International Journal of

Biology

and Chemistry

EDITORIAL

The most significant achievements in the field of natural sciences are reached in joint collaboration, where important roles are taken by biology and chemistry. Therefore publication of a Journal, displaying results of current studies in the field of biology and chemistry, facilitates highlighting theoretical and practical issues and distribution of scientific discoveries.

One of the basic goals of the Journal is to promote the extensive exchange of information between the scientists from all over the world. We welcome publishing original papers and materials of biological and chemical conferences, held in different countries (by prior agreement, after the process of their subsequent selection).

Creation of International Journal of Biology and Chemistry is of great importance, since scientists worldwide, including other continents, might publish their articles, which will help to widen the geography of future collaboration.

The Journal aims to publish the results of the experimental and theoretical studies in the field of biology, biotechnology, chemistry and chemical technology. Among the emphasized subjects are: modern issues of technologies for organic synthesis; scientific basis of the production of biologically active preparations; modern issues of technologies for processing of raw materials; production of new materials and technologies; study on chemical and physical properties and structure of oil and coal; theoretical and practical issues in processing of hydrocarbons; modern achievements in the field of nanotechnology; results of studies in various branches of biology, chemistry and related technologies.

We hope to receive papers from the leading scientific centers, which are involved in the application of the scientific principles of biological and chemical sciences on practice and fundamental research, related to production of new materials, technologies well ecological issues.

A.G. Sarıkaya[1*] , E.H. Tığlı Kaytanlıoğlu[2] , H. Fakir[2]

[1]Bursa Technical University, Faculty of Forestry, Bursa, Turkey
[2] Isparta University of Applied Sciences, Faculty of Forestry, Isparta, Turkey
*e-mail: aysegul.sarikaya@btu.edu.tr

Determination of volatile components and ethnobotanical properties of *Rhus coriaria* l. in Isparta province of Turkey

Abstract. *Rhus coriaria* L., which is from the Anacardiaceae family, is an important as a spice and medicinal plant in Turkey. In recent years, when drugs are insufficient, interest in natural plants has increased and their importance has increased in terms of being a source of raw materials in many industrial areas. In this study, it was aimed to determine the volatile components of sumac fruit samples collected from Kasnak, Kovada Lake, Barla Mountain, Aşağıgökdere and Sütçüler locations in Isparta province and their ethnobotanical use in the region. 159 volatile components of Rhus coriaria, were determined by the Head Void-Solid Phase Micro-Extraction (HS-SPME) technique combined with gas chromatography/mass spectrometry (GC/MS). The main components were α-pinene (Sütçüler 16.95%; Barla Mount 24.41%, Kovada 16.37%, Kasnak Forest 5.81%, Aşağıgökdere 18.20%, limonene (Sütçüler 7.50%; Barla Mountain 8.35%; Kovada 18.07%; Kasnak Forest 11%, 83; Aşağıgökdere 12.38%), 1,3,6-Octatriene, 3,7-Dimethyl- (Sütçüler 13.76%; Barla Mountain 19.36%; Kovada 7.97%; Kasnak Forest 5.53% ; Aşağıgökdere 15.01%) and β-caryophyllene (Sütçüler 7.70%; Barla Mountain 21.55%; Kovada 12.99%; Kasnak Forest 33.63%; Aşağıgökdere 1.18%). To determine the ethnobotanical use of Rhus coriaria in the region, a face-to-face survey of 22 questions was applied to 150 people selected by the stratified sampling model from the local people. The local people use the leaves and flowers of Rhus coriaria as tea, the fruits as a spice, and the sour sauce obtained from the fruits for food purposes. They also stated that they use it for various ailments, especially against Covid-19, for health purposes.
Key words: *Rhus coriaria*, volatile component, ethnobotany, Covid-19.

Introduction

Mankind has always been in interaction with plants from present. They tried the plants that they were sure were not harmful and poisonous and used them in the treatment of various diseases. According to the information obtained in archaeological excavations, human beings have sought healing for their problems by using plants since the early ages. Although people live in different cultures and their usage patterns have changed over time, they have generally used natural plants for religious purposes such as food, medicine, fuel, bait, broom, paint, tool making, evil eye and magic. Some natural plants and their use for various purposes have been passed down from generation to generation [1-6].

Turkey is one of the countries rich in plant diversity. Approximately 13,404 species and subspecies have been identified in our country, and 3,275 taxa of these are endemic. Our country is also rich in medicinal and aromatic plants [7].

Medicinal and aromatic plants are biological, cultural and industrial resources used in many fields. It is used as a medicine in traditional and modern medicine for the prevention of diseases and health. In addition to the use of medicinal and aromatic plants in perfumery and cosmetics, they are used in nutrition as nutritional supplements, herbal tea, flavor and spice. Interest in medicinal and aromatic plants has increased considerably in recent years and continues to increase [8].

In the group of medicinal and aromatic plants, especially those rich in essential oil have special importance. Essential oils and their aromatic extracts are widely used by the fragrance and flavor industries in the preparation of perfumes, food additives, cleaning products, cosmetics and pharmaceuticals, as a source of aroma-chemicals or as synthesis starting materials of nature-identical and semi-synthetic beneficial aroma chemicals. In recent years, it has been observed that there has been a great increase in the demand for essential oil [9].

Since Turkish society lived in rural areas for many years, they used natural plants. Today, society benefits from a part of wild plants such as food, medicine, fuel, fodder, broom, paint or in the treatment of diseases [10]. The ability of the people living in a region to benefit from the plants around them to meet their various needs can be defined as ethnobotany [11].

Despite the increase in health problems recently, it is seen that drugs are insufficient and the consumption of natural products has increased, and natural plants are used as raw materials for many human and animal medicines [12]. *Rhus coriaria* L. (leather sumac) has an important place among these species. *Rhus coriaria*, which is the only species of the *Rhus* genus in our country, is distributed in the Mediterranean, Southeastern Anatolia, Aegean, Northern Anatolia, Central Anatolia and Thrace regions. *Rhus coriaria*, which is 1-3 m long in the form of shrubs and trees, spreads between 600-1900 m in dry stony, bushes, roadsides, rocky places and forested places [13]. The antidiabetic, hypolipidemic, anti-ischemic, antiviral, antibacterial, DNA protective, antifungal, scolid, non-mutagenic, anti-cancer effects and also,

efficiency on passive avoidance learning and non-toxic, It has been determined that it has biological effects such as analgesic effect [14].

In this study, the ethnobotanical characteristics of *Rhus coriaria*, which spreads naturally in Isparta province of Turkey and has an important place in terms of consumption, and its volatile components were determined with samples taken from 5 different places. Thus, it is aimed to popularize its use among the people and to reveal the importance of natural plants against diseases.

Materıals and methods

Material. The research material consists of sumac samples collected from Kasnak forest, Kovada Lake, Barla Mountain, Aşağıgökdere and Sütçüler provinces of Isparta in 2022. Fruit samples were collected from the research areas in September (Figure 1; Figure 2). Aspect and elevation information of the sampled areas in the field were recorded. Recorded and collected plant samples were placed in Isparta University of Applied Sciences Forestry Faculty Forest Botany Laboratory for volatile component analysis according to herbarium techniques.
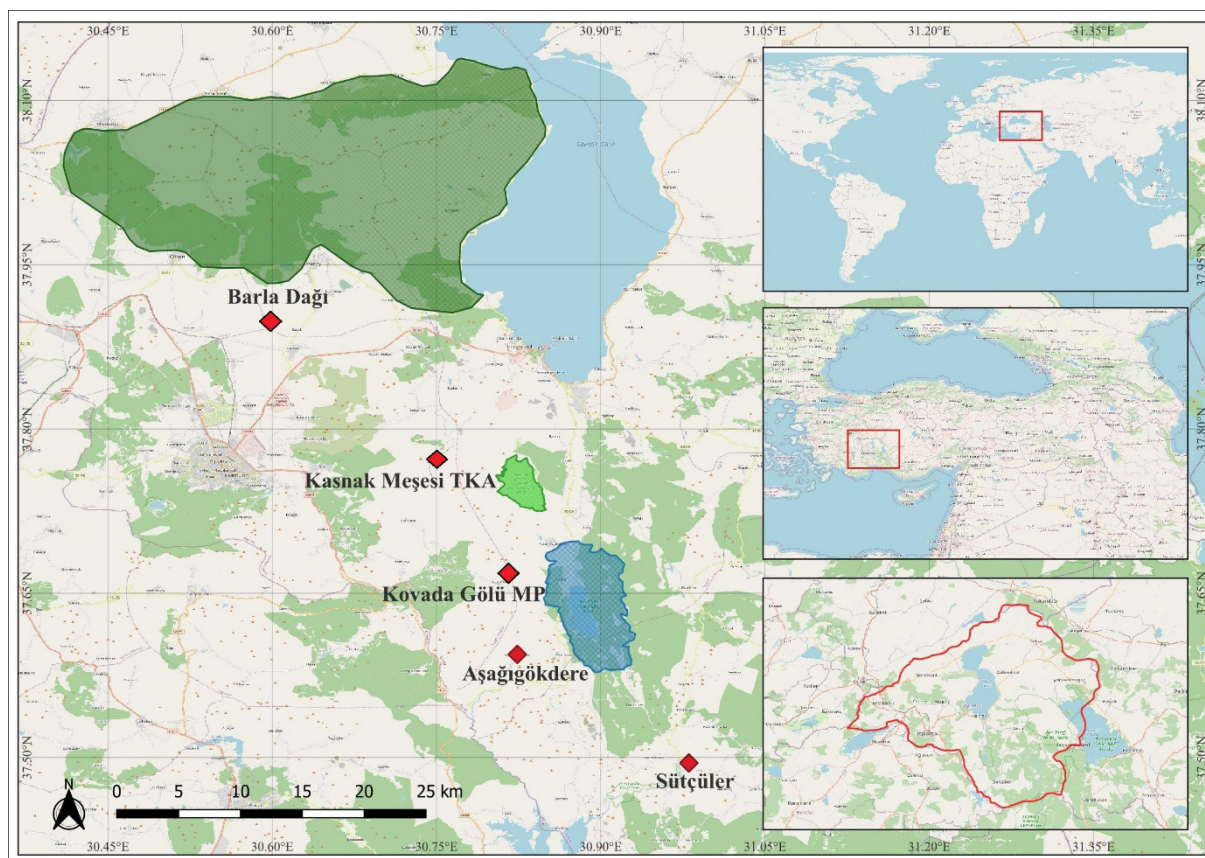

Figure 1- Sumac plant as study material

Figure 2- Areas where sumac is collected

Method for the determination of fruit volatile components. At least 1 kg of fruit was collected from each of the five sites (Kasnak Forest, Kovada Lake, Barla Mountain, Aşağıgökdere and Sütçüler) to be used in the volatile component analysis. Collected fruit samples were put into packages and labeled by coding, and information such as collection time, location and altitude were recorded on the label. It was brought to the Herbarium Laboratory of the Faculty of Forestry of Isparta University of Applied Sciences to perform volatile component analysis.

Floral aromatic components of *Rhus coriaria* fruits were determined by Head Void-Solid Phase Micro-Extraction (HS-SPME) technique combined with gas chromatography/mass spectrometry (GC/MS). Based on the solid phase microextraction method (SPME, Supelco, Germany), 2 g flower samples were incubated in a 10 mL bottle at 60°C for 30 minutes, then volatile compounds were absorbed from the headspace using 75 µm [(Thick Carboxene-Polydimethylsiloxane (CAR/PDMS)]. Coated fused silica fiber and immediately injected into the capillary column (Restek Rx-5 Sil MS 30 mx 0.25 mm, 0.25 µm) or an HS-SPME compatible GC-MS instrument (Shimadzu 2010 PLUS). The oven temperature is programmed to increase to 250ºC at a heating rate of 4ºC per minute after being kept at 40ºC for 2 minutes. Injector and detector temperatures are set to 250ºC. The ionization mode was chosen as EI (70 eV) and the carrier gas as helium (1.61 mL/min). Wiley, Nist, Tutor and FFNSC library was used to identify volatile compounds.

Method for determining ethnobotanical use. Ethnobotanical characteristics were surveyed with a questionnaire consisting of 22 questions consisting of the surrounding villages in the sample areas in the Isparta region was prepared and face-to-face interviews were conducted with the local people. This survey was conducted with 150 people selected by the stratified sampling model, consisting of people in Eğirdir Barla, Bedire, Aşağıgökdere, Yukarıgökdere, Kırıntı, Eyüpler villages and Sütçüler District Çandır villages in Isparta region (Figure 3). According to the representation ratios of each substratum in the universe, the sample groups were determined according to the simple random sampling method. The names of the participants were not taken and their information was kept confidential.
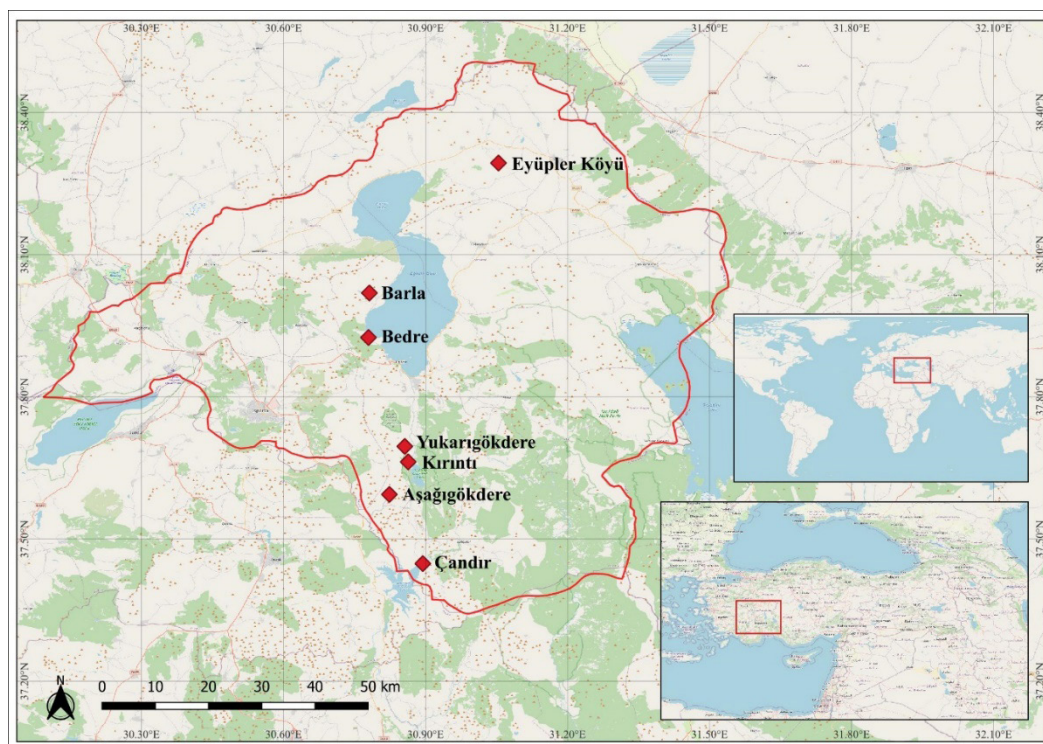
Figure 3- Areas of survey research

Results and discussion

Volatile components were determined from 100 grams of *Rhus coriaria* fruits. In the comparative study of fruit samples taken from five locations (Kasnak Forest, Kovada Lake, Barla Mountain, Aşağıgökdere and Sütçüler) in Isparta province, a total of 159 volatile components were determined, and when the component classes are examined, they consist of monoterpene hydrocarbons and sesquiterpene hydrocarbons. The main components, respectively, are α-pinene (Sütçüler 16.95%; Barla Mountain 24.41%; Kovada Lake 16.37%; Kasnak Forest 5.81%; Aşağıgökdere 18.20%), limonene (Sütçüler 7.50%; Barla Mountain 8.35%; Kovada Lake 18.07%; Kasnak Forest 11.83%; Aşağıgökdere 12.38%), 1,3,6-Octatriene, 3,7-Dimethyl- (Sütçüler 13.76%; Barla Mountain 19%) .36; Kovada Lake 7.97%; Kasnak Forest 5.53%; Aşağıgökdere 15.01%) and β-caryophyllene (Sütçüler 7.70%; Barla Mountain 21.55%; Kovada Lake 12.99%; Kasnak Forest 33.63% ; Aşağıgökdere 1.18%). The results of the volatile component analyses are given in Table 1.

Table 1 – Volatile components and classes of *Rhus coriaria*

	Components	Sütçüler	Barla Dağı	Kovada	Kasnak	A.Gökdere	Class	Formula
1	*α-Pınene*	16.95	24.41	16.37	5.81	18.20	MH	$C_{10}H_{16}$
2	Camphene	0.34	0.45	0.38	0.12	0.36	MH	$C_{10}H_{16}$
3	2-Heptenal	1.51	0.93	1.87	0.46	1.41	AA	$C_7H_{12}O$
4	Benzaldehyde	0.10	0.12	0.28	*	*	AAI	$C_{10}H_6O$
5	2-β-Pınene	1.40	*	1.54	0.97	1.95	MH	$C_{10}H_{16}$
6	1-Octen-3-One	0.34	0.24	0.34	0.13	0.34	MH	$C_8H_{14}O$
7	1-Octen-3-Ol	0.03	*	0.09	0.07	0.05	AA	$C_8H_{16}O$
8	6-Methyl-5-Hepten-2-One	0.17	0.16	0.87	0.76	0.48	AA	$C_8H_{14}O$

Table continuation

	Components	Sütçüler	Barla Dağı	Kovada	Kasnak	A.Gökdere	Class	Formula
9	β-Myrcene	6.39	6.50	13.57	4.72	9.09	MH	$C_{10}H_{16}$
10	2,4-Heptadienal	0.04	*	*	*	*	AA	$C_7H_{10}O$
11	Capronate	0.03	*	*	*	*	OC	$C_6H_{11}O_2$
12	Octanal	0.50	0.23	1.74	0.55	1.12	AA	$C_8H_{16}O$
13	L-Phellandrene	0.51	0.49	1.10	0.80	0.44	MH	$C_{10}H_{16}$
14	1,4-Dichloro-Benzene	0.05	0.06	*	*	0.02	AH	$C_6H_4Cl_2$
15	Acetic Acid	0.12	0.04	*	*	0.06	AAI	CH_3COOH
16	α-Terpınene	0.23	0.18	0.99	0.41	0.13	MH	$C_{10}H_{16}$
17	Methyl(1-Methylethyl) Benzene	1.34	*	2.06	0.75	0.86	MH	$C_{10}H_{14}$
18	3,3,6,6-Tetramethyl	0.03	*	*	*	*	OC	$\underline{C_{12}H_{26}}$
19	**Limonene**	7.50	8.35	18.07	11.83	12.38	MH	$C_{10}H_{16}$
20	Cis-Ocimene	3.33	5.10	3.11	1.81	5.84	MH	$C_{10}H_{16}$
21	Oct-3(E)-En-2-One	0.11	0.04	0.12	*	0.12	AAI	$C_8H_{12}O$
22	Benzeneacetaldehyde	0.06	0.03	0.05	*	*	OC	C_8H_8O
23	**1,3,6-Octatriene, 3,7-Dimethyl-**	13.76	19.36	7.97	5.33	15.01	MH	$\underline{C_{10}H_{18}}$
24	1,5-Heptadıene, 2-Ethyl-6-Methyl-	0.09	0.06	0.11	*	*	MH	$C_{10}H_{16}$
25	Cyclopropanemethanol	0.01	*	*	*	*	AA	$\underline{C_4H_8O}$
26	1,4-Cyclohexadiene	0.07	*	1.97	0.82	*	MH	C_6H_8
27	α-Terpınolene	0.17	0.20	0.94	0.78	0.27	MH	$C_{10}H_{16}$
28	1-Isopropenyl – Benzene	0.06	0.07	*	0.07	0.08	MH	$C_9H_{14}N_2$
29	1,3-Cyclopentadıen	0.09	0.12	*	*	*	AH	C_5H_6
30	4-Tridecene	0.07	*	*	*	*	MH	$\underline{C_{13}H_{26}}$
31	Butanoic Acid	0.14	*	*	*	*	AAI	$C_9H_{18}O$
32	Nonanal	1.92	0.58	*	1.18	2.30	AAI	$C_9H_{18}O$
33	P-Mentha-1,5,8-Triene	0.60	0.14	*	*	0.08	MH	$C_{10}H_{14}$
34	2,4,6-Octatriene	1.54	1.42	0.68	0.73	2.47	MH	$\underline{C_8H_{12}}$
35	2-Nonenal	0.18	0.08	*	*	*	AAI	$C_9H_{16}O$
36	α-Guaiene	*	*	*	0,02	*	MH	$C_{15}H_{24}$
37	Ohexene-1-Methanol	0.06	*	*	*	*	AA	C_6H_{12}
38	1-Methoxy-4-(2-Propenyl)- Benzene	0.10	*	*	*	*	SH	$C_{11}H_{16}O$
39	Dodecane	0.04	*	0.21	*	0.06	AH	$C_{12}H_{26}$
40	Capraldehyde	0.19	*	0.58	0.17	0.22	AAI	$C_{10}H_{20}O$
41	Hexyl Ester	0.05	*	*	*	*	AAI	$C_9H_{18}O$
42	Linalyl Acetate	0.40	*	0.49	*	0.50	AAI	$C_{12}H_{20}O_2$
43	2-Decenal	0.51	0.13	*	0.66	0.38	OM	$C_{10}H_{18}O$
44	Endobornyl Acetate	0.13	*	*	*	*	AAI	$C_{12}H_{20}O_2$
45	4-Terpinenyl Acetate	0.12	*	*	*	0.13	AAI	$C_{12}H_{20}O$
46	Tridecane	0.23	*	*	0.20	0.15	OC	$C_{13}H_{28}$
47	Satıven	0.08	*	*	*	*	OC	$C_{15}H_{24}$
48	2-Undecenal	0.08	0.03	0.07	*	0.04	AAI	$C_{11}H_{20}O$
49	α-Ylangene	0.57	0.07	0.10	*	*	SH	$C_{15}H_{24}$
50	α-Copaene	2.57	0.25	*	*	0.24	SH	$C_{15}H_{24}$
51	Tetradecane	0.20	*	0.13	*	0.12	AH	$C_{14}H_{30}$

	Components	Sütçüler	Barla Dağı	Kovada	Kasnak	A.Gökdere	Class	Formula
52	4,11,11-Trimethyl-8-Methylene-	0.05	*	*	*	*	SH	$C_{15}H_{24}$
53	V6-Cedren	0.07	*	*	*	*	SH	$C_{15}H_{24}$
54	10,10-Dımethyl-2,6-Bıs(Methylene)	0.16	*	*	*	0.18	OC	$\underline{C_{15}H_{24}O}$
55	β-Cubebene	0.17	*	*	*	*	OC	$C_{15}H_{24}$
56	Aromadendrene	0.32	*	*	*	0.22	SH	$C_{15}H_{24}$
57	Isoledene	0.04	*	*	0.05	*	SH	$\underline{C_{15}H_{24}}$
58	5,9-Undecadien-2-One	0.08	*	*	*	*	OC	$C_{13}H_{22}O$
59	Humulen	0.18	0.09	*	0.24	0.16	SH	$C_{15}H_{24}$
60	α-Humulene	1.10	1.87	0.98	4.00	1.65	SH	$C_{15}H_{24}$
61	Arıstolen	0.08	*	*	*	*	OC	-
62	Trans- cadina	0.84	*	*	*	*	SH	$C_{15}H_{24}$
63	Epi-Bicyclosesquiphellandrene	0.05	*	*	*	*	SH	$\underline{C_{15}H_{24}}$
64	γ-Cadinene	0.27	0.32	0.28	*	0.29	SH	$C_{15}H_{24}$
65	α-Amorphene	0.37	0.14	*	0.92	0.03	SH	$C_{15}H_{24}$
66	β-Selinene	0.14	*	*	*	*	SH	$C_{15}H_{24}$
67	1,2,4a,5,8,8a-Hexahydro-4,7-Dimethyl-1-(1-Methylethyl)	0.60	*	*	*	*	SH	$C_{15}H_{24}$
68	α-Muurolene	1.81	0.13	0.06	0.67	0.08	SH	$C_{15}H_{24}$
69	Δ-Cadinene	0.81	0.39	0.17	3.29	0.21	SH	$C_{15}H_{24}$
70	Cıs-Calamenene	0.22	*	*	*	*	SH	$C_{15}H_{22}$
71	Epızonaren	0.16	*	*	0.01	*	SH	$C_{15}H_{24}$
72	Dro-1,6-Dimethyl-4-(1-Methylethyl)	0.34	*	*	*	*	SH	$C_{15}H_{18}$
73	α-Calacorene	0.16	*	*	*	*	SH	$C_{15}H_{20}$
74	2-Cyclopenten-1-One	0.03	*	*	*	*	AAI	C_5H_6O
75	Caryophyllene Oxide	0.06	0.45	*	*	*	SH	$C_{15}H_{24}$
76	Dımethyl-2,3,4,4a,5,6-Hexahydro-Naphthalen-2-Yl)-Prop-2-E	0.04	*	*	*	*	OC	$C_{15}H_{24}O$
77	α-Cubebene	0.02	*	*	0.05	*	OC	$C_{15}H_{24}$
78	Torreyol	0.08	*	*	*	*	AA	$\underline{C_{15}H_{26}O}$
79	Cembrene	1.83	0.47	0.59	3.32	1.10	OC	$C_{20}H_{32}$
80	1,5,9-Cyclotetradecatriene, 1,5,9-Trimethyl-12-(1-Methylethenyl)-	0.03	*	*	*	*	OC	$C_{20}H_{32}$
81	Cis-Pinen-3-Ol	*	0.01	*	*	*	AA	$C_{10}H_{16}O$
82	β-Pinene	*	2.88	*	*	*	MH	$C_{10}H_{16}$
83	Trans-2-(2-Pentenyl)Furan	*	0.03	*	*	*	AAI	C_5H_6O
84	Isomyrcenol	*	0.03	*	*	*	AA	$C_{10}H_{16}O$
85	1-Methyl-4-(1-Methylethyl)- Benzene	*	0.23	*	*	*	AH	$C_{10}H_{12}$
86	Cyclopentene	*	0.09	*	*	*	MH	C_5H_8
87	4-Carene	*	0.06	*	*	*	MH	$C_{10}H_{16}$
88	İsopentyl 2-Methylbutanoate	*	0.06	*	*	*	AAI	$C_8H_{16}O_2$
89	Butyrate <2-Methylbutyl-, 2-Methyl->	*	0.01	*	*	*	AAI	$C_{10}H_{20}O$
90	1,3,5-Undecatriene	*	0.13	*	*	*	MH	$C_{11}H_{18}$
91	β-Fenchyl Alcohol	*	0.05	0.60	*	0.12	AA	$C_{10}H_{18}O$

	Components	Sütçüler	Barla Dağı	Kovada	Kasnak	A.Gökdere	Class	Formula
92	Decanal	*	0.08	*	*	*	OM	$C_{10}H_{20}O$
93	1,6-Octadien-3-Ol, 3,7-Dimethyl-, Acetate	*	0.27	*	1.12	*	AAI	$C_{11}H_{18}O$
94	Bornyl Acetate	*	0.13	0.30	0.64	0.18	AAI	$C_{12}H_{20}O_2$
95	Hept-2-Ene, 3,7,7-Trimethyl-	*	0.09	*	*	*	OC	$C_{10}H_{16}$
96	**β-Caryophyllene**	*	21.55	12.99	33.63	19.18	SH	$C_{15}H_{24}$
97	10,10-Dimethyl-2,6-Bis(Methylene)	*	0.13	*	0.28	*	OC	$C_{15}H_{24}O$
98	Decene	*	0.06	*	*	*	AH	$C_{10}H_{20}$
99	1-Butanol, 3-Methyl	*	0.13	*	0.18	*	AA	$C_5H_{12}O$
100	Neryl Acetone	*	0.04	*	*	*	AAI	$C_{13}H_{22}O$
101	α-Guaiene	*	0.05	*	0.02	*	SH	$C_{15}H_{24}$
102	α-Selinene	*	0.12	0.23	1.91	0.18	SH	$C_{15}H_{24}$
103	β-Elemene	*	0.02	*	*	*	SH	$C_{15}H_{24}$
104	2,6,10,15-Tetramethyl	*	0.01	*	*	*	AAI	$\underline{C_{21}H_{44}}$
105	Octadecamethylcyclononasıloxane	*	0.01	*	*	*	OC	$\underline{C_{18}H_{54}O_9Si_9}$
106	Δ-3 Carene	*	*	0.30	*	*	MH	$C_{10}H_{16}$
107	1,2-Dichloro-Benzene	*	*	0.22	*	*	AH	$C_6H_4Cl_2$
108	1,7-Octadıen, 3,6-Dımethylen-	*	*	0.30	*	*	AA	$\underline{C_{10}H_{18}O}$
109	1-Chloroundecane	*	*	0.03	*	*	MH	$C_{10}H_{21}Cl$
110	Hexadecane, 1-Chloro-	*	*	0.44	*	*	AH	$C_{16}H_{34}$
111	Nonanal	*	*	3.57	*	*	AAI	$C_9H_{18}O$
112	α-Campholene Aldehyde	*	*	0.05	*	0.04	AAI	$C_{10}H_{16}O$
113	2(10)-Pinen-3-One	*	*	0.36	0.14	0.26	MH	$C_{10}H_{14}O$
114	3-Cyclohexen-1-Ol, 4-Methyl-1-(1-Methylethyl)-	*	*	0.64	0.12	*	AA	$C_{10}H_{18}O$
115	Benzene, 1-Methoxy-4-(1-Propenyl)-	*	*	0.20	*	*	AH	$C_{11}H_{16}O$
116	Carvacrol Methyl Ether	*	*	0.24	*	*	OC	C_6H_3
117	2-Decenal	*	*	0.31	*	*	AAI	$C_{10}H_{18}O$
118	Heptadecane, 2,6,10,15-Tetramethyl-	*	*	0.07	*	*	AH	$C_{21}H_{44}$
119	3-Phenylhexan-3-Ol	*	*	0.11	*	*	AA	$C_{12}H_{18}O$
120	Docosanoic Acid	*	*	0.17	*	*	SH	$C_{22}H_{44}O_2$
121	Lımonen	*	*	0.21	0.35	*	MH	$C_{10}H_{16}$
122	Copaene	*	*	0.19	*	*	SH	$C_{15}H_{24}$
123	Cıs-Caryophyllene	*	*	0.08	*	*	SH	$C_{15}H_{24}$
124	Cycloheptasiloxane	*	*	0.12	*	*	OC	O_7Si_7
125	Eudesma-4(14),11-Diene	*	*	0.23	1.94	0.16	SH	$C_{15}H_{24}$
126	Selina-3,7(11)-Diene	*	*	0.11	*	*	SH	$C_{15}H_{24}$
127	Cyclooctasiloxane, Hexadecamethyl-	*	*	0.07	*	*	OC	$\underline{C_{16}H_{48}O_8Si_8}$
128	Benzaldehyde	*	*	*	0.08	0.11	AAI	C_7H_6O
129	2-Methyl-6-Methylene-2-Octene	*	*	*	0.07	0.09	SH	$C_{10}H_{18}$
130	Linalool	*	*	*	0.51	*	OM	$C_{10}H_{18}O$
131	Pentanoic Acid	*	*	*	0.10	*	AAI	$C_5H_{10}O_2$
132	1,3,8-P-Menthatrıene	*	*	*	0.21	*	sh	$C_{10}H_{14}$

	Components	Sütçüler	Barla Dağı	Kovada	Kasnak	A.Gökdere	Class	Formula
133	Limonen-10-Yl Acetate	*	*	*	0.02	*	MH	$C_{10}H_{16}$
134	α-Terpıneol	*	*	*	1.69	*	AA	$C_{10}H_{18}O$
135	Undecanal	*	*	*	0.08	*	AAI	$C_{10}H_{21}CHO$
136	2-Undecenal	*	*	*	0.03	*	AAI	$C_{10}H_{21}CHO$
137	Ylangene	*	*	*	0.38	0.12	SH	$C_{15}H_{24}$
138	6,8a-Octahydro-7-Methyl-4-Methylene-1-(1-Methylethyl)-	*	*	*	2.51	*	SH	$C_{15}H_{24}$
139	5,9-Undecadien-2-One, 6,10-Dimethyl-	*	*	*	0.14	*	AA	$C_{13}H_{22}O$
140	Octahydro-7-Methyl-3-Methylene-4-(1-Methylethyl)	*	*	*	0.05	*	SH	$C_{15}H_{24}$
141	Selina-3,7(11)-Diene	*	*	*	1.54	*	SH	$C_{15}H_{24}$
142	β-Vatirenene	*	*	*	0.07	*	SH	$C_{15}H_{22}$
143	Germacrene B	*	*	*	0.25	*	SH	$C_{15}H_{24}$
144	1,2,4a,5,8,8a-Hexahydro-4,7-Dimethyl-1-(1-Methylethyl)	*	*	*	0.09	*	SH	$C_{15}H_{24}$
145	Tetracosamethyl-cyclododecasıloxane	*	*	*	0.05	*	OC	$C_{24}H_{72}O_{12}Si_{12}$
146	β-Elemene	*	*	*	0.10	*	SH	$C_{15}H_{24}$
147	3-Carene	*	*	*	*	0.03	MH	$C_{10}H_{16}$
148	3,7-Octadien-2-Ol, 2-Methyl-6-Methylene-	*	*	*	*	0.15	SH	$C_{10}H_{16}O$
149	1,4-Hexadiene, 5-Methyl-3-(1-Methylethylidene)-	*	*	*	*	0.01	SH	$C_{15}H_{24}$
150	2-Propenamide, 2-Methyl-N-Phenyl-	*	*	*	*	0.07	SH	$C_{16}H_{16}N_2O$
151	3-Methyl-Undecane	*	*	*	*	0.03	AH	$C_{12}H_{26}$
152	Hexanoic Acid	*	*	*	*	0.06	AAI	$C_6H_{12}O_2$
153	Trans-Anethole	*	*	*	*	0.10	AA	$C_{10}H_{12}O$
154	α-Gurjunene	*	*	*	*	0.05	SH	$C_{15}H_{24}$
155	5,9-Undecadien-2-One, 6,10-Dimethyl	*	*	*	*	0.07	OC	$C_{13}H_{22}O$
156	Farnesene	*	*	*	*	0.03	SH	$C_{15}H_{24}$
157	β-Guaiene	*	*	*	*	0.06	SH	$C_{15}H24$
158	Cyclohexane	*	*	*	*	0.05	SH	C_6H_{12}
159	Tetratetracontane	*	0.02	*	*	*	MH	$C_{44}H_{90}$
	Component Number	81	63	59	63	64		
	AA: Aromatic Alcohol	2,40	1,54	6,22	3,97	3,28		
	AAI: Aromatic Aldehyde	3,57	1,44	5,77	3,42	3,76		
	AH: Aromatic Hydrocarbon	0,38	0,47	1,27	-	0,23		
	MH: Monoterpene Hydrocarbon	52,64	70,15	70,10	35,61	67,79		
	OM: Oxygenated Monoterpene	2,84	0,73	1,07	3,90	1,50		
	OC: Other Components	0,51	0,21	-	1,17	0,38		
	SH: Sesquiterpene Hydrocarbon	36,48	24,45	15,59	51,95	23,03		
	Total	100,00	100,00	100,00	100,00	100,00		

A total of 159 volatile components were determined, and when the component classes are examined, they consist of monoterpene hydrocarbons and sesquiterpene hydrocarbons. In our study, the main components were determined as α-pinene, limonene, 1,3,6-Octatriene, 3,7-Dimethyl- and β-caryophyllene.

In previous studies; Brunke et al. (1993) [15] analyzed the volatile components of *Rhus coriaria* samples collected in Adana, Şanlıurfa, Diyarbakır, Hatay, Gaziantep and Kahramanmaraş by GC-MS. Comparative studies have identified more than 120 compounds, the main components of which are terpene hydrocarbons (α-pinene, β-caryophyllene and cembrene), oxygenated terpenes (α-terpineol, carvacrol and β-caryophyllene alcohol), as well as farnesyl acetone, hexahydrofarnesylacetone and aliphatic aldehydes. have been detected.

Kurucu et al. (1993) [16] investigated the essential oils obtained from the leaf, fruit peel and twig/bark of *Rhus coriaria* by hydrodistillation by GC and GC/MS. They determined 63 components in branch/bark oil, 63 components in leaf oil and 85 components in fruit pericarp oil. The main components in pericarp oil are limonene (0.17–9.49%), nonanal (10.77–13.09%), and (Z)-2-decenal (9.90–42.35%), while the main components of leaf oil are β-caryophyllene (0.33–16%, It is a sesquiterpene hydrocarbon defined as 95 and provisionally patchulan (3.08–23.87%), the main components of branch/bark oil are β-caryophyllene (12.35–21.91%) and kembrene (10.71–26,50%).

Rediel et al. (2017) [17] analyzed the organs of *Rhus coriaria* collected in Sicily (Italy) by Gas chromatography Mass spectrometry (GC-MS). Monoterpene and sesquiterpene hydrocarbons are the most abundant, and β-caryophyllene and α-pinene components were identified as the main components.

Morshedloo et al. (2018) [18] evaluated the variability of essential oil compositions in *Rhus coriaria* fruits collected from 14 different locations in Iran. GC-FID and GC-MS analyzes of essential oils identified a total of 57 components. As main components (E)-Caryophyllene (5.9–50.3%), n-nonanal (1.8–23.3%), kembrene (1.9–21.7%), α-pinene (%) 0.0–19.7), (2E,4E)-decadienal (2.4–16.5%), and nonanoic acid (0.0–15.8%) were determined.

Zhalel et al. (2018) [19] (ATCC No. 21332) (BS) evaluated it's chemical composition and antibacterial activities. The chemical composition of *Rhus coriaria* was determined by Gas chromatography Mass Spectrometry (GC-MS). They found that the most common components in Rhus coriaria were β-caryophyllene (34.3%) and cembrene (23.8%).

When we compare other studies with our research, α-pinene, limonene, and β-caryophyllene components support our study. In our study, 1,3,6-Octatriene and 3,7-Dimethyl- components were detected differently. This difference is thought to be related to the region, climate and ecological characteristics.

Separately, a questionnaire consisting of 22 questions was prepared and interviews were conducted with the local people to determine the ethnobotanical characteristics of *Rhus coriaria* L. in the surrounding villages of Isparta province. A total of 150 people were interviewed. Considering some demographic characteristics of the participants of the survey conducted with the local people; 54.7% are female and 45.3% are male. The age of the local people participating in the survey is between 16 and 80 years old. Of the respondents, 32.66% are primary school-secondary education graduates, 36% high school, 27.32% associate degree-undergraduate, and 4% graduate-doctorate (Table 2).

Table 2 – Some demographic characteristics of the respondents

Gender	Number of people	%
Female	82	54,7
Male	68	45,3
Total	150	100
Education Status		
Primary/ Middle School	49	32,67
High School	54	36
Associate/ Bachelor Degree	41	27,33
Master/Doctorate Degree	6	4

90% of the participants in the survey study benefited from the plants that grow naturally in the region before the Covid-19 virus appeared, 84.7% started using the natural plants in the region after the onset of the Covid-19 pandemic, and 88.7% used the sumac plant (Figure 4).

It was determined that 78.7% of them had an increase in the amount of sumac plant use after the onset of the Covid-19 pandemic (Figure 4). According to the results of the research, it was determined that 4.1% of the local people did not use the sumac plant in any way, 16.7% benefited from the sumac plant for health and treatment, 77.3% for food/meal/spice, and 18% for pleasure. 32.2% of the participants in the survey research obtained the sumac plant by collecting them from nature. Of those who collect it from nature, 42% say that the area where the

plant is collected is clean and hygienic, 32% of the plants are healthy, 62% of them are harvested in the season, 12.7% of them are all the organs of the plant and 30.7% are It pays attention to the ripeness of its fruits. 83.4% of the participants in the survey study consume the sumac plant by drying its fruits, 14% consume its fruits fresh, and 12.7% consume it by making sour sauce.
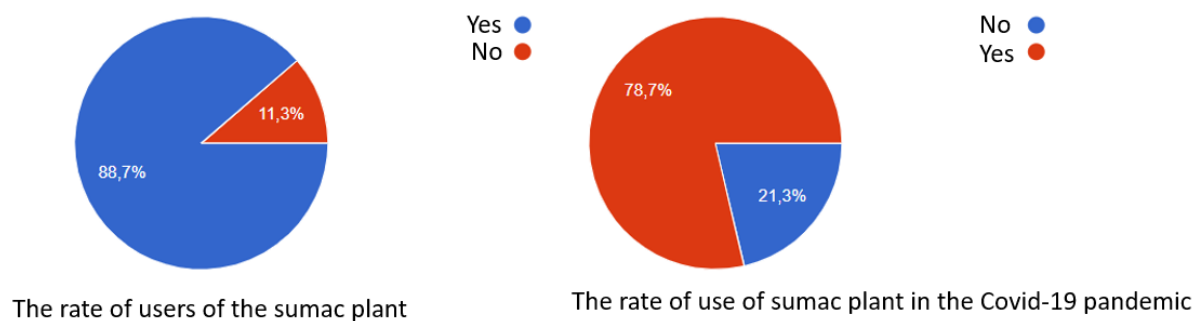

Figure 4- Use status of sumac plant

To the survey question, which parts of the plant species you supply most benefit from, 77.3% of them stated that they benefited from the fruit, 34.7% of the flower, 16% of the stem, 6.7% of the shoot and 4% of the root. Participants stated that it collects the most intensively in the months of August-September-October. They consume leaves and flowers of the sumac as as tea, its fruits as a spice in salads and meals, and the sour sauce obtained from its fruits in salads; They also stated that they use their fruits as a mouthwash against mouth sores. 85.4% of the participants obtain sumac sour from the fruits of the sumac plant. After drying the fruits, pounding them in a mortar and crushing them, they separate the seeds and boil them to obtain sumac syrup. To the question of whether you have seen or heard of any side effects from the sumac plant you are using, 96.7% said no, 2% heard but did not see any side effects, and 1.3% stated that they had side effects. 56.7% family, 45.3% people around, 2% written media, 6.7% books/magazines, 10% visual and audio media, 11.3% quotes and 1.3% of them are the factors that are effective in the consumption of the sumac plant with the rates of advertisements. 66% of the participants heard that the sumac plant can be beneficial against Covid-19. 91.3% of the participants who had Covid-19 used the sumac plant during their treatment (Figure 5).
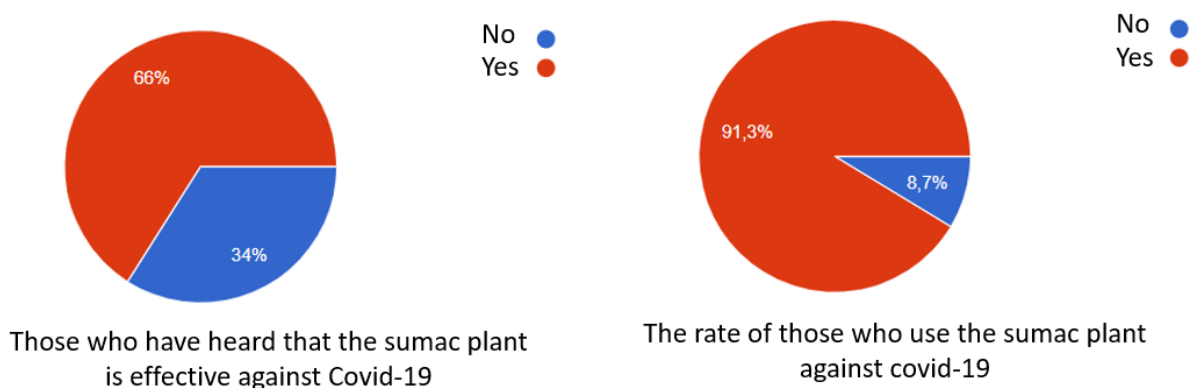
Figure 5- The use of the sumac plant against Covid-19 by the participants

Participants who used the fruits as a tea for treatment reported that they killed germs in the mouth and had a diuretic, breath-opening and throat-relaxing effect. 5.3% of the participants reported that they were selling the products they obtained from the sumac plant, that they were selling them to the surrounding provinces and their relatives, and that 94.7% of them did not. Participants who made the sale were asked whether there was an increase in their sales during and after the Covid-19 pandemic. 96.3% of the participants stated that there was an increase.

In order to determine the ethnobotanical characteristics of *Rhus coriaria* in the surrounding villages of Isparta province, 150 people were interviewed in the region. The local people consume the leaves and flowers of the Rhus coriaria they collect as tea, the fruits as a spice in salads and meals, and the sour sauce obtained from the fruits in salads; They also stated that they use their fruits as a mouthwash against mouth sores. Especially after the Covid-19 pandemic, its use has increased in the region and it has been stated that it has a therapeutic feature in addition to reducing the risk of catching the immune-boosting Covid-19. The local people benefit from the sumac plant economically, as well as for food such as spice, tea, sumac syrup, and for health purposes for the treatment of various diseases.

Previous studies stated that; the decoction prepared from the roots and leaves of *Rhus coriaria* is widely used in stomach diseases, and the decoction prepared from its fruits is widely used among people to reduce kidney stones. It is known that the fresh leaves are laid on the sole of the shoes to treat the cracks in the skin, and chewing the fruit in the form of gum is good for mouth sores and stomach cramps [20-21].

In addition to these, it has been stated that sumac is used in dysentery, liver diseases, conjunctivitis and anorexia, hair treatments, dermatitis, burns and skin diseases [22]. Setorki et al., (2012) [23] stated that sumac plant has a protective effect on oxidative stress and liver enzymes caused by foods with high fat content. The laxative obtained from its fruit is also used in hypertension and diabetes in Azerbaijan [24]. Exporting the extracts prepared from sumac fruit as an herbal tanning agent and being preferred in ink making, dyeing and veterinary medicine has increased the economic value of sumac [25-27].

Baydoun et al. (2017) [28] investigated the ethnobotanical and economic importance of wild plant species in Lebanon and found that *Rhus coriaria* was used for food and herbal medicine.

Batiha et al. (2022) [29] stated that in recent years, the use of *Rhus coriaria* (sumac) has developed not only in culinary use and human nutrition but also in the pharmaceutical industry, food industry and veterinary applications. Considered a spice, most of the antioxidant potential and therapeutic roles of *Rhus coriaria* have been increasingly attributed to its constituent tannins, flavonoids, and phenolic acids. They stated that tannin-rich sumac extracts and isolates improve food quality and oxidative stability of animal products such as meat and milk. The studies carried out support our study in terms of ethnobotanical use. Differently, its use has increased in the Covid-19 pandemic and it has been found that it has a therapeutic feature in addition to reducing the risk of catching the immune-boosting Covid-19. Our study is important in this respect.

Conclusion

Rhus coriaria is used extensively as a spice, as well as in the pharmaceutical industry, food industry, paint industry and veterinary field thanks to the secondary metabolites it contains. Instead of collecting *Rhus coriaria*, which is valuable for the economy and health, from natural areas, cultivation studies should be increased and ex-situ and in-situ protection measures should be taken for natural populations. It is recommended to increase the studies on the secondary metabolites of *Rhus coriaria* to popularize food safety with the 'clean food' label in our country, especially in the food industry, whose importance has increased in recent years. In addition, it is recommended to carry out detailed studies to evaluate it in the field of health against viruses.

References

1. Altan,Y., Uğurlu, E. ve Gücel, S. 1999. Şenkata (Erzurum) ve Çevresinin Etnobotanik Özellikleri. 1st International Symposium on Protection of Natural Environment and Ehrami Karaçam, Kütahya- Turkey, 132139.

2. Lev E., Amar Z. Ethnopharmacological survey of traditional drugs sold in Israel at the end of the 20th century. J. Ethnopharmacol. 2000;72:191–205. doi: 10.1016/S0378-8741(00)00230-0. – DOI - PubMed

3. Tütenocaklı, T. 2002. Ayvacık (B1, Çanakkale) ve Çevresinin Etnobotaniği, Yüksek Lisans Tezi. Çanakkale Onsekiz Mart Üniversitesi Fen Bilimleri Enstitüsü, Çanakkale.

4. Heinrich M, Barnes J, Gibbons, S. 2004. Fundementals of pharmacognosy and phytotherapy, Churchill Livingstone, Edinburgh.

5. Koçyiğit, M. 2005. Yalova İli'nde Etnobotanik Bir Araştırma. İstanbul Üniversitesi, Sağlık Bilimleri Enstitüsü, Yüksek Lisans Tezi, İstanbul.

6. Deniz, L., Serteser, A., Kargıoğlu, M., 2010. Uşak Üniversitesi ve Yakın Çevresindeki Bazı Bitkilerin Mahalli adları ve Etnobotanik Özellikleri. Afyon Kocatepe Üniversitesi Fen Bilimleri Dergisi 01, 57-72.

7. Tarım ve Orman Bakanlığı, 2022. Nuh'un gemisi ulusal biyoçeşitlilik veritabanı. https://nuhungemisi.tarimorman.gov.tr/public/istatistik. Erişim tarihi: 02.09.2022

8. BAKA (Batı Akdeniz Kalkınma Ajansı), (2012). Tıbbi ve Aromatik Bitkiler Sektör Raporu, 2012.

9. Weiss, E.A., (1997). Essential Oil Crops. The Journal of Agricultural Science, 129 No:121-123.

10. Baytop, T., (1984). Turkey'de bitkilerle ile tedavi (Geçmişle ve bugün), İstanbul.

11. Yıldırımlı, Ş., (2004). Etnobotanik ve Türk Etnobotaniği. Kebikeç İnsan Bilimleri için Kaynak Araştırmaları Dergisi, 17, s. 175- 193.

12. Kırbağ, S. Zengin, F. (2006): Elazığ Yöresindeki Bazı Tıbbi Bitkilerin Antimikrobiyal Aktiviteleri. J Agric Sci, 16(2), 77-80.

13. Koyuncu, M. Köröğlu, A. (1991): Rhus Coriaria Yaprak ve Meyvelerinin Anatomik İncelenmesi. Doğa-Tr J Pharmacy, 1, 89-96.

14. Saltan, F. Z., & Ünder, D. (2019). Sumak ve Önemli Biyolojik Etkileri. Çukurova Tarım ve Gıda Bilimleri Dergisi, 34(1), 69-78.

15. Brunke, E.J.; Hammerschmidt, F.J.; Schmaus, G.; Akgül, A. The Essential Oil of Rhus coriaria L. Fruits. Flavour Fragr. J. 1993, 8, 209–214. [Google Scholar] [CrossRef]

16. Kurucu,S., Koyuncu, M., Güvenç (Köroglu), A., Baser, K. H.C., Özek, T. (1993) The Essential Oils of Rhus coriaria L. (Sumac), Journal of Essential Oil Research, 5:5, 481-486, DOI: 10.1080/10412905.1993.9698267

17. Reidel, R.V.B.; Cioni, P.L.; Majo, L.; Pistelli, L. Evolution of volatile emission in Rhus coriaria organs during different stages of growth and evaluation of the essential oil composition. Chem. Biodiv. 2017, 14, e1700270. [Google Scholar] [CrossRef] [PubMed]

18. Morshedloo, M.R., Maggi, F. Maggi, Neko, H.T., Aghdam M.S., (2018). Sumac (Rhus coriaria L.) fruit: Essential oil variability in Iranian populations Industrial Crops and Products, 111 (2018), pp. 1-7

19. Zhaleh, M., Sohrabi, N., Zangeneh, Akram Zangeneh, M.M., Moradi, R., Zhaleh, H., (2018). Chemical Composition and Antibacterial Effects of Essential Oil of Rhus coriaria Fruits in the West of Iran (Kermanshah), Journal of Essential Oil Bearing Plants, 21:2, 493-501, DOI: 10.1080/0972060X.2018.1462739

20. Tuzlacı, E. (2006) Şifa Niyetine Turkey' nin Bitkisel Halk İlaçları. Alfa Yayıncılık, İstanbul.

21. Tuzlacı, E. (2011) Turkey Bitkileri Sözlüğü. Alfa Yayıncılık, İstanbul.

22. Ali-Shtayeh, M. S., Al-Assali, A. A., Jamous R. M. (2013) Antimicrobial activity of Palestinian medicinal plants against acne-inducing bacteria. African J Microbiol Res 7:2560- 2573.

23. Setorki, M., Rafieian, M., Heidarian, E., Ghatreh, K., Shahinfard, N., Ansari, R., Forouzandeh, Z. (2012) Effect of Rhus coriaria consumption with high cholesterol food on some atherosclerosis risk factors in rabbit. J Babol University of Medical Sci 14:38- 45.

24. Hasanova, G., Öztürk M, Akçiçek E, (2000) Azerbaycan' da Geleneksel Tedavide Kullanılan Bitkiler 13. BİHAT özet kitabı, İstanbul.

25. Kurt, R., Karayılmazlar, S., Çabuk, Y. (2014) Sepicilikte Kullanılan Odun Dışı Orman Ürünlerinin Dış Ticaretinin Değerlendirilmesi, Akdeniz ormanlarının geleceği: Sürdürülebilir toplum ve çevre". II. Ulusal Akdeniz Orman ve Çevre Sempozyumu, Isparta, 650- 656.

26. Kizil, S., Turk, M. (2010) Microelement contents and fatty acid compositions of Rhus coriaria L. and Pistacia terebinthus L. fruits spread commonly in the south eastern Anatolia region of Turkey. Natural Product Res 24:92-98

27. Tiryaki, G. Y. (2010). Kahramanamaraş İlinde Üretilen Simgesel Geleneksel Ürün: Sumak Ekşisi. Gıda Mühendisliği Dergisi 31:55- 58.

28. Baydoun SA, Kanj D, Raafat K, Aboul Ela M, Chalak L, et al. (2017) Ethnobotanical and Economic Importance of Wild Plant Species of Jabal Moussa Bioreserve, Lebanon. J Ecosys Ecograph 7: 245. doi: 10.4172/2157-7625.1000245

29. Batiha, G.E.; Ogunyemi, O.M.; Shaheen, H.M.; Kutu, F.R.; Olaiya, C.O.; Sabatier, J.M.; De Waard, M. Rhus coriaria L. (Sumac), a Versatile and Resourceful Food Spice with Cornucopia of Polyphenols. Molecules 2022, 27, 5179.

R.R. Tokpayev[1] , E.R. Shreider[1]*,
Z.T. Ibraimov[1] , T.M. Shalakhmetova[2] , M.K. Nauryzbayev[1]

[1]Center of physico-chemical methods of research and analysis, al-Farabi Kazakh National University, Almaty, Kazakhstan
[2]School of Biology and Biotechnology,
al-Farabi Kazakh National University, Almaty, Kazakhstan
*e-mail: vlr98@mail.ru

Decellularization of bone tissue
in a supercritical carbon dioxide environment

Abstract. The use of pig bone tissue as a graft makes it possible to obtain high-quality, relatively cheap and biocompatible ECM. This is since the mineral composition of pork bone is most similar to the mineral composition of human bone. Decellularization in $SC-CO_2$ is a promising direction, since carbon dioxide easily diffuses into the depth of the cell and is a good solvent for lipids, it is non-flammable, non-toxic and chemically non-aggressive. In this paper, the ECM in $SC-CO_2$ was obtained in three ways: 1) in dynamic mode with large $SC-CO_2$ flows; 2) in static and dynamic modes with large $SC-CO_2$ flows; 3) in static and dynamic modes with large $SC-CO_2$ flows, with preliminary exposure in ethyl alcohol as a co-solvent. According to the histological examination, the removal of ICC by the first method is 55%. The use of a co-solvent before starting the decellularization process increases the percentage of ICC removal to 98%, which allows the use of ECM as a transplant.

Key words: decellularization, tissue engineering, transplantation, supercritical extraction, carbon dioxide, biomaterials, extracellular matrix, xenografts.

Introduction

Bone tissue is in second place in terms of transplantation after blood, in this regard, the need for high-quality and inexpensive bone grafts is increasing every year. It is related to an increase in the number of patients with diseases of the musculoskeletal system, victims of various accidents that lead to injuries and infections formation. However, common methods of treatment, such as tissue/organ transplantation, surgeries, use of various mechanical devices, face several unresolved issues and problems, which aroused great interest in tissue engineering [1, 2].

Various biomaterials are used to obtain transplants. By origin, materials can be divided into allogenic (donor is another person), autogenic (donor is the recipient), alloplastic (synthetic biomaterials), xenogenic (donor is an animal) [3-5].

The use of xenogenic materials is a promising direction. This is due to their maximum availability and cheapness, which makes it possible to almost recreate the damaged area completely. Most often, bovine and pig bones are used as xenogenic material. However, in the works [6-8], it was proved that the use of bovine bone tissue leads to further rejection of the graft and inability of colonization with stem cells. That is why pig bone grafts are now widely used. The trabecular pig bone is most similar in mineral composition to the mineral composition of human bone [9-11].

The most common method of draft obtaining is decellularization. Decellularization is a method in which all intracellular components (ICC) are removed under the action of various agents. The result of decellularization is the extracellular matrix (ECM), which during the process must not be destroyed and retain its composition, as well as mechanical and biological properties. Decellularization can be chemical, biological, physical and with the help of supercritical fluid technologies. Each method has a number of advantages and disadvantages.

Chemical decellularization includes treatment with acids and bases, detergents, hypotonic and hypertonic solutions [12]. Acids and bases in the process of decellularization cause or catalyze hydrolytic degradation of biomolecules, but at the same time reduce the strength of ECM [13,14]. Detergents such as SDS (sodium dodecyl sulfate)

and Triton X-100 completely remove ICC, however, they affect structure and composition of ECM, since together with ICC, glycosaminoglycans are washed out and eliminate growth factor. The use of hypotonic and hypertonic solutions has the least effect on ECM, however, the removal of ICC does not occur completely. Biological decellularization with the help of enzymes also has a minimal effect on ECM, however, complete removal of ICC by this treatment cannot be achieved. The removal of ICC during physical decellularization occurs due to physical forces influence, but they can also affect the ECM. Physical decellularization includes such methods as freezing-thawing, osmotic pressure, ultrasonic treatment, etc. [15].

Supercritical fluid CO_2 extraction currently is of great interest to scientists. This is due to unique properties of CO_2 that it possesses under supercritical conditions. The main advantage of supercritical carbon dioxide (SC-CO_2) during the decellularization process is that it is a non-toxic, non-combustible, relatively inert gas and diffuses independently from bone tissue over time due to the transition to a gaseous state under normal conditions. Due to diffusing, more channels are formed inside the tissue. Due to the unique properties of diffusion, density and viscosity SC-CO_2 is used as a selective extraction solvent. It is especially suitable for extracting components from a solid microporous structure, including bone tissue. Due to the high transfer rate and high permeability possessed by the supercritical fluid, any endotoxins, allogeneic proteins and bio-loading are completely removed from the ECM, which leads to a decrease in the immunogenicity of the graft. Consequently, the decellularized tissue obtained by this method will be safe for the recipient after implantation, since SC-CO_2 treatment avoids the use of toxic organic solvents and does not leave a cytotoxic residue. From an economic point of view, use of SC-CO_2 is promising, since it is found in large quantities in nature, which significantly reduces its cost and increases availability. Cyclic installations used for decellularization under supercritical conditions allow carbon dioxide to be used repeatedly. The use of supercritical fluid in the decellularization process can completely or partially reduce the use of aggressive, toxic and expensive reagents. Due to this, as a result of decellularization in SC-CO_2, will be obtained commercially available, biochemically pure and structurally intact ECM [16].

In paper [17], a comparative analysis of the traditional process of decellularization using detergents and decellularization in SC-CO_2 was carried out. The obtained ECMs were examined using histological examination, scanning electron microscopy (SEM) and DNA and collagen were determined. The ECM analysis confirmed that decellularization in SC-CO_2 proceeds efficiently and does not have a significant effect on the matrix, unlike detergents. The traditional decellularization process takes on average from 3 to 14 days, whereas decellularization in SC-CO_2 at 23 ml/min flow rate took less than 3 days. In addition, in this method, the number of stages of decellularization is significantly reduced and there is no need to wash the ECM before introducing the graft into the body. While removal of ICC using SC-CO_2, there is no need to use high temperatures, since carbon dioxide goes into a supercritical state at T=31.1°C, due to which thermosensitive biomaterials can be subjected to this treatment [18].

Materials and methods

The pig trabecular bone tissue was used as a biomaterial. Sample preparation of the initial biomaterial was carried out, which included the removal of meat and fat residues using a scalpel, the production of sections using a band/saber saw, freeze drying and vacuuming.

The decellularization process using SC-CO_2 was carried out on an experimental semi-industrial supercritical installation. The installation diagram is shown in Figure 1.

Decellularization process in SC-CO_2 in dynamic mode with constant flow [19]. To carry out the decellularization process in SC-CO_2, bone sections were fixed in an extraction vessel so that the samples did not come into contact with the bottom of the vessel. The vessel was moved into the reactor, the reactor lid with a pressure gauge was tightly fixed and the outlet-underwater channels were closed. By turning on the medium-temperature refrigeration unit, the CO_2 in the condenser passes from the gaseous state to the liquid state and enters the expansion column with the help of a high-pressure pump, where the CO_2 passes into the supercritical fluid state and enters the reactor. The flow rate is 1500 g/min, the temperature is 37°C, the pressure is 190-200 atm. After the reactor, the CO_2 with extracted compounds passes into the cyclone separator, where its transition to gaseous state occurs again. Then the gas passes through the adsorber back into the condenser. Due to the cyclical nature of the installation, the CO_2 consumption is minimal. The conditions for decellularization in SC-CO_2 in a dynamic mode with a constant flow are given in Table 2.
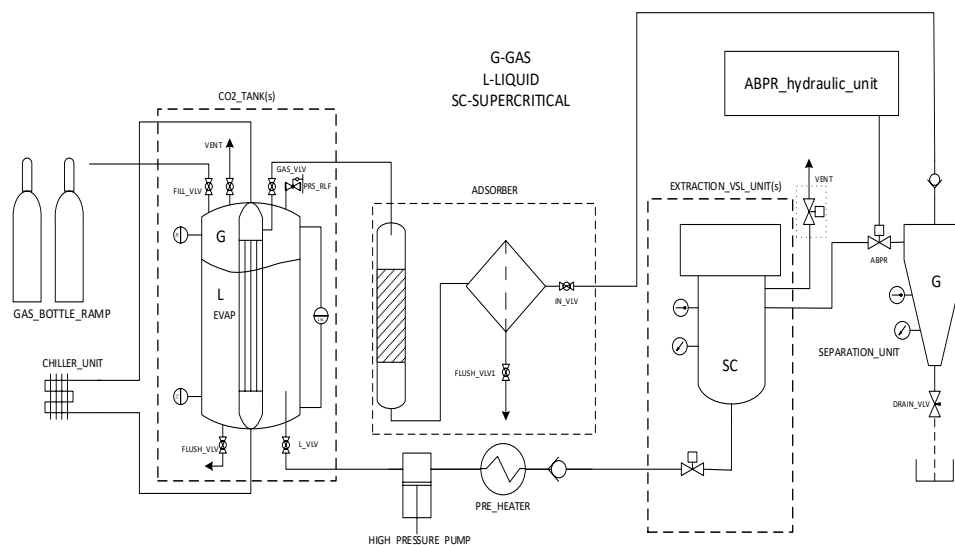
Figure 1 – Diagram of an experimental semi-industrial supercritical installation

Table 1 – Main components of an experimental semi-industrial supercritical installation

Name	On the diagram	Specifications
High pressure pump V4	HIGH_PRESSURE_PUMP	Inlet pressure: 10…80 bar, outlet pressure: 15...450 bar, CO_2 flow: 0,2…2 l/min
Condenser	CO2_TANK(s)	Working pressure: 70 bar, volume: 30 L
Medium-temperature refrigeration unit	CHILLER_UNIT	Refrigerant: R404a, cooling capacity: 10 kW at -15 °C
Cyclone separator	SEPARATION_UNIT	Working volume: 2 L, working pressure: 100 bar
Back pressure regulator	BPR	Working pressure: 30…500 bar, conditional pass: 6 mm
Hydraulic station	Not specified in the diagram	Hydraulic fluid flow: 1...10 l/min, working pressure: 160 bar
Heater block	Not specified in the diagram	Number of circuit: 2, working temperature: up to 100 °C, circuit power: 6 kW
Heat exchanger	PRE_HEATER	Shell and tube, working pressure: 450 bar

Table 2 – Conditions for decellularization in SC-CO_2 in dynamic mode with constant flow

Sample, #	Decellularization time, hours
1	0,5
2	1
3	2
4	4
5	6
6	8

Decellularization process in SC-CO_2 in static (with exposure in SC-CO_2) and dynamic (with constant flow) modes. To carry out the decellularization process under these conditions, the same preparatory operations are carried out that are given for the decellularization process in SC-CO_2 in dynamic mode, the difference is the alternation of static and dynamic modes. To carry out decellularization in static mode, SC-CO_2 is converted to a liquid state, using a high-pressure pump, the pressure in the reactor is pumped up to 200-230 atm and then the pump is turned off.

The process in dynamic mode proceeds according to the method described above. The flow rate is 1500 g/min, the temperature is 37°C, the pressure is 190-200 atm. The conditions for decellularization under supercritical conditions in static and dynamic modes are presented in Table 3.

Table 3 – Conditions for decellularization in SC-CO$_2$ in static and dynamic modes

Sample, #	Decellularization time in static mode, hours	Decellularization time in dynamic mode, hours
1	0,25	0,25
2	0,5	0,5
3	1	1
4	2	2
5	4	4
6	6	6
7	8	8

Decellularization process in SC-CO$_2$ in static (exposure in SC-CO$_2$) and in dynamic (at constant flow) modes with preliminary exposure in 96% ethyl alcohol. According to paper [20], the use of a co-solvent during decellularization in SC-CO$_2$ increases the percentage of ICC removal. 96% ethyl alcohol was used as a co-solvent. The samples were previously soaked in ethyl alcohol before the process and after the process was carried out for 6 hours in static mode and 6 hours in dynamic mode. The flow rate is 1500 g/min, the temperature is 37 °C, the pressure is 190-200 atm. The preliminary exposure time of samples in 96% ethyl alcohol is shown in Table 4.

Table 4 – Preliminary storage time of samples in 96% ethyl alcohol

Sample, #	Preliminary storage time of samples in ethyl alcohol, hours
1	0,5
2	1
3	2
4	4
5	8
6	12
7	24
8	48
9	72
10	96
11	120
12	144

Histological examination. Histological examination includes several stages: fixation, decalcification, dehydration, paraffin impregnation, paraffin filling, obtaining histological sections, deparaffinization, staining, microscopic analysis. Formalin was chosen as the fixing fluid, in which the bone tissue was kept for 24 hours. After fixation, to remove formalin residues, the samples are placed in ethyl alcohol with an increasing concentration (70, 80, 96%) for 12 hours for each solution. 5% nitric acid was used for decalcification. The samples were placed in the solution for 24 hours with constant stirring (175 rpm) using a universal orbital shaker (LOIP LS-110, РФ). The nitric acid solution must be replaced 3 times with a fresh one within 24 hours. After decalcification, the samples are crushed with a scalpel to a size of no more than 1 cm in length, 1 cm in width and 0.3 cm in thickness. After the obtained rectangular-shaped materials are subjected to dehydration in ethyl alcohol with increasing concentration (50, 80, 96, 100%). In each solution, they are kept for 24 hours. At the end of dehydration, the samples are placed in a mixture of chloroform:ethyl alcohol = 1:1 and kept for 3 hours, changing the solution to a fresh one every hour, then transferred to a pure chloroform solution for 3 hours. Then the samples are placed in a saturated solution of paraffin in chloroform for 12 hours and placed in an electric dry-air thermostat (ТС-1/80 СПУ, РФ) at 37 °C and constant stirring. After the time has elapsed, they are transferred to a pure paraffin solution for 3-4 hours and thermostated at 56-57 °C with constant stirring. Then the samples are placed in homemade paper boats and filled with paraffin and left until the

paraffin completely solidifies for 12-24 hours. After using a manual microtome (MS 2 TU 64-16, РФ), sections of bone tissue 5-7 microns thick are obtained from the obtained paraffin blocks and transferred to a slide. For further staining, it is necessary to remove the remnants of paraffin: for this, slides with samples are placed sequentially for 15 minutes in chloroform solutions (changing the solution 3 times), in solutions of ethyl alcohol with a descending concentration (100, 90, 80%) and in distilled water. After that, staining with eosin and Mayer's hematoxylin is carried out, placing samples for 10 minutes in each solution. After that, the dehydration process is carried out by placing the samples in solutions of ethyl alcohol with an ascending concentration and then in a solution of o-xylene. After that, the slices are enclosed in Canada balsam, dried in a thermostat for 12 hours at 37 °C and microscopic analysis of the obtained slices is performed [21].

Study of bone tissue surface morphology using optical microscopy. Optical microscopy was used to control changes in surface morphology during the decellularization process. The study of the morphology of the bone tissue surface was carried out on a trinocular microscope (MX-300, РФ) at a magnification of 40 times in the " Open Type National Nanotechnology Laboratory" at the al-Farabi Kazakh National University and on optical microscope (BRESSER ADVANCE ICD, China) with magnification of 20 times in the Center of Physics and-chemical methods of research and analysis (CFChMA) in the laboratory of sorption and catalytic processes.

Isolation of DNA from bone tissue followed by spectrophotometric detection. To isolate DNA from bone tissue, 400 mg of the sample is ground into powder using a mortar, 1 ml of Degestion buffer is added (4.7 ml EDTA +50 ml proteinase K +250 ml 10% N-Laurylsarcosyl) and incubated in a thermostat for 30 minutes at T = 50°C. After the sample is centrifuged at 10000 rpm for 15 minutes, the resulting supernatant is removed. Then another 1 ml of Degestion buffer is added to the precipitate, conduct incubation in thermostat at T = 50 °C for 24 hours and centrifugation at 13000 rpm for 15 minutes. The resulting supernatant is transferred to a test tube and 4 ml of Binding buffer is added (118.2 g of guanidinium thiocyanate, 10 ml of 1M tris (hydroxymethyl) is placed in a 200 ml volumetric flaskaminomethane, 8 ml 0.5 M EDTA, 1 g of N-Laurylsarcosyl and distilled water to the label), thoroughly mixed, 20 µl of silicon dioxide was added and incubated at T = 50 °C, for 3 hours.

At the end of the time, they are centrifuged for 15 minutes at 10000 rpm. The supernatant is removed, and 1 ml of cooled 80% ethyl alcohol is added to the resulting precipitate, centrifuged at 10000 rpm for 15 minutes and the supernatant is removed. 50 ml of TE buffer is added to the precipitate, incubated for 3 minutes at room temperature and centrifuged at 13000 rpm for 15 minutes. The resulting supernatant containing DNA is analyzed using a spectrophotometer (NanoDrop 2000/2000c, USA) at 260 nm wavelength [22].

Results and discussion

Histological examination is the most common method of determining the completeness of the decellularization process. Hematoxylin – stains the nuclei of cells, and eosin – stains the cytoplasm. The complete or partial absence of stained nuclei and cytoplasm characterizes the removal of ICC. At the end of the histological examination, the following microscopic images at x200 magnification were obtained for samples obtained by decellularization in SC-CO$_2$ in a dynamic mode with a constant flow (Figure 2). Based on the obtained results, it can be concluded that the time of decellularization directly affects the removal of ICC, which characterizes decrease in the number of brightly colored nuclei over time. However, according to the obtained images, it can be said that after 8 hours of the decellularization process, a small number of colored nuclei are observed in SC-CO$_2$, which characterizes the incomplete removal of ICC.

At the end of the histological examination, the following microscopic images at x200 magnification were obtained for samples obtained by decellularization in SC-CO$_2$ in static and dynamic modes (Figure 3).

Decellularization process time increase and addition of a static mode leads to a more complete removal of the ICC.

At the end of the histological examination, the following microscopic images at x200 magnification were obtained for samples obtained by decellularization in SC-CO$_2$ in static and dynamic modes with preliminary exposure in 96% ethyl alcohol (Figure 4).

Usage of 96% ethyl alcohol as a co-solvent significantly affects the decellularization process. ICC removal by this method proceeds more fully.

Results of microscopic analysis of samples obtained by decellularization in SC-CO$_2$ in dynamic mode with constant flow are shown in Figure 5.
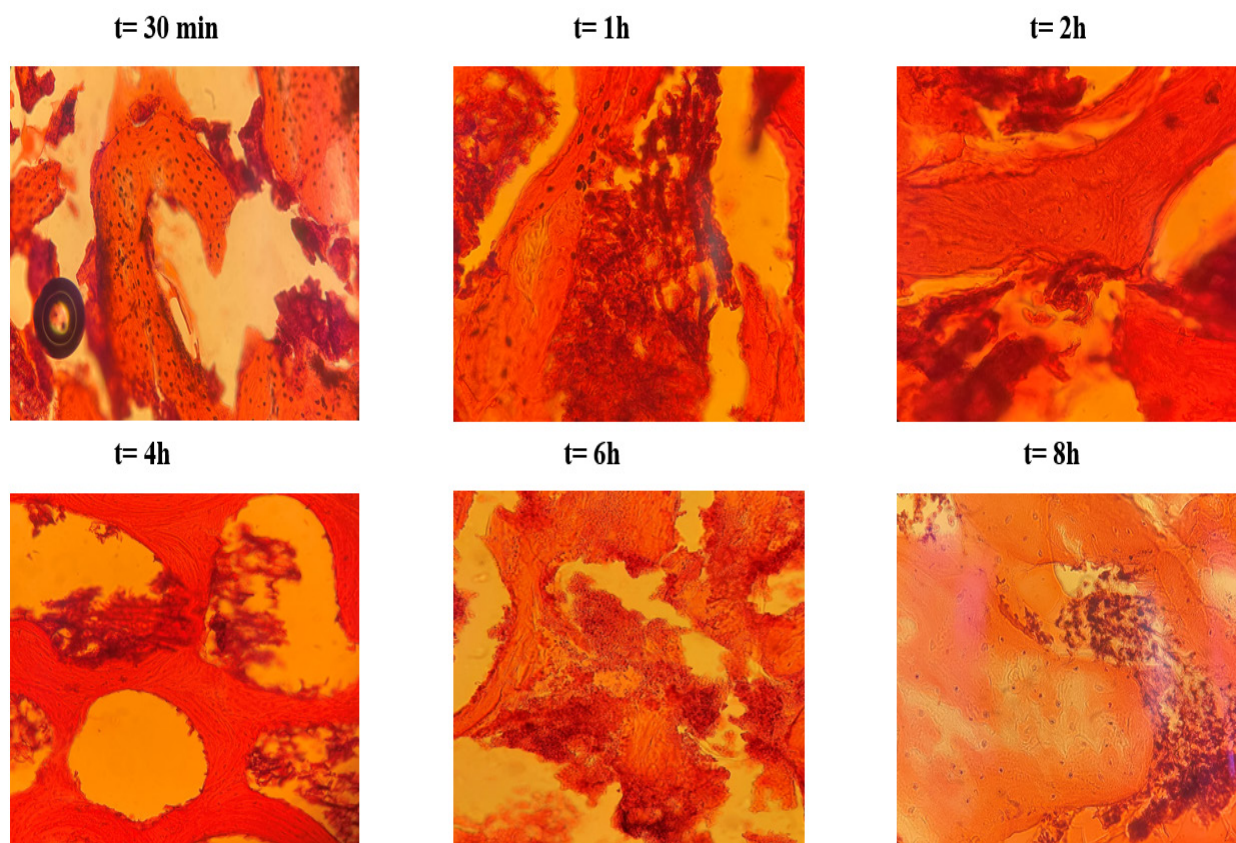
t= 30 min **t= 1h** **t= 2h**

t= 4h **t= 6h** **t= 8h**

Figure 2 – Changes in the histostructure of pig bone during decellularization

t_{st} = 15 min
t_{dyn} = 15 min

t_{st} = 30 min
t_{dyn} = 30 min

t_{st} = 1 h
t_{dyn} = 1 h

t_{st} = 2 h
t_{dyn} = 2 h

t_{st} = 4 h
t_{dyn} = 4 h

t_{st} = 6 h
t_{dyn} = 6 h

t_{st} = 8 h
t_{dyn} = 8 h
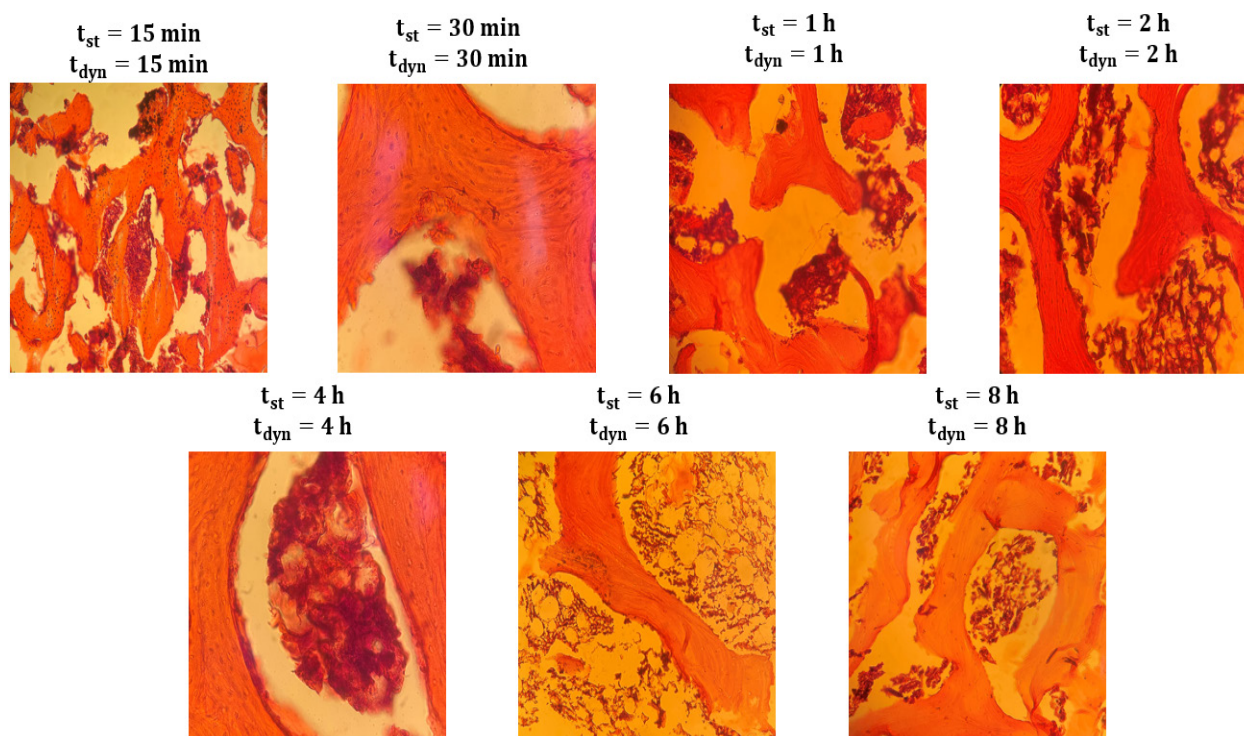
Figure 3 – Changes in the histostructure of pig bone during decellularization
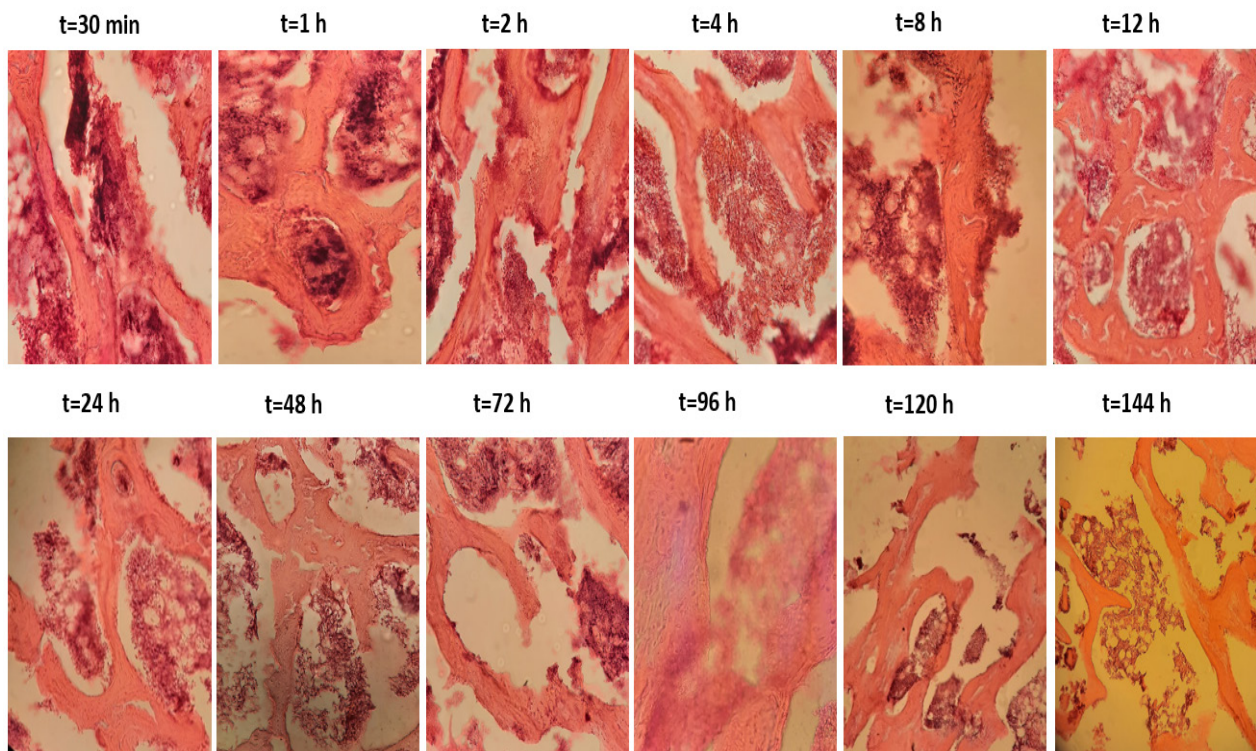
Figure 4 – Changes in the histostructure of pig bone during decellularization
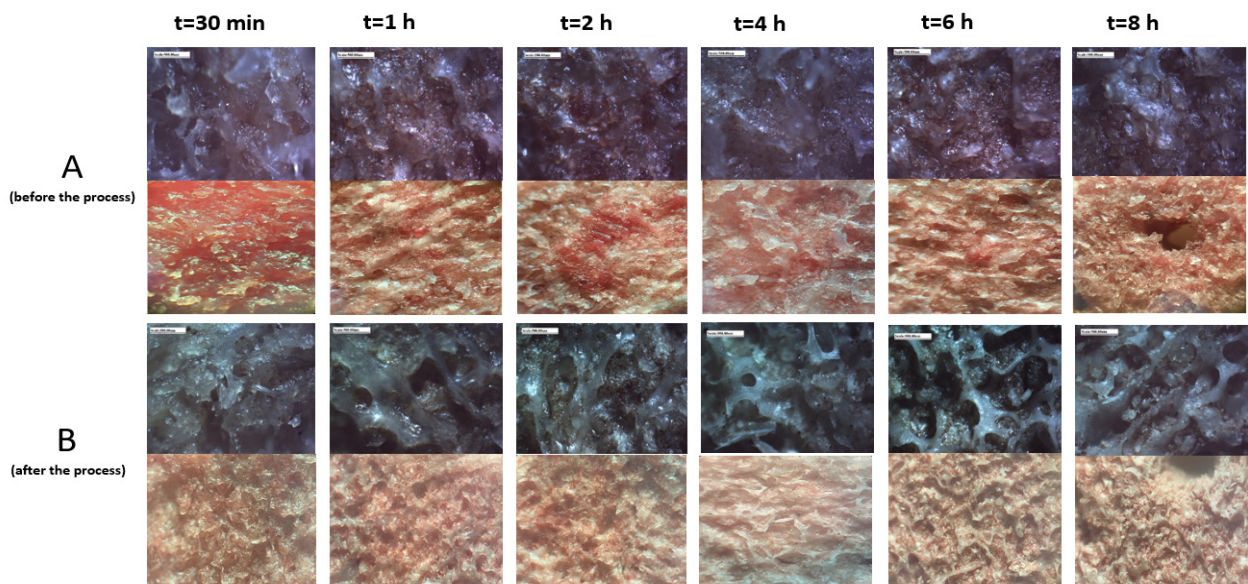
Figure 5 – Microscopic images of bone tissue surface morphology

Based on the obtained images of decellularization process, it can be concluded that the process directly depends on time. However, when decellularization of bone tissue in the SC-CO$_2$ medium with a constant flow after 8 hours, the presence of ICC is observed, which characterizes the incompleteness of decellularization and use of graft obtained by this method is doubtful.

The results of microscopic analysis of samples obtained by decellularization in SC-CO$_2$ in static and dynamic modes are shown in Figure 6.

When decellularization is carried out in SC-CO$_2$ medium in static and dynamic modes, a significant increase in the porosity of the ECM and the visual absence of ICC is observed, which characterizes the completeness of the decellularization process
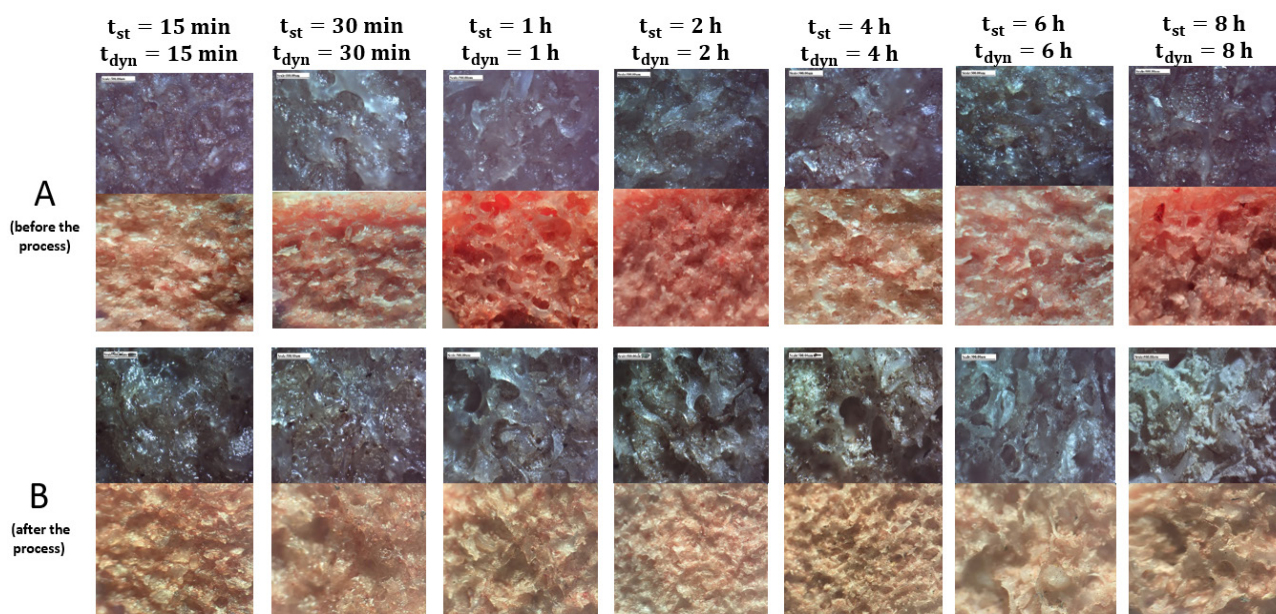
Figure 6 – Microscopic images of bone tissue surface morphology

The results of microscopic analysis of samples obtained by decellularization in SC-CO$_2$ in static and dynamic modes with preliminary exposure in 96% ethyl alcohol are shown in Figure 7.

Usage of 96% ethyl alcohol as a co-solvent and an increase in the time of the process has a positive effect on the morphology of bone tissue surface and the removal of ICC takes place most completely.

With the help of spectrophotometric analysis, the DNA concentration of the last samples was determined in each method (Figure 8).

The concentration of DNA in bone tissue after the decellularization process in SC-CO$_2$ in dynamic mode with constant flow is 69.4 ng/µl, after decellularization in SC-CO$_2$ in static and dynamic modes is 61.5 ng/µl, after decellularization in static and dynamic modes with preliminary exposure in 96% ethyl alcohol is 33.4 ng/µl.

The concentration of DNA extracted from bone tissue using the decellularization method in static and dynamic modes with preliminary exposure in ethyl alcohol is almost 2 times greater than in samples obtained by other methods.

Table 5 shows the optimal conditions for obtaining ECM using the decellularization method.
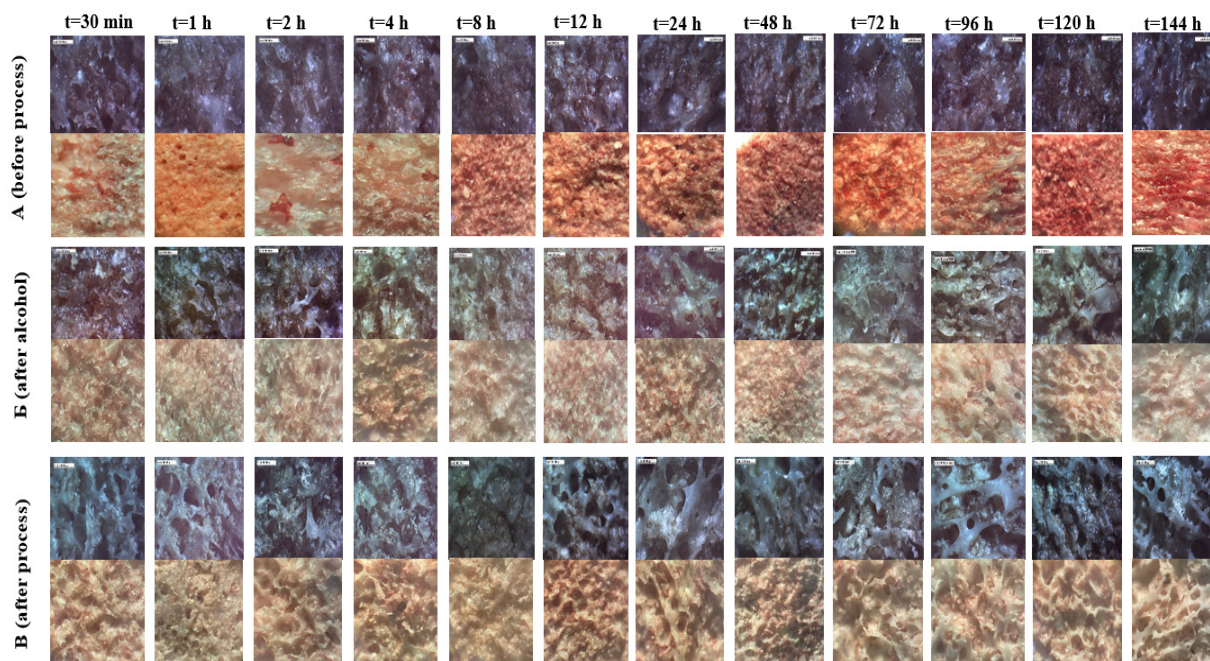
Figure 7 – Microscopic images of bone tissue surface morphology
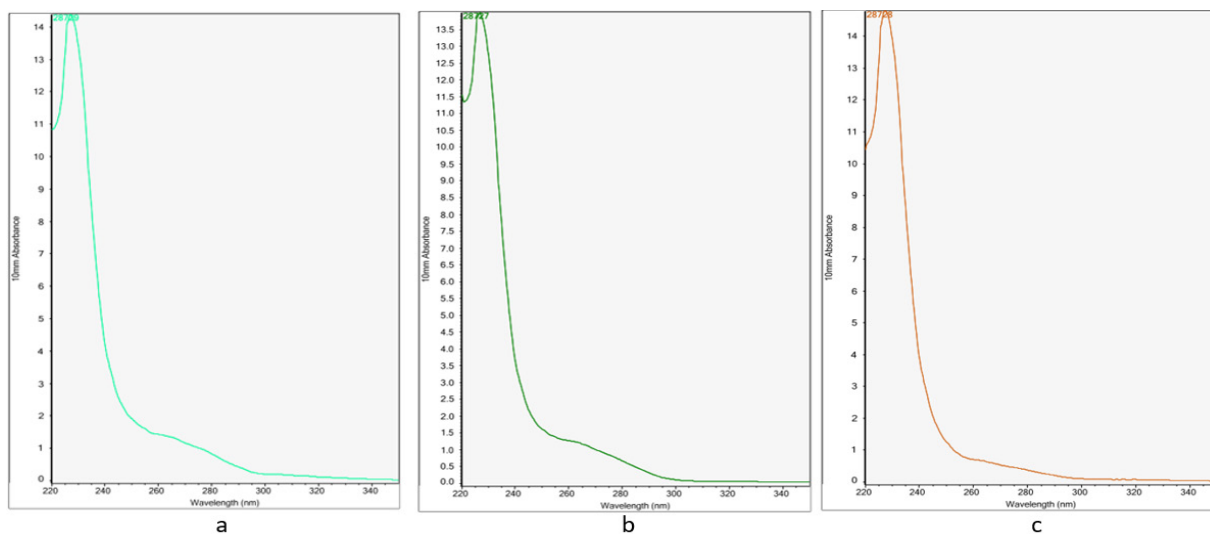
Figure 8 – Dependence of absorption coefficient on wavelength in the spectrophotometric determination
of DNA (a) the process of decellularization in dynamic mode; (b) the process of decellularization in static and dynamic modes;
(c) the process of decellularization in static and dynamic modes with preliminary exposure in 96% ethyl alcohol

Table 5 – Optimal conditions for obtaining ECM

#	Exposure time in ethyl alcohol, hours	Decellularization time in static mode, hours	Decellularization time in dynamic mode, hours
1	144	6	6

Also, according to [23], if the concentration of DNA in the decellularized material is less than 50 ng/µl, the use of this transplant is possible, since the appearance of the recipient's immune response is minimal.

Conclusion

According to the obtained microscopic images after histological examination, it can be concluded that the removal of ICC during the process of decellularization in SC-CO$_2$ in a dynamic mode with a constant flow occurs by only 70%, and the completeness of the decellularization process is 55% (visual calculation based on microscopic images of the bone surface morphology), whereas with decellularization in static and dynamic modes with preliminary exposure in ethyl alcohol, the removal of ICC is 98%, and the completeness of the decellularization process is 97%. In overall, use of the obtained ECM by decellularization in static and dynamic modes with preliminary exposure in ethyl alcohol is promising since its effect on the human body will be minimal. From an economic point of view, the use of this method is also promising, since the use of the static method leads to the possibility of increasing the process time, reducing energy consumption and wear of the pump.

References

1. Ma Z, Kotaki M, Inai R, Ramakrishna S., et al. (2005) Potential of nanofiber matrix as tissue-engineering scaffolds. *Tissue Eng.,* vol. 11, no. 1, pp. 101-109. https://doi.org/10.1089/ten.2005.11.101

2. Bigdeli A.K. et al. (2013) Nanotechnologies in tissue engineering *Nanotechnol* vol. 2, no. 4, pp. 411-425. https://doi.org/10.1515/ntrev-2013-0015

3. Matson J.B., Stupp S.I. (2012) Self-assembling peptide scaffolds for regenerative medicine *Chem. Commun.*, vol. 48, no. 1, pp. 26–33. https://doi.org/10.1039/c1cc15551b

4. Ng J. et al. (2017) Biomimetic Approaches for Bone Tissue Engineering. *Tissue Engineering – Part B: Reviews.,* vol. 23, no. 5, pp. 480-493. https://doi.org/10.1089/ten.TEB.2016.0289

5. Campana V. et al. (2014) Bone substitutes in orthopaedic surgery: from basic science to clinical practice**.** *J. Mater. Sci. Mater. Med.,* vol. 25, no. 10, pp. 2445-2461. https://doi.org/10.1007/s10856-014-5240-2

6. Elliot R.R., Richards R.H. (2011) Failed operative treatment in two cases of pseudarthrosis of the clavicle using internal fixation and bovine cancellous xenograft (Tutobone). *J. Pediatr. Orthop. Part B*. vol. 2**0**, no. **5**, pp. 349-353**.** https://doi.org/10.1097/BPB.0b013e328346c010

7. Ledford C.K. et al. (2013) Bovine xenograft failures in pediatric foot reconstructive surgery. *J. Pediatr. Orthop.,* vol. 33, no. 4, pp. 458-463**.** https://doi.org/10.1097/BPO.0b013e318287010d

8. Maffulli N. et al. (2013) Bovine xenograft locking Puddu plate versus tricalcium phosphate spacer non-locking Puddu plate in opening-wedge high tibial osteotomy: A prospective double-cohort study. *Int. Orthop.* vol. 37, no. 5, pp. 812-826. https://doi.org/ 10.1007/s00264-013-1817-5

9. Bracey D.N. et al. (2018) A decellularized porcine xenograft-derived bone scaffold for clinical use as a bone graft substitute: A critical evaluation of processing and structure. *J. Funct. Biomater*., vol. 37, no. 5, pp. 812-826. https://doi.org/ 10.1007/s00264-013-1817-5

10. Feng W. et al. (2012) The expression and distribution of xenogeneic targeted antigens on porcine bone tissue. *Transplant. Proc.,* vol.44, no. 5, pp. 1419-1422. https://doi.org/10.1016/j.transproceed.2011.11.070

11. Jian Y.K. et al. (2008) Properties of deproteinized bone for reparation of big segmental defect in long bone., *Chinese J. Traumatol. – English Ed.,* vol.11, no. 3, pp. 152-156. https://doi.org/10.1016/s1008-1275(08)60032-2

12. Hodde J., Hiles M. (2002) Virus safety of a porcine-derived medical device: Evaluation of a viral inactivation method. *Biotechnol. Bioeng*., vol. 79, no. 2. pp. 211–216. https://doi.org/10.1002/bit.10281

13. Hodde J. et al. (2007) Effects of sterilization on an extracellular matrix scaffold: Part I. Composition and matrix architecture. *J. Mater. Sci. Mater. Med.*, vol. 18, no. 4. pp. 537–543 https://doi.org/10.1007/s10856-007-2300-x

14. Gilbert T.W. et al. (2008) Collagen fiber alignment and biaxial mechanical behavior of porcine urinary bladder derived extracellular matrix. *Biomaterials. Elsevier Ltd*, vol. 29, no. 36. pp. 4775–4782. https://doi.org/10.1016/j.biomaterials.2008.08.022

15. Dmitriev R.I. et al. (2015) Imaging oxygen in neural cell and tissue models by means of anionic cell-permeable phosphorescent nanoparticles. *Cell. Mol. Life Sci.*, vol. 72, no. 2. pp. 367–381. https://doi.org/10.1007/s00018-014-1673-5

16. Sun Y. et al. (2020) Effects of SCCO2, gamma irradiation, and sodium dodecyl sulfate treatments on the initial properties of tendon allografts. *Int. J.*

Mol. Sci., vol. 21, no. 5. pp. 415-421. https://doi.org/10.3390/ijms21051565

17. Chung S., Kwon H., Kim N.P. (2019) Supercritical extraction of decellularized extracellular matrix from porcine adipose tissue as regeneration therapeutics. *J. Cosmet. Med.*, vol. 3, no. 2. pp. 86–93. https://doi.org/10.25056/JCM.2019.3.2.86

18. Fages J. et al. (1998) Bone allografts and supercritical processing: effects on osteointegration and viral safety. *J. Supercrit. Fluids.*, vol. 13, no. 1–3. pp. 351–356. https://doi.org/10.1016/S0896-8446(98)00071-0

19. Cho D. et al. (2018) Super-Critical-CO2 De-ECM Process. *MRS Adv.* vol. 3, no. 40. pp. 2391–2397. https://doi.org/10.1557/adv.2018.494

20. Duarte M.M. et al. (2021) Fast decellularization process using supercritical carbon dioxide for trabecular bone. *J. Supercrit. Fluid*s.

Elsevier, vol. 172, no. December 2020. pp. 105194. https://doi.org/10.1016/j.supflu.2021.105194

21. Rabea A.A. et al. (2020) Histological, Histochemical and Immunohistochemical Evaluation of the Role of Bone Marrow-Derived Mesenchymal Stem Cells on the Structure of Periodontal Tissues in Carbimazole-Treated Albino Rats. *Arch. Oral Biol. Elsevier Ltd,* vol. 119, no. September. pp. https://doi.org/104887 10.1016/j.archoralbio.2020.104887

22. Damgaard P.B. et al. (2015) Improving access to endogenous DNA in ancient bones and teeth. *Sci. Rep. Nature Publishing Group,*. Vol. 5. P. 1–12. https://doi.org/10.1038/srep11184

23. Crapo P.M., Gilbert T.W., Badylak S.F. (2011) An overview of tissue and whole organ decellularization processes. *Biomaterials. Elsevier Ltd*., vol. 32, no. 12. pp. 3233–3243. https://doi.org/10.1016/j.biomaterials.2011.01.057

D.I. Ismagulova [ID], A.M. Baimukhametova [ID], S.B. Baiseiit [ID], T.I. Glebova [ID],

N.G. Klivleyeva [ID], N.T. Saktaganov [ID],

N.S. Ongarbayeva [ID], G.V. Lukmanova [ID], M.G. Shamenova [ID]

Research and Production Center of Microbiology and Virology, Almaty, Kazakhstan
*e-mail: ismagulovadariya@gmail.com

Study of features of influenza virus circulation in the southern region of Kazakhstan during the 2021 epidemic season

Abstract. Influenza viruses are among the most prevalent infectious agents, leading to massive seasonal epidemics and pandemics with high mortality rates. The ability of influenza virus to antigenic variability determines the high population susceptibility, wide spread of infection, and short intervals between epidemics. In recent years, the co-circulation of influenza viruses that belong to A/H1N1pdm09 and A/H3N2 subtypes and influenza type B virus has been observed. Here we summarize the data we explored to establish the features of the influenza virus circulation in the southern region of the Republic of Kazakhstan. To conduct virological and serological studies, 590 biosamples were collected from sick patients (419 swabs and 171 blood serums). Influenza type A virus RNA was found in 39 (9.31%) samples including that of A/H1N1pdm09 virus in 15 (3.58%), A/H3N2 virus in 23 (5.49%). It has also been noted that isolates A/Almaty/10/21 and A/Almaty/15/21 were profiled by the antigenic formula A/H3N2. The results of virological, serological, and molecular genetic studies confirm the simultaneous circulation of influenza A viruses (H1N1pdm09 and H3N2), and influenza type B virus. Some thoughts on the current scenario as well as implications for the future are presented as well.

Key words: biosamples, circulation, influenza virological surveillance, serological studies.

Introduction

Being a highly contagious respiratory viral infection caused by various influenza viruses, with 290 to 650 thousand fatal cases recorded annually, seasonal influenza stays one of priority directions for the virological surveillance [1,2].

Amidst the influenza viruses that pose a grave potential threat to the national and global biological security, a special place is occupied by the genus *Alpha influenza virus* (influenza A virus) in the family Orthomyxoviridae, which includes 18 hemagglutinin subtypes (H1-H18) and 11 neuraminidase subtypes (N1-N11). Influenza A viruses containing three HA subtypes (H1, H2, and H3) and two NA subtypes (N1, N2) possess epidemic significance to humans. Type B influenza viruses also actively participate in the epidemic process [3].

As it is known, influenza A viruses periodically cause pandemics at intervals of 10-40 years. This takes place as a result of the emergence of a fundamentally novel influenza virus (subtype or variant), against which there is no immunity among the population. A unique triple-reassortant influenza A/H1N1pdm09 virus, which emerged in 2009, included a complex combination of swine, avian, and human influenza virus genes. The pandemic strain of influenza A/H1N1pdm09 virus has become the dominant agent in the etiology of subsequent epidemic seasons. It has displaced the seasonal influenza A/H1N1 virus from active circulation in the human population [4] and is currently continuing to circulate along with A/H3N2 viruses and two type B lines [5]. In this regard, one of the major tasks in solving biosecurity issues is to control the distribution of the pandemic influenza A/H1N1pdm09 virus, which has an enhanced virulence [6].

The Global Influenza Programme monitors influenza activity worldwide and publishes an update every two weeks, where information is categorized by influenza transmission zones, areas with similar influenza transmission patterns. The tireless goal of the influenza surveillance is to provide timely and high-quality epidemiological data and viral

isolates to check the duration of the influenza season as well as provide candidate viruses for vaccine production. The correct surveillance can help decision-makers prioritize resources and plan public health interventions [7-9]. The isolation of influenza virus strains from the clinical material is significant for diagnosing respiratory diseases in humans and assessing the correspondence between epidemic and vaccine strains within the limits of the surveillance over the spread of influenza infection and represents an essential component in the vaccine development and production [10-13].

Serological diagnosis is particularly important in the case of an atypical or asymptomatic course of influenza infection. The hemagglutinins inhibition assay (HAI) and enzyme-linked immunosorbent assay (ELISA) are still widely used in the diagnosis of influenza infection to determine specific antibodies in blood serums [14-17].

Materials and methods

Kazakhstan is a major transit corridor for the passage of epidemic variants of the influenza virus, which reinforces its geopolitical importance in global influenza surveillance [15, 18, 19].

In the 2021 epidemic season, 590 biosamples (419 swabs and 171 blood serums) were obtained together with medical personnel from healthcare facilities located in the southern region of Kazakhstan, of which – 248 nasopharyngeal swabs and 171 blood serums from the Almaty region, and 171 swabs from the Kyzylorda region. Primary screening of nasopharyngeal swabs for the presence of the genetic material of influenza viruses was performed in RT-PCR. The characteristics of collected material and the results of molecular analysis in RT-PCR are presented in Table 1.

Table 1 – Characterization of biosamples and RT-PCR-based primary screening of human nasopharyngeal swabs collected from the Almaty and Kyzylorda regions in 2021

Sampling point	Number of biosamples		Number of PCR-positive samples to					
	nasopharyngeal swab	blood serum	influenza virus	influenza type A virus	Subtype		influenza A virus with unidentifi-ed subtype	influenza type B virus
					A/H1N1 pdm	A/H3N2		
Almaty region	248	171	15	14	5	9	0	1
Kyzylorda region	171	-	27	25	10	14	1	2
Total	419	171	42	39	15	23	1	3
Percentage:	100%	100%	10.02%	9.31%	3.58%	5.49%	0.24%	0.72%

Results and discussion

According to our data, the genetic material of influenza virus was detected in 42 swabs (10.02% of the total number of examined samples): influenza A virus in 39 samples (9.31%), influenza virus type B in 3 swabs (0.72%). While subtyping samples positive for influenza type A virus, it was found that the A/H1N1pdm09 virus RNA was detected in 3.58% of cases, that of A/H3N2 in 5.49%. In one sample (0.24%) positive for influenza type A virus, the subtype could not be identified. The results of RT-PCR-based primary screening of clinical samples showed that influenza type A and B viruses are circulating among the population in the southern region of Kazakhstan with a predominance of influenza type A viruses.

Three hemagglutinating agents were isolated in CE during virological examination of biological samples. As a result of cloning by the method of limiting dilutions in CE and MDCK cell culture, the hemagglutination titers of isolates on CE were in the range of 1:64 – 1:1024 while those in the MDCK cell culture varied within 1:8-1:32. Negative results were obtained with serums against the influenza B virus [15]. The results obtained in the HAI and NAI assays indicate that the Kazakhstan isolate A/Kyzylorda/1/21 belongs to influenza virus with the antigenic formula A/H1N1pdm09, whereas the isolates A/Almaty/10/21 and A/Almaty/15/21 to influenza A/H3N2 virus. The antigenic formulae of the isolates was confirmed by RT-PCR [20].

In order to detect specific antibodies against influenza viruses, we used 171 blood serums collected

from the Almaty region in the spring 2021. The HAI assay results are shown in Figure 1.

As shown on Figure 1, antihemagglutinins were detected against the A/H1N1 serosubtype virus in 2.92% of cases (five samples) of the total number of examined serums, against A/H1N1pdm in 12.28% (21 samples), against A/H3N2 in 4.68% (eight samples), against type influenza B virus in 15.20% (26 samples), and antibodies against simultaneously two influenza (A+B) viruses were found in 10.53% (18 serums). The antibody titers ranged in 1:80 – 1:320.

Results obtained from a study of 171 blood serums in ELISA are shown in Figure 2.
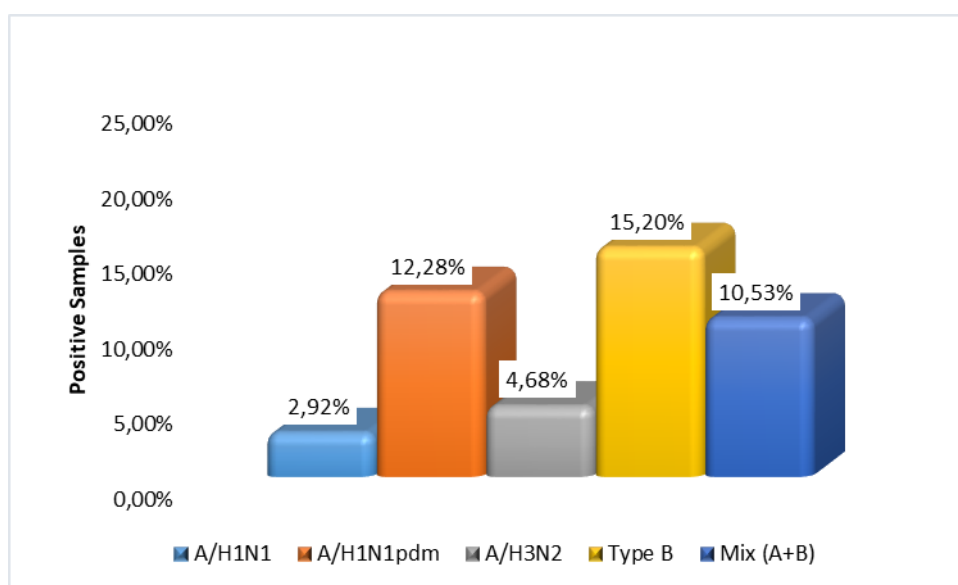
Figure 1 – Results of HAI assay on antibodies against influenza viruses in human blood serum
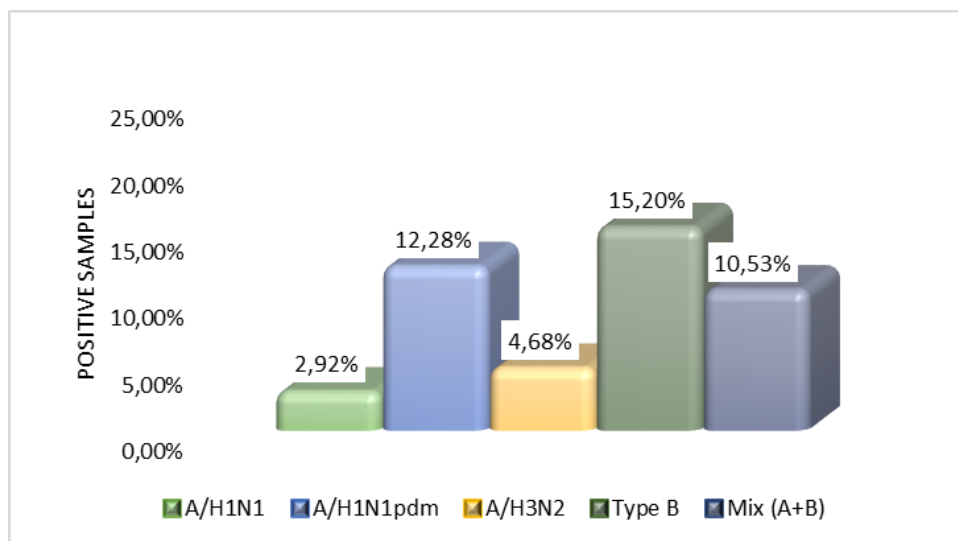
Figure 2 – Results of ELISA on antibodies against influenza viruses in human blood serum

Isolates prepared from nasopharyngeal swabs and identified in the RT-PCR, HAI and NAI assays as influenza viruses of the A/H1N1pdm09 and A/H3N2 subtypes were characterized by high hemagglutination titers both in CE and MDCK cell culture [15, 20].

Antibodies simultaneously against two subtypes of influenza A virus were identified in 46(5.9%) of blood serums, and against influenza A and B viruses in 60(7.7%) [15].

Additional considerations

Another important parameter is coinfections as was shown by us for COVID-19 [22]. The timing and severity of the 2021-2022 influenza (flu) season was different than most seasons before the COVID-19 pandemic. In 702 samples (9.85%) pathogens of respiratory infections of non-influenza etiology were detected, including adenovirus, bocavirus, coronavirus, metapneumovirus, paramyxovirus types I-IV, respiratory syncytial virus, and rhinovirus. At the same time, both before and during the COVID-19 pandemic, different influenza virus variants co-circulation (A/H1N1, A/H3N2, and type B) were discovered, with a predominance of viruses with the antigenic formula A/H1N1 (Figure 3).

The results of the study indicate the need for continuous monitoring of the viral pathogens spread, which will expand the existing knowledge of the viral etiology of respiratory diseases and highlight the importance of viruses in the respiratory infections occurrence [22]. Similar results were noted for other countries [23-29]. Though relatively mild, there was more activity during the 2021-2022 flu season than during the 2020-2021 flu season, and activity remained elevated later in the spring than any flu season on record [30]. In addition to the use of everyday preventive actions, fall influenza vaccination campaigns were thought as an important component of prevention [31].
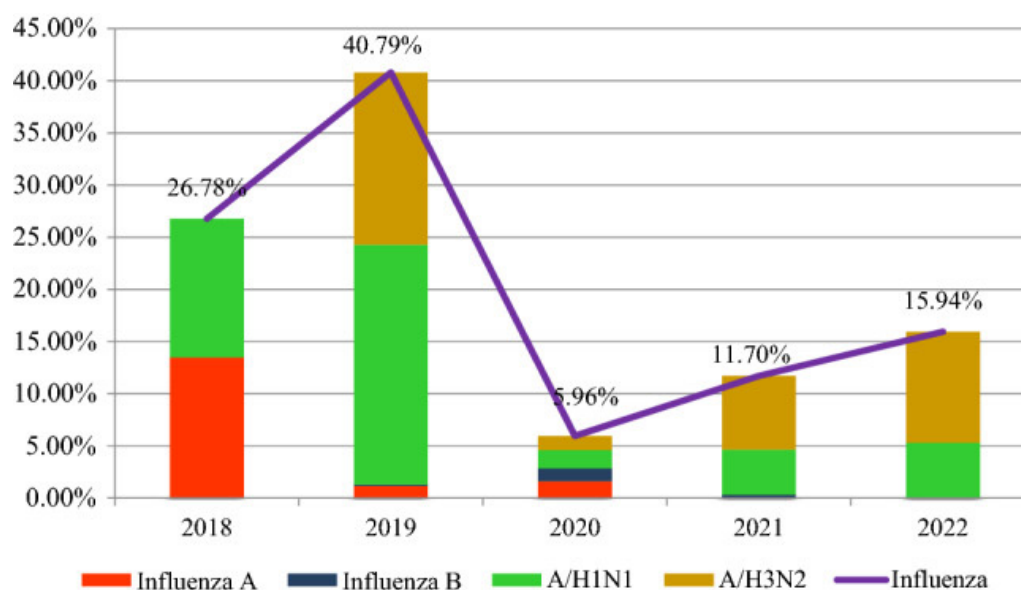

Figure 3 – Dynamics of prevalence of different influenza types

Conclusion

In recent years, a rapid spread of influenza viruses of subtypes A/H1N1, A/H3N2, and type B is being observed in Kazakhstan as well as throughout the world [18, 21]. In addition, the extraordinary complexity of the epidemic situation is associated with the emergence of reassortant viruses. The epidemiology of influenza substantially depends on the antigenic variability of influenza viruses, which are able to spread throughout the world and evolve rapidly. Gradual and relatively continuous alterations in the surface glycoproteins HA and NA promotes the emergence of new antigenic variants of the influenza virus that are resistant to immunity resulting from the previous infections or vaccination. It is for this reason that seasonal epidemics reoccur every year with varying intensity and trends.

References

1. Krasnova E. I., Karpovich G. S., Provorova V. V., Shestakov A. E., Kazakova Yu. (2021) Influenza in COVID-19 pandemic, epidemiological characteristics, approaches to vaccination. Lechaschi Vrach., vol. 4, no 24, pp 50-56. https://doi.org/10.51793/OS.2021.98.48.009.

2. Lvov D.K., Burtseva E.I., Mukasheva E.A., Kolobukhina L.V., Bogdanova V.S., Bovin, et al. (2019) Peculiarities of the influenza viruses circulation and their properties during 2018–2019 epidemic season in Russia and countries of the Northern Hemisphere. Problems of Particularly Dangerous Infections., vol. 3, pp. 66–74. (rus.). https://doi.org/10.21055/0370-1069-2019-3-66-74.

3. Dawood F.S., Jain S., Finelli L., Shaw M.W., Lindstrom S., Garten R.J., et al. (2009) Emergence of a novel swine-origin influenza A(H1N1) virus in humans. N. Engl. J. Med., vol. 360, no 25, pp. 2605–2615. https://doi.org/10.1056/nejmoa0903810.

4. Kurskaja O. G., Susloparov I.M., Durymanov A.G., et al (2011) Izuchenie pandemicheskogo grippa A/H1N1 v Sibirskom i Dal'nevostochnom regionah (sezon 2009–2010). Vestnik NGU. (Serija: Biologija, klinicheskaja medicina)., vol 9, no 2, pp 156-161.

5. Klivleyeva N.G., Ongarbayeva N.S., Baimukhametova A.M., Saktaganov N.T., et al. (2021) Detection of influenza virus and pathogens of acute respiratory viral infections in population of Kazakhstan during 2018–2019 epidemic season. Infection and Immunity, vol. 11, no. 1, pp. 137–147. https://doi.org/10.15789/2220-7619-DOI-1348.

6. Lvov D.K., Bogdanova V.S., Kirillov I.M., Shchelkanov M.Yu., Burtseva E.I., et al. (2019) Evolution of pandemic influenza virus A(H1N1)pdm09 in 2009-2016: dynamics of receptor specificity of the first hemagglutinin subunit (HA1). Problems of Virology., vol. 64, no 2, pp. 63-72. https://doi.org/10.36233/0507-4088-2020-65-6-4.

7. World Health Organization. (2014) WHO global epidemiological surveillance standards for influenza. Geneva: World Health Organization. 84 p.

8. Global influenza strategy 2019-2030. (2019). Geneva: World Health Organization, Licence: CC BY-NC-SA 3.0 IGO. Cataloguing-in-Publication (CIP) data. CIP data available at http://apps.who.int/iris.

9. Lakdawala S.S., Jayaraman A., Halpin R.A., Lamirande E.W., Shih A.R., Stockwell T.B., et al. (2015) The soft palate is an important site of adaptation for transmissible influenza viruses. Nature., vol 526, no 7571, pp: 122–1255. https://doi.org/10.1038/nature15379.

10. Krauss S., Walker D., Webster R. G. (2012). Influenza Virus Isolation. Switzerland: Springer Nature. pp 11–24. ISSN: 1064-3745.

11. Surveillance standards for vaccine-preventable diseases, second edition. (2018) Geneva: WHO. Licence: CCBY-NC-SA3.0IGO.

12. Glebova T.I., Klivleyeva N.G., Baimukhametova A.M., Saktaganov N.T., et al. (2021) Circulation of influenza viruses in the epidemic season of 2018–2019 among people residing in Northern and Western Kazakhstan. Infectious diseases., vol 19, no 2, pp. 70–75. doi: 10.20953/1729-9225-2021-2-70-75.

13. Hoffmann E, Stech J, Guan Y.A. (2001) Universal primer set for the full-length amplification of all influenza A viruses. Arch Virol., vol 146, no 12. pp. 2275-89. https://doi.org/10.1007/s007050170002.

14. Douwdal W.A., Kendal A., Noble G.R. Influenza virus (1979) Diagnostic Procedures for Viral. Washington: Rickettsial and Chlamydial Infection, pp. 585-609.

15. Shamenova MG, Glebova TI, Klivleyeva NG, Baiseiit SB, Baimukhametova AM, Saktaganov NT, Ongarbayeva NS, Ismagulova DA. Serological studies of influenza infection among population in southern region of Kazakhstan during the 2018-2021 epidemic season. J Pak Med Assoc. 2023;73(4):804-807. doi: 10.47391/JPMA.6348.

16. Mukasheva EA, Nikolaeva LI, Makhnovsky PI, Kirillova ES, Kolobukhina LV, Merkulova LN, et al. [Diagnostic capacity of detection of specific antibodies to pandemic influenza A(H1N1)pdm09 virus]. Vopr Virusol 2017; 62: 109-14.

17. Rowe T, Abernathy RA, Hu-Primmer J, Thompson WW, Lu X, Lim W, et al. Detection of antibody to avian influenza A (H5N1) virus in human serum by using a combination of serologic assays. J Clin Microbiol 1999; 37: 937-43.

18. Klivleyeva NG, Ongarbayeva NS, Baimukhametova AM, Saktaganov NT, Lukmanova GV, Glebova TI, et al. Detection of influenza virus

and pathogens of acute respiratory viral infections in population of Kazakhstan during 2018-2019 epidemic season. Russian Journal of Infection and Immunity 2021; 11: p. 137-47. 10.15789/2220-7619-DOI-1348.

19. Glebova TI, Klivleyeva NG, Baimukhametova AM, Saktaganov NT, Lukmanova GV, Ongarbayeva NS, et al. Circulation of influenza viruses in the epidemic season of 2018–2019 among people residing in Northern and Western Kazakhstan. Infekc Bolezni 2021; 19: p. 70-75.

20. Glebova T.I., Klivleeva N.G., Ongarbaeva N.S., Bayseim S.B., et al. New strain of influenza virus H1N1A/Pig/Kostanay/06/12 used for preparation of diagnostic drugs. News of Kazakhstan Science / Novosti nauki Kazahstana . 2019, 2, p. 90-98.

21. Klivleyeva NG, Lukmanova GV, Saktaganov NT et al. (2020) Acute respiratory viral infections in Kazakhstan in 2017–2019. Bull Natl Acad Sci Republic of Kazakhstan.; 3:29–35. 10.32014/2020.2518-1467.66 (ISSN 1991–3494.

22. Klivleyeva N, Lukmanova G, Glebova T, Shamenova M, Ongarbayeva N, Saktaganov N, Baimukhametova A, Baiseiit S, Ismagulova D, Kassymova G, Rachimbayeva A, Murzagaliyeva A, Xetayeva G, Isabayeva R, Sagatova M. Spread of Pathogens Causing Respiratory Viral Diseases Before and During CoVID-19 Pandemic in Kazakhstan. Indian J Microbiol. 2023;63(1):129-138. doi: 10.1007/s12088-023-01064-x.

23. Oh DY, Buda S, Biere B, et al. (2021) Trends in respiratory virus circulation following COVID-19-targeted nonpharmaceutical interventions in Germany, January–September 2020: Analysis of national surveillance data. The Lancet Regional Health – Europe.;6:100112. 10.1016/j.lanepe.2021.100112.

24. Brestovac B, Lawrence C, Speers DJ, et al.

Respiratory viral infections in Western Australians with cystic fibrosis. Respir Med. 2020;161:105854. doi: 10.1016/j.rmed.2019.105854.

25. Yum S, Hong K, Sohn S, et al. Trends in viral respiratory infections during COVID-19 Pandemic South Korea. Emerging Infectious Dis. 2021;27:1685–1688. doi: 10.3201/eid2706.210135.

26. Lagacé-Wiens P, Bullard J, Cole R, et al. (2021) Seasonality of coronaviruses and other respiratory viruses in Canada: implications for COVID-19. Canada Commun Dis Rep.;47:132–138. 10.14745/ccdr.v47i03a02

27. Biere B, Oh DY, Wolff T, et al. (2021) Surveillance of endemic human Coronaviruses in Germany, 2019/2020. The Lancet Regional Health – Europe.;11:100262. 10.1016/j.lanepe.2021.100262

28. Masse S, Capai L, Villechenaud N, et al. Epidemiology and clinical symptoms related to seasonal coronavirus identified in patients with acute respiratory infections consulting in primary care over six influenza seasons (2014–2020) in France. Viruses. 2020;12:630. doi: 10.3390/v12060630.

29. Park S, Lee Y, Michelow IC, et al. Global seasonality of human coronaviruses: a systematic review. Open Forum Infect Dis. 2020;7:ofaa44343. doi: 10.1093/ofid/ofaa443.

30. Bellizzi S, Panu Napodano CM, Pinto S, Pichierri G. COVID-19 and seasonal influenza: The potential 2021-22 "Twindemic". Vaccine. 2022;40(24):3286-3287. doi: 10.1016/j.vaccine.2022.

31. Olsen SJ, Winn AK, Budd AP, Prill MM, Steel J, Midgley CM, et al. Changes in Influenza and Other Respiratory Virus Activity During the COVID-19 Pandemic – United States, 2020-2021. MMWR Morb Mortal Wkly Rep. 2021;70(29):1013-1019. doi: 10.15585/mmwr.mm7029a1.

H.M.U. Shaheen[1] , N.A. Rajput[1*] , M. Atiq[1] ,
L. Amrao[1] , W.R. Arshad[2] ,
G.A. Kachelo[1,3] , M. Usman[1] , M.F. Tahir[1]

[1]Department of Plant Pathology, University of Agriculture, Faisalabad, Pakistan
[2]Sugarcane Research and Development Board, Faisalabad, Pakistan
[3]Crop Disease Research Institute, PARC, Karachi, Pakistan
*e-mail: nasirrajput81@gmail.com, nasir.ahmed@uaf.edu.pk

Synthetic fungicides for controlling brown leaf spot of rice caused by *Bipolaris oryzae*

Abstract. Rice (*Oryzae sativa* L) is suffering from several biotic and abiotic factors. Among biotic factors, brown leaf spot of rice (BLS) is potentially devastating disease of rice causing the severe yield losses up to 100%. The current study was designed to evaluate most effective synthetic fungicides management strategy towards BLS disease. For this purpose, 12 fungicides were screened out under *in vitro* conditions and four most effective fungicides were further demonstrated against the targeted pathogen with three different concentrations (100, 150 and 150 ppm) by using poisoned food technique. The results revealed that propiconazole and thiophanate methyl showed the strong inhibitory effect against *B. oryzae* followed by contaf plus and bavistin respectively. The promising fungicides (propiconazole and thiophanate methyl) under lab conditions were further evaluated *in vivo* against BLS disease by using 3 types of applications i.e. Pre-inoculation, Post-inoculation and after symptoms appearance. Findings showed that, Post-inoculation was found most effective as compared to other applications, furthermore combination of propiconazole and thiophanate methyl showed significant reduction in disease incidence percent as compared to solo applications. The reduction in disease incidence percent in all application methods suggested that these synthetic fungicides could be used against BLS of rice.
Key words: Propiconazole, Thiophanate methyl, Pre-inoculation, Contaf Plus, Bavistin.

Introduction

Rice (*Oryzae sativa* L) is a major cereal crop that is consumed as a staple diet by more than half of the world's population. Asia produces and consumes about 90% of the world's rice, which is a symbol of a culture's ability for survival [1,2]. Rice is also considered as the "Queen of cereals" [3]. Currently, rice is growing worldwide except Antarctica [4]. It is an important crop for containing a high amount of carbohydrates, protein, and fats. More than 1/5 of the global calorie intake for humans is provided by it [5]. It contains vitamins and minerals, and it is particularly rich in potassium, vitamin E and vitamin B (thiamin, niacin) [6]. Worldwide, its production leads 500 million tones over an area of 167.24 million hectares, while in Pakistan, it is grown on 3.3 million hectares with production of 8.4 million tonnes [7]. Punjab and Sindh are the major rice-growing provinces of Pakistan and these are accounted for the majority of the country's production [8]. There is a potential demand for rice production to be increased as continuously rising in world's population. Rice crop production is estimated to be increased up to 852million tons by the year 2035, as compared to its current production [9]. Therefore, it is necessary to boost production technology to meet the demand. However, with the development of more advanced techniques and high-yielding varieties, the crop is more vulnerable to biotic and abiotic factors.

Pakistani basmati rice varieties are famous throughout the world for their unique aroma but unfortunately, these varieties are tragically also susceptible to several diseases, including paddy blast, bacterial leaf blight, and brown leaf spot of rice [6]. Among a number of rice-related diseases, the brown spot of rice, which is brought on by the plant-pathogenic fungi *Bipolaris oryzae*, *Helminthosporium*

oryzae, and *Drechslera oryzae,* is one of the most devastating disease causing both qualitatively and quantitatively losses [10]. It is named as "chronic and orphan disease" because it affects millions of hectares of rice annually [11]. The pathogen of brown leaf spot disease of rice *(Bipolaris oryzae)* was responsible for the great "Bengal Famine 1942-43" causing the starvation death of 2 million people as a result of destruction of 50-90% of rice crops [12]. The pathogen attacks both at seedling and maturity stage [10]. As the pathogen is seed-borne [13], it causes blight on seedlings and can cause 10–58% seedling mortality because it spreads through heavily infected seeds [12]. The characteristic symptoms appear as small, circular, dark brown to purple-brown spots on leaves, panicles, glumes, and grain. Fully developed lesions are circular to oval with a light brown to grey center, surrounded by a reddish-brown margin, and ultimately kill the leaf [10]. When the infection is severe, grey mycelial growth can be seen between the sheaths and stalks and the neck turns into black color [14], and when the conditions are favorable, inadequate grain filling takes place [15].

Primarily, the weeds and the contaminated soil are the major sources for the pathogens survival. The pathogen enters the host plant by direct penetration or through the stomata [16]. It requires a temperature of 20°C and >80% relative humidity for the development of infection [17]. The disease becomes more severe when there is an excessive usage of nitrogen fertilizer. Under unfavorable environmental conditions, the rate of disease incidence become very high leading to seed discoloration, poor grain quality and yield losses [18]. Several management strategies for controlling the disease are in practices such as the use of resistant varieties, synthetic fungicides, biological and cultural control practices [19]. No doubt, use of biocontrol agents are environment friendly disease management approach [20], but the use of bio-agents in foliar spraying cannot completely manage the disease. The best strategy to manage the disease is the use of resistant varieties. The use of resistant varieties is safe, efficient, and cost-effective for controlling the rice diseases but due the lack of resistant varieties farmers mostly prefers the use of synthetic chemicals as this is the most effective management strategy for preventing brown spot disease, highly recommended method and widely used throughout the world [19].

Several studies on the use of synthetic chemicals to control the brown leaf spot disease have been reported. [21] examined four different fungicides including Carbendazim 50WP, Carboxin 50 WP,

Propiconazole 25 EC and Hexaconazole 25 EC @500ppm concentration. Among all, propiconazole was found to be effective fungicide that prevented 96.58% of fungus growth under lab conditions. [22], also evaluated different fungicides against the brown leaf spot of rice. All tested fungicides showed the best result against the *Bipolaris oryzae* under *invitro* conditions. But Bavistin performed excellent result at a concentration of 1500ppm as compared to other fungicides. Another experiment was performed in which [23] used six fungicides against brown leaf spot of rice. Among different fungicides, two (Propiconazole (1 ml per l) and Hexaconazole (2 ml per l) were found to be effective in reducing severity from 22.34% to 5.19 and 7.98% respectively, and significantly increased grain yield. [24] reported in their study about the antifungal response of different synthetic fungicides under *invitro* conditions. The most effective among chemicals was Propiconazole, while tebuconazole+trifloxystrobin and pyraclostrobin+ epoxyconazole also showed significant results at 0.75 ppm concentration.

The present study aims at determining the effectiveness of different latest fungicides for management of brown leaf spot of rice caused by *B. oryzae* and to suggest the farmers to use recommended synthetic chemicals to prevent the disease. Moreover, this research may contribute to an improved knowledge of the best times to apply fungicides at various stages of crop growth.

Materials and methods

Isolation, purification and identification of pathogen. Sample collection on the basis of visual symptoms was done from different rice growing zones of District Faisalabad, Pakistan. Leaf samples were cut into small pieces about 3-5 mm size and surface sterilized with 1% sodium hypochlorite (NaOCl) solution, then thoroughly washed with distilled water and placed on blotter paper for drying purpose. After that sterilized petri plates were poured with autoclaved potato dextrose agar (PDA) medium and samples were positioned on the center of that plates with the help of sterilized forceps. All the plates were wrapped and incubated at 28°C temperature in an incubator. Mycelial growth was regularly observed.

By using single hyphal tip method, a minute portion of fungal colony was transferred to fresh PDA plates for purification of the pathogen. On synthetic media, *B. oryzae* has been observed to grow as a cottony mycelial growth that was seen as dark grey, black, or greenish in color. Microscopically,

the spores were fucoid to cylindrical, light to dark brown, and curved with septate conidia [25].

In vitro evaluation of fungicides against Bipolaris oryzae. For management of *Bipolaris oryzae,* 12 fungicides i.e. Propiconazole, Thiophanate Methyl, Contaf Plus, Bavistin, Cabrio Top, Fossil, Amistar Top SC, Curzate M, Aliette, Polyram DF, Vidal and Score were evaluated to check their efficacy against the targeted pathogen. For this purpose, stock solutions for these fungicides were prepared separately to make different concentrations.

Preparation of stock solution. Stock solution was prepared by checking the active ingredients of concerned fungicide and dissolving the adequate amount of active ingredients in 100ml of sterilized distilled water (SDW) in glass bottles [26], stock solution was prepared [27].

Required amount of each fungicide was dissolved in SDW to make stock solution. Three different concentrations such as 50, 100 and 150ppm for each fungicide treatment were prepared by using 0.5, 1 and 1.5 ml of stock solution respectively.

Screening of fungicides under in vitro conditions against B. oryzae. 12 different fungicides were examined against *B. oryzae* by using poisoned food technique, all the fungicides were brought from local pesticide market of Faisalabad. 100 ppm concentration for each fungicide were used. Autoclaved fresh PDA media was amended with fungicide before pouring in petri plates. A 5 mm fungal plug from a pure culture of *B. oryzae* was placed in the center of each plate and incubated at 28 °C temperature. The un-amended plates were treated as control. All the treatments were replicated thrice under completely randomized design (CRD). Mycelial growth was calculated using digital Vernier caliper.

In vitro assessment of most effective fungicides against *B. oryzae*. Separate conical flasks were used for each fungicide. 100 ml PDA media was placed in each conical flask and autoclaved at 121℃ temperature and 15psi pressure for 15-20mins. Three concentrations i.e. 50, 100 and 150 ppm were prepared for each fungicide and mixed with PDA media. Certain amount of amended PDA media was poured in sterilized petri plates and inoculated with 5mm disc of pure culture of *B. oryzae*. Three replications of each treatment were used to minimize error. Control treatment were remained un-amended. After that, all plates were wrapped with parafilm and labeled with date, name of fungicide and concentration with the help of permanent marker. All plates were incubated carefully at 25°C± 2°C temperature. Data of mycelial growth was recorded for 3 days with 24 hours of

interval by measuring diameter of colony growth with the help of digital Vernier caliper.

Exploitation of most effective synthetic fungicide and their combination against brown leaf spot of rice under greenhouse conditions

The moderately susceptible variety of rice (Shaheen basmati) was sown on raised seedbeds and these were irrigated twice-daily with tap water. Rice seedlings of 45 days age were transplanted into earthen pots containing 4 kg of sterilized soil. All recommended agronomical practices were followed to ensure a healthy crop. The plants were artificially inoculated with spore suspension previously prepared by using pure mycelial culture [28]. The pots were categorized in three different groups, the first group was treated with fungicide after ensuring that the crop was well-established, and two days later it was artificially inoculated with spore suspension using a hand sprayer. The spore suspension was applied to the second group two days just before the application of synthetic fungicides. The third group of plants was given a fungicide treatment after the confirmation of disease development. The control treatment also received the similar inoculation with spore suspension, but instead of being sprayed with fungicides, they were just given the sterile distilled water. All the treatments were replicated with three replications under completely randomized design (CRD). Weekly observation of disease incidence was ensured upto three week of intervals. The percentage of disease incidence data was calculated as given below

$$\text{Disease Incidence} = \frac{\text{Number of infected Plant}}{\text{Total number of plants}} \times 100$$

Results and discussion

Screening of twelve fungicides against B. oryzae under in vitro conditions. In first experiment, 12 chemicals including Thiophanate Methyl, Propiconazole, Contaf Plus, Bavistin, Cabrio Top, Fossil, Amistar Top SC, Curzate M, Aliette, Polyram DF, Vidal, and Score were screened out at 100 ppm concentration against *B. oryzae* under lab conditions. Among all investigated chemicals, Propiconazole, Thiophanate methyl, Contaf plus, and Bavistin were the only chemicals that showed significantly inhibitory response with least mycelial growth of 7.51, 9.41, 11.44, and 12.53 mm, respectively as compared to control plate (56.35 mm). Whereas, others showed minimum effectivity against pathogen such as Cabrio top

(14.55 mm), Fossil (15.52 mm), Amistar Top SC (14.83 mm), Curzate M (16.11 mm), Aliette (19.57 mm), Polyram DF (18.88 mm), Vidal (13.66 mm), Score (15.31 mm) (Figure 1). Therefore, based on above results, these four most effective chemicals were further assessed under *in vitro* conditions by applying different concentrations i.e. 50, 100 and 150ppm for further investigation.
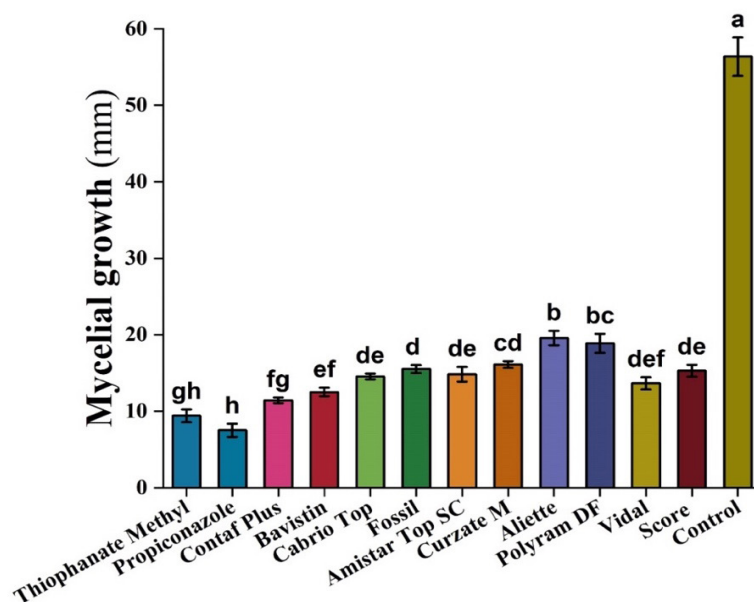

Figure 1 – Screening of different synthetic fungicides against
B. oryzae under laboratory conditions

In vitro assessment of four most effective fungicides against B. oryzae. Four fungicides were evaluated against the *Bipolaris oryzae* under *in vitro* conditions. The mycelial growth was sufficiently inhibited by all treatments. Among all fungicides, Propiconazole expressed highly effective result in reducing the mycelial growth (5.32 mm) followed by Thiophanate Methyl, Contaf Plus and Bavistin, showed the mycelial growth 5.94, 6.31, and 9.25mm, respectively as compared to control (30.13 mm) (Figure 2). Relation between treatment and concentration exhibited that Propiconazole was the most effective fungicide tested against *B. oryzae,* with mycelial growth of 6.57, 5.19, and 4.20mm at 50, 100, and 150 ppm concentrations, respectively, while Bavistin, with concentrations of 50, 100, and 150 ppm, showed the least growth inhibition (10.77, 9.38, and 7.67 mm), respectively (Figure 3). Interaction between treatment and days showed that Propiconazole exhibited excellent result against *B. oryzae* under laboratory conditions after 24, 48, and 72 hours with the lowest mycelial growth of 3.52, 5.21 and 7.23 mm, followed by Thiophanate methyl (4.40, 5.75 and 7.67 mm), Contaf plus (4.01, 6.03, and 8.87 mm) and Bavistin (6.66, 9.16, and 11.93 mm) mm as compared to control (10.63, 29.77, and 50 mm) (Figure 4).

Assessment of fungicides against brown leaf spot of rice under greenhouse conditions using pre-inoculation treatment

Two most effective synthetic fungicides Propiconazole and Thiophanate Methyl were evaluated under greenhouse conditions. The combination of Propiconazole+ Thiophanate Methyl applied before inoculation of pathogen showed the highest efficacy against brown leaf spot of rice, with disease incidence of 17.43% followed by the solo application of Propiconazole and Thiophanate Methyl with 24.96% and 28.46% disease incidence as compared to control (55.48%) (Figure 5a). Interaction between treatment and days also revealed that, at 7, 14, and 21 days, the combination of Propiconazole+Thiophanate Methyl expressed lowest disease incidence (22.00, 17.33 and 12.95%), followed by single application of Propiconazole (28.19, 25.08, and 21.62%) and Thiophanate Methyl (31.18, 28.15 and 26.04%) (Figure 5b).
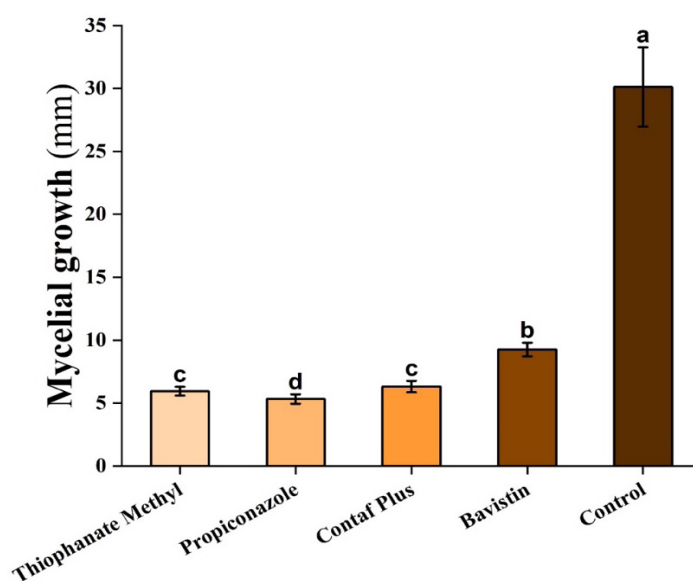
Figure 2 – Impact of treatments on mycelial growth of *B. oryzae* under *in vitro* conditions
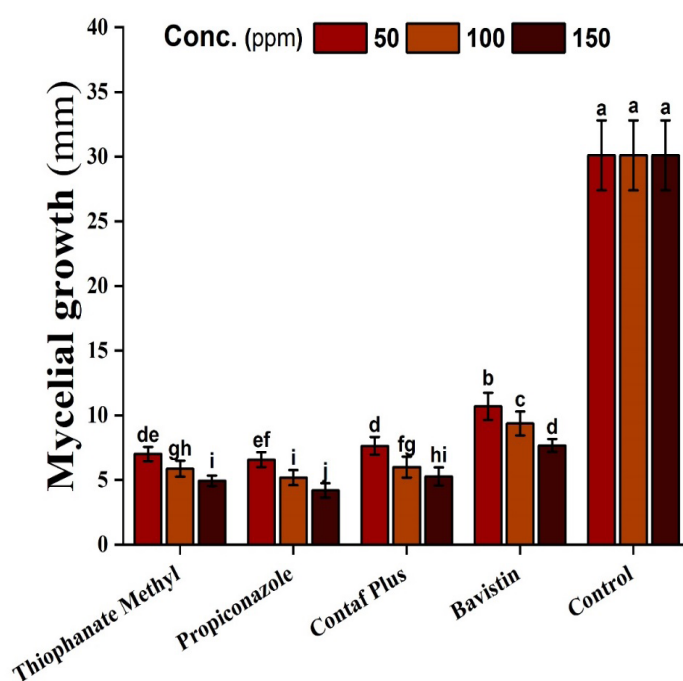

Figure 3 – Impact of an interaction between treatment and concentration on mycelial growth of *B. oryzae* under *in vitro* conditions
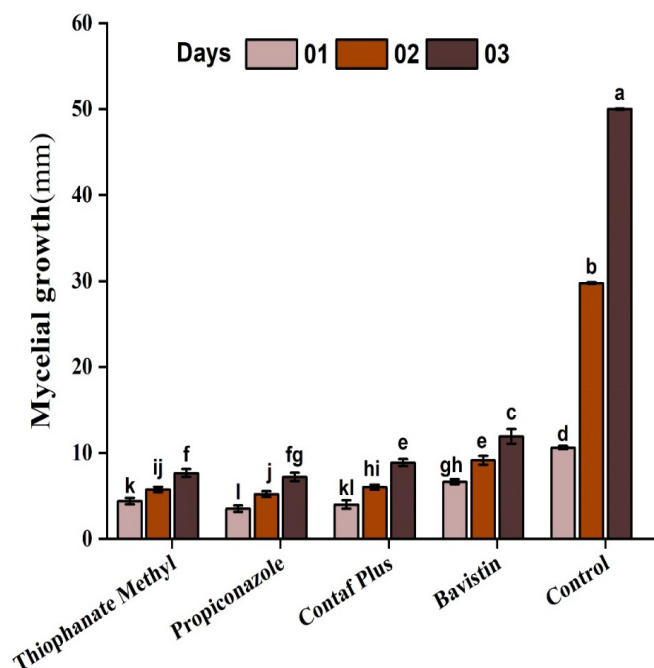
Figure 4 – Impact of interaction between treatment and days on growth
of *B. oryzae* under *in vitro* conditions

Assessment of fungicides against brown leaf spot of rice under greenhouse conditions using post-inoculation treatment

According to the findings, least disease incidence (11.04%) was expressed by the application of Propiconazole+Thiophanate Methyl in post inoculation treatment, followed by the single application of Propiconazole (17.06%) and Thiophanate Methyl (20.82%) as compared to the untreated control (55.48%) (Figure 5c). Fungicides were applied 2 days after spore inoculation under greenhouse conditions. All treated plants exhibited less disease incidence before or after inoculation as compared to the untreated control. At two days after inoculation, rice plants treated with the combination of propiconazole and thiophanate methyl showed significantly excellent result with disease incidence of 14.27, 11.52, and 7.33%. The solo application of propiconazole and thiophanate methyl showed disease incidence of (20.00, 17.01, and 14.16%) and (23.28, 21.72, and 17.46%) respectively (Figure 5d).

Assessment of fungicides against brown leaf spot of rice under greenhouse conditions using after symptom appearance treatment

In third experiment, fungicidal treatment was applied after appearance of visible symptoms. Where,

combination of Propiconazole and Thiophanate methyl expressed the lowest disease incidence percentage (15.40%) as compared solo application of propiconazole and thiophanate methyl (20.19 and 23.79%) respectively as compared to control treatment (55.48%) (Figure 5e). The application of combination of propiconazole+ thiophanate methyl was found highly effective up to three weeks with disease incidence of (19.41, 15.68 and 11.17%) followed by propiconazole (23.21, 20.20 and 17.16%) and thiophanate methyl (26.07, 23.95 and 21.36%) in comparison to untreated control (38.18, 56.50 and 71.77 %) (Figure 5f).

Brown leaf spot of rice, caused by the fungus *B. oryzae* is a potential threat to farmers causing significantly yield losses [10]. The use of resistant varieties, cultural practices, biological control and the application of synthetic fungicides are being adopted to manage this disease. Due to changes in climatic conditions, instability of pathogen is a major threat to rice crop. Cultural practices alone cannot effectively control disease. Biological control is inaccessible for larger fields. Therefore, farmers are interested towards the use of synthetic chemicals due to their quicker and effective response against disease by contributing higher yields and better quality.
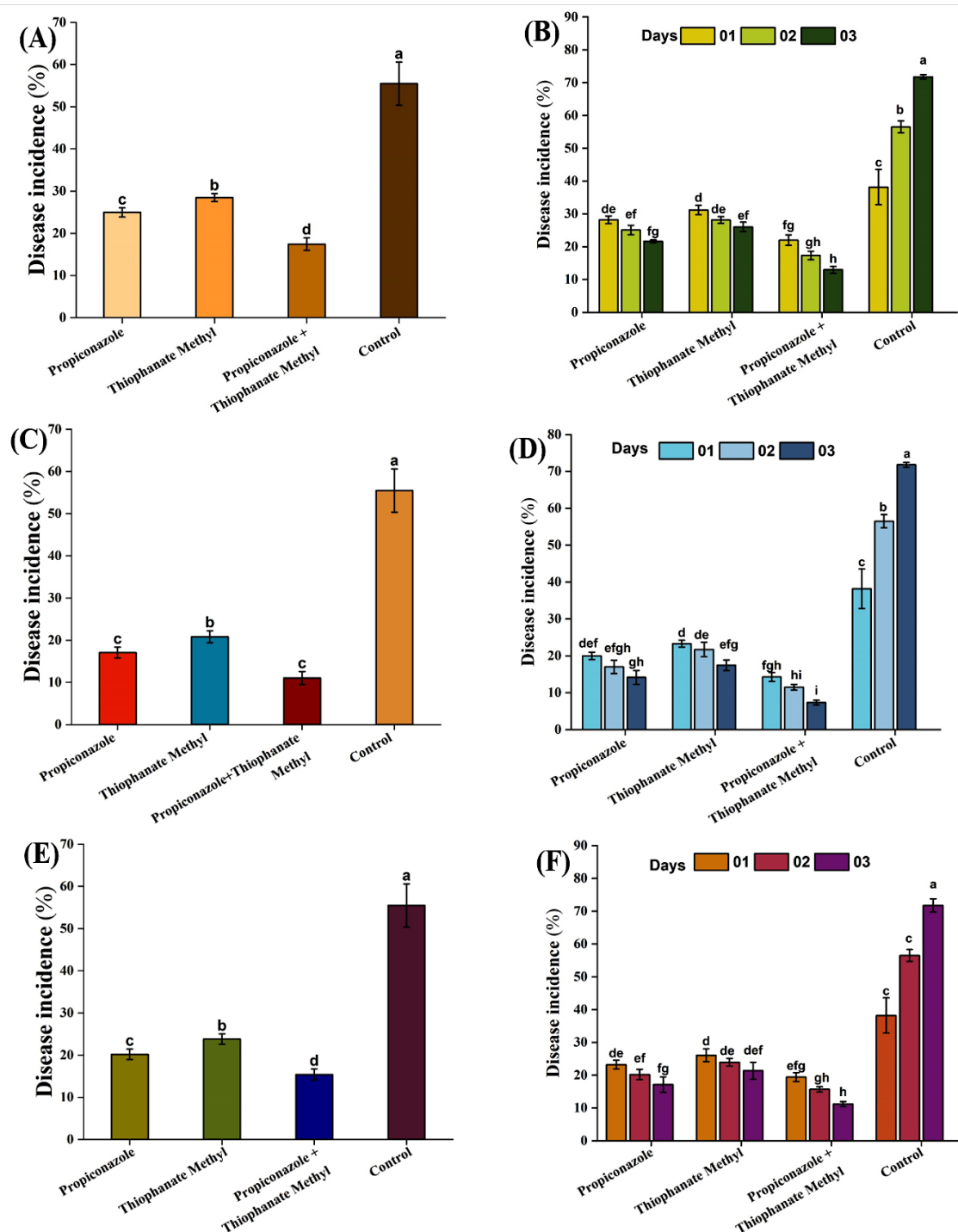
Figure 5 – Assessment of fungicides. a: Assessment of fungicides against brown leaf spot of rice
under greenhouse conditions using pre-inoculation treatment, b: Interaction of treatment and days
on disease incidence in pre-inoculation treatment, c: Assessment of fungicides against brown leaf spot
of rice under greenhouse conditions using post-inoculation treatment, d: Interaction of treatment and days
on disease incidence in post-inoculation treatment, e: Assessment of fungicides against brown leaf spot
of rice under greenhouse conditions using after symptom appearance treatment, f: Interaction of treatment
and days on disease incidence after symptom appearance

In our current study, we evaluated 12 different commercial fungicides against *Bipolaris oryzae*. All of them demonstrated an inhibitory response in reducing mycelial growth, but, surprisingly, propiconazole demonstrated the excellent response under laboratory conditions. The best performing fungicides propiconazole and thiophanate methyl were examined under greenhouse conditions. A highly significant response was seen when (propiconazole+ thiophanate methyl) were used in combination against brown leaf spot of rice. [24] studied the efficacy of 8 fungicides under *in-vitro* conditions in which three fungicides propiconazole, pyraclostrobin + epoxyconazole andtebuconazole + trifloxystrobin inhibited the mycelial growth up to 100% at 0.75ppm concentration. However, propiconazole was found to be effective at 0.1% concentration under field conditios. Our findings are also supported by the research of [29], in which they used the Khumal 9, a long-lasting rice variety in the Baglung district and applied seven fungicides. Among seven fungicides, Propiconazole, provides strongly inhibitory response in reducing disease severity and boosting economic yield. [21] evaluated four various fungicides, including Carbendazim 50WP, Carboxin 50 WP, Propiconazole 25 EC, and Hexaconazole 25EC against *B. oryzae.* At 500 ppm concentration, propiconazole was reported to be an effective fungicide that showed maximum inhibition of 96.58% of the fungal growth under lab conditions. According to [30], Azoxystrobin and propiconazole, at a concentration of 0.1%, decreased the severity of the brown spot disease in rice and increased yield. In addition, [31] reported that propiconazole 25 EC @ 0.1% was highly effective against diseases such as sheath blight, sheath rot, brown spot, and glume discoloration. The same results have been studied by [32], they evaluated several fungicides to check their efficacy against the brown leaf spot of rice. Among all tested fungicides, propiconazole was found to be highly effective against the *B. oyzae* with maximum inhibition of 97% at 250ppm concentration. They also observed that propiconazole @0.1% significantly reduces the disease incidence respectively. Four fungicides Mencozeb, Thiophanate Methyl, Iprovalicarb +Propineb and Propineb were evaluated against the *Helminthosporium oryzae* [33]. They reported that Mancozeb and Thiophanate methyl were found to be the most showing no linear colony growth (0.0 mm) at 150 and 200 ppm concentrations, respectively.

The result showed that 3rd experiment (after symptom appearance) provides satisfactory inhibitory response as compared to pre-inoculation treatment but less than that of post-inoculation treatment. Our study concluded that all three experiment either preventive (pre-inoculation treatment), curative (post-inoculation treatment) and after symptoms appearance significantly reduce the disease incidence but interestingly, post-inoculation treatment provides excellent result against brown leaf spot of rice as compared to other two experiment under greenhouse conditions.

Conclusion

We eventually came to the conclusion that propiconazole was excellent under lab conditions. However, the combination of propiconazole+thiophanate methyl were effective when applied under greenhouse conditions in all three experiment pre-inoculation, post-inoculation and after symptoms appearance respectively as compared to control. These fungicides have been proved to be effective for long-lasting control of brown leaf spot of rice, so farmers are strongly encouraged to apply and use these fungicides in large field conditions.

References

1. Chauhan B.S., Mahajan G., Sardana V., Timsina J., Jat M.L. (2012) Productivity and sustainability of the rice–wheat cropping system in the Indo-Gangetic Plains of the Indian subcontinent: problems, opportunities, and strategies. *Adv. Agron.* Vol. 117, pp. 315-369. https://doi.org/10.1016/B978-0-12-394278-4.00006-4

2. Shankar T., Malik G.C., Banerjee M., Dutta S., Maitra S., Praharaj S., Sairam M., Kumar D.S., Dessoky E.S., Hassan M.M. (2021) Productivity and nutrient balance of an intensive rice–rice cropping system are influenced by different nutrient management in the red and lateritic belt of West Bengal, India. *Plants*, Vol. 10, no. 8, pp. 1622. https://doi.org/10.3390/plants10081622

3. Abbas A., Murtaza S., Aslam F., Khawar A., Rafique S., Naheed S. (2011) Effect of processing on nutritional value of rice (*Oryza sativa*). *World J. Med. Sci.* Vol. 6, pp. 68-73.

4. Muthayya S., Sugimoto J.D., Montgomery S., Maberly G.F. (2014) An overview of global rice production, supply, trade, and consumption. *Annal. New York Acad. Sci.* Vol. 1324, pp. 7-14.

5. Fukagawa, N.K., Ziska, L.H., 2019. Rice: Importance for global nutrition. *J. Nutrit. Sci. Vitaminol.* pp. 65. https://doi.org/10.3177/jnsv.65.S2

6. Qudsia H., Akhter M., Riaz A., Haider Z., Mahmood A. (2017) Comparative efficacy of different chemical treatments for paddy blast, brown leaf spot and bacterial leaf blight diseases in rice (*Oryza sativa* L.). *Appl. Microbiol. Open Access.* Vol. 3, no. 3. https://doi.org/10.4172/2471-9315.1000138

7. FAOSTAT Statistical Database (2020) Food and Agriculture Organization of the United Nations.

8. Saqib S.E., Kuwornu J.K., Panezia S., Ali U. (2018) Factors determining subsistence farmers' access to agricultural credit in flood-prone areas of Pakistan. *Kasetsart J. Social Sci. Vol.* 39, pp. 262-268. https://doi.org/10.1016/j.kjss.2017.06.001

9. Gadal N., Shrestha J., Poudel M.N., Pokharel B. (2019) A review on production status and growing environments of rice in Nepal and in the world. *Arch. Agric. Environ. Sci.* Vol. 4, no. 1, pp. 83-87. https://doi.org/10.26832/24566632.2019.0401013

10. Manandhar H.K., Timila R.D., Sharma S., Joshi S., Manandhar S., Gurung S.B., Sthapit S., Palikhey E., Pandey A., Joshi B., Manandhar G., Gauchan D., Jarvis D.I., Sthapit B.R. (2016) A field guide for identification and scoring methods of diseases in the mountain crops of Nepal. In Biover. Int.

11. Zanao J.L.A., Rodrigues F.A., Fontes R.L.F., Korndo G.H., Neves J.C.L. (2009) Rice resistance to brown spot mediated by silicon and its interaction with manganese. *Phytopathol.* Vol. 157, pp. 73-78. https://doi.org/10.1111/j.1439-0434.2008.01447.x

12. Bowbrick P. (2020) Toxic Famine research – And how it suppresses its critics. SSRN *Elect. J.* pp. 101970. https://dx.doi.org/10.2139/ssrn.3657078

13. Sato H., Ando I., Hirabayashi H., Takeuchi Y., Arase S., Kihara J. (2008) QTL analysis of brown spot resistance in rice (*Oryzae sativa L.*). *Breeding Sci.* Vol. 58, pp. 93-96. https://doi.org/10.1270/jsbbs.58.93

14. Sunder S., Singh R., Dodan D., Mehla, D. (2005) Effect of different nitrogen levels on brown spot (*Drechslera oryzae*) of rice and its management through host resistance and fungicides. *Plant Dis. Res.* Vol. 20, pp. 111-114.

15. Huynh V.N., Gaur A. (2004) Role of *Bipolaris oryzae* in producing abnormal seedling of rice (*Oryzae sativa*). *Omonrice,* Vol. 12, pp. 102-108.

16. Carvalho M.P., Rodrigues F.A., Silveira P.R., Andrade C.C.L., Baroni J.C.P., Paye H.S., Loureiro J.E., (2010) Rice resistance to brown spot mediated by nitrogen and potassium. J *Phytopathol.* Vol. 158, pp. 160-166. https://doi.org/10.1111/j.1439-0434.2009.01593.x

17. Kaiser W.J. (1973) Factors affecting growth, sporulation, pathogenicity, and survival of Ascochyta rabiei. *Mycol.* Vol. 65, no. 2, pp. 444-457. https://doi.org/10.1080/00275514.1973.12019452

18. Goel R., Lore J., Thind, T. (2007) Performance of different fungicides against multiple diseases of rice. *Ind. Pytopathol.* Vo. 60, no. 3, pp. 296-301.

19. Nancy D.J.H.B. (2019) Brown patch & large patch diseases of lawns. Home & Garden Information Center. https://hgic.clemson.edu/factsheet/ brown-patch-large-patch-diseases-of-lawns.

20. Schantz S.L., Gasior D.M., Polverejan E., McCaffrey R.J., Sweeney A.M., Humphrey H., Gardiner J.C. (2001) Impairments of memory and learning in older adults exposed to polychlorinated biphenyls via consumption of Great Lakes fish. *Environ. Health Perspec.* Vol. 109, no. 6, pp. 605-611. https://doi.org/10.1289/ehp.01109605

21. Kumar V., Chaudhary V.P., Kumar D., Kumar A., Sagar S., Chaudhary S. (2017) Efficacy of botanicals and fungicides against *Rhizoctonia solani* inciting sheath blight disease on Rice (*Oryza sativa L.*). *J. Appl. Nat. Sci.* Vol. 9, no. 4, pp. 1916-1920. https://doi.org/10.31018/jans.v9i4.1463

22. Sandeep P. (2015) *In vitro* study of Fungicides in controlling *Helminthosporium oryzae* causal organism of leaf brown spot of Rice. *Int. Res. J. Biol. Sci.* Vol. 4, no. 10, pp. 48-51.

23. Sunder S., Singh R., Dodan D.S. (2010) Evaluation of fungicides, botanicals and non-conventional chemicals against brown spot of rice. *Ind. Phytopathol.* Vol. 63, no. 2, pp. 192-194.

24. Chouhan V., Kumar, A. (2022). Evaluation of fungicides for management of brown leaf spot disease of rice. SSRN 4005520. https://dx.doi.org/10.2139/ssrn.4005520

25. Marwein R., Singh S., Maharana J., Kumar S., Arunkumar K.P., Velmurugan N., Chikkaputtaiah C. (2022) Transcriptome-wide analysis of north-east indian rice cultivars in response to *Bipolaris oryzae* infection revealed the importance of early response to the pathogen in suppressing the disease progression. *Gene*, Vol. 809, pp. 146049. https://doi.org/10.1016/j.gene.2021.146049

26. Borum D.F., Sinclair J.B. (1968) Evidence for systemic protection against *Rhizoctonia solani* with vitavax in cotton seedlings. *Phytopathol,* Vol. 58, no. 7, pp. 976-980.

27. Gul A., Nissa T., Ahmed E., Parveen S., Khoso H.A., Naseem M. (2015) In vitro screening of different fungicides against fruit rots of chilli. *Life Sci. Int. J.* Vol. 9, no. 1, pp. 3217-3222.

28. Kachelo G.A., Rajput N.A., Atiq M., Sahi S.T., Khan N.A. Hameed A., Muhammad N.,

Mushtaq M.S. (2022) Antifungal efficacy of plant extracts and chemicals against alternaria leaf spot disease of spinach. *Pak. J. Agric. Res.* Vol. 35, no. 2, pp. 380-387. https://dx.doi.org/10.17582/journal.pjar/2022/35.2.380.387

29. Poudel N.S., Bharatee P., Acharya M. (2019) Influence of different chemical fungicides against rice brown leaf spot disease caused by *Bipolaris oryzae*. *Int. J. Curr. Microbiol. Appl. Sci.* Vol. 8, no. 01, pp. 441-446. https://doi.org/10.20546/ijcmas.2019.801.046

30. Hossain I., Dey P., Hossain M.Z. (2011) Efficacy of Bion, Amistar, and Tilt in controlling brown spot and narrow brown spot of rice cv. BR 11(Mukta). *J. Bang. Agric. Uni.* Vol. 9, no. 2, pp. 201-204. http://dx.doi.org/10.22004/ag.econ.208639

31. Lore J.S., Thind T.S., Hunjum M.S., Goel R.K. (2007) Performance of different fungicides against multiple diseases of rice. *Ind. Phytopathol.* Vol. 60, pp. 296-301.

32. Gupta V., Shamas N., Razdan V.K., Sharma B.C., Sharma R., Kaur K. (2013) Foliar application of fungicides for management of brown spot disease in rice (*Oryza sativa* L.) caused by *Bipolaris oryzae*. *Afr. J. Agric. Res.* Vol. 8, no. 25, pp. 3303-3309. http://dx.doi.org/10.5897/AJAR2013.7182

33. Jatoi G.H., Keerio A.U., Abdulle Y.A., Qiu D. (2019) Effect of selected fungicides and Bio-Pesticides on the mycelial colony growth of the *Helminthosporium oryzae* brown spot of rice. *Acta Ecol. Sinica,* Vol. 39, no. 6, pp. 456-460. https://doi.org/10.1016/j.chnaes.2018.09.018

A.B. Kusmangazinov[1*] (iD), M.S. Kurmanbayeva[1] (iD), A.A. Sumbembayev[1,2] (iD),

A.N. Danilova[2] (iD), G.A. Alimtay[3] (iD), K.A. Daulet[1] (iD),

D.E. Karabalayeva[1] (iD), N.V. Terletskaya[4] (iD)

[1]Al-Farabi Kazakh National University, Almaty, Kazakhstan
[2]Altai botanical garden, Ridder, Kazakhstan
[3]Kazakh-Russian Medical University, Almaty, Kazakhstan
[4]Institute of Genetics and Physiology, Almaty, Kazakhstan
*e-mail: adil_06.1996@mail.ru

Study of *Hedysarum theinum* (Fabaceae Lindl.) in the flora of Kazakhstan

Abstract. Analysis of historical data on the distribution of *Hedysarum theinum* Krasnob. in Kazakhstan presented in this paper is based on herbarium collections kept at the Institute of Botany and Phytointroduction, Almaty and the Digital Herbarium of Moscow State University, Moscow, as well as a list of species of *Hedysarum theinum* on the Ivanovsky Ridge, Kazakhstani Altai with specimens collected as a result of expedition trips to the study area. The cenoflora includes 176 species from 120 genera and 41 families. The hierarchical order of the leading families is as follows: Asteraceae Dumort, Poaceae Barnhart, Ranunculaceae Juss., Rosaceae Juss. Comparative analysis of life forms shows that short rhizomatous plants prevail – 33%, taproot plants – 24% and tussock plants – 11%. The basis of communities in relation to temperature, moisture and substrate structure are the following ecological groups of plants: mesophytes – 30%, in a smaller proportion are mesohygrophytes – 19%, mesoxerophytes – 20% and mesopsychrophytes – 18%.

Key words: *Hedysarum theinum,* herbarium collections, Kazakhstani Altai, cenoflora.

Introduction

The genus *Hedysarum* (H.) L. (Fabaceae) comprises about 285 species. Some of its representatives are known for their medicinal properties, while other are valuable forage and ornamental plants [1]. *H. theinum* is an endemic for Central Asian-South Siberian area [2], which is also present in Kazakhstani Altai (Figure 1).

Biological features of the species (slow growth, irregular fruiting, narrow ecological plasticity) and anthropogenic impact (intensive logging, deforestation and grazing) led the species to the threat of extinction [3]. *H. theinum* as an independent species, which differs from *H. neglectum* by the structure and chemical constitution of the root, inflorescences, pedicels, flowers and fruits [4]. In earlier works, *H. theinum* was referred to *H. obscurum* and *H. austrosibiricum* [5].

The study of the *H. theinum* cenopopulation was carried out by Russian botanists in the highlands of the Russian and Kazakhstani Altai at an altitude of 1600-2100 m above sea level [6]. In Eastern Europe and Siberia major research was performed by M.S. Knyazev [7]. The scientists S.Y. Syeva, N.A. Karnaukhova, O.V. Dorogina; T.P. Sviridova, N.S. Zinner and Sh.M. Zubairova made a special contribution to the study of cultivation, ecological and biological features, introduction, reintroduction and ontogenesis of *H. theinum* [8-10].

Figure 1 – In nature: A – community involving *H. theinum*,
B – generative individual of *H. theinum*

The above-ground part of *H. theinum* contains monosaccharides, disaccharides, tannins, vitamin C, carotene, substances of xanthone nature mangiferin and isomangiferin. Such compounds as polyphenols, alkaloids, saponins, coumarins, carbohydrates, and vitamin C are present in the under-the-ground part [11-13].

A number of works are focused on anatomy [14], phytochemistry [15-18], introduction [19-22], genetics [23-25], and microclonal reproduction of *H. theinum* [26, 27]. At the same time, geobotanical studies have been conducted insufficiently both throughout the range [28-31] and in Kazakhstan, in particular [32]. At the present time, clarification of the geographical distribution of the species in nature and the inventory of species of the *H. theinum* cenoflora in a comparative aspect with previous floristic studies in the Kazakhstani Altai is an important and relevant direction.

Our goal was to study the actual distribution of *H. theinum* on the basis of historical herbarium finds and our own expeditionary data, as well as to identify the floristic composition of communities associated with *H. theinum* in Kazakhstani Altai.

Materials and methods

Creation of inventory of herbarium material stored in the Institute of Botany and Phytointroduction Herbarium (AA) – more than 50 documented sheets, and the Digital Herbarium of Moscow State University (MW) – 3 herbarium sheets, was aimed at added clarification of the composition and distribution of *H. theinum*. Herbarium specimens from different places

in Kazakhstan and other neighboring regions cover the period of 1843-2000.

Statistical processing of the results was performed in STATISTICA 10.0. The Latin names are given according to the "WCSP" [33] and according to the electronic resource "Plant list" [34]. Families were structured according to A.L. Takhtajian [35]. Species and genera in the families were arranged alphabetically. The names of floristic regions were given according to the "Flora of Kazakhstan" [36].

The floristic composition of communities associated with *H. theinum* on the territory of Kazakhstani Altai was studied in natural habitats of the Ivanovsky Ridge in the Southwestern Altai. The eastern part, as the highest (about 2800 m above sea level), begins at the eastern border of Kazakhstan, at the sources of the Belaya and Chernaya Uba and stretches westward to the Gromatukha River valley, in the vicinity of the town of Ridder. In the south, it borders with the Ulbinskiy range, and in the northwest, the Gromatukha River separates it from the Ubinskiy range. The elevation ranges from 2000-2800 m above sea level [37].

Results and discussion

To establish the historical locations of *H. theinum* in Kazakhstan, an inventory of AA and MW was conducted. The actual distribution sites in three floristic regions were identified: 22 in Altai, 24 in Dzungar Alatau, and 25 in Trans-Ili Kungei Alatau (Figure 2).

Table 1 shows the collections of *H. theinum* stored in AA, MW and collected mainly by Krasnoborov I.M., who discovered the species.

Figure 2 – Distribution of *H. theinum* in floristic regions of Kazakhstan, where: 1. Spurs of the common Syrt; 2. Tobol-Ishim; 3. Irtysh; 4. Semipalatinskiy boar; 5. Kokchetav; 6. Precaspian; 6a. Bukey; 7. Aktobe; 7a. Mugodzhar; 8. Embi; 9. Turgay; 10. Western shallow hills; 10a. Ulutau; 11. Eastern cretaceous; 11a. Karkaraly; 12. Zaisan; 13. Northern Ust-Urt; 13a. Buzachi; 13b. Mangyshlak; 14. Priaralskiy; 15. Kzyl-Orda; 16. Betpak-dala; 17. Muyun-Kum; 18. Balkhash-Alakul; 19. South Ust-Urt; 20. Kzyl-Kum; 21. Turkestan; 22. Altai; 23. Tarbagatai; 24. Dzungarian Alatau; 25. Trans-Ili Kungei Alatau; 25a. Ketmen-Terskey Alatau; 26. Chu-Ili Mountains; 27. Kyrgyz Alatau; 28. Karatau; 29. Western Tien Shan.

Table 1 – Collections of *H. theinum* in AA and MW

Floristic Area	Region	Location	Date	Identifier
Altai	Western Altai	Western Altai. Golukha Mountain. Northwest of Ridder. On the northern slope of Golukha Mountain, in a fir forest at an altitude of 1600 m	27.07.1947	Krasnoborov I.M. (AA)
Altai	Western Altai	Altai. Ridder. The surroundings of Ridder. The outskirts of the Botanical Gardens. On top of the hill 820 m	29.06.1926	Krasnoborov I.M. (AA)
Altai	Southern Altai	Altai, Sarymsakty ridge, the headwaters of the Ush-Kungei River	19.08.1958	Krasnoborov I.M. (AA)
Dzungarian Alatau	Northern part	Lepsinsk. Glinovka. Meadow near the snow on the top of the mountain Abl-tau close to Glinovskii village	07.07.1928	Krasnoborov I.M. (AA)
Trans-Ili Kungei Alatau	Trans-Ili Alatau	Trans-Ili Alatau. Kaz. state reserve. Sarsai, the height above the sea 2200 m	1932	Krasnoborov I.M. (AA)
Trans-Ili Kungei Alatau	Trans-Ili Alatau	Trans-Ili Alatau, the right bank of the Middle Talgar River, rocky slopes near the Semenov glacier of the Eastern peak	19.07.1935	Krasnoborov I.M. (AA)
Dzungarian Alatau		Kazakhstan, Taldy-Kurgan region, Sarkand district, vicinity of Pokatilovo village, Dzungarian Alatau, valley of the Baskan river, granite kurums, shrub thickets	20.07.1995	Krasnoborov I.M. (AA)
Dzungarian Alatau	Southwestern spurs	Altyn-Emel, Mantai mountains. Itmurun river gorge. Along the northern meadow slopes near the peaks	26.06.1926	Goloskokov V.P. Krasnoborov I.M. (MW)
Dzungarian Alatau	Northern part	Lepsi. A meadow near the snow, on top of Abyl-Tau Mountain, in the vicinity of the village of Glinovka	7.07.1928	Lipshits S., Krasoborov I.M. (MW)
Altai	Southern Altai	In the subalpine Tarbagatai near the Cheshak Assu brook, as well as in the Narym Alps	1840	Karelin et Kiriloff, Krasnoborov I.M. (MW)

Based on the inventory of historical summaries, the route of expeditionary research was laid on the Ivanovsky Ridge as the most typical habitat of the species in the Kazakhstani Altai. The community with *H. theinum* occupies an area up to 35 km^2 in the upper reaches of the Bolshaya Poperechka River on the northwestern slope. Coordinates are 50º 19' 02'' N, 83º 52' 32'' E, elevation 1860 m above sea level [32].

According to the results, the studied cenoflora includes 176 species belonging to 120 genera from 40 families (Table 2).

Table 2 – Cenoflora of *H. theinum* in Kazakhstani Altai (Ivanovsky Ridge)

Names of species	Family	Life forms (Raunkiaer 1934)	Ecological groups
Achillea ledebourii Heimerl *(Ptarmica ledebourii* (Heimerl) Klok.)	Asteraceae	Tp	M
Achillea millefolium L.	Asteraceae	Lrp	M
Antennaria dioica (L.) Gaertn.	Asteraceae	Tp	MX
Aster alpinus L.	Asteraceae	Tp	MP
Crepis chrysantha (Ledeb.) Turcz.	Asteraceae	Srp	M
Crepis sibirica L.	Asteraceae	Srp	M
Doronicum altaicum Pall.	Asteraceae	Lrp	GM
Erigeron speciosus (Lindl.) DC.	Asteraceae	Tp	M
Leuzea carthamoides (Willd.) DC. *(Stemmacantha chartamoides* (Willd.) M. Dittrich)	Asteraceae	Srp	MP
Ligularia glauca (L.) O.Hoffm.	Asteraceae	Tp	M
Omalotheca sylvatica (L.) Sch.Bip. & F.W.Schultz	Asteraceae	Tp	M
Saussurea frolowii Ledeb.	Asteraceae	Srp	MP
Saussurea latifolia Ledeb.	Asteraceae	Srp	MP
Saussurea parviflora (Poir.) DC.	Asteraceae	Srp	M
Saussurea schanginiana (Wydler) Fisch. ex Herder	Asteraceae	Srp	M
Senecio nemorensis L.	Asteraceae	Srp	M
Serratula coronata L.	Asteraceae	Srp	MP
Solidago dahurica (Kitag.) Kitag. ex Juz.	Asteraceae	Srp	MP
Solidago virgaurea L.	Asteraceae	Brp	M
Taraxacum ceratophorum (Ledeb.) DC.	Asteraceae	Brp	M
Tragopogon pratensis L.	Asteraceae	Tp	MX
Tripleurospermum inodorum (L.) Sch.Bip. *(Tripleurospermum perforatum* ((Mérat) M.Laínz)	Asteraceae	Tp	MX
Aconitum anthora L. *(Aconitum anthoroideum* DC.*)*	Ranunculaceae	Bbp	MX
Aconitum glandulosum Rapaics *(Aconitum altaicum* Steinb.)	Ranunculaceae	Lrp	M
Aconitum leucostomum Vorosch.	Ranunculaceae	Srp	M
Aconitum monticola Steinb.	Ranunculaceae	Srp	M
Aconitum septentrionale Koelle	Ranunculaceae	Srp	GM
Anemonastrum crinitum (Juz.) Holub	Ranunculaceae	Brp	M
Anemonastrum narcissiflorum (L.)	Ranunculaceae	Brp	M
Anemonoides caerulea (DC.) Holub *(Anemone caerulea* DC.*)*	Ranunculaceae	Brp	M
Aquilegia glandulosa Fisch. ex Link.	Ranunculaceae	Tp	GM

Names of species	Family	Life forms (Raunkiaer 1934)	Ecological groups
Clematis alpina subsp. sibirica (L.) Kuntze (*Atragene sibirica* L.)	Ranunculaceae	Srp	GM
Delphinium elatum L.	Ranunculaceae	Srp	GM
Thalictrum alpinum L.	Ranunculaceae	Tp	GM
Thalictrum flavum L.	Ranunculaceae	Tp	M
Trollius altaicus C.A.Mey.	Ranunculaceae	Srp	GM
Ranunculus grandifolius C.A. Mey.	Ranunculaceae	Srp	GM
Ranunculus monophyllus Ovcz. (*Ranunculus krylovii* Ovcz.)	Ranunculaceae	Lrp	GM
Callianthemum alatavicum Freyn	Ranunculaceae	Srp	M
Aegopodium alpestre Ledeb.	Apiaceae	Srp	M
Angelica decurrens (Ledeb.) B.Fedtsch.	Apiaceae	Lrp	GM
Bupleurum longifolium ssp. aureum (Fisch. ex Hoffm.) Soó	Apiaceae	Tp	MX
Neogaya simplex (L.) Meisn. (*Pachypleurum alpinum* Ledeb.)	Apiaceae	Srp	M
Pachypleurum alpinum Ledeb.	Apiaceae	Srp	GM
Schulzia crinita (Pall.) Spreng.	Apiaceae	Tp	GM
Seseli condensatum (L.) Rchb.f.	Apiaceae	Bbp	M
Agrostis gigantea Roth	Poaceae	Tsp	MX
Alopecurus pratensis L.	Poaceae	Tsp	MX
Anthoxanthum monticola (Bigelow) Veldkamp (*Hierochloe alpina* (Sw. ex Willd.) Roem. & Schult.)	Poaceae	Tp	MX
Anthoxanthum nipponicum Honda (*Anthoxanthum alpinum* Á.Löve & D.Löve)	Poaceae	Tp	MX
Calamagrostis arundinacea (L.) Roth	Poaceae	Tsp	MX
Calamagrostis epigejos (L.) Roth	Poaceae	Tsp	X
Calamagrostis obtusata Trin.	Poaceae	Tsp	X
Dactylis glomerata L.	Poaceae	Tsp	M
Elymus mutabilis (Drobow) Tzvelev	Poaceae	Tp	M
Deschampsia cespitosa (L.) P. Beauv.	Poaceae	Tp	M
Festuca altaica Trin.	Poaceae	Tsp	MX
Festuca borissii Reverd.	Poaceae	Tp	MP
Festuca kryloviana Reverd.	Poaceae	Tp	MX
Festuca rubra L.	Poaceae	Tp	MX
Koeleria altaica (Domin) Krylov	Poaceae	Tp	MX
Milium effusum L.	Poaceae	Tsp	MX
Phleum alpinum L.	Poaceae	Tsp	MX
Phleum phleoides (L.) H.Karst.	Poaceae	Tsp	MX
Poa alpigena Lindm.	Poaceae	Tp	MX
Poa attenuata Trin.	Poaceae	Tp	M
Poa pratensis L.	Poaceae	Tp	GM
Poa sibirica Roshev.	Poaceae	Tsp	MP

Table continuation

Names of species	Family	Life forms (Raunkiaer 1934)	Ecological groups
Helictochloa versicolor (Vill.) Romero Zarco *(Helictotrichon versicolor* (Vill.) Pilg.)	Poaceae	Tp	MX
Deschampsia cespitosa (L.) P. Beauv.	Poaceae	Tp	MX
Alchemilla altaica Juz.	Rosaceae	Srp	MP
Alchemilla vulgaris L. *(Alchemilla acutiloba* Opiz)	Rosaceae	Srp	MP
Alchemilla xanthochlora Rothm.	Rosaceae	Srp	MP
Cotoneaster uniflorus Bunge	Rosaceae	C	MPt
Dasiphora ruticose (L.) Rydb. *(Pentaphylloides ruticose* (L.) O.Schwarz)	Rosaceae	C	M
Potentilla chrysantha Trevir.	Rosaceae	Srp	M
Rosa acicularis Lindl.	Rosaceae	C	M
Rosa spinosissima var. spinosissima *(Rosa pimpinellifolia* L.)	Rosaceae	C	M
Rubus idaeus L.	Rosaceae	C	GM
Sibbaldia procumbens L.	Rosaceae	Srp	GM
Sanguisorba alpina Bunge	Rosaceae	Srp	GM
Sibiraea laevigata (L.) Maxim.	Rosaceae	Srp	GM
Spiraea chamaedryfolia L.	Rosaceae	C	M
Spiraea media Schmidt	Rosaceae	C	MX
Allium altaicum Pall.	Amaryllidaceae (Alliaceae)	Bp	MPt
Allium flavidum Ledeb.	Amaryllidaceae (Alliaceae)	Bp	MX
Allium schoenoprasum L.	Amaryllidaceae (Alliaceae)	Bp	GM
Bistorta elliptica (Willd. ex Spreng.)	Polygonaceae	Srp	MP
Koenigia alpina (All.) T.M.Schust. & Reveal *(Aconogonon alpinum* (All.) Schur)	Polygonaceae	Srp	MP
Rheum compactum L.	Polygonaceae	Srp	MP
Rumex acetosa L.	Polygonaceae	Srp	MX
Rumex acetosella L.	Polygonaceae	Srp	M
Campanula cervicaria L.	Campanulaceae	Tp	M
Campanula stevenii subsp. altaica (Ledeb.) Fed. *(Campanula altaica* Ledeb.)	Campanulaceae	Tp	M
Carex aterrima Hoppe	Cyperaceae	Tsp	GM
Carex capillaris L.	Cyperaceae	Tsp	GM
Carex glomerata Thunb.	Cyperaceae	Tsp	M
Carex melanocarpa Cham. ex Trautv.	Cyperaceae	Tsp	M
Carex pediformis var. macroura (Meinsh.) Kük. *(Carex macroura* Meinsh.)	Cyperaceae	Tsp	M
Berberis sibirica Pall.	Berberidaceae	C	M
Saxifraga sibirica L.	Saxifragaceae	Srp	MPt
Bergenia crassifolia (L.) Fritsch	Saxifragaceae	Lrp	MP
Micranthes punctata (L.) Losinsk. *(Saxifraga punctata* L.)	Saxifragaceae	Srp	MPt

Table continuation

Names of species	Family	Life forms (Raunkiaer 1934)	Ecological groups
Betula rotundifolia Spach	Betulaceae	T	P
Cerastium pauciflorum Steven ex Ser.	Caryophyllaceae	Tp	MX
Dianthus superbus L.	Caryophyllaceae	Tp	MX
Dichodon cerastoides (L.) Rchb.	Caryophyllaceae	Tp	M
Silene repens Patrin	Caryophyllaceae	Tp	GM
Silene vulgaris (Moench) Garcke *(Oberna behen* (L.) Ikonn.)	Caryophyllaceae	Tp	M
Corydalis bracteata (Stephan ex Willd.) Pers.	Papaveraceae	Tp	GM
Papaver nudicaule L.	Papaveraceae	Tp	M
Dracocephalum grandiflorum L.	Lamiaceae	Srp	MX
Dracocephalum nutans L.	Lamiaceae	Srp	MX
Dracocephalum ruyschiana L.	Lamiaceae	Tp	X
Lamium album L.	Lamiaceae	Tp	MX
Origanum vulgare L.	Lamiaceae	Srp	M
Phlomoides alpina (Pall.) Adylov, Kamelin & Makhm.	Lamiaceae	Srp	MP
Epilobium angustifolium L. *(Chamaenerion angustifolium* (L.) Scop.)	Onagraceae	Srp	MP
Erythronium sibiricum (Fisch. & C.A.Mey.) Krylov	Liliaceae	Bbp	MP
Lloydia serotina (L.) Rchb.	Liliaceae	Bbp	M
Euphorbia pilosa L.	Euphorbiaceae	Bbp	MPt
Galium boreale L.	Rubiaceae	Tp	MP
Galium verum L.	Rubiaceae	Tp	MX
Gentiana algida Pall.	Gentianaceae	Bbp	MP
Gentiana decumbens L.f.	Gentianaceae	Bbp	MP
Gentiana uniflora Georgi	Gentianaceae	Bbp	MP
Gentianella amarella (L.) Börner	Gentianaceae	Bbp	MP
Gentianopsis barbata (Froel.) Ma	Gentianaceae	Bbp	M
Swertia obtusa Ledeb.	Gentianaceae	Tp	GM
Geranium albiflorum Ledeb.	Geraniaceae	Srp	GM
Geranium collinum Stephan ex Willd.	Geraniaceae	Srp	GM
Hedysarum neglectum Ledeb.	Fabaceae	Lrp	MP
Lathyrus gmelinii (Fisch. ex Ser.) Fritsch	Fabaceae	Lrp	MP
Lathyrus vernus (L.) Bernh.	Fabaceae	Lrp	M
Thermopsis alpina (Pall.) Ledeb.	Fabaceae	Srp	MP
Vicia cracca L.	Fabaceae	Lrp	M
Trifolium lupinaster L. *(Lupinaster pentaphyllus* Moench)	Fabaceae	Srp	GM
Oxytropis alpina Bunge	Fabaceae	Srp	GM
Hylotelephium ewersii (Ledeb.) H.Ohba *(Sedum ewersii* Ledeb.)	Crassulaceae	Srp	GM
Rhodiola algida (Ledeb.) Fisch. & C.A.Mey.	Crassulaceae	Srp	MPt
Rhodiola rosea L.	Crassulaceae	Srp	MPt
Iris ruthenica Ker Gawl.	Iridaceae	Srp	MX
Juniperus communis var. saxatilis Pall. *(Juniperus sibirica* Burgsd.)	Cupressaceae	C	MPt

Table continuation

Names of species	Family	Life forms (Raunkiaer 1934)	Ecological groups
Lagotis globosa Hook.f.	Plantaginaceae	Brp	MX
Veronica krylovii Schischk.	Plantaginaceae	Srp	MX
Larix sibirica Ledeb.	Pinaceae	T	MP
Picea obovata Ledeb.	Pinaceae	T	P
Pinus sibirica Du Tour	Pinaceae	T	P
*Lonicera caerulea subsp. altaica (*Pall.) Gladkova (*Lonicera altaica (*Pall.))	Caprifoliaceae	C	MP
Lonicera hispida Pall. ex Schult.	Caprifoliaceae	C	MP
Patrinia sibirica (L.) Juss.	Caprifoliaceae	Srp	MX
Valeriana pratensis Dierb. *(Valeriana collina* Wallr.)	Caprifoliaceae	Bbp	M
Veronica krylovii Schischk.	Plantaginaceae	Srp	M
Macropodium nivale (Pall.) W.T.Aiton	Brassicaceae	Srp	MPt
Myosotis scorpioides subsp. Scorpioides (Myosotis palustris (L.) Hill*)*	Boraginaceae	Srp	GM
Paeonia anomala L.	Paeoniaceae	Brp	M
Pedicularis condensata M.Bieb.	Orobanchaceae	Srp	MX
Pedicularis elata Willd.	Orobanchaceae	Srp	MX
Pedicularis oederi Vahl	Orobanchaceae	Srp	MX
Polemonium caeruleum L.	Polemoniaceae	Tp	M
Polygala sibirica L.	Polygalaceae	Tp	MP
Primula nivalis Pall.	Primulaceae	Tsp	MP
Primula pallasii Lehm.	Primulaceae	Srp	M
Ribes atropurpureum C.A.Mey.	Grossulariaceae	C	M
Ribes rubrum L.	Grossulariaceae	C	M
Salix lanata L.	Salicaceae	T	GM
Salix nummularia Andersson	Salicaceae	T	GM
Salix rectijulis Ledeb. ex Trautv.	Salicaceae	T	GM
Thesium repens Ledeb.	Santalaceae	Ds	MP
Vaccinium myrtillus L.	Ericaceae	Hs	GM
Vaccinium vitis-idaea L.	Ericaceae	Hs	GM
Veratrum lobelianum Bernh.	Melanthiaceae	Srp	MP
Viola altaica Ker Gawl.	Violaceae	Tsp	M
Viola biflora L.	Violaceae	Tsp	M
Viola disjuncta W.Becker	Violaceae	Tsp	M

* Life forms according to Raunkiaer (1934): M – Mesophanerophytes, N – Nanophanerophytes, Ch – Chamaephyts, H – Hemicryptophytes, C – Cryptophytes. Life forms according to Serebryakov, (1962): T – tree; S – shrub; Hs – half-shrub; Ds – dwarfshrub; Lrp – long rhizomatous plant; Srp – short rhizomatous plants; Bbp – bulbotuberiferous plants; Bp – bulbous plants; Tp –taproot plants; Brp – brushy root plants; Tsp – tussock plants; Cm – club-moss. Ecological groups of plants in relation to the temperature, moisture and ston nature of the substrate: H – hygrophytes, HP – hygropsychrophytes, GM – hygromesophytes, M – mesophytes, MX – mesoxerophytes, MP – mesopsychrophytes, X – xerophytes, XPt – xeropetrophyte, P – psychrophytes, MPt – mesopetrophytes [38]

The most numerous are representatives of the following families: Poaceae Barnhart (13.7%), Asteraceae Dumort. (12.6%), Ranunculaceae Juss. (9.7%), Rosaceae Juss. (8%), which account for 44% of the total (Figure 3).

In the aspect of life forms, short rhizomatous plants prevail – 33%, taproot plants – 24% and tussock plants – 11% (Figure 4).

Regarding the composition of life forms in relation to temperature, moisture and substrate structure, the basis of phytocenoses are ecological groups of plants: mesophytes – 30%, in a smaller proportion are mesohygrophytes – 19%, mesoxerophytes – 20% and mesopsychrophytes – 18% (Figure 5).

The results of comparisons of *H. theinum* cenoflora on the Ivanovsky Ridge with data on the species composition of the flora of the Kazakhstani Altai show that the families Fabaceae Lindl., Ranunculaceae Juss., Rosaceae Juss., Gentianaceae Juss. differ significantly in the proportion of participation in the formation of the floral composition (Table 3). This is associated with the low number of xeromesophytic species and the predominant number of mesophytic species typical of dark coniferous forests and subalpine meadows. The Spearman rank correlation coefficient is 0.615, and the relationship is moderate and direct.
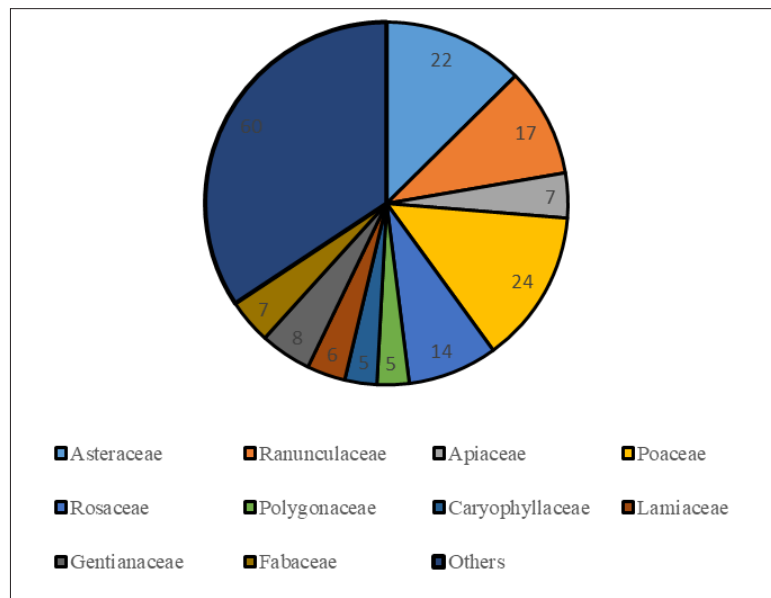
Figure 3 – Spectrum of the leading families
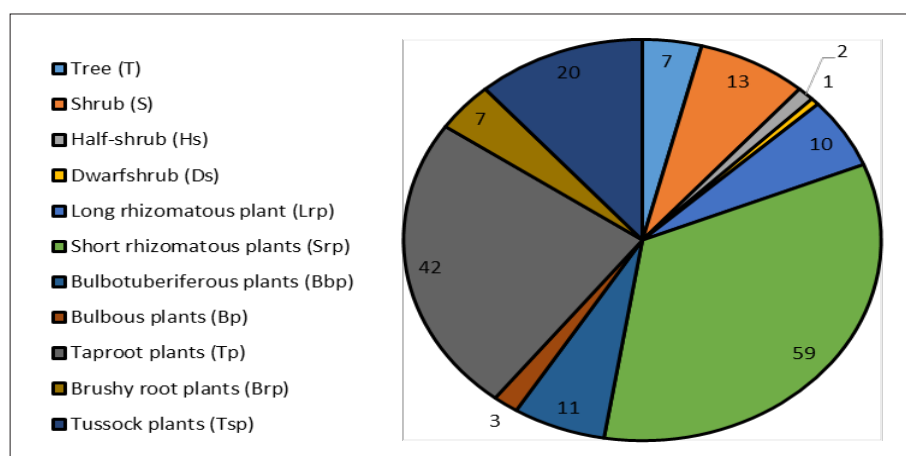
Figure 4 – Life forms according to Serebryakov (1962)
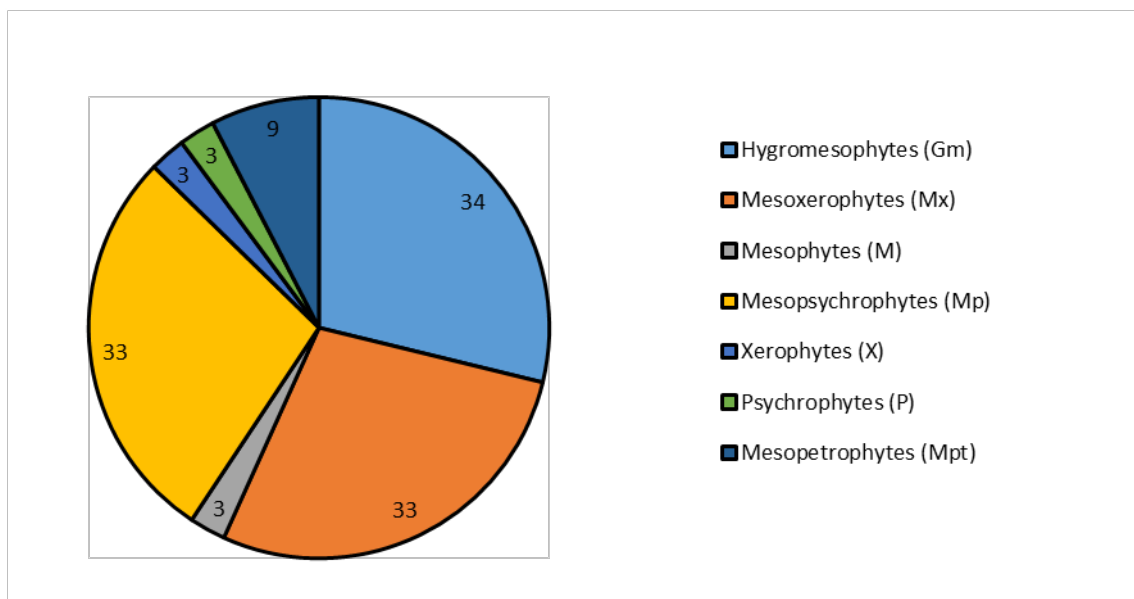
Figure 5 – Ecological groups of plants

Table 3 – Leading families of the flora of *H. theinum* populations by the number of species

Family	Cenoflora of *H. theinum* populations, Ivanovo Ridge		Flora of Kazakhstani Altai
	Number of genera, % of total number	Number of species, % of total number	Number of species, % of total number
Apiaceae Lindl.	7/6	7/4	71/2,9
Asteraceae Dumort.	16/13	22/12	324/13,3
Caryophyllaceae Juss.	4/3	5/3	81/3,3
Fabaceae Lindl.	6/5	7/4	183/7,5
Lamiaceae Martinov	4/3	6/3	77/3,2
Gentianaceae Juss.	4/3	8/5	29/1,2
Poaceae Barnhart	14/12	24/14	308/12,6
Ranunculaceae Juss.	10/8	17/10	10/4,2
Rosaceae Juss.	9/7	14/8	109/4,5
Caryophyllaceae Juss.	4/3	5/3	81/3,3
Total	78/65	115/66	1256/51,8

According to the spectrum of the 10 leading families, the flora of associated species for *H. theinum* is significantly similar to the flora of the entire Kazakhstani Altai. The high percentage of species falling within the main ten families – 66% – indicates a high degree of anthropogenic pressure and transformation of the flora, which is much higher than the overall figures for the Kazakhstani Altai – 51.8%. Weed species in the cenoflora: *Crepis sibirica, Poa pratensis, Lamium album* also confirm the presence of anthropogenic pressure on *H. theinum* communities.

Conclusion

The study of the current state of rare and economically valuable *H. theinum* in Kazakhstan should have a comprehensive character. The first stage in the study was an inventory of historical herbarium materials of the main repositories: the herbarium fund of the Institute of Botany (AA) and the herbarium fund of the Moscow State University (MW). Establishment of the actual places of growth served as the basis for the construction of expedition routes. The second stage of the study was the analysis

of the *H. theinum* cenoflora in the Kazakhstani Altai, the natural habitat of the species. The study of *H. theinum* cenoflora showed a high similarity of species ratio with the whole flora of Kazakhstani Altai. The high number of mesophytic species influenced the predominance of such families as Asteraceae Dumort., Poaceae Barnhart, Ranunculaceae Juss. and Rosaceae Juss. At the same time the high percentage of species falling on the leading families and the presence of weed species confirms the high anthropogenic load on the *H. theinum* communities. The species requires further detailed study with the purpose of preservation and protection.

Acknowledgements

References

1. Zinner, N.S., Nekratova, A.N., Shchukina, A.V., Kovaleva, A.L. (2021). Biological features of high altitude rare medicinal plant species Hedysarum theinum Krasnob. in western Siberia cultivation. Acta Biologica Sibirica, 7, 77-85. doi:10.3897/abs.7.e67122

2. Karnaukhova, N.A., Selyutina, I.J., & Syeva, S.Y. (2021). Reproductive biology of Hedysarum theinum (Fabaceae). Botanicheskii Zhurnal, 106(6), 556-566. doi:10.31857/S0006813621060065

3. Dorogina, O.V., Karnaukhova, N.A., Agafonova, M.A. (2009). Relationships between the variability of electrophoretic profiles of seed polypeptides and ecological-geographic conditions of the habitats of populations of Hedysarum theinum Krasnob. (Fabaceae). Contemporary Problems of Ecology, 2(6), 506-509. doi:10.1134/S1995425509060022

4. Krasnoborov I.M., Azovtsev G.R., Orlov V.P. (1985). A new species of the genus Hedysarum (Fabaceae) from Southern Siberia [Novyj vid roda Hedysarum (Fabaceae) iz Yuzhnoj Sibiri] // Bot. journal. Vol. 70, No. 7. pp. 968-973.

5. Zhmud, E.V., Zinner, N.S., & Dorogina, O.V. (2020). Trypsin inhibitor activity in representatives of the genus Hedysarum (Fabaceae): The polyvariance of seasonal dynamics in southern siberia. Proceedings on Applied Botany, Genetics and Breeding, 181(3), 25-31. doi:10.30901/2227-8834-2020-3-25-31

6. Karnaukhova, N.A., & Selyutina, I.Y. (2013). Assessment of Hedysarum theinum Krasnob. (Fabaceae) population status in Altai. Contemporary Problems of Ecology, 6(4), 408-414. doi:10.1134/S1995425513040021

7. Knyazev M.S. (2013). Review of Eastern European and some Siberian Hedysarum, Fabaceae [Obzor vostochno-evropejskih i nekotoryh sibirskih kopeechnikov (Hedysarum, Fabaceae)]. Botanical Journal. Vol. 98. No. 10. pp. 1261-1273.

8. Syeva S.Ya., Karnaukhova N.A., Dorogina O.V. (2008). Hedysarum of the Altai Mountains [Kopeechniki Gornogo Altaya] Gorno-Altaysk, p.184.

9. Sviridova, T.P., Zinner, N.S. (2008). Prospects for growing Hedysarum alpinum L. and Hedysarum theinum Krasnob. in the conditions of the Tomsk region [Perspektivy vyrashchivaniya Hedysarum alpinum L. i Hedysarum theinum Krasnob. v usloviyah Tomskoj oblasti]. Bulletin of Tomsk State University. Biology, (2 (3)), 5-11.

10. Zubairova Sh.M. (2013). Features of seed productivity Hedysarum daghestanicum Boiss. Ex Rupr. in natural populations [Osobennosti semennoj produktivnosti Hedysarum daghestanicum Boiss. Ex Rupr. v prirodnyh populyaciyah] // Fundamental Research, No. 6-2. – pp. 352-355

11. Nechepurenko, I.V., Komarova, N.I., Kuzovkina, I.N., Vdovitchenko, M.Y., Polovinka, M.P., & Salakhutdinov, N.F. (2009). Isolation and identification of 4',6-dimethoxy-7-hydroxyisoflavone from roots of Hedysarum theinum cultivated in vitro. Chemistry of Natural Compounds, 45(3), 420-421. doi:10.1007/s10600-009-9327-9

12. Liu, Y., Yang, H., Wang, W., Zhao, Y., Chen, H., Liang, H., Zhang, Q. (2019). Chemotaxonomy studies on the genus Hedysarum. Biochemical Systematics and Ecology, 86. doi:10.1016/j.bse.2019.05.010

13. Nechepurenko, I.V., Polovinka, N.P., Sal'Nikova, O.I., Pokrovskii, L.M., Komarova, N.I., Salakhutdinov, N.F., & Nechepurenko, S.B. (2007). Components of the ethylacetate extract of Hedysarum theinum roots. Chemistry of Natural Compounds, 43(1), 5-9. doi:10.1007/s10600-007-0052-y

14. Karnaukhova, N.A. (2016). Anatomo-morphological features of the leaves of Hedysarum theinum (Fabaceae) in western Altai. Contemporary Problems of Ecology, 9(3), 349-354. doi:10.1134/S1995425516030057

15. Fedorova, Y.S., Kulpin, P.V., Kotova, T.V., Denisova, S.V., Beregovykh, G.V. (2021). Study of

the antidepressant properties of some plants. Paper presented at the AIP Conference Proceedings, 2419. doi:10.1063/5.0069670

16. Vdovitchenko, M.Y., Kuzovkina, I.N., Paetz, C., Schneider, B. (2007). Formation of phenolic compounds in the roots of Hedysarum theinum cultured in vitro. Russian Journal of Plant Physiology, 54(4), 536-544. doi:10.1134/S1021443707040164

17. Nechepurenko, I.V., Polovinka, M.P., Komarova, N.I., Korchagina, D.V., Salakhutdinov, N.F., Nechepurenko, S.B. (2008). Low-molecular-weight phenolic compounds from Hedysarum theinum roots. Chemistry of Natural Compounds, 44(1), 31-34. doi:10.1007/s10600-008-0009-9

18. Nechepurenko, I. V., Komarova, N.I., Gerasimova, Y.V., Koval, V.V., Polovinka, M.P., Korchagina, D.V., Salakhutdinov, N.F. (2009). Structure of oligomeric proanthocyanidines from Hedysarum theinum roots studied by thiolysis and MALDI-TOF MS. Chemistry of Natural Compounds, 45(1), 32-39. doi:10.1007/s10600-009-9216-2

19. Karnaukhova N.A. (2007). Features of Hedysarum theinum Krasnob. (Fabaceae) development. in natural conditions and during introduction to the Central Siberian Botanical Garden (Novosibirsk) [Osobennosti razvitiya Hedysarum theinum Krasnob. (Fabaceae) v prirodnyh usloviyah i pri introdukcii v Central'nyj sibirskij botanicheskij sad (g. Novosibirsk)] // Plant Resources, Vol. 43, issue 3. – pp. 14-25.

20. Elisafenko, T.V., Dorogina, O.V., Achimova, A.A., & Yamtyrov, M.B. (2013). Problems of reintroduction and restoration on the example of species of the genus Hedysarum L. and Viola L. [Problemy reintrodukcii i restavracii na primere vidov roda Hedysarum L. i Viola L.]. Problems of Botany in Southern Siberia and Mongolia, (12), 232-234.

21. Agafonova O.V., Volodarskaya S.B. (2000). Productivity and content of oligomeric catechins in Hedysarum theinum Krasnob. in the Central and South-Western Altai [Produktivnost' i soderzhanie oligomernyh katekhinov u Hedysarum theinum Krasnob. v Central'nom i Yugo-Zapadnom Altae] // Plant resources, Vol. 36, issue 3. – pp. 47-52.

22. Karnaukhova, N.A., Selyutina, I.J., Syeva, S.Y. (2021). Reproductive biology of Hedysarum theinum (Fabaceae). Botanicheskii Zhurnal, 106(6), 556-566. doi:10.31857/S0006813621060065

23. Nuzhdina, N.S., Bondar, A.A., Dorogina, O.V. (2018). New data on taxonomic and geographic distribution of the trnLUAA intron deletion of chloroplast DNA in Hedysarum L. (Fabaceae L.).

Russian Journal of Genetics, 54(11), 1282-1292. doi:10.1134/S1022795418110108

24. Yurkevich, O.Y., Samatadze, T.E., Selyutina, I.Y., Romashkina, S.I., Zoshchuk, S.A., Amosova, A.V., Muravenko, O.V. (2021). Molecular cytogenetics of eurasian species of the genus Hedysarum L. (Fabaceae). Plants, 10(1), 1-15. doi:10.3390/plants10010089

25. Zviagina, N.S., Dorogina, O.V. (2013). Genetic differentiation of Altai-sayan endemic Hedysarum theinum Krasnob. (Fabaceae) evaluated by inter-simple sequence repeat analysis. Genetika, 49(10), 1183-1189. doi:10.7868/s0016675813100135.

26. Erst, A.A., Zvyagina, N.S., Novikova, T.I., & Dorogina, O.V. (2015). Clonal micropropagation of a rare species Hedysarum theinum Krasnob. (Fabaceae) and assessment of the genetic stability of regenerated plants using ISSR markers. Russian Journal of Genetics, 51(2), 158-162. doi:10.1134/S1022795415020076

27. Erst, A.A., Zheleznichenko, T.V., Novikova, T.I., Dorogina, O.V., Banaev, E.V. (2014). Ecological and geographic variability of Hedysarum theinum and features of its propagation in vitro. Contemporary Problems of Ecology, 7(1), 67-71. doi:10.1134/S1995425514010053

28. Dong Y., Tang D., Zhang N., Li Y., Zhang C., Li L., Li M. (2013). Phytochemicals and biological studies of plants in genus Hedysarum. Chem Cent J. 7(1):124. doi: 10.1186/1752-153X-7-124. PMID: 23866043; PMCID: PMC3727964.

29. Selyutina, I.Yu., Zibzeev, E.G. (2010). Ontogenetic structure of coenopopulations of Hedysarum theinum (Fabaceae) in various ecological-cenotic conditions of the Ore Altai [Ontogeneticheskaya struktura cenopopulyacij Hedysarum theinum (Fabaceae) v razlichnyh ekologo-cenoticheskih usloviyah Rudnogo Altaya]. Journal of the Siberian Federal University. Biology, 3(2), 130-145.

30. Fedorova, Y.S., Kuznetsov, P.V., Cherkasova, T.L. (2013). Features of the development of botanical research of plants of the genus Hedysarum [Osobennosti razvitiya botanicheskih issledovanij rastenij roda Hedysarum]. Medicine in Kuzbass, (1), 63-66.

31. Karnaukhova, N.A., Dorogina, O.V., Selyutina, I.Y. (2018). The anatomical structure of leaf in species of Hedysarum Sect. gamotion basin in south Siberia. Turczaninowia, 21(4), 150-160. doi:10.14258/turczaninowia.21.4.15

32. Kubentayev S.A. (2018). Ontogenetic structure and resource indicators of Hedysarum theinum Krasnob cenopopulations on the Ivanovsky

ridge in Eastern Kazakhstan [Ontogeticheskaya struktura i resursnye pokazateli cenopopulyacij Hedysarum theinum Krasnob. na hrebte Ivanovskom v Vostochnom Kazahstane]. Diversity of the plant world, (3 (15)), 24-36.

33. World Checklist of Selected Plant Families. By the Royal Botanic Gardens.

34. The Plant List (2013). Version 1.1. Available at: http://www.theplantlist.org

35. Takhtajan A.I. (2021). Flowering plants [Cvetkovye rasteniya]. 2 ed. – p. 871.

36. Flora of Kazakstan [Flara Kazahstana] (1956), Alma-Ata, AS KazSSR, T.1, p. 353.

37. Artemov, I.A. (2021). Using marginal species localities for the revision of the western boundary of the altai-yenisei floristic province. Vestnik Tomskogo Gosudarstvennogo Universiteta, Biologiya, (55), 6-18. doi:10.17223/19988591/55/1

38. Kubentayev S.A., Zhumagul M.Z., Kurmanbayeva M.S., Alibekov D.T., Kotukhov J.A., Sitpayeva G.T., Mukhtubayeva S.K., Izbastina K.S. Current state of populations of Rhodiola rosea L. (Crassulaceae) in East Kazakhstan. Bot Stud. 2021;62(1):19. doi: 10.1186/s40529-021-00327-4

F.A. Al-Ghamdi* [iD], J.A. Al-sulami [iD], H. Al-Nahari [iD]

University of Jeddah, Jeddah, Saudi Arabia
*e-mail: faalgamdi@uj.edu.sa

Possible positive effect of gum Arabic against the toxicity of the drug furosemide on newborn rats

Abstract. Medicinal plants received special attention due to their biological and medicinal activities, aspects of safety in their use, and low cost. This study aimed to prove gum Arabic (GA) extract's preventive and therapeutic role against furosemide toxicity. Moreover, histological findings, renal functions, and the level of MDA and GSH in the serum and kidney tissues of newborn rats were assessed. Thirty pregnant rats were divided into six groups (n = 5 per group). The first group is the control group, with no treatment. The second is the GA group, administered 15% w/v GA in drinking water daily from conception day 0 until the end of pregnancy. The third group is the furosemide group; furosemide (20 mg/k, ip) was taken daily from conception day 0 until the end of pregnancy. The fourth group is the protective group (preventive group); GA was taken daily (15% w/v in drinking water) from conception day 0 to day 10, followed by furosemide (20 mg/kg, ip) daily until the end of pregnancy. The fifth group is the therapeutic group; furosemide (20 mg/kg, ip) was taken daily from conception day 0 to day 10, followed by GA (15% w/v in drinking water) daily until the end of pregnancy. The sixth group is the mixed group; GA and furosemide were administered together from conception day 0 until the end of pregnancy.

Key words: gum arabic; furosemide; kidney failure; loop diuretics; newborn rats.

Introduction

Loop diuretics are widely utilized pharmaceutical agents in medicine and are considered the most potent diuretics [1]. The loop diuretics have been regarded as a significant advancement in medical treatment. Their effectiveness is particularly notable in patients with insufficient response to alternative medications, including individuals with chronic impaired kidney function and severe cardiovascular disease [2].

According to epidemiologic studies, oliguria increases the risk of death. Moreover, based on observational studies, many intensivists employ loop diuretics, particularly furosemide [3].

The documented mechanisms of sodium-potassium-chloride cotransporters suggest that loop diuretics exert vasodilatory effects inside the renal system [4]. Loop diuretics can potentially decrease metabolic demands and oxygen utilization in renal tubular cells, thereby protecting renal function under ischemic conditions [5].

Loop diuretics are organic anions with a negative charge, exhibiting limited lipid solubility. This characteristic enables them to firmly bind to serum albumin, with a binding capacity of over 95 percent. Consequently, their filtration at the glomerulus is restricted, leading to a reduction in their bioavailability. For instance, the bioavailability of furosemide is roughly 50 percent [6].

Furosemide may be classified as a weak organic acid. The primary route of elimination for this substance is renal excretion, accounting for around 85% of its clearance. Roughly half of the substance is metabolized, while the other half is actively secreted in its original form by the organic acid transporters in the proximal tubules [7].
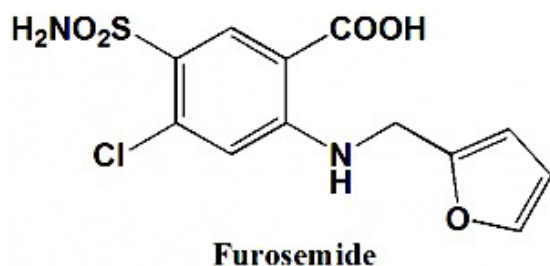
Furosemide has the potential to mitigate and lessen the intensity of renal damage. Similarly, furosemide may assist in controlling excessive fluid volume by enhancing sodium excretion and promoting diuresis [3].

Furosemide can be taken orally as tablets or as an oral solution and can be inhaled as well. The efficacy of intravenous furosemide is twice that of oral furosemide [8]. Furosemide is synthesized by a significant number of manufacturers located in Bulgaria, Brazil, China, Israel, Hungary, Italy, Switzerland, Poland, USA [9].

The furosemide chemical formula is 4-chloro-N-(2-furyl methyl)-5-sulfamoyl-anthranilic acid [10]. Figure 1A shows the structure formula of furosemide,

and a commercially available furosemide medication, named Lasix, is shown in Figure 1B.

Furosemide exerts its pharmacological effects by targeting the medullary thick ascending loop of Henle, where it inhibits the activity of the $Na^+/K^+/Cl^-$ pump located on the luminal cell membrane. This action mechanism can decrease the demand for oxygen in the renal tubules. Furosemide is further recognized for its significant adjunctive function in preserving fluid balance and enhancing nutritional provision in critically sick patients with acute kidney injury (AKI) [11].

Figure 1 – Structural formula of furosemide (A) and a commercially available furosemide medication Lasix (B)

There is a correlation between the presence of furosemide in plasma and the presence of albumin. The protein-bound fraction of furosemide is transported into the proximal tubule epithelial cells by the bloodstream and then translocated to its target locations, which are the lumens of the ascending limbs of Henle's loop tubules [12].

Moreover, the kidneys regulate fluid and sodium balance, which is seen in the case of kidney failure, where fluid retention is evident [13].

However, furosemide has adverse effects, including hepatic insufficiency, diabetes, hypoproteinemia, and some infrequent symptoms such as indigestion, thirst, dizziness, dehydration, drowsiness, weakness, muscle cramps, tinnitus, and deafness [14].

In the case of individuals diagnosed with cirrhosis, furosemide is often deliberated as a treatment option. Nevertheless, its use is associated with certain risks, including the potential for severe muscle contracture and the depletion of skeletal muscle mass, as indicated in a prior study [15]. Notably, furosemide was categorized as a Pregnancy Category C medication, warranting caution among healthcare providers when prescribing it to pregnant women. This caution stems from findings in animal reproductive experiments revealing the transfer of furosemide across the placenta and its propensity to induce adverse effects [16].

Intensive diuretic therapy can potentially lead to a reduction in breastfeeding. In cases where nursing a newborn or a premature infant is involved, it might be advisable to consider an alternative medication. Markedly, administering furosemide at lower doses may not necessarily hinder or suppress lactation [16].

Furthermore, several studies have reported that the administration of furosemide in preterm newborns has been shown to significantly influence the development and advancement of renal calcification and nephrolithiasis, often referred to as the formation of renal calcifications and stones. It causes sensorineural hearing loss and is more common in premature babies [17].

Numerous research investigations have shown the extensive use of GA and many traditional therapeutic practices. These studies have revealed various advantageous effects associated with Gum Acacia or Gum Arabic (GA; here is shown on Figure 2), which encompasses health-related, aesthetic, nutritional, and industrial aspects [18]. It refers to a desiccated gum fluid often obtained by incisions made on the stems and branches of acacia trees, namely those belonging to the *A. senegal* and *A. seyal* species within the Fabaceae family. The gum exudate is commonly found in the shape of tears, spheres, or semi-spheres [19]. *A. senegal* is a drought-tolerant tree that grows natively in desert, subtropical, and semi-arid climates. It is a tiny, spiky shrub that grows 2-6 m or even 12 m tall from the ground [20].

Figure 2 – General view of GA

GA comprises glycoproteins, proteins that include a carbohydrate co-factor or prosthetic group, and polysaccharides. The predominant constituents of these polysaccharides are galactose and arabinose. GA is widely recognized as an environmentally sustainable and nutritionally viable option [21, 22].

The scientific classification of GA places it in the plant kingdom within the *Fabaceae* family (subfamily *Mimosoideae*), belonging to the *Acacia* genus, with the primary species being *Acacia senegal* and *Acacia seyal* [19].

Materials and methods

Chemicals. In this investigation, furosemide, a member of the loop diuretic class, was employed. Furosemide was procured as commercial vials (Lasix® 20 mg, Sanofi-Aventis Deutschland GmbH, Germany) and administered intraperitoneally at 20 mg per kilogram, following established precedents in scientific literature.

Gum Arabic. GA, obtained in solid spheres, was sourced commercially from a perfumery establishment in Khartoum, Sudan. These spheres constitute pure extracts derived from the *Senegalese acacia* tree and do not contain any additives. The specimens underwent a grinding process and subsequent preparation in potable water, with a concentration of 15% (Figure 3), following procedures delineated in previous studies.
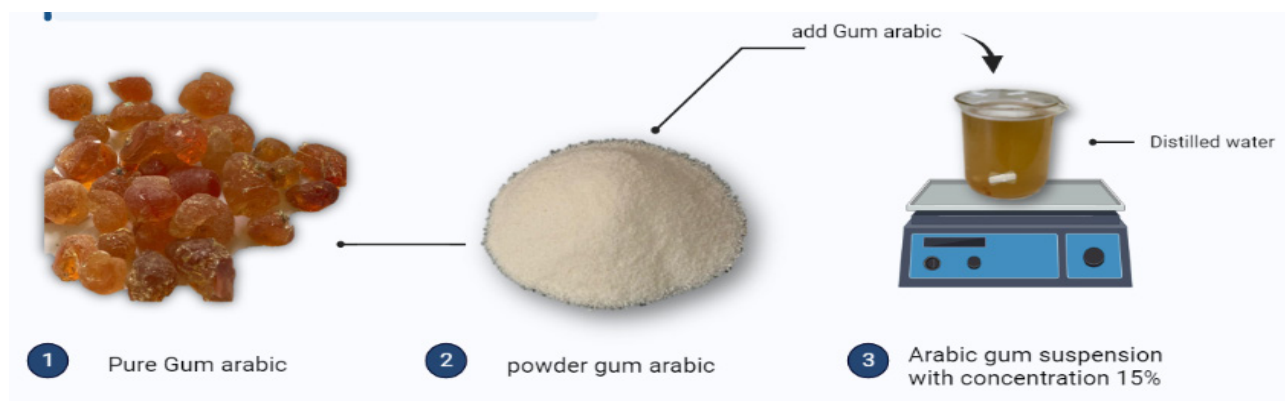
Figure 3 – Preparation of GA suspension

Experimental animals. The research employed pregnant Wistar albino rats, specifically those displaying albinism, as the subjects for experimentation. These rats were initially assessed for weight, demonstrating an average weight ranging from 200 to 250 grams at the study's outset. The specimens were sourced from the animal housing facility associated with the Faculty of Pharmacy at King Abdulaziz University. The rats were housed under carefully controlled laboratory conditions, specifically in plastic cages, where the temperature

was maintained at 20 ± 22°C. They were subjected to a light-dark cycle, each lasting 12 hours, and the light phase commencing at 07:00 AM. Throughout the experiment, the rats had unrestricted access to food and water (Figure 4).

Ethical approval. The animal studies in this research adhered to the ethical guidelines established by the Committee on Bioethics for Animal Studies at the College of Pharmacy, King Abdulaziz University. Trial registration number: PH-1443-64 and date of registration: 1/6/2022.

Figure 4 – Experimental setup for housing
of rats under controlled laboratory conditions

Experimental design. The implemented experimental design is summarized on Figure 5. The animal subjects were categorized into six distinct groups as follows:

1. Control Group (G 1): No specific treatment was administered.

2. Gum Arabic Group (G 2): GA (15% w/v in drinking water) was administered daily from conception (day 0) throughout the entire pregnancy period [23, 24].

3. Furosemide Group (G 3): Furosemide (20 mg/kg, intraperitoneal) was administered daily from conception (day 0) until the conclusion of the pregnancy [25].

4. Protective (Preventive) Group (G 4): GA was administered daily (15% w/v in drinking water) from conception (day 0) until day 10, followed by daily administration of furosemide (20 mg/kg, intraperitoneal) until the end of pregnancy.

5. Therapeutic Group (G 5): Furosemide (20 mg/kg, intraperitoneal) was administered daily from conception (day 0) until day 10, followed by daily administration of GA (15% w/v in drinking water) until the end of pregnancy.

6. Mixed Group (G 6): GA and furosemide were administered concurrently from conception (day 0) until the conclusion of the pregnancy period.

Morphological studies. At the age of two weeks, an assessment of the newborns was conducted across all groups. The evaluation aimed to determine mortality rates, examine the external characteristics of the newborns, and measure parameters including body weight, length, and kidney weight in the treated groups, with comparisons made against the control group for analysis.

A laboratory digital balance was used to measure the body weight and kidney weight of newborn mice. A meter was used to measure the body length of newborn mice.

Histological studies. Kidney samples were obtained from juvenile rats (aged two weeks) and immediately fixed in a 10% formalin solution. Following fixation, the specimens underwent a series of standard processing steps involving alcohol and xylol treatment, ultimately leading to their embedding in paraffin. Subsequently, the paraffin-embedded samples were sectioned into slices with a thickness ranging from 4 to 6 micrometers. These slices were then subjected to staining using the hematoxylin and eosin (H&E) stain method, facilitating the examination of histopathological changes and alterations within the kidney tissue.
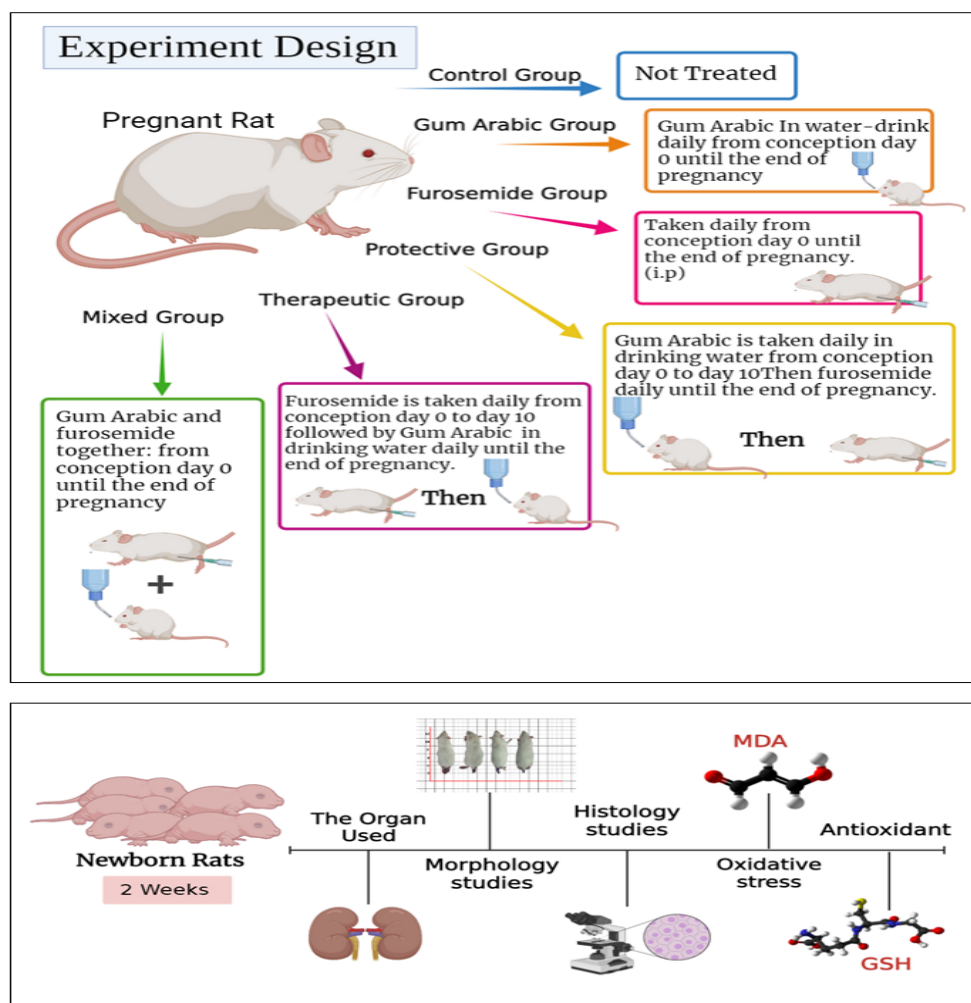
Figure 5 – Design of the experiment

Biochemical analysis. Malondialdehyde (MDA) levels were assessed to evaluate the impact of oxidative stress on both kidney tissue and serum. An enzyme-linked immunosorbent assay (ELISA) kit designed for precise quantitative detection of Rat MDA was employed. The procedure involved introducing MDA monoclonal antibodies into pre-coated wells, enabling the addition of MDA. After incubation, a biotin-conjugated anti-Rat MDA antibody was introduced and bound to Rat MDA.

Glutathione (GSH) levels were also measured to assess kidney tissue and serum antioxidant levels. In this study, an ELISA kit was utilized to determine the concentration of GSH in the serum and tissue of the rats.

Statistical analysis. Statistical analysis involved the calculation of the mean values for both the control group and the treatment groups. Furthermore, the

standard deviation of these means was determined, and a T-test was performed at a significance level of 5% to assess the statistical significance of observed differences. The statistically significant data ($P < 0.05$) compared to the control group were denoted as "a," while statistically significant data ($P < 0.05$) compared to the furosemide group were denoted as "b."

Results and discussion

Morphological studies. Mortality and survival rate. Table 1 shows the number of births, deaths, and lived births as well as the mortality rate for the control group, the Arabic gum group, the furosemide group, the preventive group, the treatment group, and the mixed group at the age of two weeks. The data in Table 1 revealed an elevated mortality rate

within the mixed group compared to the control group. The results also indicated no statistically significant difference in the total number of deliveries among the GA, furosemide, protective, therapeutic, and mixed groups compared to the control group (Figure 6).

Table 1 – The number of births, deaths, lived births, and mortality rates for all groups at the age of two weeks

Group number	Number of births	Number of deaths	Number of live births	Mortality rate (%)
G1	26	0	26	0
G2	26	0	26	0
G3	25	0	25	0
G4	27	0	27	0
G5	24	9	15	37.5
G6	24	4	20	16
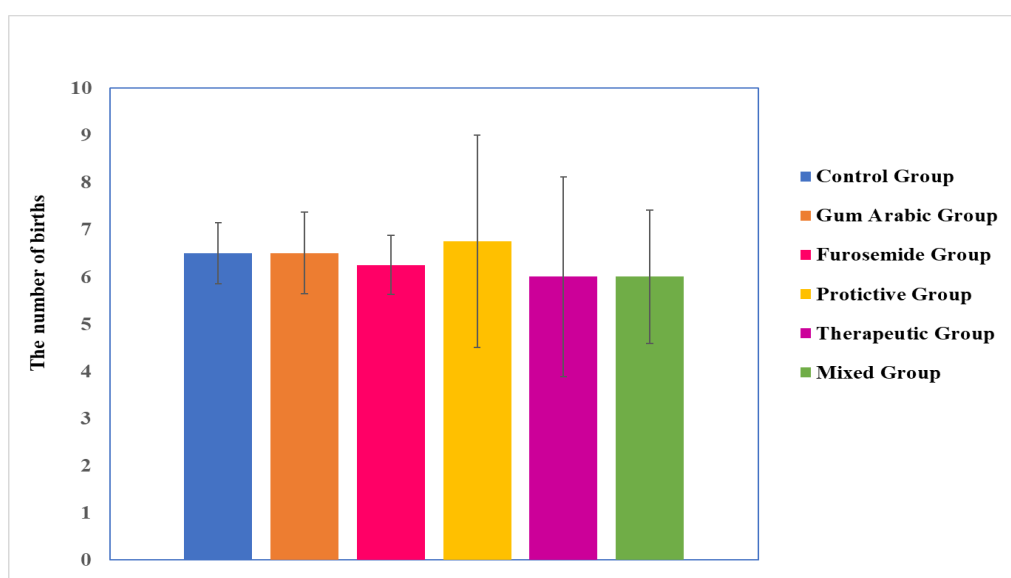
Figure 6 – The number of births for all studied groups

Malformations. In the context of our study, several noteworthy observations were made concerning malformations associated with different treatment groups. Firstly, an increased incidence of preterm labor was observed in both the furosemide and the mixed treatment groups, indicating a potential association between these treatments and the risk of preterm birth. Secondly, delayed hair growth was noted in individuals receiving furosemide and mixed treatment, suggesting a potential adverse effect on fetal development. Moreover, infants born to mothers in the furosemide and mixed groups exhibited smaller birth sizes than those in the control group, indicating a possible impact on fetal growth. Additionally, our findings indicated an elevated occurrence of bleeding in

pregnant mothers within the preventive group, warranting further investigation into the safety and efficacy of the preventive treatment. Lastly, it is crucial to highlight the unfortunate occurrence of maternal mortality in the therapeutic group.

Body weight and body length. Compared to the control group, the weight of newborn rats in the GA and the treatment groups increased significantly in the second week, whereas weight decreased significantly in the furosemide and mixed groups.

The group administered with GA and the therapeutic group displayed a notable and statistically significant increase in body weight. In contrast, compared to the furosemide-treated group, the mixed group exhibited a significant reduction in body weight (Figure 7).
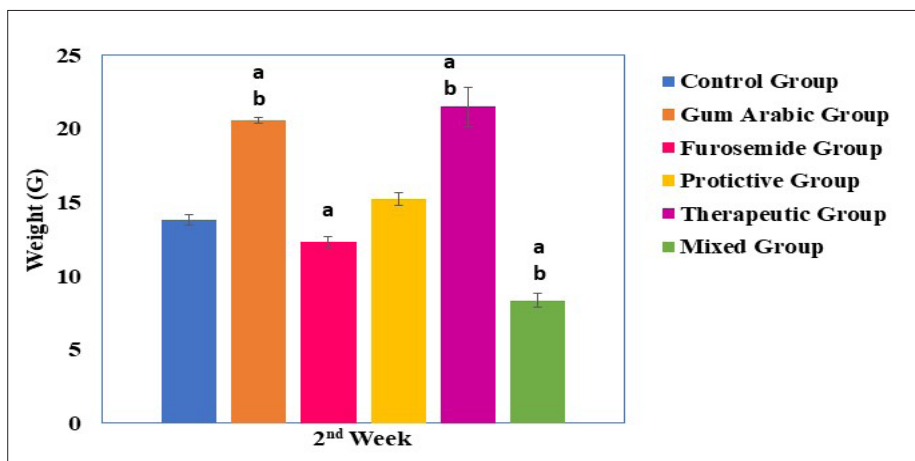
Figure 7 – The newborn rats' body weight (g) for all studied groups

In the second week of the study, noteworthy findings emerged regarding the length measurements among the various groups. The group administered with GA displayed a statistically significant increase in length. In contrast, both the group treated with furosemide and the mixed group exhibited significant decreases in length compared to the control group.

Furthermore, the group subjected to GA treatment, as well as both the preventive and treatment groups, exhibited statistically significant increases in length. Conversely, a significant decrease in height was observed in the mixed group when compared to the cohort receiving furosemide treatment (Figure 8).
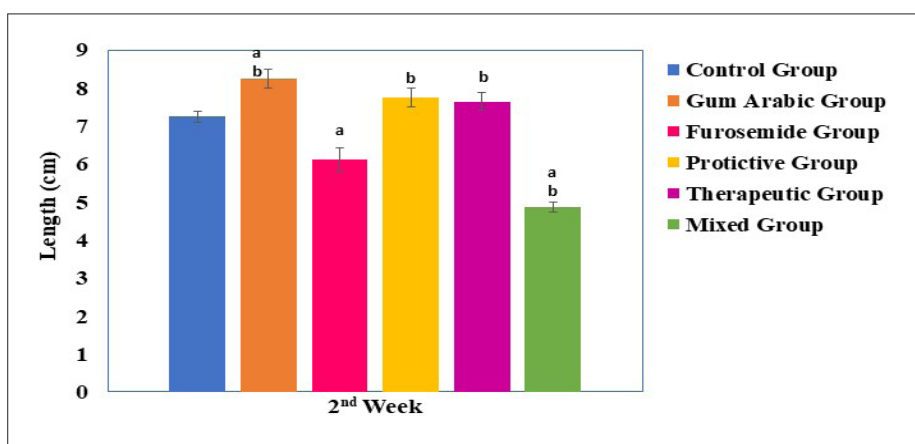
Figure 8 – The newborn rats' length (cm) for all studied groups

Figure 9 shows photographs of rats from all studied groups with their corresponding body weights and body lengths after two weeks.

Kidney weight. The study's findings indicated a statistically significant increase in kidney weight in both the group treated with GA and the therapeutic group. In contrast, a notable decrease in kidney weight was recorded in the mixed group compared to the control group. Furthermore, the study revealed

a substantial increase in kidney weight within the group that received GA treatment and the therapeutic group. Conversely, a significant decrease in kidney weight was observed in the mixed group compared to the group subjected to furosemide treatment (Figure 10).

Figure 11 shows photographs representing the change in the kidney weights among all studied groups after two weeks.
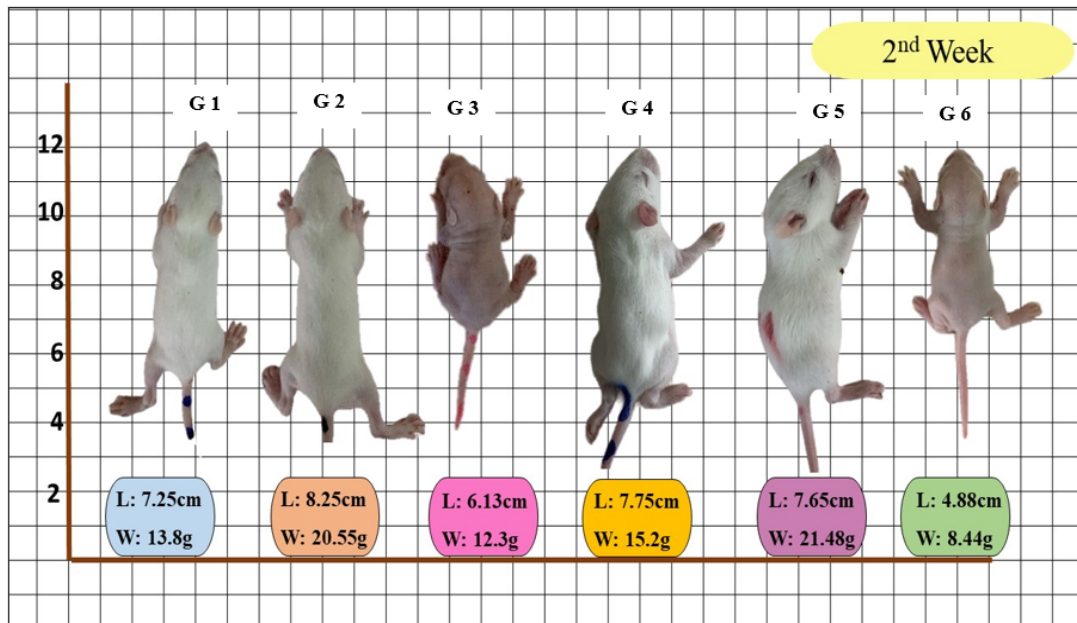
Figure 9 – Photographs of rats from all studied groups after two weeks
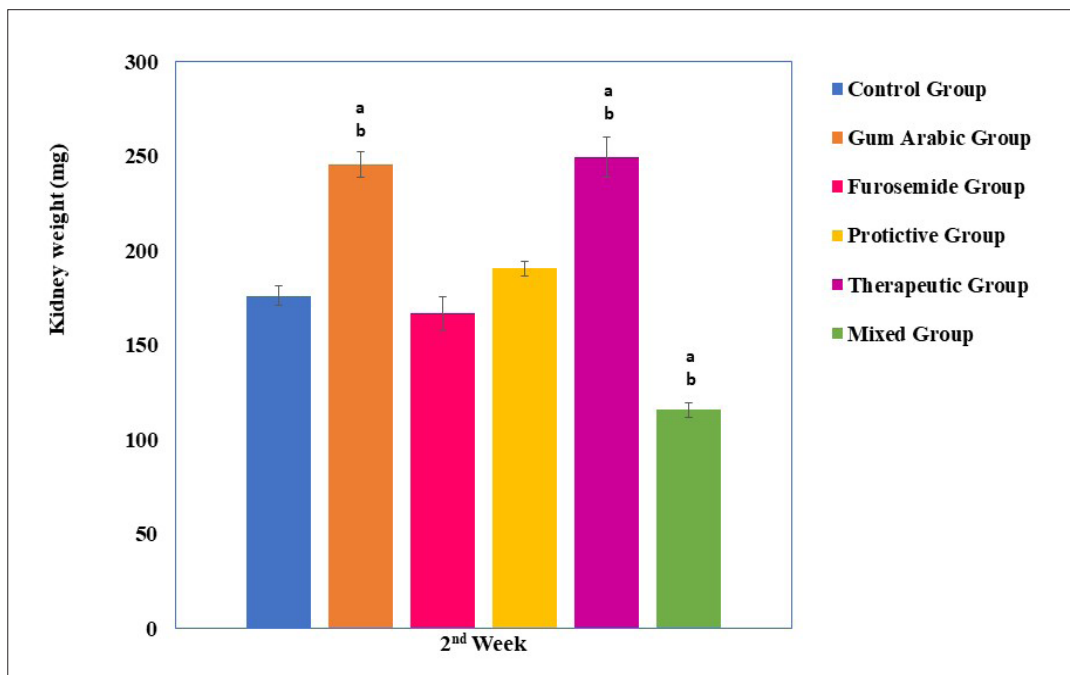

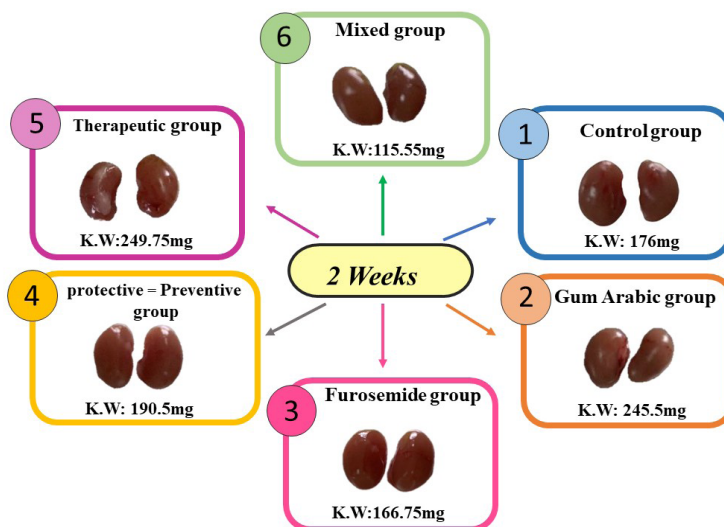**Figure 10** – The newborn rats' kidney weight (mg) for all studied groups

Figure 11 – Photographs of the kidneys of rats from all studied groups after the two weeks.

Histological studies. The kidney cortex of newborn rats in the control group showed normal kidney structure and tissue and a complete absence of interstitial fibrosis. The normal histological appearance of the kidney consists of the glomerulus, tufts of the glomerulus, Bowman's capsules, proximal tubule, and distal tubules (Figure 12-1). The renal cortex of the kidneys of newborn rats in the GA group was not damaged by the treatment with GA and was similar to the control group in histological structure (Figure 12-2). In contrast, the renal cortex of newborn rats in the furosemide group exhibited several notable histological changes associated with administering furosemide. These changes included the dilation of Bowman's space and increased cell pigmentation intensity. Significantly, the impact on the glomeruli exceeded that on the renal tubules, characterized by severe glomerular shrinkage, resulting in a loss of both structural integrity and function. Conversely, the effect on the renal tubules appeared relatively straightforward, with observable spaces between the tubules and the presence of fatty droplets. This appearance of droplets is a commonly recognized indicator of tissue damage in many tissues (Figure 12-3). In contrast, rats in the protective group exhibited signs of histological improvement, as evidenced by the relatively healthier appearance of the renal tubules. Notably, the damage manifested as a reduced Bowman's area size and a moderate separation of the glomerular tufts (Figure 12-4).

The rats displayed histological improvement in the therapeutic group, notably in preserving glomerular integrity. The Bowman's space exhibited a crescent shape, and the glomerular tufts remained intact. However, indications of damage were observed at the level of the renal tubules, characterized by cytoplasmic decomposition and the presence of hemorrhage (Figure 12-5).

In contrast, the rats in the mixed group exhibited distinct histological differences in their kidney tissues. Notably, there were alterations in the shape of the glomeruli, with evidence of atrophy and fragmentation in some of the glomerular tufts. A noticeable degree of cytoplasmic decomposition was observed at the renal tubule level (Figure 12-6).

Note: (1) Control group, showing normal kidney architecture and histology. (2) Gum Arabic group, showing normal kidney architecture and histology. (3) Furosemide group, showing several effects on the histological structure of the kidney: (➡) space expansion in Bowman space, (➡) the intensity of the pigmentation of the cells, (★) the appearance of spaces between the installation of renal tubules, and (<) severe shrinkage of many glomeruli and pyknotic. (4) Preventive group, an effect appeared on the histological structure of the kidney. (*) Relative decrease in space around the glomerulus (Bowman's distance). Many glomeruli and renal tubules appear intact. (5) Therapeutic group, the glomeruli appear intact, the crescent-shaped void appears and the tufts intact, damage appears on the tubes, (0) where cytoplasmic decomposition appears, and (□) hemorrhage. (6) Mixed group, several effects appeared on the histological structure of the kidney. (>) A few of the glomeruli showed shrinkage and nuclear atrophy, and many of them were intact. (➡) Protrusion of the nuclei into the tubular cavity and (*) relative fragmentation of some of the glomerulus tufts.
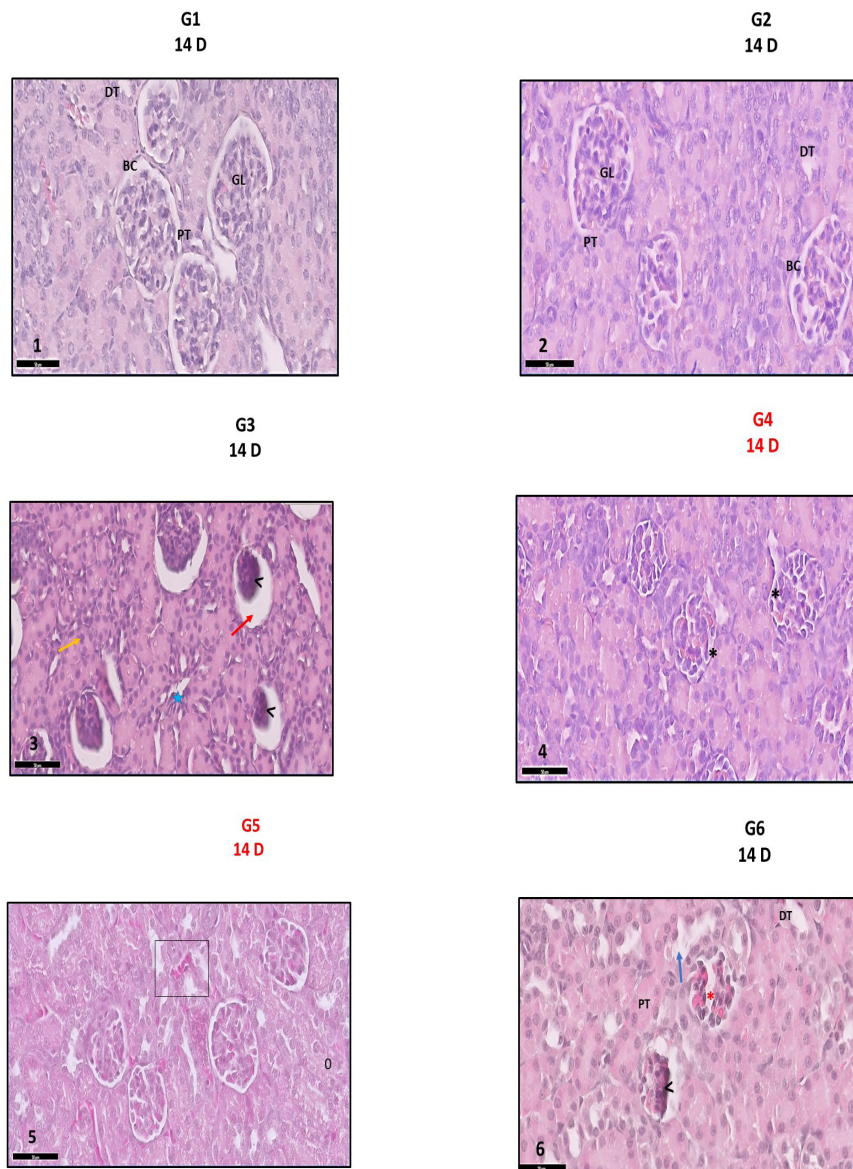
Figure 12 – Representative photograph of renal tissue under a light microscope of newborn rats
at age 2 weeks. Hematoxylin and eosin staining (H&E). Scale bars: 50 μm

Malondialdehyde (MDA). The study's findings revealed noteworthy variations in the serum MDA levels across the different treatment groups during the second week of observation. Specifically, a significant elevation in serum MDA levels was observed in the group receiving furosemide treatment and in the preventive and therapeutic groups compared to the control group. Conversely, a significant reduction in serum MDA levels was noted in the group treated with GA, along with the preventive, therapeutic, and mixed groups, when contrasted with the group subjected to furosemide treatment (Figure 13).

The study's findings unveiled notable alterations in tissue MDA levels among the various treatment groups during the second week of investigation. Specifically, compared to the control group, a significant increase in tissue MDA levels was observed in the group treated with furosemide and the preventive group. In contrast, there was a significant reduction in tissue MDA levels noted in the mixed group compared to the control group.

Additionally, the results indicated a significant decrease in tissue MDA levels in the GA, preventive, therapeutic, and mixed groups during the second week compared to the group treated with furosemide (Figure 14).

Glutathione (GSH). The findings indicated a notable reduction in serum GSH levels during the second week in the group administered furosemide and in the preventive and therapeutic groups compared to the control group. Conversely, the results documented a substantial elevation in serum GSH levels within the group treated with GA, the

preventive group, the therapeutic group, and the mixed group during the second week when contrasted with the furosemide-treated group (Figure 15).

The findings revealed a marked reduction in tissue GSH levels during the second week in the group treated with furosemide and in the preventive and therapeutic groups compared to the control group. In contrast, a significant increase in tissue GSH levels was observed in the group treated with GA, the preventive group, the therapeutic group, and the mixed group during the second week compared to the furosemide-treated group (Figure 16).
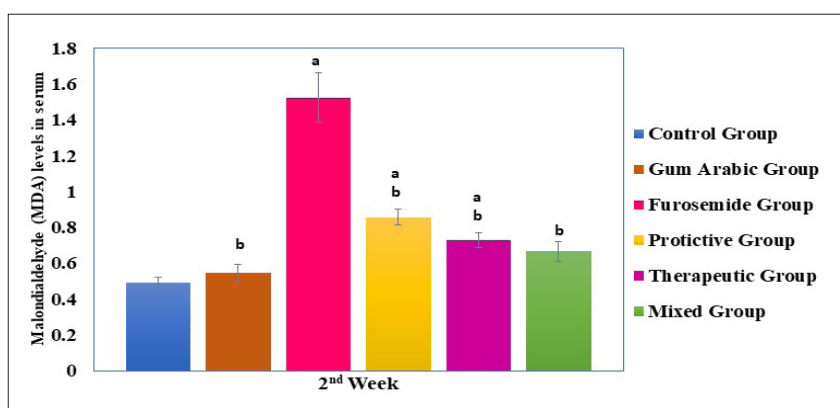
Figure 13 – The malondialdehyde (nmol/ml) levels in the serum
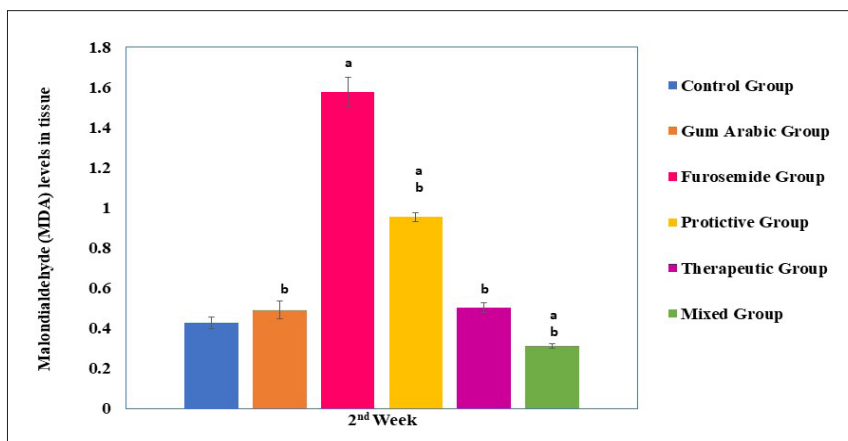of newborn rats for all studied groups.

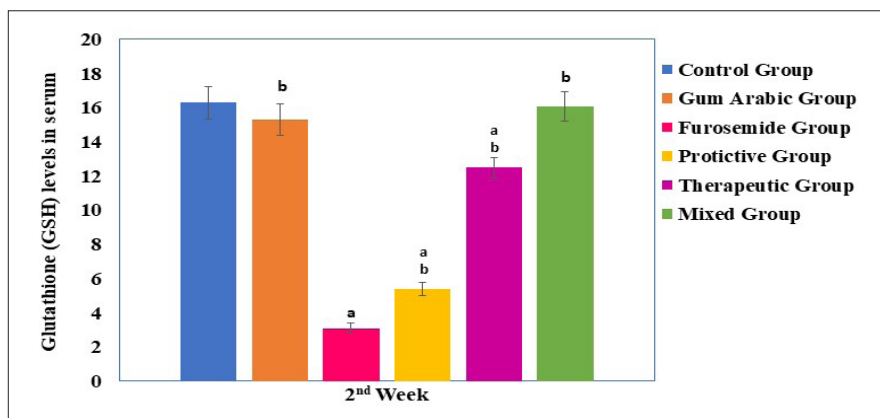**Figure 14 –** All studied groups' malondialdehyde levels
in newborn rats' kidney tissue.

Figure 15 – The glutathione level in the serum of newborn rats for all studied groups
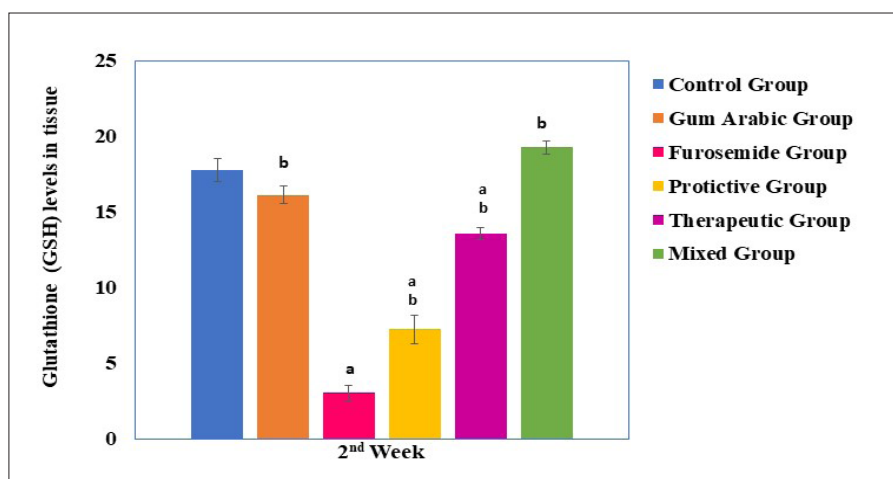

Figure 16 – Glutathione levels in the kidneys of newborn rats for all studied groups

As demonstrated in a rat model investigation conducted by Rokutan and colleagues [26], chronic administration of furosemide is associated with fatal outcomes. Furthermore, in a study involving elderly patients, furosemide contributed to increased mortality rates, thus underscoring the significance of this factor for healthcare providers [27].

In alternative investigations, loop diuretics, notably furosemide, have been employed during pregnancy to address conditions such as pulmonary edema, severe hypertension in the context of chronic kidney disease, or congestive heart failure, despite the associated risk of hyperbilirubinemia in newborns. Additionally, it has been demonstrated that loop diuretics can traverse into breast milk, potentially impeding breastfeeding [28].

Animal reproduction investigations have revealed unfavorable fetal effects when diuretics, specifically

furosemide, are administered during pregnancy. The findings indicated a higher incidence of premature birth within both the furosemide and mixed groups, in contrast to the control group. Additionally, instances of maternal bleeding were observed in the preventive group.

Nakatsuka and colleagues, in their study from 1988 [29], reported that administering furosemide via intraperitoneal injection to pregnant rats leads to the relaxation of uterine muscles, potentially resulting in various fetal deformities. Furthermore, the administration of diuretics during pregnancy was found to be linked to differences in fetal birth weight and the incidence of preterm delivery [30].

The present investigation revealed a significant reduction in both body weight and length during the second week in the group treated with furosemide compared to the control group.

Our findings align with prior research [13, 31], which reported that the administration of furosemide reduced body weight and decreased extracellular water due to increased diuresis. This is consistent with the observed positive correlation between the decrease in extracellular water and body weight. Additionally, our results concur with the findings from other studies [32, 33].

The study demonstrated a noteworthy increase in both body weight and length during the second week in the group treated with GA, in contrast to the control group. This finding is consistent with the results reported in another study [34].

The study revealed a substantial increase in kidney weight during the second week in the group treated with GA compared to the control group.

Upon histological examination of the kidney composition in the control group, it is evident that the cortex region contains numerous renal or urinary corpuscles and renal tubules. Each renal corpuscle comprises a glomerulus, characterized by a tuft of capillaries resting on the basement membrane of the glomerulus and Bowman's capsule. The Bowman's capsule consists of two distinct layers: the outer parietal layer, lined with simple flat squamous cells featuring thin nuclei and a delicate basement membrane, and the inner visceral layer. The visceral layer is lined with large circular cells containing prominent, circular, basal-shaped nuclei known as foot cells resting on the outer surface of the glomerulus's capillaries. The space between these two layers, the parietal and visceral layers, is termed the urothelial space. Within the cortical region, the urinary tubules can be differentiated into proximal convoluted tubules, characterized by cuboidal cells with central nuclei and a narrow lumen, and distal convoluted tubules. The distal convoluted tubules are lined by cuboidal cells with apical nuclei, and their lumens appear broader and more irregular. These findings follow prior observations reported in other studies [35-37].

The tissue composition in the group treated with GA exhibited similarities to that of the control group, which aligns with the findings reported in reference [38].

The tissues in the group treated with furosemide exhibited notable effects on the histological structure of the kidney. These effects included the expansion of Bowman's space and an increase in cell pigmentation intensity. The impact on the glomeruli was more pronounced than the renal tubules, as there was significant shrinkage of the glomeruli, resulting in a loss of their normal shape and function. The

effect on the tubules was relatively straightforward, characterized by the presence of spaces between the renal tubules and the appearance of fatty droplets. These findings are consistent with the observation that furosemide adversely affects organs, particularly the kidneys.

Dilken et al. 2023, as reported in their study [39], asserted that furosemide induces damage to both the renal cortex and medulla, elevates the risk of renal injury and diminishes oxygen levels even under control conditions.

In a study conducted by Araujo et al. in 2020 [40], they documented that furosemide impacts the renal tubules of rats. This effect can be elucidated by considering that the thin tubule represents the location of the highest flow resistance within the Henle loop.

The findings from both the preventive and therapeutic groups indicated that renal tissue was affected to a lesser extent than the group treated with furosemide yet to a greater extent than the group treated with GA.

According to Hammad and colleagues in 2019 [41], the impact of GA on inflammatory markers and oxidative stress was associated with robust histological protective attributes.

As reported by Said and colleagues in 2019 [42], the utilization of GA effectively alleviated renal damage. This beneficial effect can be attributed to the antioxidant and anti-inflammatory properties of GA.

In his 2019 review [43], Jaafar reported that GA had substantiated its pharmacological effects and therapeutic advantages in numerous studies conducted across various diseases.

The preventive effect of GA on renal function significantly reduces renal function markers in patients with diabetic renal failure and exerts a direct antioxidant effect [44].

In the mixed group (comprising treatment with both GA and furosemide simultaneously), noticeable differences were observed in the shape of the glomeruli, including atrophy and fragmentation of certain glomerular tufts. Furthermore, relative cytoplasmic degeneration was noted at the renal tubule level. However, these effects were milder than those observed in the group treated with furosemide alone and more pronounced than those observed in the preventive and therapeutic groups.

In another study, it was reported that GA helps preserve the normal structure of the renal cortex, except for some tubules showing degeneration and expansion [42].

MDA is a critical marker for assessing oxidative levels in biological fluids and tissues. It is an organic

compound considered one of the foremost indicators of lipid peroxidation, particularly polyunsaturated fatty acids [45].

The findings revealed a substantial increase in MDA levels in both the kidney tissues and serum of the group treated with furosemide compared to the control group.

As elucidated by Silbert and colleagues in their 2019 study [46], furosemide diminishes the metabolic activity in the ascending loop of Henle. This, in turn, can result in an enduring elevation of renal oxidative stress via multiple mechanisms. Furosemide's inhibition of glomerular tubular feedback leads to increased nephron blood flow and filtration, necessitating elevated solute transport. Consequently, the stimulation of renin release may further contribute to oxidative stress. Therefore, it is affirmed that using furosemide acts as a catalyst for oxidative stress.

Studies have consistently demonstrated that urinary furosemide administration increases renal oxidative stress in all patients, with the most severe cases of acute kidney injury (AKI) exhibiting the most significant increase. Notably, in this study, the group treated with GA showed no statistically significant change in MDA levels in the second week following birth compared to the control group.

GSH is a significant antioxidant enzyme within the body, serving as a vital defender of cells. It plays a pivotal role in facilitating the conversion of GSH from its oxidized form to the reduced form, thereby contributing to apoptosis regulation and cell development. Furthermore, GSH assumes a crucial protective function in the detoxification processes in various organs, including the liver, kidneys, lungs, intestines, and epithelia. The GSH redox cycle offers valuable insights into the mechanisms underlying injuries caused by toxic substances, diseases, or the regulation of redox-sensitive pathways within organisms [47-49].

The results indicate a significant decrease in the level of GSH in both kidney tissue and serum of the furosemide-treated group compared to the control group. However, in the group treated with GA in this study, no statistically significant change was observed in GSH levels during the second week following birth compared to the control group.

In another study [50], it was demonstrated that the treatment with GA at doses of 2.5%, 5%, and 10% w/v in water did not result in any significant changes in the concentrations of GSH. This suggests that GA does not exert an antioxidant effect in the tissues of both treated and normal rats. Therefore, its potential beneficial effect in patients with chronic renal failure is unlikely to be attributed to an antioxidant action.

Ahmed et al.'s perspective, as presented in reference [51], contradicts the previously mentioned finding. According to Ahmed et al. 2015, the use of GA to prevent nephrotoxicity in chronic kidney disease is based on the belief that it contains a high percentage of antioxidants. This difference in interpretation highlights the ongoing debate and research regarding the exact mechanisms of GA's effects on kidney health.

Conclusion

A high dose of furosemide can result in toxicity, leading to renal and histopathological changes and disturbances in renal function tests in newborn rats. However, the administration of gum Arabic as a protective and therapeutic agent mitigates the toxic manifestations induced by furosemide.

Acknowledgments

References

1. Schetz, M., Loop Diuretics, in Critical Care Nephrology. 2009, Elsevier. p. 547-551.

2. Brater, D.C., (2000).Pharmacology of Diuretics. The American Journal of the Medical Sciences, 319(1): p. 38-50.DOI: 10.1016/s0002-9629(15)40678-0.

3. Bagshaw, S.M., R. Bellomo, and J.A. Kellum, (2008).Oliguria, volume overload, and loop diuretics. Critical Care Medicine, 36(Suppl): p. S172-S178.DOI: 10.1097/ccm.0b013e318168c92f.

4. Wang, J., et al., (2012).Hemodynamic Effects of Furosemide on Renal Perfusion as Evaluated by ASL-MRI. Academic Radiology, 19(10): p. 1194-1200.DOI: 10.1016/j.acra.2012.04.021.

5. Hamishehkar, H., et al., (2017).The Effect of Furosemide on the Level of Neutrophil Gelatinase-associated Lipocalin in Critically Hospitalized Patients with Acute Kidney Injury. Indian journal of critical care medicine : peer-reviewed, official publication of Indian Society of Critical Care Medicine, 21(7): p. 442-447.DOI: 10.4103/ijccm. IJCCM_93_17.

6. McMahon, B.A. and L.S. Chawla, (2021). The furosemide stress test: current use and future potential. Renal failure, 43(1): p. 830-839.DOI: 10.1080/0886022X.2021.1906701.

7. Ho, K.M. and B.M. Power, (2010).Benefits and risks of furosemide in acute kidney injury. Anaesthesia, 65(3): p. 283-293.DOI: 10.1111/j.1365-2044.2009.06228.x.

8. Grogono, J.C., et al., (2018).Inhaled furosemide for relief of air hunger versus sense of breathing effort: a randomized controlled trial. Respiratory research, 19(1): p. 181-181.DOI: 10.1186/s12931-018-0886-9.

9. Mariano, F., et al., (2019).Furosemide as a functional marker of acute kidney injury in ICU patients: a new role for an old drug. Journal of Nephrology, 32(6): p. 883-893.DOI: 10.1007/s40620-019-00614-1.

10. Abo Zaid, M.H., et al., (2023).Use of green fluorescent nano-sensors for the determination of furosemide in biological samples and pharmaceutical preparations. BMC chemistry, 17(1): p. 25-25.DOI: 10.1186/s13065-023-00937-y.

11. Bagshaw, S.M., et al., (2010).The SPARK Study: a phase II randomized blinded controlled trial of the effect of furosemide in critically ill patients with early acute kidney injury. Trials, 11: p. 50-50. DOI: 10.1186/1745-6215-11-50.

12. Lee, T.H., et al., (2021).Diuretic effect of co-administration of furosemide and albumin in comparison to furosemide therapy alone: An updated systematic review and meta-analysis. PloS one, 16(12): p. e0260312-e0260312.DOI: 10.1371/journal.pone.0260312.

13. Mose, F.H., et al., (2021).Effect of furosemide on body composition and urinary proteins that mediate tubular sodium and sodium transport-A randomized controlled trial. Physiological reports, 8(24): p. e14653-e14653.DOI: 10.14814/phy2.14653.

14. Carone, L., et al., (2016).Furosemide. Journal of Pain and Symptom Management, 52(1): p. 144-150.DOI: 10.1016/j.jpainsymman.2016.05.004.

15. Sawada, Y., et al., (2019).Effect of furosemide on muscle cramps in patients with liver cirrhosis. Journal of Gastroenterology and Hepatology, 35(1): p. 76-81.DOI: 10.1111/jgh.14820.

16. Khan, T.M., R. Patel, and A.H. Siddiqui, Furosemide. 2022: StatPearls Publishing, Treasure Island (FL).

17. Jackson, W., et al., (2018).Association between furosemide in premature infants and sensorineural hearing loss and nephrocalcinosis: a systematic review. Maternal health, neonatology and perinatology, 4: p. 23-23.DOI: 10.1186/s40748-018-0092-2.

18. Jarrar, A.H., et al., (2021).The Effect of Gum Arabic (Acacia Senegal) on Cardiovascular Risk Factors and Gastrointestinal Symptoms in Adults at Risk of Metabolic Syndrome: A Randomized Clinical Trial. Nutrients, 13(1): p. 194.DOI: 10.3390/nu13010194.

19. Ashour, M.A., et al., (2022).A Review on the Main Phytoconstituents, Traditional Uses, Inventions, and Patent Literature of Gum Arabic Emphasizing Acacia seyal. Molecules (Basel, Switzerland), 27(4): p. 1171.DOI: 10.3390/molecules27041171.

20. Prasad, N., et al., (2022).Gum arabic – A versatile natural gum: A review on production, processing, properties and applications. Industrial Crops and Products, 187: p. 115304.DOI: 10.1016/j.indcrop.2022.115304.

21. Musa, H.H., A.A. Ahmed, and T.H. Musa, Chemistry, Biological, and Pharmacological Properties of Gum Arabic, in Bioactive Molecules in Food. 2019, Springer International Publishing. p. 797-814.

22. Verma, C. and M.A. Quraishi, (2021).Gum Arabic as an environmentally sustainable polymeric anticorrosive material: Recent progresses and future opportunities. International Journal of Biological Macromolecules, 184: p. 118-134.DOI: 10.1016/j.ijbiomac.2021.06.050.

23. Dakhil, A.S. and L. Alhasan, (2020).THE POSSIBLE PROTECTIVE EFFECTS OF GUM ARABIC IN KIDNEY INJURY INDUCED BY ADENINE. Plant Archives, 20(2): p. 4142-4149.

24. Ali, B.H., et al., (2020).Gum arabic reduces inflammation, oxidative, and nitrosative stress in the gastrointestinal tract of mice with chronic kidney disease. Naunyn-Schmiedeberg's Archives of Pharmacology, 393(8): p. 1427-1436.DOI: 10.1007/s00210-020-01844-y.

25. Casanova, A.G., et al., (2021).The furosemide stress test and computational modeling identify renal damage sites associated with predisposition to acute kidney injury in rats. Translational Research, 231: p. 76-91.DOI: 10.1016/j.trsl.2020.11.011.

26. Rokutan, H., et al., (2012).Furosemide induces mortality in a rat model of chronic heart failure. International Journal of Cardiology, 160(1): p. 20-25.DOI: 10.1016/j.ijcard.2011.03.005.

27. Rodríguez-Molinero, A., et al., (2022).Mortality in Elderly Patients Taking Furosemide: Prospective Cohorts Study. International journal of hypertension, 2022: p. 4708259-4708259.DOI: 10.1155/2022/4708259.

28. Ghanem, F.A. and A. Movahed, (2008).Use of Antihypertensive Drugs during Pregnancy and Lactation. Cardiovascular Drug Reviews, 26(1): p. 38-49.DOI: 10.1111/j.1527-3466.2007.00036.x.

29. Nakatsuka, T., (1988).Role of myometrial constriction in the induction of wavy ribs in rat fetuses. Teratology, 37(4): p. 329-334.DOI: 10.1002/tera.1420370406.

30. Bozzo, P. and A. Einarson, (2009).Use of diuretics during pregnancy. Canadian Family Physician, 55(1): p. 44-45.

31. Murugan, P.S. and G.S. Selvam, (2014). Furosemide and Potassium Chloride-induced Alteration in Protein Profile of Left Ventricle and its Associated Risk for Sudden Cardiac Death. Toxicology international, 21(1): p. 1-7.DOI: 10.4103/0971-6580.128781.

32. Lee, C.-T., et al., (2007).Effects of furosemide on renal calcium handling. American Journal of Physiology-Renal Physiology, 293(4): p. F1231-F1237.DOI: 10.1152/ajprenal.00038.2007.

33. Dussol, B., et al., (2012).A pilot study comparing furosemide and hydrochlorothiazide in patients with hypertension and stage 4 or 5 chronic kidney disease. Journal of clinical hypertension (Greenwich, Conn.), 14(1): p. 32-37.DOI: 10.1111/j.1751-7176.2011.00564.x.

34. Nasir, O., (2013).Renal and Extrarenal Effects of Gum Arabic (<i>Acacia Senegal</i>) – What Can be Learned from Animal Experiments? Kidney and Blood Pressure Research, 37(4-5): p. 269-279.DOI: 10.1159/000350152.

35. Verlander, J.W., (1998).Normal Ultrastructure of the Kidney and Lower Urinary Tract. Toxicologic Pathology, 26(1): p. 1-17.DOI: 10.1177/019262339802600101.

36. Zhuo, J.L. and X.C. Li, (2013).Proximal nephron. Comprehensive Physiology, 3(3): p. 1079-1123.DOI: 10.1002/cphy.c110061.

37. Dixit, S.G., et al., (2013).To study the effect of monosodium glutamate on histomorphometry of cortex of kidney in adult albino rats. Renal Failure, 36(2): p. 266-270.DOI: 10.3109/0886022x.2013.846865.

38. Ali, B.H., et al., (2013).New model for adenine-induced chronic renal failure in mice, and the effect of gum acacia treatment thereon: Comparison with rats. Journal of Pharmacological and Toxicological Methods, 68(3): p. 384-393.DOI: 10.1016/j.vascn.2013.05.001.

39. Dilken, O., et al., (2023).Furosemide exacerbated the impairment of renal function, oxygenation and medullary damage in a rat model of renal ischemia/reperfusion induced AKI. Intensive care medicine experimental, 11(1): p. 25-25.DOI: 10.1186/s40635-023-00509-3.

40. Araujo, M., et al., (2020).Renal Nerve Deafferentation Attenuates the Fall in GFR during Intravenous Infusion of Furosemide in Anesthetized Rats. Kidney and Blood Pressure Research, 45(1): p. 70-83.DOI: 10.1159/000504223.

41. Hammad, F.T., et al., (2019).The Effect of Arabic Gum on Renal Function in Reversible Unilateral Ureteric Obstruction. Biomolecules, 9(1): p. 25.DOI: 10.3390/biom9010025.

42. Said, A.M., S.A.E. Atwa, and O.A. Khalifa, (2019).Ameliorating effect of gum arabic and lemongrass on chronic kidney disease induced experimentally in rats. Bulletin of the National Research Centre, 43(1).DOI: 10.1186/s42269-019-0086-x.

43. Jaafar, N.S., (2019).Clinical effects of Arabic gum (Acacia): A mini review. Iraqi Journal of Pharmaceutical Sciences (P-ISSN: 1683 – 3597 , E-ISSN : 2521 – 3512), 28(2): p. 9-16.DOI: 10.31351/vol28iss2pp9-16.

44. Ali Alshehry, G., (2022).The Role of Gum Arabic for a Protective Kidney Dysfunction Induced Gentamicin on Diabetes Rats. Advances in Materials Science and Engineering, 2022: p. 1-8.DOI: 10.1155/2022/8617445.

45. Roxana-Nicoleta, V.-N. and M. Marius, (2019).Side comparation of two methods for quantifying malondialdehyde levels in animal tissue extracts. Journal of Experimental and Molecular Biology, 20(4): p. 61-66.

46. Silbert, B.I., et al., (2017).Does Furosemide Increase Oxidative Stress in Acute Kidney Injury? Antioxidants & Redox Signaling, 26(5): p. 221-226.DOI: 10.1089/ars.2016.6845.

47. Tipple, T.E. and L.K. Rogers, (2012). Methods for the determination of plasma or tissue glutathione levels. Methods in molecular biology (Clifton, N.J.), 889: p. 315-324.DOI: 10.1007/978-1-61779-867-2_20.

48. Adem, S. and M. Ciftci, (2016).Purification and biochemical characterization of glucose 6-phosphate dehydrogenase, 6-phosphogluconate dehydrogenase and glutathione reductase from rat lung and inhibition effects of some antibiotics. Journal of Enzyme Inhibition and Medicinal Chemistry, 31(6): p. 1342-1348.DOI: 10.3109/14756366.2015.1132711.

49. Jawad, Z.J.M. and D.A. Hussien, (2018). Biochemical changes of serum Glutathione and Malondialdehyde by Paraqu at and Olive Oil on Adult Male Reproductive system of albino Rats. International Journal of Biosciences (IJB), 13(04): p. 55-60.DOI: 10.12692/ijb/13.4.55-60.

50. Ali, B.H., (2004).Does Gum Arabic Have an Antioxidant Action in Rat Kidney? Renal Failure, 26(1): p. 1-3.DOI: 10.1081/jdi-120028536.

51. Ahmed, A.A., et al., (2015).Gum Arabic extracts protect against hepatic oxidative stress in alloxan induced diabetes in rats. Pathophysiology, 22(4): p. 189-194.DOI: 10.1016/j.pathophys.2015.08.002.

Sh.K. Bakhtiyarova[1]* , Y.K. Makashev[1] , B.I. Zhaksymov[1] ,

Y.E. Makashev[1] , A.M. Kalekeshov[1] , A.B. Zhunusova[1] ,

U.N. Kapysheva[1] , I.S. Tazhibaev[1] , A.N. Zhiengazina[2] ,

Zh.N. Zhalimbetova[2]

[1] Institute of Genetics and Physiology, Almaty, Kazakhstan
[2] National Center for Sports Medicine and Rehabilitation, Almaty, Kazakhstan
*e-mail: bifara.66@mail.ru

Reserve capabilities of the cardiorespiratory system in athletes of certain sports under conditions of intense muscular activity

Abstract. This study provides data on the peculiarities of adaptation of the cardiorespiratory system to muscle load in athletes engaged in certain types of martial arts (judo, Thai boxing, MMA, and jiu-jitsu). Changes in physiological indicators such as weight, height, vital capacity, glossopharyngeal inhalation (GI), blood pressure, heart rate, physical performance, endurance according to the physical work capacity test at a heart rate of 170 beats per minute (PWC_{170}) and membrane patch colorimetry (MPC) tests, and heart rate variability are shown, with the calculation of the main indices of the humoral-vegetative balance. The results showed that the vital capacity of the lungs and tidal volume in athletes were 6-8% lower than the required values and corresponded to the "average level" of the functional capabilities of the respiratory system. Calculations of the Skibinsky, Robinson, and Shapovalova indices showed a functional insufficiency in the adaptation of the cardiorespiratory system to physical activity. Against the background of the development of muscle strength functions, indicators of physical performance and endurance of athletes (PWC_{170} and maximum oxygen consumption (MOC) tests) turned out to be "below average" levels in absolute and relative values. To identify hidden functional disorders of the cardiovascular system, variability studies were conducted on heart rate (HRV), the results of which showed that 60% of athletes (in all groups), regardless of the type of sport, had a good level of functional capability of the cardiovascular system. The remaining athletes revealed a low level of adaptation mechanisms and functional state of the cardiorespiratory systems, the reason for which was insufficient training of the body of endurance athletes. Research has shown that athletes who have not previously engaged in special training for endurance and increased performance need to develop cardiorespiratory capabilities that ensure the activity of metabolic processes and replenish energy reserves for successful sports activities.
Key words: athletes, health assessment, physical performance, endurance, cardiorespiratory system, heart rate variability.

Introduction

The sports activity of any athlete depends on the development of such qualities as endurance, strength and speed of reaction. The focus of training cycles is based on various combinations of three criteria: the predominant power of loads (maximum, submaximal, moderate), the predominant cyclicity and the predominant development of speed and strength in the athlete [1]. At the same time, athletes training in cyclic sports often experience myocardial dystrophy and hypertension due to maximum physical stress,

problems with the musculoskeletal system, and disturbances in homeostasis (tendency to thrombus formation), the cause of which scientists associate with accelerated catabolism of proteins and impaired microcirculation [2]. Very often, researchers associate the causes of diseases in athletes with improper organization of the training process, irrational use of means and methods of physical activity, which leads to overload and overstrain of individual systems and organs [3,4]. As shown in scientific studies by foreign scientists, the physiological reaction to overexertion is expressed at the first stage in a decrease in the athlete's

performance and endurance associated with extreme stress on the cardiorespiratory system and hormonal stress [5-7]. According to the recommendations of many researchers, to identify abnormalities in the functioning of the cardiorespiratory system in young athletes at the initial stage of their sports activity, it is necessary to apply an integrated approach using various functional tests [8]. This approach makes it possible to study the systemic mechanisms of sports activity, identifying the connection between an athlete's performance and the "physiological price" of the sports results achieved by him. It is known that the effectiveness of an athlete's activity is mainly determined by the coordinated work of the heart, breathing and circulatory system, which ensures the supply of oxygen to intensively working organs. The main functional indicators of synchronization of the heart and breathing in humans are health indices, which are informative and characterized by simplicity and accessibility [8-10]. In this study, the health indices of Quetelet, Skibinsky, Robinson, Shapovalova, the life index GI according to vital capacity data were determined, and an analysis of heart rate variability (HRV) was carried out in groups of athletes involved in speed-strength sports [8-11]. These studies substantiate the need for the constant use of a comprehensive assessment of physical activity and the level of adequate preparedness of the cardiorespiratory system of young athletes under conditions of maximum physical activity.

The purpose of the study is to determine the characteristics of physical performance, endurance and hidden forms of functional insufficiency of the cardiorespiratory system in professional young athletes involved in various types of martial arts.

Materials and methods

The subjects of the survey. Athletes involved in martial arts – judo (n=10), MMA (n=10), Muay Thai (n=20) and jiu jitsu (n=20). A total of 60 athletes were examined – 52 boys and 8 girls aged from 17 to 22 years old, training in sports where they do not undergo special endurance training.

Methods of study. Body composition was determined using a professional body composition analyzer (Tanita S S-330 S, TANITA Corporation, Japan). The software Strain Gauge Load Cell recorded data on the physical parameters of the athletes' bodies.

Spirometry. To study the level of somatic health of athletes, the vital capacity of the lungs (VC, ml) was measured on a computer spirometer for functional diagnostics of the state of the lungs (Spiro

Spectrum – 100, Neurosoft, Russia), tidal volume (TR), inspiratory reserve volume (RIV, norm 500-800 ml), expiratory reserve volume (ROV, norm 1500-2000 ml), and vital index (LI) in relation to VC, ml/weight, kg (norm 50-70 ml/kg). The value of proper vital capacity (DVL) was calculated using the following formula: for young men, DVL = height, cm x0.052 – age (years) x0.022-3.6; for girls, VEL = height, cm × 0.041–age (years) x 0.018-2.68 [12]. The volumes of ROvyd and ROVD were considered. The spirography results were also compared with the normative indicators between the groups. It was considered that in healthy young athletes, the spirometry parameters of VC and VC should be more than 80%, but not more than 120% of the normative indicators. An additional examination by specialists is recommended at values less than 70% of the norm additional examination by specialists was recommended.

Indices. The Quetelet index, which characterizes the degree of harmony between physical development and physique, was calculated using the following formula: I kettle = body weight (kg) = body length 2 (m). The Skibinsky index for a reliable assessment of the oxygen supply system was calculated using the formula: I skib = 0.01 VC (ml) × time of held breathing during inspiration (Stange test, sec.): heart rate (beats per minute); The Robinson index was calculated using the formula IRob = (resting heart rate x blood pressure system):100; The Shapovalova Power Index (SPI), which shows the development of speed-strength qualities, is calculated using the formula SPI = body weight (g) x number of bends in 60 sec/height (cm) x 60 [13].

Physical performance test. The PWC_{170} test [14,15] is based on a stepwise bicycle ergometer test on a bicycle ergometer (Seca, Germany) to determine the minimum power of physical activity at a heart rate of 170 beats/min, which reflects the optimal capabilities of the cardiorespiratory system.

Test for maximum oxygen consumption (MOC). The method for determining MOC is directly related to the PWC_{170} value, which makes it possible to determine the absolute values of MIC by the value of PWC_{170} using the formula proposed by V. L. Karpman [16]: MIC = 1.7 PWC_{170} +1240, ml/min and relative values of MIC ml/min/kg, that is, by the ratio of MIC per mass athlete's body in kg.

Heart rate variability (HRV). In order to identify the hidden forms of functional insufficiency of autonomic support based on spectral analysis of HRV [17,18]. A special computer program was used (Poly-Spectrum-8EX, Neurosoft LLC, SP 9441-

017-13218158-2008, Russia). Based on the analysis of the power spectral density of oscillations, the distribution of power was determined depending on the oscillation frequency, which made it possible to quantify the various frequency components of the heart rhythm oscillations and visually (graphically) present the ratios of the different components of the heart rhythm, reflecting the activity of certain parts of the regulatory mechanism. The use of HRV has made it possible to reveal the hidden functional features of the cardiorespiratory system in young athletes.

Results and discussion

To determine the level of health and adaptation of the cardiorespiratory system to muscle load, such physiological indicators as weight, height, VC, LI, BP, heart rate, and heart rate variability before and after exposure to physical activity were determined in athletes and the main health indices were calculated. The results of the studies on the main indicators of lung capacity are presented in the Table 1.

It turned out that the vital capacity of the lungs of judokas, athletes involved in MMA, Muay Thai and jiu-jitsu was within the proper level of lung volume, while the tidal volume indicators exceeded the maximum limit of the physiological norm (0.8 l/min) by 15 -84% (Figure 1).

It was found that the vital capacity of the lungs, inspiratory reserve volume, and tidal volume in judokas and athletes involved in MMA and jiu jitsu were 6-8% lower than the proper level of lung volume, while boxers (Muay Thai) showed 32% more vital capacity (table). The vital index of all athletes, determined by the ratio of vital capacity to body weight (ml/kg), fluctuated within the physiological norm (from 60 to 75 ml/kg). Measuring the vital capacity of the lungs–This study is one of the links in the pulmonary breathing system – the ventilation apparatus. It is the violation of pulmonary ventilation in the vast majority of diseases of the respiratory system that lead to complex pathophysiological disorders and largely determine the clinical picture of pulmonary failure, reducing the functional capabilities of the athlete's body. The study of vital capacity and determination of the vital index (VI) showed an average level of respiratory system development.

Table 1 – Indicators of the functional state of the cardiorespiratory system and its reserves in young athletes involved in various types of martial arts

Indicator/Group	Dzudo (n= 10)	MMA (n= 10)	Muay Thai (n= 20)	Jiu-Jitsu (n= 20)
Weight, kg	67.1± 5.7 *	72.4± 4.2 *	67.4± 3.5	76.1 ± 3.9 *
VC, l	4.17±0.44 *	4.25±0.62	5.06±0.28 *	4.64±0.32
JEL, l	3.90±0.23	3.98±0.22 *	4.57±0.23 **	4.80±0.43 *
%JEL	106.8	105.7	132.0	100.4
Rovdokha, l	1.45±0.07 *	1.51±0.06	2.21±0.20 *	1.98±0.05
Expiratory RO, l	2.09±0.25 *	0.79±0.02 *	1.14±0.04	1.03±0.04
Breathing volume, l	0.92±0.50 *	1.12±0.04	1.19±0.05	1.47±0.06 *
Life index	62.0	58.7	75.0	61.0
Iskib ml/min	25.0	32.0	42.0	32.0
Iketle kg/ ^{m2}	23.2	23.3	23.3	24.8
Ishapov. c.u.	240.0	267.6	241.0	253.3
Irobins. u.u.	87.5	84.6	86.3	91.2
PWC$_{170}$ abs.kgm/min	1056.1±20.5 *	1220.8±43.7 *	1125.3±49.1	1199.2±40.0 *
PWC$_{170}$ relates	15.7	16.9	17.0	16.0
MIC ml/min/kg	3034.5±34.81 *	3314.8±74.2	3220.2±130.8	3264.7±75.1 *
IPC relates.	45.0	45.8	48.6	42.8
* P ≤0.05 between groups of athletes, ** P ≤0.02				
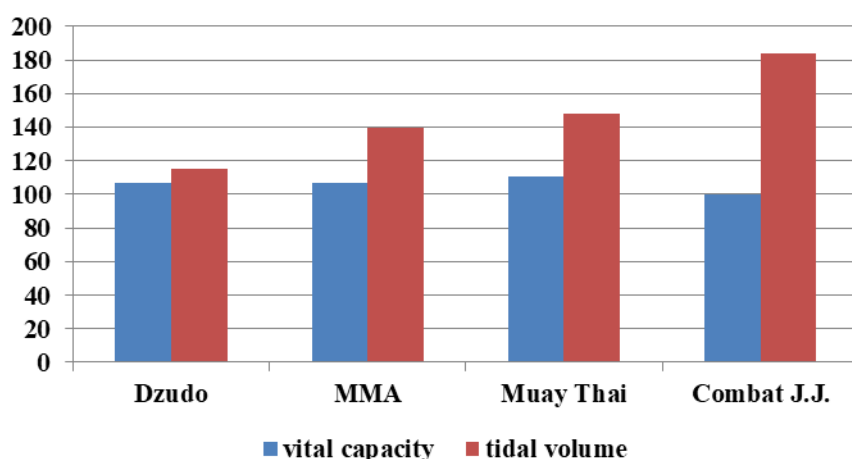
Figure 1 – Indicators of vital capacity of the lungs and tidal volume in athletes of different
types of martial arts (physiological norm -100%)

Calculations of the Quetelet index showed that all athletes had harmonious development and no body mass deficiency was identified. It should be noted that the athletes in the jiu-jitsu group have body mass index values on the border of normal and overweight (24.8 kg/m 2).

Skibinsky index Iskib . Determination of the state of the reserve mechanisms for providing the lungs with oxygen during breath-holding, that is, determination of the Skibinsky index, showed a good level of adaptation of the cardiorespiratory system to physical activity in all athletes, except for judokas, who showed a satisfactory level of resistance to hypoxic loads.

The Robinson Index (RI), as an indicator of a double product, characterizes the quality of the regulation and functional state of the cardiovascular system, showing the oxygen demand in the myocardium. Index calculations showed that athletes have a functional insufficiency of the cardiorespiratory system, since at a rate of up to 85 c.u., index values were above the maximum limit in all groups of athletes and ranged from 84.6 to 91.2 units, which corresponds to the average level (Table). It is known that the higher the IR values, the more significant the violations of CCC regulation.

The Shapovalova Power Index (SPI), which shows the development of speed-strength qualities among athletes, ranges from 240 units. up to 267.6 units, which corresponds to an "above average" level of development of athletes' physical abilities (table). When comparing the results obtained with physiological norms in athletes, it was shown that

there was good development in strength, speed, and speed endurance.

Modern studies have shown that athletes of different sports have inequality in the metabolic shifts of working muscles [29], changes in energy supply and the state of autonomic regulation of the cardiorespiratory system, and different mechanisms of adaptation to physical activity have been shown [21-23]. Currently, special attention is being drawn to studies related to new ways to increase the endurance of athletes, such as hypoxic training, which affects the activity of oxidative processes in muscles, the redistribution of blood flow and adapting cardiorespiratory mechanisms to increase the performance and endurance of athletes [24]. In this case, it is necessary to take into account health indices showing the effectiveness of aerobic metabolism in a comprehensive assessment of the stress of the cardiorespiratory system during intense physical activity in athletes [25]. The Skibinsky, Shapovalova, and Robinson indices reflect the vagosympathetic balance in the human body. Shifts in this balance change the hemodynamic parameters of heart rate and blood pressure and show hidden insufficiency of development or adaptation of the cardiorespiratory system [30,31].

The use of an integral approach reveals the features of athletes' adaptation to high physical loads, shows the need to include various tests to identify hidden functional features of the cardiorespiratory system, the state of physical performance and endurance of system mechanisms that ensure the success of the sports career of athletes involved in speed-strength sports, including martial arts.

To study physical performance and endurance, all athletes underwent a bicycle ergometer test to determine PWC_{170} and maximum oxygen consumption (VO_2). The data obtained were compared with the results of the PWC_{170} test in qualified athletes involved in martial arts and not specifically training for endurance, as shown in the reference table [16]. It turned out that judokas (average weight 67.1 kg), boxers (Muay Thai, average weight 67.4 kg), in the group of athletes involved in MMA (72.4 kg), as well as jiu-jitsu (average weight 76.1 kg) physical performance in absolute and relative values, is "below average" level. Figure 2 shows intragroup differences in physical performance and maximum oxygen consumption per minute among athletes training in the Combat Jiu-Jitsu group.
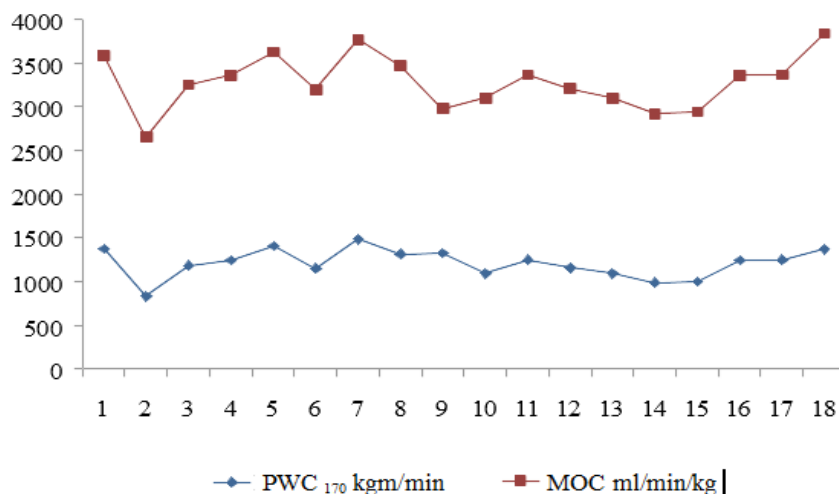

Figure 2 – Physical performance (PWC_{170}) and endurance (MOC) data for athletes training in the Combat Jiu-Jitsu group

Maximum oxygen consumption (VO_2) is the maximum amount of oxygen in ml that a person can consume within 1 minute; that is, it is aerobic performance capacity. In these groups of athletes, the MPC abs. and rel. units also corresponded to "average" and "below-average levels of endurance.

As shown by the results of a survey of young athletes involved in various types of martial arts, who did not specifically train for endurance due to their sports directions, they showed average resistance to physical activity, functional insufficiency of the cardiorespiratory system, physical performance and endurance, but high development of the muscular system, the ability to quickly rehabilitation after muscle strain. Currently, many researchers consider it necessary to use training cycles to develop endurance and increase the performance of athletes whose main activities are aimed at speed-strength and cyclic sports [19,20]. However, in the system of training athletes involved in martial arts, most of the training cycles are aimed at developing muscle-strength functions, while the problem of expanding the cardiorespiratory capabilities of athletes is not solved by such loads [21,22]. The data obtained are confirmed by the results of studies of heart rate variability in martial arts athletes.

To identify hidden functional features of the cardiovascular system, studies of heart rate variability (HRV) were conducted [18,19]. The results of HRV studies showed that 60.0% of athletes (boys and girls), regardless of the type of sport, had good functional capabilities of the cardiovascular system. The remaining athletes showed a decrease in adaptive capabilities and functional state of the cardiovascular system. Below are examples of HRV indicators with good FS and reduced FS for athletes aged 17–23 years (Figure 3).
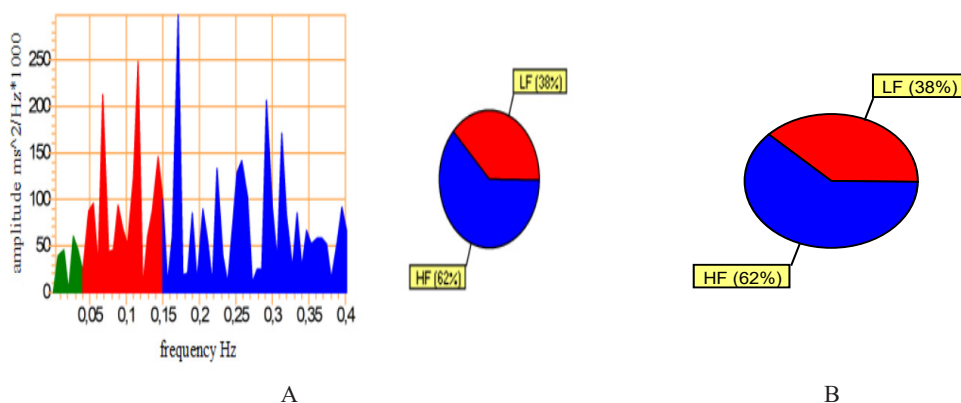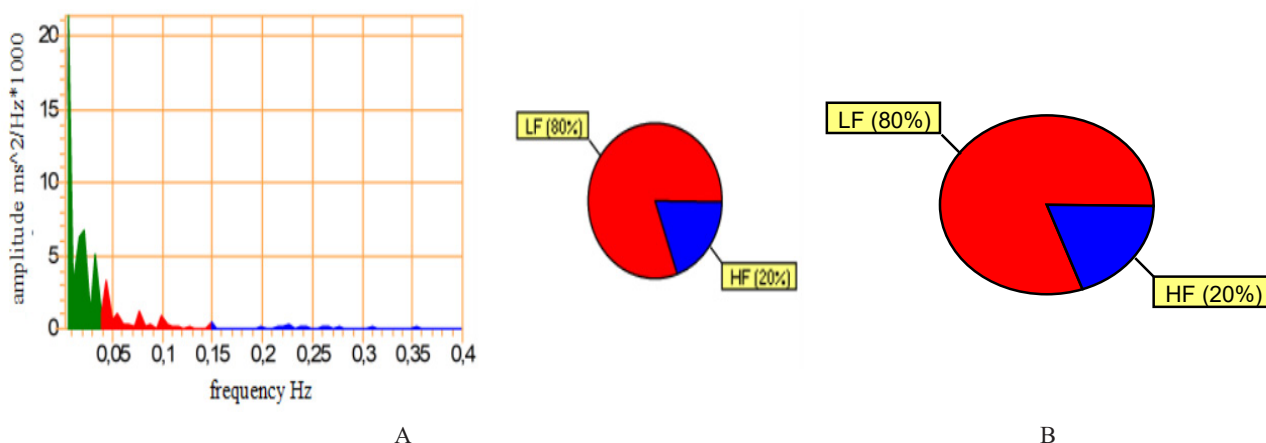
Figure 3 – Good functional state (A) according to spectral analysis of HRV
and diagram of vegetative balance (B) in boys 17-20 years old, practicing MMA

Medical and physiological interpretation of HRV indicators and assessment of the rhythmogram and type of sinus rhythm regulation show that the rhythmogram of heart rate variability corresponds to class 1 and is characterized by well-defined waves of short, long, and very long periods. In this case, the modulating sympatho-parasympathetic effect prevails over the humoral-metabolic and cerebral ergotropic influences; that is, aerobic processes prevail over anaerobic metabolic mechanisms. The parasympathetic autonomic nervous system (resting background vagotonia) makes the greatest contribution to heart rate regulation. This variant of heart rate regulation characterizes the good physical condition of the athlete. From spectrogram evaluation and spectral analysis indicators. It follows that the total power of the spectrum of neurohumoral modulation is high. A balance is maintained between the parts of the autonomic nervous system with a mixed (balanced) autonomic modulation of the heart rate, showing a good functional state at the current moment [23].

With a reduced functional state, revealed in some athletes from the groups of judo (3 people), Thai boxing (7 people) and jujitsu (12 people), the pattern of HRV parameters in 40% of athletes differs significantly from the data of a good state of the FS (Figure 4).

Figure 4 – Decrease in functional state (A) according to spectral analysis of HRV and
diagram of vegetative balance (B) in athletes involved in judo, Muay Thai and jiu-jitsu

This variant of the rhythmogram and the structure of heart rate variability indicate a transition of its regulation from a reflex, vegetative level of regulation to a lower one – humoral – metabolic (anaerobic type of energy supply), which is not able to quickly provide energy to muscle cells. The state of neurohumoral regulation is characterized by a low level of humoral and metabolic influences in the modulation of heart rate. The balance of the departments of the autonomic nervous system is characterized by the predominance of activity of the sympathetic department (high emotional background) of the autonomic nervous system (Figure 2B). The current functional state with such a balance decrease [24].

The identified characteristic changes in HRV due to fluctuations in the tone of the sympathetic nervous system were observed in all athletes after muscle-strength training. According to the obtained HRV data, more than half (60-68% in each group) of the examined athletes after intense training maintain a balance of parts of the autonomic nervous system, ensuring an active and emotionally stable state of athletes who are able to withstand maximum physical exertion without pathological abnormalities in the functioning of the cardiovascular system. systems. In athletes who have shown increased activity of sympathetic regulation associated with a high level of emotional component, the functional capabilities of the cardiovascular system are reduced, which may affect the success of their performances in the future [25,26]. Perhaps this condition reflects the insufficiency of the development and formation of the main regulatory systems for athletes from 17 to 19 years old, for whom further monitoring of the development of cardiovascular system and timely correction of vegetative-vascular abnormalities is necessary [27]. Moreover, as researchers note, increasing functional capabilities in athletes is possible only with the development of endurance, adaptation of the body to gradually increasing physical activity and maintaining vagosympathetic balance when heart rate changes without a significant increase in blood pressure [28].

Modern studies have shown that athletes of different sports have an inequality of metabolic shifts in working muscles [29], issues related to metabolism, energy processes and the state of autonomic regulation of the cardiorespiratory system and its adaptation to physical loads have been deeply studied [21-23]. Currently, special attention is drawn to studies related to new ways to increase the endurance of athletes, such as hypoxic training, which affects the activity of oxidative processes in muscles, redistributes blood flow, and adapts cardiorespiratory mechanisms to increase the performance and endurance of athletes [24]. In this case, it is necessary to use health indices that show the effectiveness of aerobic metabolism in a comprehensive assessment of the stress of the cardiorespiratory system during increased physical activity in athletes [25]. The Skibinsky, Shapovalova, Robinson indices reflect the vagosympathetic balance in the human body. Shifts in this balance change the hemodynamic parameters of heart rate and blood pressure, show a latent insufficiency in the development or adaptation of the cardiorespiratory system [30,31].

The use of an integral approach reveals the features of athletes' adaptation to high physical loads, shows the need to include various tests to identify hidden functional features of the cardiorespiratory system, the state of physical performance and endurance of system mechanisms that ensure the success of the sports career of athletes involved in speed-strength sports, including martial arts.

Conclusion

The use of an integrated approach to assessing the prospects of the physical capabilities of martial arts athletes shows resistance to physical activity, functional characteristics of the cardiorespiratory system, reveals individual abilities to increase physical performance and endurance and rapid rehabilitation after muscle loads. It has been shown that 60-70% of martial arts athletes maintain the balance of parts of the autonomic nervous system after maximum physical exertion without significant deviations in the functioning of the cardiovascular system, while the remaining 30% of athletes showed insufficiency of the adaptive capabilities of the cardiovascular system, which may be associated with age-related processes of formation of the vegetative-vascular system.

Acknowledgments

References

1. Roklicer R., Trivic T., Minovancev A., Drid P. Cardio remodels: improvement in elite judo athletes and health assessments/Integration of science and sports practice in combat sports Proccedings of XX International scientific and practical conference of young researchers, dedicated to the 100th Anniversary of E.M.Chumakov. – Moscow: GCOIFK. – 2021.-pp. 91-97

2. Arakawa K, Hosono A, Shibata K, Ghadimi R, Fuku M, Goto C, Imaeda N, Tokudome Y, Hoshino H, Marumoto M, Kobayashi M, Suzuki S, Tokudome S.Changes in blood biochemical markers before, during, and after a 2-day ultramarathon // J Sports Med. 2016. Vol.7. P. 43-50. https://doi.org/10.2147/OAJSM.S97468.

3. Schwellnus M, Soligard T, Alonso JM, Bahr R, Clarsen B, Dijkstra HP, Gabbett TJ, Gleeson M, Hägglund M, Hutchinson MR, Janse Van Rensburg C, Meeusen R, Orchard JW, Pluim BM, Raftery M, Budgett R, Engebretsen L. How much is too much? (Part 2). International Olympic Committee consensus statement on load in sport and risk of illness // Br J Sport Med. 2016. Vol.50, №17. P. 1030-41. https://doi.org/10.1136/bjsports-2016-096581.

4. Kreher J. Diagnosis and prevention of overtraining syndrome: an opinion on education strategies // Open Access J Sports Medicine. 2016. Vol.7. P. 115-22.

5. Cordeiro LMS, Rabelo PCR, Moraes MM, Teixeira-Coelho F, Coimbra CC, Wanner SP, Soares DD. Physical exerciseinduced fatigue: the role of serotonergic and dopaminergic systems // Braz J Med Biol Res. 2017. Vol.50, №12. e6432. https://doi.org/10.1590/1414-431X20176432.

6. Corbalan R., Bassand J.P., Illingworth L., Kayani G., Pieper K.S., Ambrosio G., et al. Analysis of outcomes in ischemic vs nonischemic cardiomyopathy in patients with atrial fibrillation: a report from the garfield-af registry. JAMA Cardiology. 2019;4(6):526-548. https://doi.org/10.1001/jamacardio.2018.4729

7. Spassky A.A., Myagkova M.A., Levashova A.I., Kukushkin S.K., Kurshev V.V., Yanova Yu.V., Veselova L.V. Methodology for a comprehensive assessment of an athlete's adaptation potential to stress. Metodologiya kompleksnoj ocenki adaptacionnogo potenciala sportsmena k nagruzke. //Sports medicine: science and practice. 2019;9(3):49-61. https://doi.org/10.17238/ISSN2223-2524.2019.3.49

8. Agadzhanyan N.A. Pankova N.B., Nadorov N.A. Informativeness of various functional tests of the state of the human cardiorespiratory system in normal conditions and in pathology. Informativnost' razlichnyh funkcional'nyh prob sostoyaniya kardiorespiratornoj sistemy cheloveka v norme i pri patologii // Bulletin of Restorative Medicine. – 2008. – No. 1 – P. 67−71.

9. Orlov V. A., Sudakov K. V., Andryunin M. A. Measurement and assessment of physical health and performance. Izmerenie i ocenka fizicheskogo zdorov'ya i rabotosposobnosti. // Collection of materials of the scientific symposium of the Moscow State Academy of Physical Culture. – M., 2001. – P. 20−29.

10. Razinkin S.M., Petrova V.V., Artamonova I.A., Fomkin P.A. Development and justification of a criterial apparatus for assessing the level of health of an athlete. Razrabotka i obosnovanie kriterial'nogo apparata ocenki urovnya zdorov'ya sportsmen. // Bulletin of neurology, psychiatry and neurosurgery. – 2015. – No. 2. – P. 72-80.

11. Vaguine Yu.E., Klassina S.Y., Fudin N.A. Heart rate variability during speed-strength load of athletes after hypoventilation training // Sports medicine: research and practice. 2022;12(2):67-72. (rus.) https://doi.org/10.47529/2223-2524.2022.2.5

12. Cherkashin D.V., Sharova N.V., Kuchmin A.N. Spirography in clinical practice. Spirografiya v klinicheskoj praktike. Textbook, ed. A.S. Svistova. -2nd edition. -SPb.: Politekhnika.-2019.-139p.

13. Sharykina A.S., Badtieva V.A., Pavlov V.I. Sports cardiology. Sportivnaya kardiologiya // Textbook. – Moscow: Ikar. – 2016. – 328 p.

14. Astakhov A.V. Physical performance and methods of its determination. Fizicheskaya rabotosposobnost' i metodika ee opredeleniya // Theory and practice of physical culture. – Moscow: Scientific Center TiPFC. -2007.-No. 8.-P.20-32.

15. Andriyanova E.Yu. Advantages and disadvantages of tests to assess the level of general physical performance of athletes and people involved in physical education. Preimushchestva i nedostatki testov po ocenke urovnya obshchej fizicheskoj rabotosposobnosti sportsmenov i lic, zanimayushchihsya fizicheskoj kul'turoj. // Science and sport: modern trends. -2022.-Vol.10, No.3.-P.6-13.

16. Karpman V.L., Belotserkovsky Z.B., Gudkov I.A. Testing in sports medicine. Testirovanie v sportivnoj medicine. Monograph. -M.: Physical education and sports. – 1988-208p.

17. Baevsky R.M., Barsukova Zh.V., Berseneva A.P. and others. Assessment of the functional state of the body based on mathematical analysis of

heart rhythm. Ocenka funkcional'nogo sostoyaniya organizma na osnove matematicheskogo analiza ritma serdca. // Methodological recommendations. – Vladivostok. – 1987. – 73 p.

18. Mikhailov V.M. Heart rate variability: experience of practical application of the method. Variabel'nost' ritma serdca: opyt prakticheskogo primeneniya metoda. Ivanovo: Ivan. state honey. Academy, 2002.- 290 p.

19. Sergeeva E.G., Ibragimova T.V., Didur M.D. Biofeedback and correction of heart rate variability in athletes training for endurance. Biologicheskaya obratnaya svyaz' i korrekciya variabel'nosti ritma serdca u sportsmenov, treniruyushchihsya na vynoslivost'. // Interactive Science. – St. Petersburg: Interactive Plus. – 2018. – No. 4 (26. – P. 32-36.

20. Isaev A.P., Erlikh V.V., Zalyapin V.I. Analysis of the main components of the integrative activity of the body of middle-distance runners. Analiz glavnyh komponent integrativnoj deyatel'nosti organizma begunov na srednie distancii. // Theory and practice of physical culture. – 2015. – No. 8. – pp. 27-29.

21. Menlu L., Cherkashin I.A., Kudrin E.P., Fedorov E.P. Construction of the educational and training process of mixed martial arts athletes. Postroenie uchebno-trenirovochnogo processa sportsmenov smeshannyh edinoborstv //Pedagogical-psychological and medical-biological problems of physical culture and sports//M.: LLC "Corsica". – 2023. – T.18, No. 2. – P.30-35

22. Pashintsev V.G., Surkov A.M. Development of speed-strength glycolytic endurance in judo. Razvitie skorostno-silovoj glikoliticheskoj vynoslivosti v dzyudo. Theory and practice of physical culture. 2015. – No. 3. – P. 20-22.

23. Malpas S.C. Neural influences on cardiovascular variabiliti: possibilities and pitfalls// Am. J. Physiol. Heart Circ. Physiol.- 2002.- Vol.282(1).-pp. 6-20.

24. Boutcher S.H., Park Y., Dunn S.L., Boutcher Y.N. The relationship between cardiac autonomic function and maximal oxygen uptake response to high-intensity intermittent-exercise training//Journal of Sports Sciences.- 2013.-Vol. 31(9).-pp. 1024-1029. DOI: 10.1080/02640414.2012.762984.

25. Baevsky R., Chernikova A. Analysis of heart rate variability: physiological foundations and basic methods Analiz variabel'nosti serdechnogo ritma: fiziologicheskie osnovy i osnovnye metody provedeniya □ //Cardiometry. – 2017.- Issue 10.-pp. 66–76; DOI: 10.12710/cardiometry.2017.6676 Online access: www.cardiometry.net/issues/no10-may-2017/heart-rate-variability-analysis

26. Kiviniemi A.M., Hautala A.J., Makikallio T.H., Seppanen T., Huikuri H.V., Tulppo M.P. Cardiac vagal outflow after aerobic training by analysis of high-frequency oscillation of the R-R interval// European Journal of Applied Physiology. – 2006.- Vol.96(6). – pp. 686-692. DOI: 10.1007/s00421-005- 0130-4.

27. Vanyushin Yu.S., Khairullin R.R., Elistratov D.E., Fedorov N.A. Adaptation of the cardiorespiratory system of athletes to motor activity. Adaptaciya kardiorespiratornoj sistemy sportsmenov k dvigatel'noj deyatel'nosti. Theory and practice of physical culture. 2020; 2: 30-32.

28. Vanyushin Yu.S., Elistratov D.E., Ishmukhametova N.F. Reserve capabilities of the cardiorespiratory system are the key to high athletic achievements in cyclic sports. Rezervnye vozmozhnosti kardiorespiratornoj sistemy – zalog vysokih sportivnyh dostizhenij v ciklicheskih vidah sporta. Pedagogical-psychological and medical-biological problems of physical culture and sports // Russian Federation: LLC "Corsica"-2022.- T. 17, No. 1.- P. 144-149.

29. Bragada J.A., Santos P.J., Maia J.A., Colaco P.J., Lopes V.P., Barbosa T.M. Longitudinal study in 3000 m male runners: Relationship between performance and selected physiological parameters// Journal of Sports Science and Medicine. – 2010.-N 9.-pp. 439-444.

30. Vanyushin Yu.S., Khairullin R.R., Elistratov D.E. The value of the coefficient of complex assessment of the cardiorespiratory system for diagnosing the functional state of athletes. Znachenie koefficienta kompleksnoj ocenki kardiorespiratornoj sistemy dlya diagnostiki funkcional'nogo sostoyaniya sportsmenov. Theory and practice of physical culture. 2017; 5: 59-61.

31. Gorbachev A.V. Comparative characteristics of methods for assessing the level of health and the factors that form it. Sravnitel'naya harakteristika metodov ocenki urovnya zdorov'ya i formiruyushchih ego faktorov // Bulletin of public health and healthcare of the Russian Far East. – 2016. – No. 1 (22). – P. 7-14.

T.V. Vostrikova[1,2] , A.Yu. Potapov[2] , N.V. Stolpovskaya[2] ,

A.A. Kruzhilin[2] , K.S. Shikhaliev[2] , A.M. Abekova[2*]

[1]Voronezh State University, Voronezh, Russia
[2]A.L. Mazlumov All-Russian Research Institute of Sugar Beet and Sugar, Voronezh, Russia
*e-mail: aabekova@mail.ru
(*Received June 9 2023; received in revised form July 6 2023; accepted July 14 2023*)

Seeds diversity of different species in the genus *Rhododendron* after pre-sowing treatment

Abstract. The purpose of the study is the evaluation seeds diversity of different species in the genus *Rhododendron* after pre-sowing treatment with organic compounds. As the signs of the seeds diversity is understood the seed germination and the seedling height. The research was conducted at the B.M. Kozo-Polyansky Botanical Garden of Voronezh State University (geographic coordinates: E 39°12', N 51°42'; 168.2 meters above sea level), Central Chernozem region (chernozem soil) in 2019-2020. It has been used ornamental shrubs. The study was made about the pyrimidinecarboxylic acids effect on the seed germination and the seedling height of *Rhododendron* species. The diversity of seeds is manifested in their heterogeneity according to morphological characteristics (the seedling height) and sowing qualities (seed germination) of *Rhododendron* species. The sowing properties (germinating capacity, seedling growth) were improved after treating the seeds with the organic compounds. There is the trend of increasing the seed germination and the seedling height of *Rhododendron* depended on the concentration of applied compounds. The seed germination for *Rh. ledebourii*, *Rh. luteum*, *Rh. molle* was increased from 5 to 7%, for *Rh. schlippenbachii* – from 5 to 10%. The seed treatment with pyrimidinecarboxylic acids at concentrations 0.01%, 0.05% and 0.1% allows to increase the seedling height for *Rh. ledebourii* from 37.5 to 75%, for *Rh. luteum, Rh. molle* – from 18.2 to 45.5%, for *Rh. schlippenbachii* from 20 to 40% concerning the control. To increase the seedling height, 2-benzylamino-4-methylpyrimidine-5-carboxylic acid at concentrations 0.05% and 0.1% is most effective. Morphologically close *Rhododendron* species (*Rh. luteum, Rh. molle*) indicated similar reactions to the seed treatment with compounds of the pyrimidinecarboxylic acid series.

Key words: seeds diversity, seed germination, seedling height, ornamental shrubs.

Introduction

Seeds diversity often means seed quality or sowing qualities, depending on the genotype and growing conditions. Breeding and testing are carried out and aimed at increasing the yield, resistance of agricultural plants to adverse environmental conditions [1]. Productivity is increased with breeding techniques and modes for obtaining highly productive cultivars, various agricultural practices, and the use of new technologies for growing plant material. It was noted that the productivity of the fruiting plant and its resistance to adverse factors are antipodal in nature since the same metabolites are involved in their creation but in different quantities [2]. Thus, productivity and stability are formed from the same photosynthesis products but redistributed in different directions following genetic regulation

[3]. Therefore, it is necessary to increase the plant resistance to adverse factors. The use of some biological growth regulators, organic and chemical fertilizers makes it possible to obtain more tolerant plants and their progeny with better qualities [3-5]. The example of species-specific reactions to external environmental factors (and internal factors of the organism) is the different quality of seeds. Sowing properties (germination capacity) of seeds as well as the growth processes can be improved by different growth stimulators [4, 5].

Sowing qualities of seeds and morphological characteristics of seedlings depend on the genotype and growing conditions. The leading indicators of the different plant quality is the germination energy and the germination capacity, which depend on the genotype [6]. For instance, the diversity of seeds manifests in their heterogeneity according to

morphological characteristics and sowing qualities [7]. The influence of agricultural practices at the seeds diversity exceeds genetic factors [6]. An increase in yield and sugar content of mother roots after the seed treatment with organic compounds were revealed [8]. Further, the seeds yield and sowing properties (germination capacity) were improved, when planted roots were used for the hybrids reproduction [8].

Maintenance of seed quality is mandatory for final yields, so seed lots are assessed, based on their germination capabilities and vigor [9, 10]. A lot of tests are used to evaluate seed physiological characteristics require time and skilled labor, making it costly [9, 10, 11, 12]. For instance, cytogenetic and molecular studies of the growth process and the seeds diversity [13] are modern, but complex and cost. It was reported about revealing of gamma-rays and microwave irradiation influence using I – markers assisted selection for responding to mutagenic agents [14]. Plant screening with the optical chlorophyll counter made it possible to determine the responses of genotypes to the heat and water stress conditions [12]. However, there are simple characteristics, for example, biometric indicators, including plant height, seedling length and others.

As provocative backgrounds for the study of the seedling reaction to external influences, meteorological conditions, mutagenic agents, and agricultural practices, chemical compounds are often used. But a promising area of the study, related to the growing need for the development of effective and safe drugs, is the synthesis of new heterocyclic systems, containing a pyrimidine fragment [15-18]. For instance, a phosphomide contains two ethyleneimine groups and a pyrimidine base. Ethyleneimine causes mutations, the pyrimidine base is included in the DNA chromosome. The mutagenic effect of phosphomide was previously studied for the model object Crepis capillaris L. [19] and later – for Triticum aestivum L. [20]. Agrobiological characteristics were defined: field germination of seeds, morphological characteristics of the ear, stem, leaves and others [20]. The variability of quantitative traits under the environmental conditions influence is a traditional investigation. Laboratory seed germination and morphometric parameters of woody plants and agricultural crop were studied after seed treatment with heterocyclic compounds [21, 22]. So organic compounds with the pyrimidine fragment have the biological activity. In addition, it was reported about the antioxidant and antimicrobial activity of some selected derivatives with the pyrimidine fragments [23, 24]. The antioxidant [25] and antimicrobial [26]

activity was found in *Rhododendron* leaves, flowers. That's why the representatives of the *Rhododendron* genus are valuable resource plant.

The purpose of the study is evaluation the seeds diversity, namely seed germination and the seedling height, of different species in the genus *Rhododendron* after the pre-sowing treatment with compounds of the pyrimidinecarboxylic acid series.

Materials and methods

The research was conducted at the B.M. Kozo-Polyansky Botanical Garden of Voronezh State University (geographic coordinates: E 39°12', N 51°42'; 168.2 meters above the sea level), Central Chernozem region (chernozem soil) in 2019-2020. The map of area is presented on Figure 1.

As research objects were used seeds and seedlings of ornamental woody plants. *Rhododendron ledebourii* Pojark. is a semi-evergreen shrub, and *Rhododendron luteum* Sweet, *Rhododendron molle* (Blume) G. Don, *Rhododendron schlippenbachii* Maxim. are deciduous shrubs. In controlled environment these species grow up to 2-meter in height and are highly decorative [26]. The long history of studying these species at Russian Federation has demonstrated, that *Rhododendron* species are winter-hardy, drought-resistant, and fruit-bearing shrubs [7, 26].

It was focused at the pyrimidinecarboxylic acids effect on the height of *Rhododendron* species seedlings. The following compounds were used: 4-methyl-2-piperidin-1-ylpyrimidine-5-carboxylic acid (1), 2-benzylamino-4-methylpyrimidine-5-carboxylic acid (2), and 4-methyl-2-morpholin-4-pyrimidine-5-carboxylic acid (3) synthesized at the Department of Organic Chemistry of Voronezh State University (presented on Figure 2).

Prior to the sprouting process, the seeds of *Rhododendron* species (*Rh. ledebourii, Rh. luteum, Rh. molle* and *Rh. schlippenbachii*) were soaked in a water suspension of the above listed compounds with concentrations of 0.01 %, 0.05 %, and 0.1 % for 18 hours.

The control group consisted of the same type of seeds soaked in tap water solution of a commonly used growth stimulator, Epibrassinolide (commercial fraction Epin Extra produced by NNPP NEST M, Russia), with the concentration of 0.05 % (according to the instruction [21, 22]). In case of each studied acid concentration (0.01%, 0.05%, 0.1%), as well as the control group, the experiment was conducted three times using a set of 100 seeds. After soaking, the rhododendron seeds were placed in Petri dishes

containing blotting paper, and germinated in the laboratory conditions at a constant temperature 22 ºC. The laboratory seed germination was determined as the ratio of the number of germinated seeds to the total number of seeds and was expressed in %. *Rhododendron* seedlings were counted to study the laboratory germination and planted in crates in closed ground on 21 day after the start of the experiment. The seedling height was measured using a ruler. An increase in the seedling height was determined as the ratio of the difference between the average seedling height in the experimental group and in the control group to the average seedling height in the control group and was expressed in %.

Figure 1 – The map of the B.M. Kozo-Polyansky Botanical Garden of Voronezh State University [27].
Note: Place for an introductory conversation, Memorial, Historical part of the botanical garden, Tuetum, Dry forest, Pinetum, Larch forest, Forest belts, Arboretum, Michurinsky garden, Fallow plots, Protected oak forest, Grassy slopes, Bayrachnaya oak forest, Collection of wild fruit and stone fruit crops, Geographical arboretum [27].

(1)   (2)   (3)
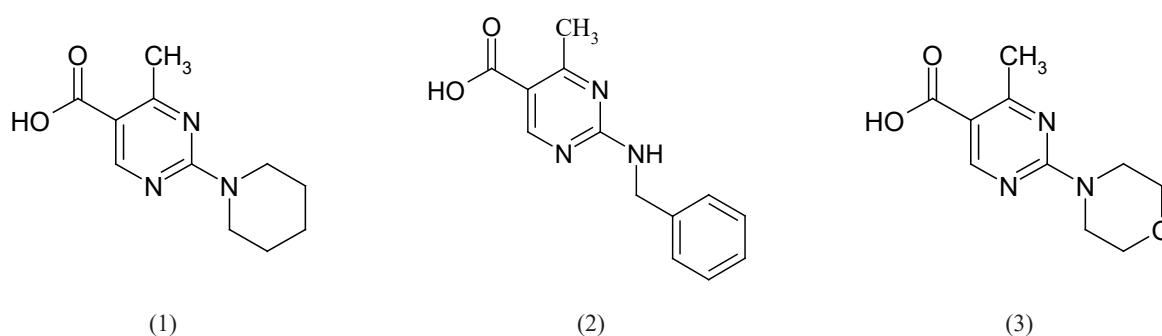
Figure 2 – Synthesized organic compounds of the pyrimidinecarboxylic acid series.
Note: 4-methyl-2-piperidin-1-ylpyrimidine-5-carboxylic acid (1), 2-benzylamino-4-methylpyrimidine-5-carboxylic acid (2), and 4-methyl-2-morpholin-4-pyrimidine-5-carboxylic acid (3)

Computer statistical processing was performed using the Stadia software package. The procedures for grouping data and their processing were described in A. P. Kulaichev work [28]. The seed germination in the control and experimental variants was compared according to the criterion of frequency agreement using Z-test for equality of frequencies. Average values of seedling lengths were compared using Student's *t*-test. The influence of the treatment factor at different concentrations on growth rates was determined using two-way analysis of variance. Coefficient of variation (Cv) was counted according to G.F. Lakin [28]. If Cv was below 10%, it means that the degree of variation was low, with Cv between 10 and 25 % it was medium, and when Cv was over 25 % – the degree of variation was high [29].

Results and discussion

The results of the seeds treatment with pyrimidinecarboxylic acids on the germination and the height of *Rhododendron* seedlings are presented in tables 1-4. The laboratory germination of seeds was determined in the control group, Epin group, experimental groups for each species. An average height of seedling was estimated respectively. It wasn't revealed the significant difference between control group and Epin group in the seed germination, as well as in the seedling height for *Rhododendron* species.

The seed germination wasn't strongly increased for *Rhododendron ledebourii* (Table 1). But there were significant differences between control and experimental groups for all acids in the 0.1% concentration, for 4-methyl-2-piperidin-1-ylpyrimidine-5-carboxylic and 2-benzylamino-4-methylpyrimidine-5-carboxylic acids in the 0.5% concentration.

It was indicated the most increase in the seedling height for 2-benzylamino-4-methylpyrimidine-5-carboxylic acid at the 0.1% concentration – 75% (the seedling height in the control group was 0.8±0.2 cm). The increase in the seedling height was smaller for 4-methyl-2-piperidin-1-ylpyrimidine-5-carboxylic acid (62%) and the smallest for 4-methyl-2-morpholin-4-pyrimidine-5-carboxylic acid (50%). The similar trend was saved for other acid concentrations. So 2-benzylamino-4-methylpyrimidine-5-carboxylic acid was the most effective for *Rhododendron ledebourii* at all tested concentrations (Table 1). The seed germination of *Rhododendron luteum* was increased by 2-benzylamino-4-methylpyrimidine-5-carboxylic, 4-methyl-2-piperidin-1-ylpyrimidine-5-carboxylic acids at the 0.1% concentration and by the last at the 0.05% concentration. This reaction is differ from responses of other *Rhododendron* species, where the 0.1% concentration was effective in all compounds (Table 2). That means the special stimulating impact for sowing qualities in *Rhododendron luteum* seeds or specific seeds reaction for the treatment.

Table 1 – The seeds diversity signs of *Rhododendron ledebourii* after treating the seeds with the synthesized organic compounds

Concentration, %	The average seedling height, cm	The seed germination, %	Cv, %	The increase in the seedling height, %
Control group	0.8±0.2	32.3	10.4	–
Epin group	0.9±0.2	35.7	11.8	–
4-methyl-2-piperidin-1-ylpyrimidine-5-carboxylic acid				
0.01%	1.1±0.2*[1]	35.4	11.6	37.5
0.05%	1.2±0.1**[2]	37.6*	9.2	50.0
0.1%	1.3±0.2***[3]	38.6*	10.3	62.5
2-benzylamino-4-methylpyrimidine-5-carboxylic acid				
0.01%	1.2±0.2**[2]	37.1	10.5	50.0
0.05%	1.3±0.2***[3]	39.4*	11.5	62.5
0.1%	1.4±0.3***[3]	40.8*[1]	10.9	75.0
4-methyl-2-morpholin-4-pyrimidine-5-carboxylic acid				
0.01%	1.1±0.2*[1]	35.2	10.4	37.5
0.05%	1.1±0.2**[2]	37.1	10.7	37.5
0.1%	1.2±0.2**[2]	39.6*	11.3	50.0

Note: Cv – variation coefficient; * – differences with the control group are reliable (p<0.05); ** – differences with the control group are reliable (p<0.01); *** – differences with the control group are reliable (p<0.001); [1] – differences with the Epin group are reliable (p<0.05); [2] – differences with the Epin group are reliable (p<0.01); [3] – differences with the Epin group are reliable (p<0.01)

Table 2 – The seeds diversity signs of *Rhododendron luteum* after treating the seeds with the synthesized organic compounds

Concentration, %	The average seedling height, cm	The seed germination, %	Cv, %	The increase in the seedling height, %
Control group	1.1±0.2	37.2	9.5	–
Epin group	1.2±0.2	40.5	10.1	–
4-methyl-2-piperidin-1-ylpyrimidine-5-carboxylic acid				
0.01%	1.3 ±0.3*	37.4	11.8	18.2
0.05%	1.4±0.1**[1]	40.6*	8.2	27.3
0.1%	1.5±0.2***[2]	42.4*	9.3	36.4
2-benzylamino-4-methylpyrimidine-5-carboxylic acid				
0.01%	1.4 ±0.2*[1]	37.1	9.7	27.3
0.05%	1.5±0.2**[2]	40.4	10.5	36.4
0.1%	1.6±0.3***[3]	42.5*	12.3	45.5
4-methyl-2-morpholin-4-pyrimidine-5-carboxylic acid				
0.01%	1.3±0.2*	37.2	9.7	18.2
0.05%	1.4±0.2*[1]	38.1	9.8	27.3
0.1%	1.4±0.2**[1]	39.7	10.3	27.3

Note: Cv – variation coefficient; * – differences with the control group are reliable (p<0.05); ** – differences with the control group are reliable (p<0.01); *** – differences with the control group are reliable (p<0.001);
[1] – differences with the Epin group are reliable (p<0.05); [2] – differences with the Epin group are reliable (p<0.01); [3] – differences with the Epin group are reliable (p<0.01)

But there were significant differences between control and experimental groups at all acids in each concentration for *Rhododendron luteum* (the seedling height in the control group was 1.1±0.2 cm, Table 2), as well as for other *Rhododendron* species into the seedling height (Table 1, 3, 4). The increase in the seedling height for *Rhododendron luteum* was smaller (Table 2), than for *Rhododendron ledebourii* (Table 1). However, the similar trend of the increase in the seedling height from low (0.01%) to high (0.1%) concentration was observed for each *Rhododendron* species.

Table 3 – The seeds diversity signs of *Rhododendron molle* after treating the seeds with the synthesized organic compounds

Concentration, %	The average seedling height, cm	The seed germination, %	Cv, %	The increase in the seedling height, %
Control group	1.1±0.2	40.8	10.5	–
Epin group	1.2±0.2	42.5	11.6	–
4-methyl-2-piperidin-1-ylpyrimidine-5-carboxylic acid				
0.01%	1.3 ±0.3*	43.4	14.8	18.2
0.05%	1.4±0.2**[1]	44.6	12.3	27.3
0.1%	1.5±0.2***[2]	46.4*	12.5	36.4
2-benzylamino-4-methylpyrimidine-5-carboxylic acid				
0.01%	1.4 ±0.2*[1]	43.8	11.7	27.3
0.05%	1.5±0.2**[2]	45.8	12.5	36.4
0.1%	1.6±0.3***[3]	47.7*[1]	12.3	45.5
4-methyl-2-morpholin-4-pyrimidine-5-carboxylic acid				
0.01%	1.3±0.2*	41.8	10.7	18.2
0.05%	1.4±0.2*[1]	45.6	10.8	27.3
0.1%	1.5 ±0.2**[1]	46.8*	13.3	36.4

Note: Cv – variation coefficient; * – differences with the control group are reliable (p<0.05); ** – differences with the control group are reliable (p<0.01); *** – differences with the control group are reliable (p<0.001); [1] – differences with the Epin group are reliable (p<0.05); [2] – differences with the Epin group are reliable (p<0.01); [3] – differences with the Epin group are reliable (p<0.01)

The seed germination of *Rhododendron ledebourii* and *Rhododendron molle* was increased by all tested chemical compounds at the concentration of 0.1% concerning the control (Table 3). But the plant height was significantly higher in each experimental group (the seedling height in the control group was 1.1±0.2 cm). The similar dynamic of the parameter increase was revealed for all acid concentrations in the height of *Rhododendron molle* seedlings.

The seed germination of *Rhododendron schlippenbachii* was differ from other species. This trait was significantly higher in each experimental group, than in control, as well as the plant height (Table 4). The same trend was observed for all acid concentrations in the height of *Rhododendron schlippenbachii* seedlings.

The seed germination for *Rh. ledebourii*, *Rh. luteum*, *Rh. molle* under the influence of pyrimidinecarboxylic acids in the tested concentrations was increased from 5 to 7%, for *Rh. schlippenbachii* – from 5 to 10%.

Morphologically close species (*Rh. luteum, Rh. molle*) reacted in a similar way to the seed treatment with pyrimidinecarboxylic acid series. Moreover, this species of Rhododendron genus are similar according to ITS1-ITS2 nucleotide sequence [30]. This species (*Rh. luteum, Rh. molle*) are characterized the similar form and size of seeds. The differences in the change in their germination and the size of seedlings were insignificant. The range of variation in the seedling height of these species was practically the same, although the seed progeny of *Rh. luteum* is more uniform, characterized by the low and medium coefficient of variation (Cv). This trait in *Rh. molle* is characterized by medium Cv, indicating greater heterogeneity of the offspring (Tables 2-3). The low coefficient of variation can mean that the population of *Rh. luteum* is more stable, than the one of *Rh. molle.*

Table 4 – The seeds diversity signs of *Rhododendron schlippenbachii* after treating the seeds with the synthesized organic compounds

Concentration, %	The average seedling height, cm	The seed germination, %	Cv, %	The increase in the seedling height, %
Control group	1.0±0.3	30.2	14.5	–
Epin group	1.1±0.3	33.8	14.6	–
4-methyl-2-piperidin-1-ylpyrimidine-5-carboxylic acid				
0.01%	1.2 ±0.3*	35.4*	15.6	20.0
0.05%	1.3±0.2*[1]	37.6*	12.2	30.0
0.1%	1.4±0.3**[1]	38.6*	14.3	40.0
2-benzylamino-4-methylpyrimidine-5-carboxylic acid				
0.01%	1.2 ±0.3*	37.1*	14.5	20.0
0.05%	1.3±0.3*[1]	39.4*	15.6	30.0
0.1%	1.4±0.3**[1]	40.8*[1]	14.9	40.0
4-methyl-2-morpholin-4-pyrimidine-5-carboxylic acid				
0.01%	1.2 ±0.2*	35.2*	13.4	20.0
0.05%	1.3±0.2*[1]	37.1*	12.7	30.0
0.1%	1.4±0.3**[1]	39.6*	14.3	40.0

Note: Cv – variation coefficient; * – differences with the control group are reliable ($p<0.05$); ** – differences with the control group are reliable ($p<0.01$); *** – differences with the control group are reliable ($p<0.001$);
[1] – differences with the Epin group are reliable ($p<0.05$); [2] – differences with the Epin group are reliable ($p<0.01$); [3] – differences with the Epin group are reliable ($p<0.01$)

The first statement is also true for *Rh. ledebourii* (low and medium Cv) and the second statement is also true for *Rh. schlippenbachii* (medium Cv) (Tables 1, 4). The lower coefficients of variation and smaller increases in the seedling height were illustrated in cases of 4-methyl-2-piperidin-1-ylpyrimidine-5-carboxylic and 4-methyl-2-morpholin-4-pyrimidine-5-carboxylic acids.

The germination capacity increase of *Rhododendron* species under the influence of 2-benzylamino-4-methylpyrimidine-5-carboxylic acid was observed mainly in concentrations of

0.05% and 0.1%. This compound had the strongest effect at the plant height for all *Rhododendron* species. The increase in the seedling height in comparison with the control was revealed in all experimental variants. But 2-benzylamino-4-methylpyrimidine-5-carboxylic acid indicated the highest stimulating activity at concentrations of 0.01%, 0.05% and 0.1% for the tested species of the genus *Rhododendron* (Tables 1-4). It was illustrated by the largest increases in the seedling height, especially for *Rh. ledebourii* (Table 1). Although cytogenetic and molecular studies can reveal the seed difference [13] more exactly, morphometric investigations adequately reflect parameters of the seeds diversity.

Apparently 2-benzylamino-4-methylpyrimidine-5-carboxylic acid retains its stimulating effect longer than other compounds and is more active, while Rh. ledebourii is most responsive to seed treatment with compounds. So in experiments with pyrimidine-carboxylic acids, as tested heterocycles, the "benzylamino" fragment increases the activity of the compounds. This is consistent with the results of O.N. Kulaeva and her colleagues, who have showed that the "benzylamino" substituent increases the activity of synthetic cytokinin: 6-benzylaminopurine is superior in activity to kinetin [31]. Two-way analysis of variance has showed a significant effect of "chemical treatment" and "concentration" factors on the seedling height Rh. ledebourii (P<0.05), Rh. luteum (P<0.05), Rh. molle (P<0.05), Rh. schlippenbachii (P<0.05).

The germination rate at Rh. ledebourii, Rh. luteum, Rh. molle increases from 5 to 7% under the influence of synthesized organic substances of pyrimidinecarboxylic acids, at Rh. schlippenbachii – from 5 to 10% in concentrations of 0.01%, 0.05% and 0.1%. The seeds treatment with compounds of pyrimidinecarboxylic acids in concentrations of 0.01%, 0.05% and 0.1% allows to increase the seedling height at Rh. ledebourii from 37.5 to 75%, at Rh. luteum, Rh. molle – from 18.2 to 45.5%, at Rh. schlippenbachii from 20 to 40% relatively to the control. To increase the seedling height, 2-benzylamino-4-methylpyrimidine-5-carboxylic acid in concentrations 0.05% and 0.1% is most effective.

Thus, parameters of the seed germination can be improved by the pre-sowing treatment with compounds of the pyrimidinecarboxylic acid series. The similar trends of the seed germination were revealed in this investigation. The strongest stimulating effect was demonstrated by all the studied compounds with a concentration of 0.1% for all Rhododendron species. The same dynamic of the increase in the seedling height from low (0.01%) to high (0.1%) concentration was observed for each Rhododendron species. On the other hand, there are some facts prove to be seeds diversity. The seed germination of Rhododendron luteum is differ from responses of other Rhododendron species. That means special stimulant impact for sowing qualities in Rhododendron luteum seeds or specific seeds reaction for the treatment. Rhododendron ledebourii had the largest increases in the seedling height. Morphologically close species (Rh. luteum, Rh. molle) reacted in a similar way to the seed treatment. But there is the difference between their parameters. The low coefficient of variation can mean that the population of Rh. luteum is more stable, than the one of Rh. molle.

Conclusion

There is the trend of increasing the seed germination and the height of Rhododendron seedlings depended on the concentration of applied organic compounds. A direct correlation can be noted: the higher concentration of 2-benzylamino-4-methylpyrimidine-5-carboxylic acid (within the range between 0.01 and 0.1%) leads the increase in the seed germination and the seedling height of Rhododendron species. The same correlation was demonstrated for the seeds germination and the seedlings height, when 4-methyl-2-piperidin-1-ylpyrimidine-5-carboxylic and 4-methyl-2-morpholin-4-pyrimidine-5-carboxylic acid was applied. But the last acid is weaker, than other. Morphologically close Rhododendron species (Rh. luteum, Rh. molle) indicated similar reactions to the seed treatment with compounds of the pyrimidinecarboxylic acid series. However, the diversity of seeds is manifested in their heterogeneity according to morphological characteristics (the seedling height) and sowing qualities (seed germination) of Rhododendron species including Rh. luteum, Rh. molle. The sowing properties (germinating capacity, the seedling growth) were improved after treating the seeds with the synthesized organic compounds in all studied species. The organic compounds of pyrimidinecarboxylic acids are characterized by high biological activity. These substances stimulate the growth of ornamental shrubs Rhododendron when their concentrations are low.

Acknowledgments

References

1. Dyakov A.B., Trunova M.V., Vasiliev T.A. (2009) Evaluation of the potentials of productivity and drought tolerance of soybean varieties [Ocenka potencialov urozhajnosti i zasuhoustojchivosti sortov soi]. Oilseeds. Scientific and Technical Bulletin of the All-Russian Research Institute of Oilseeds [Maslichnye kul'tury. Nauchno-tehnicheskij bjulleten' Vserossijskogo nauchno-issledovatel'skogo instituta maslichnyh kul'tur], no. 2(141), pp. 78-86.

2. Doroshenko T.N. (2000) Physiological and environmental aspects of southern fruit growing [Fiziologo-jekologicheskie aspekty juzhnogo plodovodstva]. Krasnodar: KubSAU, 235 p.

3. Doroshenko T.N., Zakharchuk N.V., Ryazanova L.G. (2010) Adaptive potential of fruit plants in the south of Russia [Adaptivnyj potencial plodovyh rastenij juga Rossii: Monografija]. Krasnodar: Publishing House LLC "Enlightenment-South", 192 p.

4. Khodaei-Joghan A., Gholamhoseini M., Agha-Alikhani M., et al. (2018) Response of sunflower to organic and chemical fertilizers in different drought stress conditions. Acta agriculturae Slovenica, no. 111(2), pp. 271–284. https://doi:10.14720/aas.2018.111.2.03.

5. Nesterkina I.S., Musalov M.V., Gurina V.V., et al. (2019) The effect of a new non-toxic water-soluble selenorganic substance on antioxidant protection and development of seedlings of oilseed radish (Raphanus sativus L. var. oleiferus Metzg.). Acta agriculturae Slovenica, no. 114/1, pp. 61–67. https://doi:10.14720/aas.2019.114.1.7

6. Balagura O.V., Levshakov LV. (2013) Diversity of sugar beet seeds and its significance [Raznokachestvennost' semjan saharnoj svekly i ee znachenie]. Bulletin of the Kursk State Agricultural Academy [Vestnik Kurskoj gosudarstvennoj sel'skohozjajstvennoj akademii], no. 9, pp. 52-54.

7. Vostrikova T.V. (2011) Ecological and biological features of rhododendrons during introduction in the conditions of the Central Chernozem region [Jekologo-biologicheskie osobennosti rododendronov pri introdukcii v uslovijah Central'nogo Chernozem'ja]. Bulletin of Krasnoyarsk State Agrarian University [Vestnik Krasnojarskogo gosudarstvennogo agrarnogo universiteta], no. 4, pp. 27–30.

8. Tsareva L.E. (2013) Technique of improving yielding features of seeds in reproduction of sugar beet hybrids [Careva L.E. Sposob povyshenija urozhajnyh svojstv semjan pri vosproizvodstve gibridov saharnoj svekly]. Bulletin of Altai State Agrarian University [Vestnik Altajskogo gosudarstvennogo agrarnogo universiteta], no. 1(99), pp. 17–19 (in Russian).

9. Sudhakar P., Latha P., Reddy P.V. (2016) Seed physiological and biochemical traits. In Phenotyping Crop Plants for Physiological and Biochemical Traits, pp. 17-24. https://doi:10.1016/B978-0-12-804073-7.00002-8.

10. Fachi L.R., Krause W., Duarte H., et al. (2019) Digital image analysis to quantify genetic divergence in passion fruit (Passiflora edulis) seeds. Genetics and Molecular Research, no. 18(3). https://doi:10.4238 / gmr18331.

11. Baranova T.V. (2013) Accelerated production of plants resistant to urban conditions [Uskorennoe poluchenie ustojchivyh k gorodskim uslovijam rastenij]. Ecology and Industry of Russia [Jekologija i promyshlennost' Rossii], no. 4, pp. 65–67 (in Russian).

12. Bome N.A., Salekh S., Korolev K.P., et al. (2022) Biological potential of winter cereals in the Northern Trans-Urals, Russia. SABRAO J. Breed. Genet., no. 54(4), pp. 789-802. http://doi.org/10.54910/sabrao2022.54.4.10

13. Hassanien A.M., Mohammed A.H., Allah H.A. A.B.D., et al. (2020) Cytogenetic and molecular studies on two faba bean cultivars revealed their difference in their aluminum tolerance Acta agriculturae Slovenica, no. 116(2), pp. 273-285. http://dx.doi.org/10.14720/aas.2020.116.2.1346

14. Khaled K.A.M., Sultan F.M., Azzam C.R. (2022) Gamma-rays and microwave irradiation influence on guar (Cyamopsis tetragonoloba): I – markers assisted selection for responding to mutagenic agents. SABRAO J. Breed. Genet., no. 54(2), pp. 331-349. http://doi.org/10.54910/sabrao2022.54.2.10

15. Azizian J., Delbari A. S., One-Pot K.Y. (2014) Three-Component Synthesis of Pyrimido[4,5-b]quinoline-tetraone Derivatives in Water. Synthetic Commun., no. 44 (22), pp. 3277–3286.

16. Ghoneim A.A., Assy M.G. (2015) Synthesis of Some New Hydroquinoline and Pyrimido[4,5-b]

Quinoline Derivatives. Current Research in Chemistry, no. 7(1), pp. 14–20. doi: 10.3923/crc.2015.14.20

17. Tkachenko E. V., Gubar S. N., Zhuravel I. A., et al. (2018) Synthesis and antimicrobial activity of amides 2,4-dioxo-1,4-dihydro-2H-thieno [3,2-d] pyrimidin-3yl) carboxylic acids [Sintez i protivomikrobnaja aktivnost' amidov 2,4-diokso-1,4-digidro-2N-tieno[3,2-d]pirimidin-3il)karbonovyh kislot]. Bulletin of the Kazakh National Medical University [Vestnik Kazahskogo Nacional'nogo medicinskogo universiteta], no. 1, pp. 347–350.

18. Vostrikova T.V., Kalaev V.N., Potapov A.Yu., et al. (2020) Using synthesized organic compounds as environmentally friendly retardants for ornamental plants. Southern Brazilian Journal of Chemistry, no. 28 (28), pp. 40-44.

19. Weisfeld L.I. (2015) About cytogenetic mechanism of chemical mutagenesis. In Ecological consequences of increasing crop productivity. Plant breeding and biotic diversity. Toronto-New Jersey: Apple Academic Press Inc., pp. 259-269.

20. Bome, N.A., Weisfeld, L.I., Babaev, E.V., et al. (2017) Influence of phosphomide, a chemical mutagen, on agrobiologial signs of soft spring wheat Triticum aestivun L. [Agrobiologicheskie priznaki jarovoj mjagkoj pshenicy (Triticum aestivum L.) pri obrabotke semjan himicheskim mutagenom fosfemidom] Agricultural Biology [Sel'skohozjajstvennaja biologija], no. 52 (3), pp. 570-579 (Ru). doi: 10.15389/agrobiology.2017.3.570rus

21. Vostrikova T.V., Kalaev V.N., Potapov A.Yu., et al. (2021) Use of new compounds of the quinoline series as growth and yield stimulants of agricultural crop. Periódico Tchê Química, no. 18 (38), pp. 123-136.

22. Vostrikova T.V., Kalaev V.N., Potapov A.Yu., et al. (2020) Use of new compounds of the quinoline series as effective stimulants of growth processes. Periódico Tchê Química, no. 17 (35), pp. 781-790.

23. El-Gazzar A.B.A., Hafez H.N., Nawwar G.A.M. (2009) New acyclic nucleosides analogues as potential analgesic, anti-inflammatory, anti-oxidant and anti-microbial derived from pyrimido[4,5-b] quinolines. European Journal of Medicinal Chemistry, no. 44(4), pp. 1427–1436.

24. Elkholy Y.M., Morsy M.A. (2006) Facile Synthesis of 5, 6, 7, 8-Tetrahydropyrimido[4, 5-b]-quinoline Derivatives. Molecules, no. 11, pp. 890–903.

25. Vostrikova, T.V., Burmenko, J.V., Kalaev, V.N., et al. (2022) Anthropogenic Pollution Influence on the Antioxidant Activity in Leaves and on the Cytogenic Structures in the Seedlings of the Representatives of the Rhododendron Genus. In Biological Assessment of Natural and Anthropogenic Ecosystems: Trends in Diagnosis of Environmental Stress. Burlington: Apple Academic Press Inc., pp. 121-136.

26. Alexandrova M.S. (2003) Rhododendrons [Rododendrony]. Moscow: ZAO Fiton+, 192 p. (in Russian).

27.The map of the B.M. Kozo-Polyansky Botanical Garden of Voronezh State University. https://hb.karelia.ru/files/img/01b31d63629c5eea37 dda39f6a9c3fd2.jpg

287. Kulaichev A.P. (2006) Methods and tools for integrated data analysis [Metody i sredstva kompleksnogo analiza dannyh]. Moscow: FORUM: INFA-M, 512 p.

29. Lakin G.F. (1990) Biometry [Biometrija]. Moscow: Higher School, 352 p.

30. Baranova T.V., Kalendar R.N., Kalayev V.N. (2014) To the Question of Rhododendron L. Genus Phylogeny Based on ITS1-ITS2 Spacers Sequence Studies [K voprosu filogenii vidov roda Rhododendron L. na osnovanii issledovanij posledovatel'nosti spejserov ITS1-ITS2]. Siberian Forestry Journal [Sibirskij lesnoj zhurnal], no. 6, pp. 30–46.

31. Muromtsev G.S, Chkanikov D.I., Kulaeva O.N., Hamburg K.Z. (1987) Fundamentals of chemical regulation of plant growth and productivity [Osnovy himicheskoj reguljacii rosta i produktivnosti rastenij]. Moscow: Agropromizdat, 383 p.

M. Ozturk[1] , N.R. Sagdollina[2] , M.M. Ibrayeva[3*]

[1]Mugla Sıtkı Koçman University, Mugla, Turkey
[2]S. Amanzholov East Kazakhstan University, Ust-Kamenogorsk, Kazakhstan
[3*]Yessenov University, Aktau, Kazakhstan
*e-mail: ibrayevamanshuk@mail.ru

Component composition and biological activity of essential oil of plant *Zinnia elegans*

Abstract. By the method of steam distillation, samples of essential oil were obtained from a plant cultivated in the East Kazakhstan region. The essential oil was obtained with a yield in terms of air-dry raw materials. By the gas liquid chromatography investigated a quantitative analysis of the essential oil components. Essential oil components of quantitative content calculated from the areas of gas chomatographic peaks. From plant of genus *Zinnia elegans* obtained main compounds of essentiol oil such as α-terpineol, β-myrcene, camphene and myrtenal. Terpineol has nice smell of lilac and is a sought-arter substance in the production of perfumes, fragrances and cosmetics. Pleasant smelling oily liquid. Myrcene has a large number of beneficial properties for the body, whether pure or in aromatherapy through the essential oils that contain it: Sedative and muscle relaxant, anti-inflammatory, interferon inhibition, gastric and duodenal ulcers, antalgic and antinociceptive, reduces sensitivity to pain by self-healing endogenous derivatives of morphine. Myrtenal – has an anti-inflammatory, resolving effect on acne, infiltrates. Increases the protective barrier of the epidermis. Antioxidant, rejuvenating. Camphene components are effective in the treatment of fungal, viral and bacterial infections that affect the respiratory system.
Key words: *Asteraceae, Zinnia elegans,* chemical composition, essential oils, *α-terpineol*, *β-myrcene*, gas chromatography-mass spectrometry (GC/MS), antioxidant activity.

Introduction

Zinnia elegant annual herbaceous plant, species of the genus *Zinnia* of *Asteraceae* families, it consists of species grown all over the world for their decorative role. Genus *Zinnia* there are about 20 species of herbaceous and semi-shrub annual and perennial plants from the family *Asteraceae*. In nature, the culture grows in the regions of South and Central America. The genus is named after the German professor of botany and pharmacology, director of the Botanical garden in Göttingen Johann Gottfried Zinn [1].

Nothing its predominant use as an ornamental plant, many studies have been devoted to the analysis of secondary metabolites identified in the plant in correletion with the therapeutic potential of the plant. Many studies have revealed the presence of several classes of biological active (natural) compounds in some plants organs. Studies of ethanol-water extracts obtained from the whole leaf or plant have revealed the presence of flavonoids, saponins, steroids, polyphenols and glycosides [2].

Certain spesies within the *Zinnia* genus have undergone extensive research due to their potential biological effects. These studies have uncovered various properties, including antifungal, antioxidant, hepatoprotective, antibacterial, antiviral, antimalarial, cytotoxic (evident in cancer cell lines), and insecticidal activities. Furthermore, the literature contains specific investigations into the antioxidant, hepatoprotective, antifungal, and antimalarial capabilities of these species [3].

Considering the constant requirement to explore novel plants and indirectly discover new sources of secondary metabolites with therapeutic potential for the treatment of inflammatory diseases and cancer, our focus was directed towards analyzing an excessively cultivated ornamental plant. Previous identification of certain classes of compounds, particularly polyphenols, within this plant suggested possible therapeutic benefits. Additionally, the ethnopharmacological data surrounding this plant highlighted its traditional usage as an infusion for pain relief. Therefore, this study aimed to conduct

a comprehensive phytochemical analysis of the hexane extract derived from the inflorescences of *Zinnia elegans*, along with its respective fractions. Furthermore, we aimed to evaluate the antioxidant activity of the extract though two distinctive mechanisms – inhibition of lipoxygenase and cheletion of iron [4].

Romanian scientists conducted a comprehensive study on the component composition and biological activity of the essential oil derived from plants belonging ti the *Z. elegans* species. The phytochemical analysis of *Zinnia elegans* plants grown in East Kazakhstan had not been previously explored. Hence, the study of the chemical composition of Kazakhstan's *Zinnia* species is of great significance in terms of discovering new medicinal recources [5].

Materials and methods

One commonly used method obtaining essential oil from dried and crushed aboveground parts of plants, steam distillation was carried out with hexane as a trap in a Clevenger apparatus for 2 hours. The essential oil's component composition

The component composition of essential oil of plants of the genus *Zinnia* was determined on a gas chromatograph with a mass spectrometric detector (GC/MS) using a RestekRxi®-1ms capillary column (0.25mm × 30 m × 0.25 µm), sample volume 1.0 µl, carrier gas flow rate 1 ml/min, scanning time from 4 to 120 min, ion scanning mode 39-500 m/z [6,7]. The components were identified by comparing retention time, mass spectral fragments using the NIST library. Table 1 shows the GC/MS analytical results for *Z.elegans* essential oil. *Z.elegans* essential oil contained 43 components, which accounted for 99.46% of the total number of oil components, the main volatile components of which were: β-myrcene (14.07%), *α*-terpineol (9.45%), myrtenal (7.87%) and camphene (5.36%). (presented on Figures 1 and 2, and Table 1).

Results and discussion

The antioxidant activity of fractions isolated from the essential oil of *Z. elegans* inflorescences was determined using two established methods: the iron chelating activity test and the 15-LOX inhibition test. The effectiveness of the test samples in chelating iron irons and inhibiting lipoxygenase was quantified using EC50 and IC50 values (as presented in Table 2). The obtained results were also compared to those of positive controls (terpinol and ethylenediaminetetraacetic acid EDTA) in order to assess their efficacy [8].
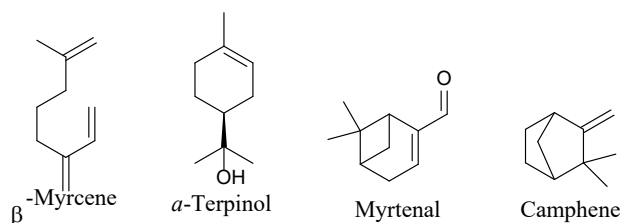
Figure 1 – Structural formulas of essential oils identified in *Zinnia Elegans*

As for the activity of inhibition of lipoxygenase, Fraction 2, where contains α-terpineol common compounds, showed the most promising activity (18.98 ± 0.22 micrograms / ml of the final solution), similar to the activity of positive control (terpineol). Other fractions, such as Fraction 3 and Fraction 4, have also exhibited significant inhibitory activity against the enzyme. In contrast, Fraction 5, which consists of fewer polar compounds compared tothe previous fractions, displayed a similar level of activity to that of the original extract. It is worth nothing that the fractions obtained generally demonstrate improved IC50 values for the analysis of lipoxygenase inhibition when compared to the total extract [9]. Interestingly, while the iron chelating activity was most promising in the initial essential oil, with a final solution concentration of 0.615± 0.001 mg/ml, this activity was not observed to the same extent in its selective fractions. However, it is noteworthy that the calculated value was found to be 10 times higher than that obtained for EDTA, a well-known metal chelator. This suggests the presence of a lower concentration of an effective iron chelator in the essential oil. Overall, these findings highlight the potential of different fractions in exhibiting inhibitory activity against the targeted enzyme. Moreover, the initial essential oil demonstrated remarkable iron-chelating properties, surpassing the efficacy of a widely recognized metal-chelating agent. There results suggest the presence of novel bioactive compounds within the fractions and essential oil, which can be further explored for potential therapeutic applications.
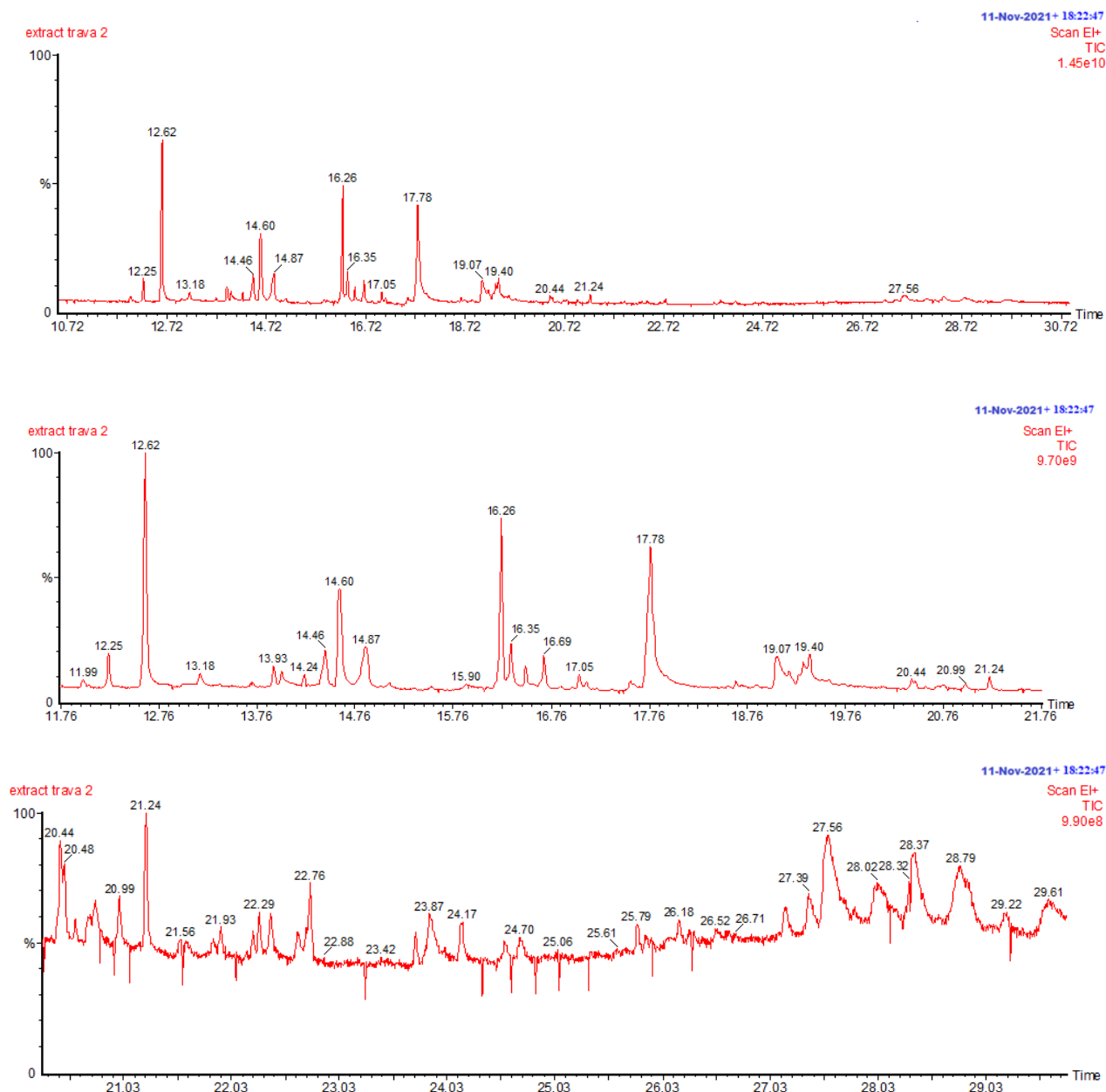
Figure 2 – GC/MS analytical results for *Zinnia elegans* essential oil

Table 1 – Component composition of *Zinnia Elegans* essential oil,%

№	RT	Component name	Content, %
	11,9843	α -Bulnesene	0,18
	12,2497	4-methylene-1-methyl-2-(2-methyl-1-propen-1-yl)-1-vinyl-cycloheptane	1,42
	12,6185	α -terpineol	9,45
	13,1776	1 α,2,3,5,6,7,7 α,7 β -octahydro-1,1,7,7 α -tetramethyl-, [1 α R-(1 α α,7 α,7 α α,7b α)]-1H-Cyclopropa[a]naphthalene	0,24
	13,927	3,7,11-trimethyl-, (E,E)-2,6,10-Dodecatrien-1-ol	0,09
	14,2403	Diepicedrene-1-oxide	0,12

Table continuation

№	RT	Component name	Content, %
1	14,4594	α -Bisabolol	1,61
2	14,5978	1-ethylideneoctahydro-7 α -ethyl-, (1E,3 α,7 α β)-1H-Indene	1,65
3	14,8747	1,2,3,4,4 α,7,8,8 α -octahydro-1,6-dimethyl-4-(1-methylethyl)-, [1R-(1a,4 β,4 α β,8 α β)]-1-Naphthalenol	1,63
4	16,2586	23-dien-3-ol, (3 β)-26,27-Dinorergosta-5	2,16
5	16,3507	6-Methyl-2-tridecanone	0,78
6	16,6854	2,6,10-Trimethylundeca-1,3-diene	1,45
7	17,0465	6-Methyl-2-tridecanone	0,76
8	17,7795	1,5-diethenyl-3-methyl-2-methylene-, (1 α,3 α,5 α)-Cyclohexane	1,99
9	19,0688	3,7,11-trimethyl-, acetate, (E,E)-2,6,10-Dodecatrien-1-ol	1,52
10	19,397	3-(3-methyl-1-butenyl)-(E)-Cyclohexene	1,48
11	19,9334	6-Isopropenyl-4,8 α -dimethyl-4 α,5,6,7,8,8 α -hexahydro-1H-naphthalen-2-one	0,45
12	20,4435	Camphene	5,36
13	20,4843	4,8,12-Trimethyltridecan-4-olide	3,07
14	20.9851	tetrahydro-6-octyl-2H-Pyran-2-one	1,97
15	21,2390	β-myrcene	14,07
16	21,5640	Nickel tetracarbonyl	1,76
17	21,9353	Adipic acid, 2-ethylhexyl octyl ester	1,80
18	22,7563	Dodecanoic acid, ethyl ester	2,18
19	22,8788	Tridecanoic acid, methyl ester	1,68
20	23,4241	Hexacosanoic acid, methyl ester	1,70
21	23.8689	9-Octadecyne	1,94
22	24,1717	methyl ester, (E)-2-Hexadecenoic acid	1,86
23	24,7086	Undecanoic acid, ethyl ester	1,78
24	25,0634	Benzoic acid, nonadecyl ester	1,71
25	25,6143	Benzoic acid, heptadecyl ester	1,74
26	25,7912	Benzoic acid, pentadecyl ester	1,84
27	26,1823	Benzoic acid, tridecyl ester	1,87
28	26,5256	Benzoic acid, undecyl ester	1,82
29	26,7134	Benzoic acid, octyl ester	1,81
30	27,3967	n-Hexadecanoic acid	1,98
31	27,5567	myrtenal	7,87
32	28,0227	3-hydroxy-6-isopropenyl-4,8 α -dimethyl-1,2,3,5,6,7,8,8 α -octahydronaphthalen-2-yl ester Acetic acid	2,20
33	28,3278	6-Isopropenyl-4,8 α -dimethyl-4 α,5,6,7,8,8 α -hexahydro-1H-naphthalen-2-one	2,21
34	28,3719	4,14-dimethyl-, acetate, (36,4 α,5 α)-9,19-Cycloergost-24(28)-en-3-ol	2,42
35	28,7987	Benzoic acid, tetradecyl ester	2,00
36	29,2225	Eicosanoic acid, ethyl ester	1,88
37	29,6154	Acetic acid, 3-hydroxy-6-isopropenyl-4,8 α -dimethyl-1,2,3,5,6,7,8,8 α -octahydronaphthalen-2-yl ester	1,96
		Total	99,46

Table 2 – *Zinnia elegans's* fractions antioxidant activity results

	Inhibition of lipoxygenase	Iron chelating activity
Name of sample	IC 50 (mg / ml)	EC 50 (mg / ml)
Fr 1	65,65 ±0,70[a*]	0,719 ±0,001[a]
Fr 2	19,99 ±0,23[d]	1,036 ±0,003[d]
Fr 3	31,65 ±0,74[c]	1,634 ±0,006[c]
Fr 4	43,54 ±1,47[b]	1,199 ±0,011[a]
Fr 5	69,43 ±6,78[a]	1,665 ±0,011[b]
The original extract	69,95 ±0,89[a]	0,645 ±0,001[f]
Positive control	20,45 ±0,44[d]	0,078 ±0,003[g]

* The values are the average values ± standard deviation, n = 3. a-g The average values in the column without a common uppercase letter differ ($p < 0.05$), as indicated by a one-factor analysis of variance.

Six strains were used in the study, which included four Gram-positive cocci strains, three of which were reference strains; *Staphylococcusaureus* ATCC 6538 (used in the determination of disinfectant – test), *Staphylococcusaureus* ATCC 25923 (used in the determination of antibiotic susceptibility – test), *Staphylococcusaureus* TS 77 (QacA/B harbor and disinfectant resistant gene and vancomycin resistant *Enterococcus* (VRE). In addition, three gramm-negative bacilli, which included 2 reference strains: *Pseudomonas aeruginosa* ATCC 27853 and *Escherichia coli* ATCC 25922 (both used for antibiotic susceptibility testing) and one carbapenem-resistant strain of Klebsiella pneumoniae (CRKP). All initial and clinical strains were obtained from the Department of Medical Microbiology, Faculty of Medicine, Istanbul University.

All strains of bacteria were cultivated on yryptic soy agar, supplied by OXOID in Turkey. The agar plates were incubated aerobically at a temperature of 35ºC for a period of 24 hours. After the incubation period, the bacterial cultures were suspended in sterile saline solution containing 0.85% NaCl. The suspension was carefully adjusted to a concentration of 108 colony-forming units per milliliter. A 96-well round bottom microtiter was used, including a negative (plant extract only medium) and positive control (bacteria only medium) and 10 serial two-fold dilutions of each of the two plant extracts ranging from 9.765 to 5000 µg/mL with a final concentration a suspension of bacterial cells equivalent to $1*10^5$ cfu/ml. All grafted plates were incubated as above. The microphones were evaluated after 24 hours. Minimum bactericidal concentration (MBC) was performed by subculturing 10 ml from all wells in which no visible growth was observed (concentration equal to or higher than MIC) on a plant extract without Muller Hinton agar (OXOID, Turkey) and incubated as above [10]. (Table 3).

Table 3 – Minimum inhibitory concentration (MIC) for various plant extracts against various strains

Bacterium	Minimum inhibitory concentration (MIC), mcg/ml	
	T1	T2
S.aureus ATCC 6538	R	625
S.aureus ATCC 25923	R	R
S.aureus TS 77	R	R
E.coli ATCC 25922	1250	1250
P.aeruginos ATCC 27853	625	R
B.subtilis ATCC 6633	625	625
Carbapenem resistant *K.penumoniae* (CRKP)	625	625
Vankomycin resistant Enterococci (VRE)	312,5	312,5

Abbreviation: R – the strain is resistant to the high concentration of the tested plant extract of 5000 µg/ml.

The tests were repeated twice or more and averages were calculated. In the study, two plant extracts (T1 and T2) had different effects on the strains. T1 microphones for *E. coli* ATCC 25922, *P. aeruginos* ATCC 27853, *Vankomycin resistant Enterococci* (VRE) and *B. subtilis* ATCC 6633 cells produced 625 mg/ml, 321.5 mg/ml and 1250 mg/ml, 625 mg/ml, respectively. The extract exhibited a remarkable capability to eliminate all strains mentioned above, as evidenced by its minimum bactericidal concentration (MBC) of 250 mg\ml, 625 mg/ml, and 1250 mg/ml. On the other hand, T2 microflora for *S. aureus* ATCC 6538, *E. coli* ATCC 25922, *B. Subtilis* ATCC 6633 and *Vankomycin resistant Enterococci* (VRE) were 625 µg/mL, 1250 µg/mL, 625 µg/mL and 312.5 µg/mL, respectively

Table 4 – Minimum bactericidal concentration (MBC) of various plant extracts against various strains

Bacterium	Minimum inhibitory concentration (MIC), µg/ml	
	T1	T2
S.aureus ATCC 6538	NT	5000
E.coli ATCC 25922	2500	2500
P.aeruginosa ATCC 27853	625	NT
B.subtilis ATCC 6635	625	2500
Vankomycin resistant Enterococci (VRE)	1250	>5000

Abbreviation: NT – not tested because the MBC value was not available as it was resistant to high tests at an herbal extract concentration of 5000 µg/mL.

The MBC T2 values for the aforementioned strains were 5000 mg/ml, 2500 mg/ml, 2500 mg/ml, >5000mg/ml, respectively. Comparison of MBC of these two extracts showed the superiority of T1 (625 µg/ml) in the fight against the *P. aeruginosa* strain and T2 (5000 µg/ml) in the destruction of S. aureus strains (Table 4).

Conclusions

It is shown that *Zinnia Elegans*, growing in the East Kazakhstan region, is a promising source of essential oils. Essential oil's of plant main components are monoterpenes, contained 43 components, which amounted to 99.46% of the total number of oil components, the main volatile components of them were: *β*-myrcene (14.07%), *α*-terpineol (9.45%), myrtenal (7.87%) and camphene (5.36%). This fraction of hydrocarbons of essentiol oil has a wide spectrum of pharmacological action, mainly determining the biological effects. It is concluded that all essential oils have a weak antioxidant effect, and this is one of the facets of their biological activity. Of all the studied in the work, *Z. elegans* essential oil, which has the highest content of *β*-myrcene (14.07%), shows great antioxidant activity. The research results indicate the pharmacological potential of *Z. elegans* essential oil, which grows in the East Kazakhstan region, which allows it possible to consider it as a promising component for obtaining phytopreparations and natural medicinal products.

References

1. Pavlov N.V. (1960). Flora of Kazakhstan. 3. 20-45. [in Russian].

2. Ojha S.K., Nandave M., Arora S., Narang N., Dinda A.K., Arya D.S. (2008) Optimal conditions for cleaning and drying furostanol saponins from tribulus terrestris. *International Journal of Pharmacology*, 1–10.

3. Yakusheva L.A., Myagkova R.I., Sarycheva I.K., Evstigneeva R.P. (1984). Arachidonic acid and ways of its isolation from natural objects. *Chemistry of natural compounds.* 2. 233-241. [in Russian].

4. «Vegetable oils and animal fats. Mass fraction determination by gas chromatography». GOST 51483-99. [in Russian].

5. Trineeva O.V., Safonova I.I., Safonova E.F.(2013). Identification of organic acids by TLC in extracts from plant objects. *Sorption and chromatographic processes*. 6. 896-901. [in Russian].

6. Kashkan G.V., Kuleshov V.I., Baranova V.O. (1988). Atomic emission determination of trace

elements in biological samples. *Analytical Chemistry.* 18-19. [in Russian].

7. Adams R.P. (2007) Identification of Essential Oil Components by Gas Chromatography / Mass Spectrometry. *Allured Pub-lishing Corporation, Carol Stream, Illinois,* 803-806

8. Muzychkina R.A., Korulkin D.Yu., Abilov Zh.A. (2004) Qualitative and quantitative analysis of the main groups of biologically active substances in medicinal plant raw materials and phytopreparations.

Chemistry of natural compounds. 288-299. [in Russian].

9. Wahba HE, Motawe HM, Ibrahim AY. Chemical composition of essential oil, anthocyanins and fatty acids of Zinnia pauciflora. World Journal of Pharmaceutical Sciences. 2014;2(12):1657-63.

10. Alexenizer M., Dorn A. Screening of medicinal and ornamental plants for insecticidal and growth regulating activity. *J. Pest Sci.* 2015;80:205–215. doi: 10.1007/s10340-007-0173-x.

D.S. Nazarova[1] , N.A. Satybayeva[1] , S.S. Satayeva[1]* , V.A. Burakhta[2] ,

I.A. Kazarinov[3] , A.N. Mukambetkaliyeva[2] , A.K. Abdygaliyeva[1] ,

A.A. Yesmagulova[1] , D.A. Baimurzin[1]

[1]Zhangirkhan West-Kazakhstan agrarian technical university, Uralsk, Kazakhstan
[2]West Kazakhstan University of Innovation and Technology, Uralsk, Kazakhstan
[3]Saratov State University named after N.G. Chernyshevski, Saratov, Russia
*e-mail: sataeva_safura@mail.ru

Use of natural material (flask) of the Taskalinsky deposit of the West Kazakhstan region to obtain thermal insulation material

Abstract. Modern construction market is experiencing a shortage of highly efficient thermal insulation materials. Alkali-silicate raw mixtures in combination with high-performance fillers currently make it possible to create porous heat-insulating materials with unique properties: rigid cellular structure, specified geometric dimensions and shape, low thermal conductivity, incombustibility, high processability, environmental friendliness, etc. at a relatively low cost. The use of such heat-insulating materials in construction allows solving the problems of energy saving, accessibility and cost-effectiveness. The article considers possibility of obtaining heat-insulating material based on sodium silicate (silicate glue "Polipax") and natural material – flasks from Taskalinsky deposit of West Kazakhstan region. Technical characteristics of Polypax glue are given. Using a scanning electron microscope, elemental, chemical, and oxide compositions of the flask were studied. A recipe for a heat-insulating composite material (HCM) has been compiled. To assess the quality of the obtained HCM, its physical and mechanical characteristics were determined: density, water resistance, thermal conductivity, strength. Samples I-II in terms of density and strength showed the best results, and samples III-IV differ slightly from the technical conditions in terms of the studied indicators. It has been determined that the obtained HCM using flask as filler has a positive effect on the performance properties of the heat-insulating material, and is also economically viable, because local raw materials are used. Thus, it is possible to use flask from Taskalinsky deposit of West Kazakhstan region as filler for heat-insulating material.

Key words: flask, liquid glass, heat-insulating material, water absorption, strength, thermal conductivity coefficient.

Introduction

It is economically unprofitable to use materials such as traditional brick, lightweight concrete for thermal protection of enclosing structures. In the manufacture of building structures, the use of indestructible highly efficient heat-insulating materials is required.

To compensate for heat losses, it is necessary to increase the heating of building or use more efficient heat-insulating materials. The last case is advantageous, because in this case, 17% of fuel is saved. In addition, the use of highly efficient thermal insulation materials reduces construction costs and material consumption.

The introduction of resource-saving technologies is an important direction in the development of building materials industry. In various regions of the country, resource conservation is facilitated by the involvement of industrial waste and by-products in the production [1-4]. At the same time, raw materials of technogenic origin with a high degree of technological readiness are the most effective in terms of resource saving.

The use of two-layer heat-insulating elements with a dense finished structure will make it possible to complete the construction of buildings in less time and increase the degree of industrialization. Science has accumulated a real potential for creating new effective materials based on the improvement of processes and equipment.

So, for example, in [5] the results of studies on the production of heat-insulating, heat-insulating-structural and heat-resistant building materials based on filled liquid glass compositions using low-energy foaming technologies are presented. As a raw material, ultrafine microsilica was used, a waste of a ferroalloy plant. Regularities of structure formation were determined, which provide strength, heat-insulating and heat-resistant characteristics of the building material. The advantages of technological solutions that ensure the stability of technical characteristics of materials were noted, which is important when using foaming technologies.

The authors [6] studied composite material liquid glass–graphite microparticles with increased thermal stability and thermal insulation properties. A composition consisting of graphite (42% by mass), liquid glass $Na_2O(SiO_2)_n$ (50% by mass) and hardener – sodium fluorosilicone Na_2SiF_6 (8% by mass) was proposed. Values of limit loads, nature of discontinuous surface, numerical values of specific heat capacity and coefficient of thermal conductivity were determined. Studies have confirmed the increased thermal insulation properties of the proposed composition.

No less interesting is the work [7], which presents an overview of the world experience in the production of foam glass materials using various raw materials, and also describes the results of research into the technology of foam glass foaming based on various types of silicate raw materials. The properties of synthesized samples and their microstructure have been studied. The conclusion is made about the applicability of silicate raw materials in the production of porous materials.

The paper [8] considers a method for manufacturing foam glass using float glass waste and sodium hydroxide. Titanium dioxide TiO_2 was introduced as hardening additive. The compositions consisted of, % (by mass): titanium dioxide – 20, sodium hydroxide – 3-17, ground glass – the rest. It is shown that samples containing 11% (by mass) NaOH and 20% (by mass) TiO_2, and without it, have the following strength values, respectively 3.40 and 0.48 MPa.

Over the past decades, composites have actively entered practice and replaced traditional materials in energy, transport, electronics and other fields of activity. The difference between most composite materials and traditional ones is that the process of their manufacture can be combined with the process of manufacturing the product [9]. There is also world experience in the use of composite technologies based on carbon fibers [10-15].

Liquid soda glass, powdered mineral fillers and special additives are used as raw materials for foamed liquid glass materials. Foam production consists of special processes (fig. 1):
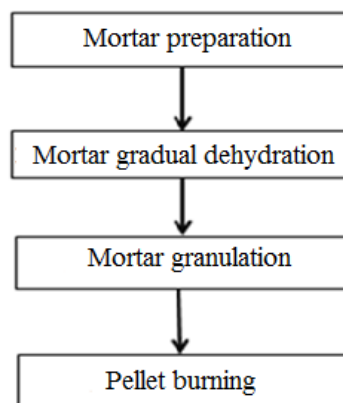

Figure 1 – Foam materials production scheme

In connection with the foregoing, the purpose of this work is to obtain composite heat-insulating materials based on liquid glass using flasks (local raw materials) from Taskalinsky deposit of West Kazakhstan region as filler.

Materials and methods

The main raw material for the production of the proposed materials is the flask from Taskalinsky deposit of West Kazakhstan region, which is a homogeneous mixture of light green color (Fig. 2), consisting of opal silica (60-80%), clay (10-40%) and soil-aleurite (up to 10%) material. A feature of the flask is the mesocompatibility of the structure, mechanical strength, high dispersion, and, as a result, high water absorption capacity. Physical and mechanical properties of the flask: bulk density – 1.49-1.59 (1.54) g/cm^3, natural moisture content -14.3-23.83 (17.88)%, activity – 17.81-44, 5 (37.1)%. Chemical composition of the flask is represented mainly by silicon dioxide SiO_2. These properties of the flask make it possible to use it as filler for the manufacture of heat-insulating materials.

The binder in the work is the liquid silicate glue Polypax, the basis of which is sodium silicate. Features of Polypax glue: when foaming, it ceases to conduct heat, therefore it is used to create heat-saving materials; withstands heating to very high temperatures, for some brands the limit is more than + 1000 degrees. The table 1 shows the technical characteristics of the glue.

Figure 2 – Flask from Taskalinsky deposit of West Kazakhstan region

Table 1 – Technical characteristics of Polypax glue

Appearance	Thick yellowish or slightly greenish liquid
Density	1.36-1.45 g/cm³
Mass fraction of insoluble substances	0.2 %
Shelf life in closed containers	2 years
Freeze/Defrostpossibility	allowed
Operating temperature of insulating layer	1300 ⁰C

The flask has a strengthening effect when introduced as filler into liquid glass, which is an inorganic polymer. This action depends on the binding properties of liquid glass.

Results and discussion

Physico-mechanical properties of the flask have been determined. Experimental data are shown in Table 2.

Table 2 – Physical and mechanical properties of flask

Fraction sizes, mm	Bulk density, g/cm³	Water absorption, %	Splitting up, %	Thermal conductivity, W/m K
5-10	561	44.50	28.29	0.08
10-20	553	46.60	28.57	0.08
20-40	528	45.20	28.16	0.07

Chemical composition of the flask was studied by physicochemical methods using X-ray phase (X-600, France) and differential thermal analyzes (DTG-60, Japan), as well as using a scanning electron microscope (Hitachi SU8220, Japan). Figure 3 shows the flask radiography.

Using a scanning electron microscope, the elemental and oxide compositions of powdered, chipped and thin sections of the flask were determined.As an example, in fig. 4 shows the elemental composition of the flask in the form of a chip.
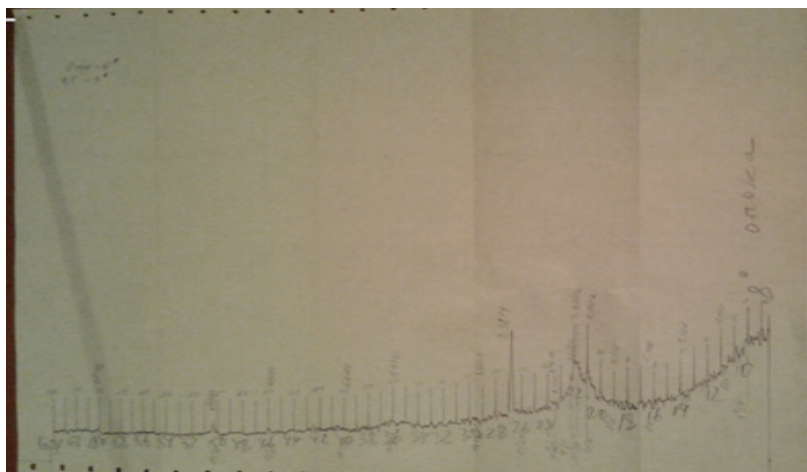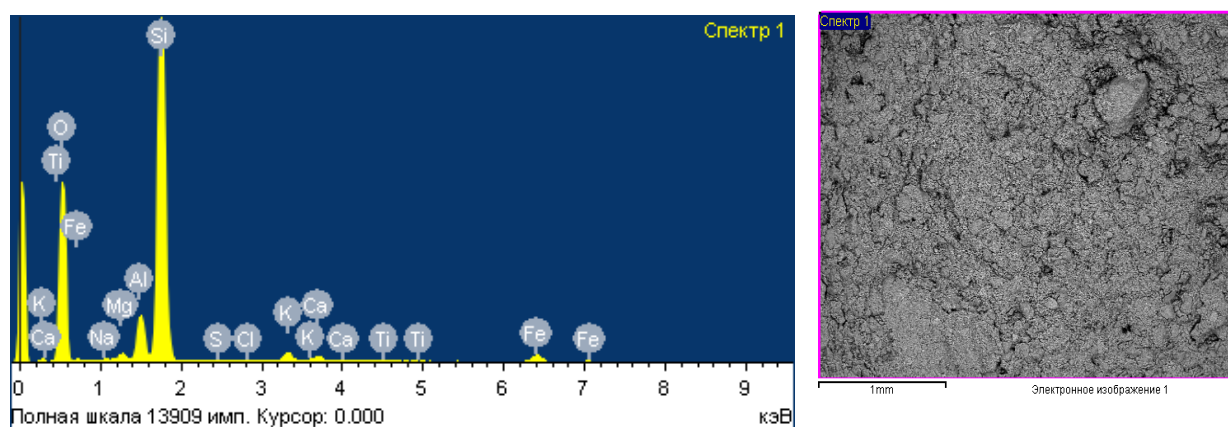
Figure 3 – X-ray of the flask

Figure 4 – Elemental composition of flask in the form of chip

Figure 5 shows the oxide composition of the studied raw material (flask).

To prepare composite material samples, the flask was crushed using a ball mill. The crushed flask was removed every 15 minutes in the amount of 250 g. Physical parameters of the crushed flask were determined using PSKh-K device (Table 3).

Effective composition of heat-insulating material based on liquid glass and flask has been developed. 4 composite material compositions were made. Mass ratios of the components are presented in table 4.

Composite materialpreparation method: the components were placed in glass beakers and stirred for 10-20 minutes until a paste-like mass was formed. Then the masses were transferred into porcelain crucibles and placed in a muffle furnace heated to 600 ^{0}C. And kept in the oven for 15 minutes.

Physical and mechanical properties of the obtained samples of composite material were studied (Table 5).

Table 5 shows that using siliceous rock (flask) it is possible to obtain heat-insulating materials with different pore sizes. Heat insulators obtained on the basis of liquid glass and flask in terms of density, water resistance, thermal conductivity coefficient and strength meet technical requirements.
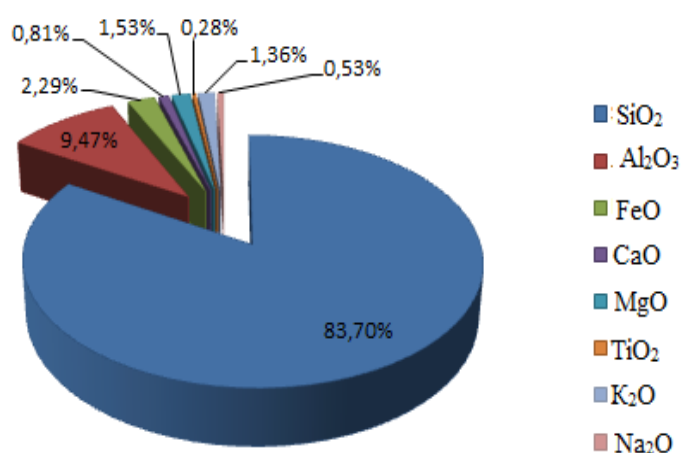
Figure 5 – Oxide composition of flask

Table 3 – Physical indicators of the crushed flask

Specific surface, cm²/g	Average particle size, microns	Density, g/cm³
3891	9.6	1.61
5458	6.8	1.61
6130	6.1	1.61
6390	5.8	1.61

Table 4 – Component composition of composite material

Sample No.	Component, wt. %	
	Flask (average particle size, μm)	Liquid glass (Polypax glue) (ρ=0.9 g/cm³)
I	50 (9.6)	50
II	50 (6.8)	50
III	50 (6.1)	50
IV	50 (5.8)	50

Table 5 – Physical and mechanical characteristics of the manufactured samples of composite material

Sample No.	Density, ρ, kg/m³	Water resistance, K_p	Coefficient of thermal conductivity,λ, W/mK	Strength, Rc, MPa
I	610.0	0.900	0.116	4.34
II	594.5	0.870	0.113	4.20
III	574.0	0.859	0.109	4.00
IV	563.0	0.847	0.107	3.90
GOST 7076-99	400-600	1.000	0.100-0.140	1.20-4.00

The main problem of the widespread use of foam glass materials is their high price relative to other heat-insulating materials. In the world practice, the production of heat-insulating foam-glass materials based on cheap natural and technogenic silica raw materials is being studied. In this article, samples of heat-insulating material are made, obtained on the basis of sodium silicate and local natural raw materials – flask. 4 samples of composite material were made in a percentage ratio of 1:1 (50% – flask, 50% – sodium silicate), but with different particle sizes of flask. The best result was shown by the 1st sample with a particle diameter of 9.6 μm, which exceeds the values according to GOST in terms of density and strength. Good results were shown by the second sample with strength of 0.2 MPa more than the maximum permissible norms (MPN), the density and thermal conductivity values correspond to the technical conditions. The results of analyzes for samples III and IV are satisfactory. However, it should be noted that all 4 composite materialsamples slightly differ from MPN in terms of water resistance values. It has been determined that, in general, it is possible to use flask from Taskalinsky deposit of West Kazakhstan region as filler for liquid glasses.

Conclusion

The paper synthesized heat-insulating materials that are most widely used in construction, studied their properties and selected the most effective heat-insulating material – foam glass, which has good thermal properties and has the best environmental performance, as well as resistance to aggressive factors.The resulting heat-insulating material is a silicate material with evenly spaced pores separated by thin vitreous partitions, has the necessary properties and, due to the foregoing, can be accepted for research aimed at its improvement (modification). The research results can be applied in the production of foam glass, which is used for thermal insulation of buildings and structures, equipment, pipelines.

Thus, according to the results of the conducted studies, it was proved that flask from Taskalinsky deposit of West Kazakhstan region can be used as filler for the production of heat-insulating materials. The possibility of obtaining building materials based on local raw materials (flasks) is shown, which contributes to saving material and energy costs in the production of multi-purpose building materials. The use of flask will expand the mineral resource base of plants for the production of thermal insulation materials.

References

1. Kopanitsa, NO. (2011) Influence of complex modifiers on properties of peat-wooden constructive heat-insulation materials. Vestnik of Tomsk State University of Architecture and Building, 3, 140-144.

2. Lukash, A.A., Lukuttsova, N.P. (2017) Effective building materials from industrial waste for housing. Vestnik of Volga State University of Technology.Ser. Materials.Constructions. Technologies, 2, 26-37.ISSN 2542-114X

3. Steshenko, A. B.; Kudyakov A. I. (2018) Cement based foam concrete with aluminosilicate microspheres for monolithic construction. Magazine of Civil Engineering, 8:86-96. DOI:10.18720/MCE.84.9

4. Belykh, S.A., Lebedeva, T.A., Vasilyeva, D.S. (2020) Study of the molding properties of sodium silicate mixtures in the manufacture of building materials using sol-gel technology. Technical science. Construction, 10(4), 544-551. DOI: 10.21285/2227-2917-2020-4-544-551

5. Belykh, S.A., Lebedeva, T.A., Daminov, A.M. (2017) Construction materials based on filled liquid-glass compositions and the field of their application. Systems Methods Technologies. Construction materials, 36, 176-181.DOI: 10.18324/2077-5415-2017-4-176-181

6. Gostev, V.A., Pituhin, E.A., Ustinov, A.S., Yakovleva, D.A. (2014) Thermal insulation properties research of the composite material water glass–graphite microparticles. Scientific and Technical Journal of Information Technologies, Mechanics and Optics, 3(91), 81-87. ISSN 2226-1494 (PRINT), ISSN 2500-0373 (ONLINE)

7. Goltzman, B.M., Yatsenko, E.A., Gerashchenko, V.S., Komunzhieva N.Yu.,Yatsenko, L.A., Smoliy, V.A. (2020) Chia-Chi Cheng. Porous heat-insulating materials based on various types of siliceous raw materials. IzvestiyaVuzov. Severo-Kavkazskiy region.technical science, 1, 55-60. DOI: 10.17213/1560-3644-2020-1-55-60

8. Martin, S.,Martin, N.,Tomas, O.,Radomir, S.(2022) Preparation and Characterization of Glass-Ceramic Foam from Clay-Rich Waste iatomaceous Earth. Materials (Basel),15(4), 1384. DOI:10.3390/ma15041384

9. Bento, A., Kubaski, E., Sequinel, T., Pianaro, S., Varela, J. Tebcherani, S. (2013) Glass foam of macroporosity using glass wasteand sodium hydroxide as the foaming agent. Ceramics International, 39(3), 2423-2430.DOI:10.1016/j.ceramint.2012.09.002

10. Murariu, M., Dechief, A.L., Bonnaud, L., Paint, Y., Gallos, A., Fontaine, G., Bourbigot, S., Dubois, P. (2010) The production and properties of polylactide composites filled with expanded graphite. Polymer Degradation and Stability, 95(5), 889-900. doi.org/10.1016/j.polymdegradstab.2009.12.019

11. Huang, J., Baird, D.G., McGrath, J.E. (2005) Development of fuel cell bipolar plates from graphite filled wet-lay thermoplastic composite materials. Journal of Power Sources, 150(1–2), 110–119. doi.org/10.1016/j.jpowsour.2005.02.074

12. Sadasivuni, K.K., Ponnamma, D., Thomas, S., Grohen, Y. (2014) Evolution from graphite to graphene elastomer composites. Progress in Polymer Science, 39(4), 749–780. doi.org/10.1016/j.progpolymsci.2013.08.003

13. Das, A., Kasaliwal, G.R., Jurk, R., Boldt, R., Fischer, D., Stöckelhuber, K.W., Heinrich, G. (2012) Rubber composites based on graphenenanoplatelets, expanded graphite, carbon nanotubes and their combination: A comparative study. Composites Science and Technology, 72(16), 1961–1967. doi.org/10.1016/j.compscitech.2012.09.005

14. Barreto, C., Proppe, J., Fredriksen, S., Hansen, E., Rychwalski, R.W. (2013) Graphite nanoplatelet/pyromelliticdianhydride melt modified PPC composites: Preparation and characterization. Polymer, 54(14), 3574–3585. doi.org/10.1016/j.polymer.2013.04.068

15. Wang, B., Jiao, Y., Gu, A., Liang, G., Yuan, L. (2014) Dielectric properties and mechanism of composites by superposing expanded graphite/cyanate ester layer with carbon nanotube/cyanate ester layer. Composites Science and Technology,91, 8–15.doi.org/10.1016/j.compscitech.2013.11.014

A.A. Minkayeva ⓘ , Sh.M. Mamashev ⓘ , A.K. Nurlybekova ⓘ ,

A.A. Kudaibergen ⓘ , Ye. Shybyray ⓘ , U. Amzeyeva ⓘ , J. Jenis* ⓘ

The Research Center for Medicinal Plants, Al-Farabi Kazakh National University, Almaty, Kazakhstan
*e-mail: janarjenis@kaznu.kz

Chemical constituents of *Dianthus superbus*, *Matricaria chamomilla* and *Glycyrrhiza glabra*

Abstract. Currently, one of the main directions of science is the study of plants with medicinal properties, the determination of biological activity and its use for medical purposes. In this supplied research work, the quantitative and qualitative composition of phytochemical components of plants *Dianthus superbus, Matricaria chamomilla* and *Glycyrrhiza glabra* growing in the Republic of Kazakhstan were investigated first-ever. The results of our studies showed the maximum amount of organic acids (0.317 %) and flavonoids (0.296 %) in the plant *D. superbus*. The content of extractive substances *M. chamomilla* (30.01 %) and *G. glabra L.* (35.30 %), and the content of polysaccharides is higher in plants *G. glabra L.* (1.475 %) and *D. superbus* (1.434 %). The plant *M. chamomilla* showed good results i n the amount of elements needed daily by the human body, including – K (23.97 mg/g), Na (5.39 mg/g), Mg (2.26 mg/g), Ca (4.31 mg/g) and Fe (0.32 mg/g). The results of the conducted analyses showed that the studied objects contain a sufficient amount of bioactive substances that may enhance the variety of successful home pharmaceuticals in the future based on plant raw materials of the Republic of Kazakhstan.

Key words: *Glycyrrhiza glabra, Dianthus superbus, Matricaria chamomilla*, phytochemical components, macroelements, microelements.

Introduction

Dianthus superbus is well-known traditional herbal medicine recognized for its anti-inflammatory effects in ancient Mongolian and Chinese oriental medicine. Even in the modern day, Mongolians are using *D. superbus* for reducing inflammation and reported to have plentiful with cyclic peptides, which showed strong anticancer activity on a wide range of cancer cells. Additionally, organic extraction of *D. superbus* exhibited antiviral activity against diverse strains of influenza A and B viruses. Moreover, quercetin derivative isolated from *D. superbus* showed stronger anti-influenza activity than the commercial drug Oseltamivir and was found to block viral RNA (vRNA) replication through binding to PB2 subunit of viral polymerase [1].

Matricaria chamomilla has various and ancient uses, including herb tea, natural medicine, and pharmaceutical preparations. It contains anti-inflammatory, antibacterial, anti-allergic effects, acts as a diuretic, sedative, carminative, and secretogog for bile, and is applied externally for healing skin wounds,

mouth sores, and haemorrhoids. Chamomile's medical and pharmacological benefits are mostly associated with its essential oil, which has antispasmodic, antibacterial, and disinfectant characteristics. The essential oil of chamomile is widely utilised in the culinary, cosmetics, and pharmaceutical sectors. Chamazulene, epi--bisabolol, -bisabolol oxide, -carvacrol, p-cymene, (E)--ocimene, (Z)--ocimene, (E,E)-farnesol, and en-yn-dicycloethers are the most important therapeutically relevant chemicals found in essential oil. Flavonoids, coumarins, hydroxycinnamic acids, mucilages, and a few other primary metabolites are also pharmacologically active. In vitro, chamomile displayed moderate antibacterial and antioxidant characteristics, as well as considerable antiplatelet activity and tentative anticancer outcomes. Chamomile essential oil was found to be a potential antiviral agent against herpes simplex virus type 2 (HSV-2) in vitro [2].

Glycyrrhiza glabra L. is widely used as a medicinal plant. *Glycyrrhiza* genus of flowering plants of the Fabaceae family, is a flowering native plant to Asia. There are five species growing in

Kazakhstan (Flora Kazakhstan). Phytochemical analysis indicated biologically active complexes of *G. glabra* are triterpene, flavonoids, polysaccharides, simple sugars, amino acids, mineral salts, fat, protein, resins, starches, glycosides, and various other substances. Several research [3, 4, 5, 6] have found that *G. glabra* extract or its derivatives, primarily glycyrrhizin, have expectorant, diuretic, laxative, sedative, antipyretic, antibacterial, and anxiolytic, antiviral, anti-inflammatory, and antioxidant properties. G. glabra has long been used to cure coughs and colds, as well as to soothe upset stomach, whilst diammonium glycyrrhizinate has anti-inflammatory properties and is used to treat liver damage caused by hepatitis B. According to Professor Hong Ding of Wuhan University presented a COVID-19 treatment combining diammonium glycyrrhizinate and vitamin C, and clinical studies have recently been allowed [7].

In this study, medicinal plants *Dianthus superbus, Matricaria chamomilla* and *Glycyrrhiza glabra L.* growing in Kazakhstan were studied for the quantitative content of biological active complexes namely flavonoids, carboxylic acids and polysaccharides for the first time. Comparatively, previous studies showed the results of amino acids and vitamins content from *Chamomilla recutita* (German chamomile) [8]. In the course of the work, the analysis of common biologically active components was carried out, such as the determination of the amount of organic acids, flavonoids, and polysaccharides, moisture content, total ash, and extractive content measured. The multi-element atomic emission spectrum analysis approach was also used to determine the levels of macro- and microelements in ashes and plants.

Materials and methods

Plant material *Matricaria chamomilla* was harvested in Southeast region, foothills of Alatau mountain Kazakhstan in the summer of 2021. Plant material *Glycyrrhiza glabra L.* was collected in in the vicinity of the city of Shardara, Kazakhstan in early autumn 2020. *Dianthus superbus*, *M. chamomilla*, and *G. glabra* L. air-dried parts were chopped into tiny pieces and kept at room temperature.

Methods described in the monograph [9] were used to conduct quantitative and qualitative analyses of bioactive compounds of *D. superbus*, *M. chamomilla*, and *G. glabra* L. A quantitative content of biologically active complexes namely the flavonoids, carboxylic acid and polysaccharides was

investigated. The flavonoids content was identified by measuring optical density of the prepared appropriate solution with an application of spectrophotometer at the wavelength of 430 nm. For the determination of polysaccharides the water extraction of plant obtained and combined with 95% ethyl alcohol in the ratio 1:3 and centrifuged at a speed of 4000 rpm for 30 minutes. The supernatant was filtered under vacuum through a glass PORE filter and dried to a constant mass that was calculated to a percentage value. The quantitative determination of carboxylic acids is carried out by titration method. The extractive content of three analyzing plant samples was measured using 80% ethanol solutions in water, as described in the State Pharmacopoeia X [10].

A Shimadzu 6200 series spectrometer was used to identify the mineral composition. In a pre-calcined and precisely weighed porcelain crucible, 3 g of raw material was inserted. The crucible was then slowly heated, first allowing the material to burn at the lowest feasible temperature before gradually increasing the flame. Calcination was carried out at 500°C to get a consistent mass. The crucible was cooled in a desiccator at the end of the calcination, and the resultant ash was burnt again at 600°C until a uniform grey color was achieved. Heating was used to dissolve plant ash in 10.0 mL of 40% nitric acid. The resultant solution was then boiled to produce wet salts. It was subsequently dissolved in 15.0 mL of 1 N nitric acid and transferred to a volumetric flask of 25.0 mL for analysis. Thus, it must be done for each of the three plants.

Results and discussion

Bioactive components, moisture content, total ash, and extractives were quantified and qualitatively analysed in *Dianthus superbus*, *Matricaria chamomilla*, and *Glycyrrhiza glabra* L. The findings are shown in Table 1.

Moisture and ash content vary within specified limitations for each plant and are determined by the nature of the plant material itself, as well as how it is harvested and dried. These data will be required for additional computations throughout the research, therefore determining these contents was required to demonstrate the high quality of *D. superbus*, *M. chamomilla*, and *G. glabra* L.

Using 80% alcohol, the most extractive compounds were extracted from all three plant species. As a result, this appropriate solvent can be employed in extraction. The identification of extractive compounds using an appropriate solvent is

critical since the quantity of biological metabolites dictates the plant's quality.

Flavonoids are the most abundant dietary polyphenolic class. They are a varied category of around 4000 distinct physiologically active chemicals synthesised during plant metabolism [11]. Flavonoids may contribute to a number of positive biological actions in humans after ingestion. Strong and consistent evidence currently suggests that flavonoids can maintain and boost nitric oxide status while also improving endothelial function. There is also evidence that these substances can affect blood pressure, oxidative damage, inflammation, platelet function and thrombosis, blood lipids, and glucose metabolism [12, 13]. These actions may assist to explain the results that flavonoids and flavonoid-rich diets have cardioprotective and antineoplastic activities [14, 15].

Organic acids are responsible for the taste, flavour, microbiological stability, and product consistency of plant-derived drinks, and they are employed in food preservation due to their antibacterial properties. Polysaccharides are unique chemicals that may maintain moisture in the dermis, keep the skin elastic, increase collagen fiber synthesis, and boost cell immunity.

Table 1 – Quantitative and qualitative analysis of biologically active constituents of *Dianthus superbus*, *Matricaria chamomilla* and *Glycyrrhiza glabra L.*

Plant Component	*Dianthus superbus*	*Matricaria chamomilla*	*Glycyrrhiza glabra L.*
	Content, %		
Moisture	5.00	6.70	5.10
Ash	6.40	12.68	4.80
Extractives	20.53	30.01	35.30
Organic acids	0.317	0.126	0.071
Flavonoids	0.296	0.105	0.150
Polysaccharides	1.434	0.643	1.475

The results of our research have shown the maximum content of organic acids and flavonoids in the plant *Dianthus superbus*. The content of extractive substances was higher in the plant *Matricaria chamomilla* and *Glycyrrhiza glabra L.*, and the content of polysaccharides was higher in the plants *G. glabra L.* and *D. superbus*. Eleven macro- and microelements were extracted (received) from plant ash. As demonstrated in Table 2, the most common were K, Na, Ca, and Mg. All three plants are an excellent source of minerals and vital elements that are required for the proper functioning of the muscular, cardiovascular, immune, as well as nervous systems and play a role in the synthesis of vital compounds, metabolic procedures, hematopoiesis, digestion, and metabolic product neutralization. The results visually illustrated in Figure 1 and 2 in order to the difference can be seen properly.

Nutrients work in concert to sustain physiologic cellular and tissue processes, and their dysregulation can have a negative impact on organ function [16]. Magnesium is the human body's fourth most prevalent mineral. This vitamin acts as a cofactor or activator in over 600 enzymes and has an effect on extracellular calcium levels. Magnesium is required for optimal physiological processes since it is used in RNA and DNA synthesis, antioxidant level maintenance in the cell, and energy metabolism. Magnesium is found predominantly in bones and teeth (60%) as well as in the intracellular space (40%) [17, 18]. Potassium (K) is the most abundant exchangeable cation in the human body and exists predominantly in the intracellular fluid [19]. It helps regulate fluid balance, muscle contractions, and nerve signals, helps reduce blood pressure (therefore, lower the hypertension rate) and water retention, protects against stroke, and prevents osteoporosis and kidney stones [20].

Dietary calcium shortage has been associated to a number of chronic conditions, including osteoporosis, osteomalacia, hypertension, colon cancer, and obesity, according to epidemiological studies. Calcium is a mineralized tissue component that is essential for appropriate growth and development of the skeleton. Calcium consumption must be optimal in order to maximise adult bone mass growth, maintain it, and prevent bone loss in the elderly. Calcium alone accounts for around 2% of total body weight, with the majority of this being distributed in the bones.

The bones and teeth contain the majority of calcium, around ninety-nine percent [21]. The remainder, or one percent, is found in serum, extracellular fluid, muscles, and other tissues. As a result, getting enough calcium aids in increasing bone metabolism and improving overall bone health [22].

Table 2 – Composition of macro-micro elements in the ash and plant of *Dianthus superbus*, *Matricaria chamomilla* and *Glycyrrhiza glabra L.*

Element	*Dianthus superbus*		*Matricaria chamomilla*		*Glycyrrhiza glabra L.*	
	Conc. in ash, mg/g	Conc. in plant, mg/g	Conc. in ash, mg/g	Conc. in plant, mg/g	Conc. in ash, mg/g	Conc. in plant, mg/g
K	154.45	9.39	202.58	23.97	328.02	14.95
Na	14.41	0.876	45.52	5.386	9.445	0.4304
Ca	62.15	3.779	36.45	4.313	4.909	0.2237
Mg	30.77	1.871	19.07	2.256	12.605	0.5744
Cu	0.0362	0.0022	0.0786	0.0093	0.0463	0.0021
Cd	0.0017	0.0001	0.0021	0.0002	0.0010	0.00005
Pb	0.0095	0.0006	0.0231	0.0027	0.0109	0.0005
Fe	0.1973	0.0120	2.6972	0.3192	2.0342	0.0927
Mn	3.3276	0.2023	0.3869	0.0458	0.3287	0.0150
Ni	0.0121	0.0007	0.0225	0.0027	0.0126	0.0006
Zn	0.0613	0.0037	0.1414	0.0167	0.2932	0.0134
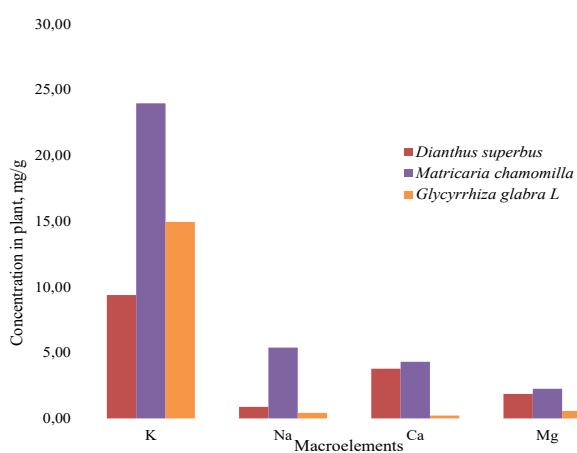
Figure 1 – Composition of macroelements in the plant of *Dianthus superbus*, *Matricaria chamomilla* and *Glycyrrhiza glabra L.*
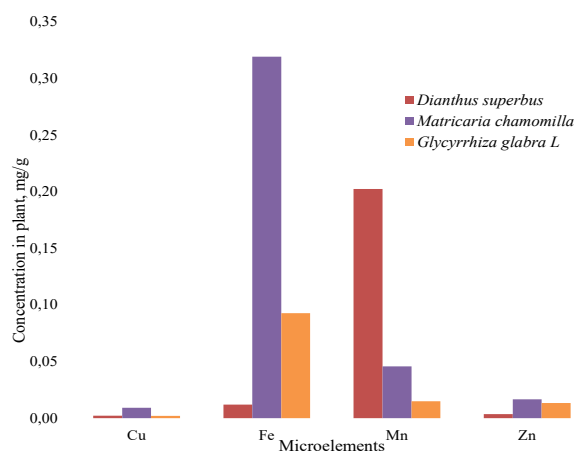
Figure 2 – Composition of microelements in the plant of *Dianthus superbus*, *Matricaria chamomilla* and *Glycyrrhiza glabra L.*

As a result of our research, it was found that in the studied plants from macronutrients K, Na, Mg, Ca predominate, and from trace elements a high content of Cu, Fe, Zn, Mn. Thus, all three tested plants can be considered as potential sources of trace elements, which in the future may allow to expand the scope of application of this plant raw material.

Conclusion

Within the framework of the project AP09259567 "Multi-natural additive suppressing the spread of acute respiratory viral infections in humans", a quantitative analysis of the plants *Dianthus superbus, Matricaria chamomilla* and *Glycyrrhiza glabra L.*,

which were collected on the territory of the Republic of Kazakhstan, was carried out, which may claim the presence of these biological active complexes as a qualitative indicator. During the study, the total number of biologically active components and the content of macro-, microelements of plant raw materials were established. It is particularly worth noting that the chamomile showed excellent results in the amount of elements needed daily by the human body (K, Na, Mg, Ca). The identified substances from the three plants have medicinal properties, thanks to which these plants can be used for the prevention of leukemia and other blood diseases, in the manufacture of medicines against diseases of the gastrointestinal tract, urinary tract, lungs, respiratory organs and reproductive system. Since the composition is rich in useful substances, the quantitative and qualitative analysis of these plants will be continued in the future.

Acknowledgment

References

1. Nile, S. H., Kim, D. H., Nile, A., Park, G. S., et.al. (2020) Probing the effect of quercetin 3-glucoside from Dianthus superbus L against influenza virus infection- In vitro and in silico biochemical and toxicological screening. Food and Chemical Toxicology, vol. 135, pp. 110985. https://doi.org/10.1016/j.fct.2019.110985

2. Mohammad S.M. (2011) Study on cammomile (Matricaria chamomilla L.) usage and farming. Advances in Environmental Biology, vol. 5, no. 7, pp. 1446-1453.

3. Mubarak M., Hussain A., Jan I., Alam S. (2020) Phytochemical Investigations and Antimicrobial Activities of Glycyrrhiza Glabra (Linn.). Fresenius Environmental Bulletin, vol. 1, pp. 251-259.

4. El-Saber Batiha G, Magdy Beshbishy A, El-Mleeh A, Abdel-Daim MM, Prasad Devkota H. (2020) Traditional Uses, Bioactive Chemical Constituents, and Pharmacological and Toxicological Activities of Glycyrrhiza glabra L. (Fabaceae). Biomolecules, vol. 10, no. 3, pp. 352. https://doi.org/10.3390/biom10030352

5. Jalal B. Z., Zahra M. K., Masoud K. G. (2013) Licorice (Glycyrrhiza glabra Linn) As a Valuable Medicinal Plant. Advanced Biological and Biomedical Research, vol. 1, no. 10, pp. 1281-1288.

6. Jain, Hemant et al. (2019) Formulation and evaluation of an antimicrobial mucoadhesive dental gel of Azadirachta indica and Glycyrrhiza glabra. International Journal of Applied Pharmaceutics, vol. 11, pp. 176-184. http://dx.doi.org/10.22159/ijap.2019v11i2.29723

7. Ding H., et al. (2020) Glycyrrhetinic acid and its derivatives as potential alternative medicine to relieve symptoms in nonhospitalized COVID-19 patients. Journal of Medical Virology, vol. 92, pp 2200-2204. https://doi.org/10.1002/jmv.26064

8. Ashirova, Z. B., Kuzhantaeva, Z. Z., Abdrassulova, Z. T., Shaimerdenova, G. Z., & Atanbaeva, G. K. (2021). Studying Phytochemical Features of Three Asteraceae Herbs Growing Wild in Kazakhstan. Floresta e Ambiente, 28. https://doi.org/10.1590/2179-8087-FLORAM-2021-0060

9. Muzychkina R.A., Korulkin D.Yu., Abilov Zh.A. (2004) Kachestvennyy i kolichestvennyy analiz osnovnykh grupp BAV v lekarstvennom rastitel'nom syr'ye i fitopreparatakh [Qualitative and quantitative analysis of the main groups of BASes in medicinal raw materials and phytopreparations] Almaty: Kazakh University.

10. USSR State Pharmacopoeia (1968) X ed., M: Medicine, p. 1080

11. Cook N.C., Samman S. (1996) Flavonoids—chemistry, metabolism, cardioprotective effects, and dietary sources. Nutritional Biochemistry, vol. 7, no. 2, pp. 66–76. https://doi.org/10.1016/S0955-2863(95)00168-9

12. Hodgson J.M., Croft K.D. (2010) Tea flavonoids and cardiovascular health. Molecular aspects of medicine, vol. 31, no. 6, pp. 495–502. https://doi.org/10.1016/j.mam.2010.09.004

13. Rice-Evans C. (2001) Flavonoid antioxidants. Current Medicinal Chemistry, vol. 8, no. 7, pp. 797–807. https://doi.org/10.2174/0929867013373011

14. Ivey K.L., Hodgson J.M., Croft K.D., Lewis J.R., Prince R.L. (2015) Flavonoid intake and all-cause mortality. American Journal of Clinical Nutrition, vol. 101, no. 5, pp. 1012–1020. http://dx.doi.org/10.3945/ajcn.113.073106

15. Androutsopoulos V. P., Mahale S., Arroo R. R., Potter G. (2009) Anticancer effects of the flavonoid diosmetin on cell cycle progression and proliferation of MDA-MB 468 breast cancer cells due to CYP1 activation. Oncology reports, vol. 21, no. 6, pp. 1525–1528. https://doi.org/10.3892/or_00000384

16. Brown R.B., Razzaque M.S. (2018) Phosphate toxicity and tumorigenesis. Biochimica et Biophysica Acta. Reviews on Cancer, vol. 1869, no. 2, pp. 303–309. https://doi.org/10.1016/j.bbcan.2018.04.007

17. Razzaque M.S. (2018) Magnesium: Are We Consuming Enough? Nutrients, vol. 10, no. 12, pp. 1863. https://doi.org/10.3390/nu10121863

18. Noronha J. L., Matuschak G. M. (2002) Magnesium in critical illness: metabolism, assessment, and treatment. Intensive care medicine, vol. 28, no. 6, pp. 667–679. https://doi.org/10.1007/s00134-002-1281-y

19. Thier S. O. (1986) Potassium physiology. The American journal of medicine, vol. 80, no. 4A, pp. 3–7. https://doi.org/10.1016/0002-9343(86)90334-7

20. Sun H., Weaver C. M. (2020). Rise in Potassium Deficiency in the US Population Linked to Agriculture Practices and Dietary Potassium Deficits. Journal of agricultural and food chemistry, vol. 68, no. 40, pp. 11121–11127. https://doi.org/10.1021/acs.jafc.0c05139

21. Matkovic, V. (1996). Nutrition, genetics and skeletal development. Journal of the American College of Nutrition, vol. 15, no. 6, pp. 556–569. https://doi.org/10.1080/07315724.1996.10718630

22. Kaushik R., Sachdeva B., Arora S. (2015) Heat stability and thermal properties of calcium fortified milk. CyTA – Journal of Food, vol. 13, no. 2, pp. 305–311. http://dx.doi.org/10.1080/19476337.2014.971346

G. Burashev[1] , B. Tatykayev[1] , M. Baláž[2] , N. Khan[1] ,

A. Seysembekova[1] , S. Tugelbay[1] , N. Turgynbay[1] ,

M. Burkitbayev[1] , Zh. Shalabayev[1*]

[1]Al-Farabi Kazakh National University, Almaty, Kazakhstan
[2]Institute of Geotechnics, Slovak Academy of Sciences, Košice, Slovakia
*e-mail: zhandos.shalabay@gmail.com
(Received 16 October 2023; received in revised form 13 November 2023; accepted 03 December 2023)

All solid-state fabrication strategy of CdS@ZnS nanocomposites and their photocatalytic performance in water purification

Abstract. Herein a systematic study of two-step solid-phase synthesis of CdS@ZnS nanocomposites and their photocatalytic activity is presented. First, CdS nanoparticles were synthesized in a planetary ball mill through a solid-state ion exchange reaction. In the second step, Cd^{2+} ions were partially replaced by Zn^{2+} ions at the surface of the nanoparticles using solvent free long-term activation in a high-energy planetary ball mill. The optimal activation time in a ball mill was determined to be 45 min. Spherical CdS nanoparticles with a diameter of 10 nm and modified CdS@ZnS (45 min) nanocomposites were characterized by X-ray diffraction analysis, Raman and UV-vis spectroscopy, and scanning electron microscopy. The ability of nanocomposites for photocatalytic water purification was tested on the degradation of the model organic dye Orange II in an aqueous solution under the visible light irradiation. The modified CdS@ZnS nanocomposites showed higher photocatalytic activity compared to the original CdS nanoparticles.
Key words: solid-state synthesis; mechanochemistry; cadmium sulfide; zinc sulfide; photocatalysis; hydrogen evolution.
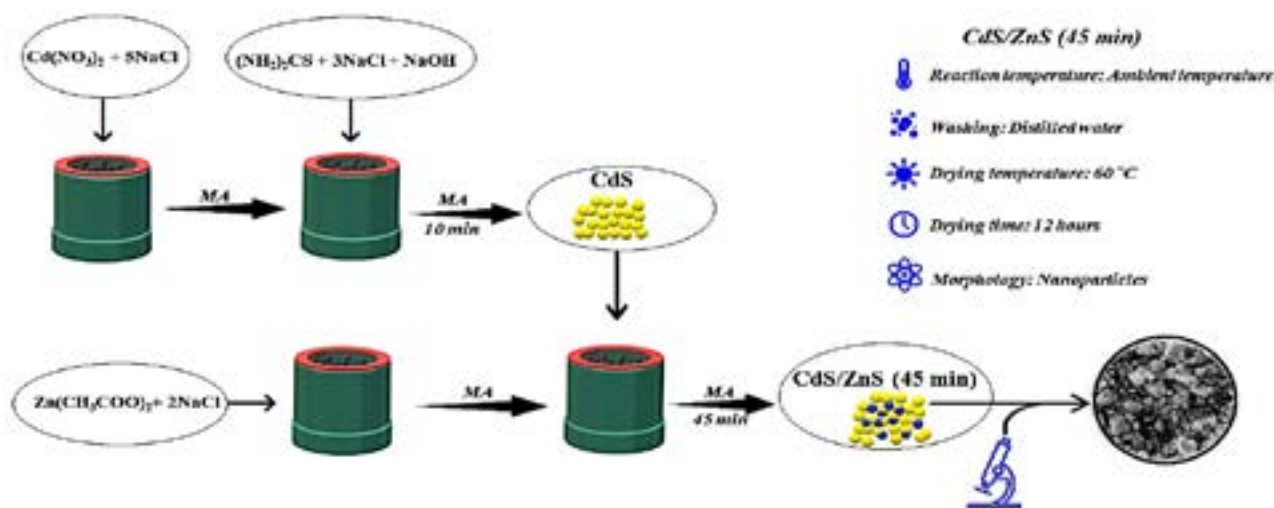
Introduction

Wastewater pollution poses a significant environmental and public health challenge globally [1]. Various human activities, including industrial processes, agriculture, and domestic sewage, contribute to the discharge of wastewater containing a range of contaminants into water. These contaminants include organic and inorganic pollutants, nutrients, heavy metals, and pathogens [2].

Photocatalysis has emerged as a highly effective method for wastewater treatment [3].

Semiconductor photocatalysts, such as metal sulfide nanoparticles and binary, ternary nanocomposites based on them, harness light energy to initiate photocatalytic reactions that can efficiently degrade organic pollutants and remove contaminants from wastewater [4]. The photocatalytic process involves the generation of electron-hole pairs upon light absorption, which induces redox reactions and breaks down pollutants into less harmful byproducts. Semiconductor photocatalysts offer advantages such as high efficiency, versatility, and the ability to operate under ambient conditions [5, 6].

Nanocomposites based on CdS nanoparticles and their composites with other semiconducters have been recommended as strong photocatalysts in water purification and hydrogen production [7]. Their ability to absorb visible light enables efficient degradation of organic pollutants and removal of harmful substances from water. Additionally, these nanoparticles exhibit remarkable performance in photocatalytic water splitting, facilitating the production of clean and sustainable hydrogen gas. CdS@ZnS nanoparticles offer promising solutions for addressing water pollution and advancing renewable energy technologies.

Also, CdS@ZnS nanocomposites find applications in diverse fields such as solar cells and photovoltaics [8], optoelectronics and light-emitting diodes [9], as well as sensing and biosensing [10]. Their unique properties enable enhanced light absorption, improved charge transport, and efficient photocatalytic activity, making them promising materials for next-generation energy devices, environmental remediation technologies, and advanced sensing platforms [11].

There are many preparation methods of CdS@ZnS nanocomposites such as aqueous synthesis [12], reverse micellar [13], microjet reactor technology [14], *in situ* synthesis [15], hydrothermal [16], chemical [11], microwave-assisted synthesis [17], electrosynthesis [18], microemulsion technique [19], and mechanochemical approach [20, 21].

The last one is of particular interest because mechanochemistry, the process of using mechanical force to initiate chemical reactions, offers several advantages in the field of chemistry [22]. Firstly, it enables reactions to occur without the need of using of toxic chemicals as precursors and high temperatures, making it environmentally friendly and energy-efficient. Secondly, mechanochemistry often leads to higher yields and purer products compared to traditional methods, reducing waste and improving overall efficiency [23]. Additionally, it allows the

synthesis of compounds that might be challenging to produce using conventional methods, expanding the scope of possible materials and innovations in various industries [24].

In this work, the surface of mechanochemically synthesized CdS nanoparticles was coated with ZnS. CdS nanoparticles were co-milled with zinc acetate in a high-energy planetary ball mill for a long time. According to our strategy, Cd^{2+} ions from the surface CdS nanoparticles were replaced by Zn^{2+} ones. As a result, CdS@ZnS with high photocatalytic activity was obtained.

Materials and methods

Materials. Cadmium nitrate tetrahydrate ($Cd(NO_3)_2 \cdot 4H_2O$, Sigma-Aldrich, Taufkirchen, Germany), thiourea ($CS(NH_2)_2$, Sigma-Aldrich, Taufkirchen, Germany), sodium hydroxide (NaOH, Sigma-Aldrich, Taufkirchen, Germany), sodium chloride (NaCl, Sigma-Aldrich, Taufkirchen, Germany), zinc acetate dihydrate ($Zn(CH_3COO)_2 \cdot 2H_2O$, Sigma-Aldrich, Taufkirchen, Germany), and Orange II sodium salt ($C_{16}H_{11}N_2NaO_4S$, Sigma-Aldrich, Taufkirchen, Germany) were of analytical grade and used without further purification.

Characterization. X-ray diffraction patterns were obtained on a MiniFlex 600 diffractometer (Rigaku, Japan) in a digital form using copper radiation. Sample analysis modes were as follows: X-ray tube voltage – 40 kV, the tube current – 15 mA, goniometer movement step size – 0.02 °, and step time 0.12 sec. During shooting, the sample was rotated in its plane at a speed of 60 rpm. For phase analysis, the ICCD-PDF2 Release 2016 database and the PDXL2 software have been used.

The study of optical phonon modes was carried out via Raman spectroscopy on a LabRAM HR Evolution spectrometer, Horiba Scientific (Japan), in the range of 100-2000 cm^{-1} (acquisition time – 15 seconds, accumulation – 3) and a laser with a wavelength of 532 nm (objective – 10X, hole – 300).

A UV-2600i compact UV spectrophotometer was used to evaluate the absorption spectra in the UV-visible region to determine the band gap energy of semiconductors.

The morphology and size of the prepared samples were investigated utilizing scanning electron microscopy (SEM). SEM images were obtained with the help of a scanning electron microscope ZEISS Crossbeam 540.

Mechanochemical synthesis of CdS/ZnS nanocomposites. The synthesis process of the ZnS

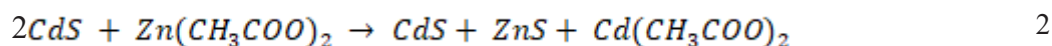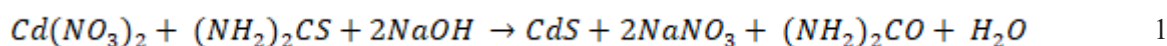doped CdS NPs (CdS/ZnS) involved two primary stages.

In the first stage, 0.8181 g of dehydrated $Cd(NO_3)_2$ was used and activated alongside 1.0111 g of NaCl, which served as a diluent. Another component, $(NH_2)_2CS$ 0.2634 g, underwent similar activation with 0.6067 g of NaCl to create a homogeneous mixture. Subsequently, all reactants were placed in a ball mill for mechanochemical synthesis. The experiment was conducted in the presence of 0.1384 g of NaOH. The resulting CdS product was subjected to multiple washes with bidistilled water to eliminate unwanted by-products. Subsequently, the CdS nanoparticles were dried for 12 hours at 60 °C.

In the subsequent stage, 0.6350 g of $Zn(CH_3COO)_2$ was also activated in the presence of 0.4045 g of NaCl. The activated product was combined with the pre-dried CdS from the first stage for mechanical activation, yielding the CdS/ZnS composite. The resulting product underwent a similar series of washes with bidistilled water and was then dried at 60 °C for approximately 12 hours.

The mechanochemical experiments were conducted within the Activator 2SL ball mill (Activator, Russia). The specific experimental conditions were as follows: the rotational speed was maintained at 400 rpm, and the ball-to-powder ratio was set to 37, employing 10 mm diameter silicon nitride balls, with a total of 20 balls utilized. The grinding chamber's volume was 100 mL, made from silicon nitride (Si_3N_4), and the milling was performed in air. The synthesis duration comprised two stages: the initial stage lasting 10 minutes and the subsequent stage 15, 30, 45 and 60 minutes.

The chemical reaction for both stages proceeded as follows:

$$Cd(NO_3)_2 + (NH_2)_2CS + 2NaOH \rightarrow CdS + 2NaNO_3 + (NH_2)_2CO + H_2O \qquad 1$$

$$2CdS + Zn(CH_3COO)_2 \rightarrow CdS + ZnS + Cd(CH_3COO)_2 \qquad 2$$

Synthesis of CdS/ZnS (45 min) doped NiS nanostructures. To investigate the photocatalytic production of hydrogen, we incorporated a co-catalyst, specifically nickel sulfide (NiS), to enhance the photocatalytic activity. Catalysts play a pivotal role in augmenting catalytic activity by efficiently collecting photoexcited electrons or holes [25]. In this study, we synthesized a NiS co-catalyst using nickel nitrate hexahydrate ($Ni(NO_3)_2 \times 6H_2O$) and sodium sulfide nonahydrate ($Na_2S \times 9H_2O$). We applied the NiS co-catalyst onto the surface of the photocatalyst during the deposition process, resulting in a composite material with approximately 1.5% NiS by weight, ensuring the presence of the requisite co-catalyst in the final material.

Photocatalytic experiments. The protocol of investigation of photocatalytic activity of the prepared nanocomposites was similar to our previous studies [26-28]. To study the photocatalytic properties of the resulting nanocomposites Orange II organic dye at a concentration of 20 mg/L was used. Specifically, 20 mg of the nanocomposite was transferred into 40 mL of an aqueous solution of Orange II. The experiments were conducted under visible light illumination using an Osram Vita Lux lamp (300 W) with a light intensity of 15 mW/cm². The lamp was positioned 20 cm above the model solution's surface, and an organic glass cut-off filter was utilized to restrict irradiation to wavelengths above 400 nm.

Before initiating light irradiation, the suspensions were stirred in the dark for 60 minutes. Every 30 minutes during this period, 2.5 mL of the suspension was taken to assess the adsorption-desorption properties between the photocatalyst and the model solution. Subsequently, light irradiation was started, and the extraction of 2.5 mL of the suspension every 30 minutes was conducted, to measure the degree of photocatalytic degradation. The absorption spectra were recorded with the help of a UV-Vis spectrophotometer (SF-56, LOMO, Russia). To ensure the accuracy of the obtained results, all photocatalytic tests were repeated two times.

The stability of the photocatalysts was studied over 5 cycles of Orange II degradation. After each cycle photocatalyst was washed with deionized water and reused in the next cycle.

Hydrogen generation. The experiment utilized a flask-shaped reactor equipped with three necks and an external light source. A xenon arc lamp with a power rating of 300 watts served as the light source. This visible light source was positioned at a distance of 20 cm from the reactor and was fitted with an ultraviolet filter with a threshold wavelength of $\lambda = 420$ nm,

restricting the range of wavelengths employed. The light irradiation intensity inside the photoreactor was maintained at 15 mW/cm².

In the photocatalytic experiment for hydrogen production from water, a CdS/ZnS composite doped with NiS was employed as the photocatalyst. For the preparation of the reaction solution, 10 mL of glycerin and 90 mL of bidistilled water were added to 30 mg of the photocatalyst. The mixture was dissolved using a magnetic stirrer to ensure uniform dispersion of the photocatalyst. To eliminate excess dissolved oxygen from the reactor, argon gas was introduced (with a purity of 99.99% by weight) through the reaction mixture. The argon bubbling process was sustained for 60 minutes at a 100 mL/min flow rate. It is important to note that during this stage, the reaction mixture was shielded from light radiation. Once the bubbling process concluded, the light source was activated, and argon continued to be supplied at a rate of 5 mL/min. Argon also functioned as a carrier for the transfer of hydrogen produced as a result of the photocatalytic reaction from the reactor to a gas chromatograph (Chromos 1000, Russia) for subsequent analysis. The reactor maintained a continuous connection with the gas chromatograph in real time for the purpose of continuous monitoring. Hydrogen concentration measurements were taken every 30 minutes following the initiation of irradiation.

Results and discussion

XRD analysis. X-ray diffraction analysis was employed to investigate the crystal structure and phase purity of the synthesized nanocomposites. The presence of multiple diffraction peaks, exhibiting a broad profile in this spectrum can be attributed to the polycrystalline nature of the synthesized CdS nanoparticles [29]. Additionally, the indistinct background in the X-ray spectrum may be attributed to amorphous characteristics resulting from the irregular arrangement of lattice elements. The observed intense diffraction peaks align perfectly with the cubic phase of cadmium sulfide (JCPDS card no. 80-0019). The broadened peaks suggest that the particle sizes are within the nanoscale range [30, 31].

Furthermore, in the subsequent figure, it is noteworthy that the X-ray diffraction pattern of CdS/ZnS reveals additional peaks at 24.5° (111), 44.5° (220), and 56.4° (311). The X-ray diffraction pattern does not exhibit peaks corresponding to the crystal planes of the standard cubic structure of ZnS. Instead, the peaks at the (111), (220), and (311) planes correspond closely to the standard cubic ZnS (JCPDS card no. 05-0492) [32]. No other phases were detected. Given the limited quantity of synthesized ZnS, it is possible that their peaks are concealed amid the CdS peaks, which strongly suggests the presence of a zinc-blende ZnS shell [33].
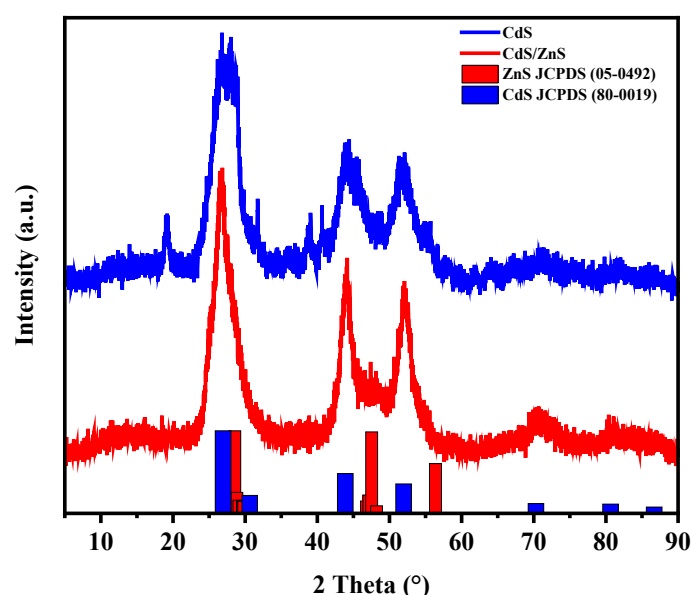

Figure 1 – XRD patterns of the a) CdS and b) CdS/ZnS nanoparticles

Raman spectroscopy. On Figure 2, the Raman spectrum of heterostructured CdS and CdS/ZnS nanocomposites is shown. For CdS and CdS/ZnS nanocrystals, three characteristic peaks were equally observed at 297.9 cm^{-1}; 598.1 cm^{-1} and 820 cm^{-1}, the corresponding second- and third-order overtones of the optical phonons 1LO, 2LO and 3LO, respectively [34]. The obtained spectra of CdS and CdS/ZnS nanocomposites are not completely different in longitudinal optical phonon modes, but the intensity of the CdS mode is somewhat sharper [35]. The optical (LO) phonon peaks of ZnS at 353 cm^{-1} may be lost between the larger peaks of CdS, which is similar to the report [36]. The observed LO Raman peak position aligns well with the reported LO phonon peak position characteristic of the cubic CdS structure. Additionally, no discernible peaks corresponding to hexagonal CdS were detected, providing indirect confirmation of the cubic zinc-blende structure in the CdS microspheres [37, 38].
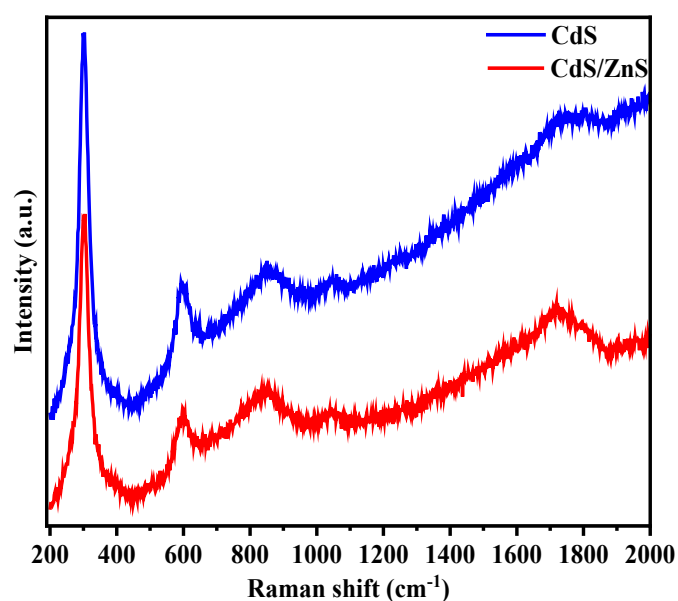

Figure 2 – Comparative Raman spectroscopy of CdS and CdS/ZnS samples employing a 532 nm laser

UV-Vis spectroscopy. Figure 3 shows the UV-Vis spectra of the mechanochemically synthesized CdS and CdS/ZnS samples. The results show that the absorption spectrum of CdS/ZnS lies higher than that of CdS. In order to find the band gaps of the synthesized samples, the Tauc plot method and the plot of $(\alpha h\gamma)^2$ versus photon energy (hν) were used. Additionally, the formula $\alpha h\nu = (h\nu - E_g)1/2$ (1) was employed, where α is the absorption coefficient, hν is the photon energy, and E_g is the direct band gap energy.

The absorption edge of CdS synthesized mechanochemically is at 565 nm (2.29 eV) [30, 39]. Compared with other CdS synthesis works, it is red shifted. It is believed that the shift in the absorption peak is obviously caused by the quantum confinement effect. The absorption edge of CdS/ZnS was at slightly lower wavelength, namely at 555 nm (2.33 eV) [40, 41].

SEM analysis. Cadmium sulfide nanoparticles have a size in range from 0.1 to 10 μm, as shown in Figure 4a. The nanoparticles are agglomerated into particles of different sizes, where the sizes range up to 10 microns. But these agglomerates are easily destroyed into individual nanoparticles when dispersed in water with ultrasonic radiation. When using nanoparticles as photocatalysts, the nanoparticle powder is dispersed in an aqueous solution. Cadmium sulfide nanoparticles were modified with zinc sulfide by solid-phase doping, and SEM images of prepared CdS/ZnS nanocomposites are presented in Figure 4b. The morphology and texture of the CdS/ZnS nanocomposites are the same as cadmium sulfide nanoparticles before modification.
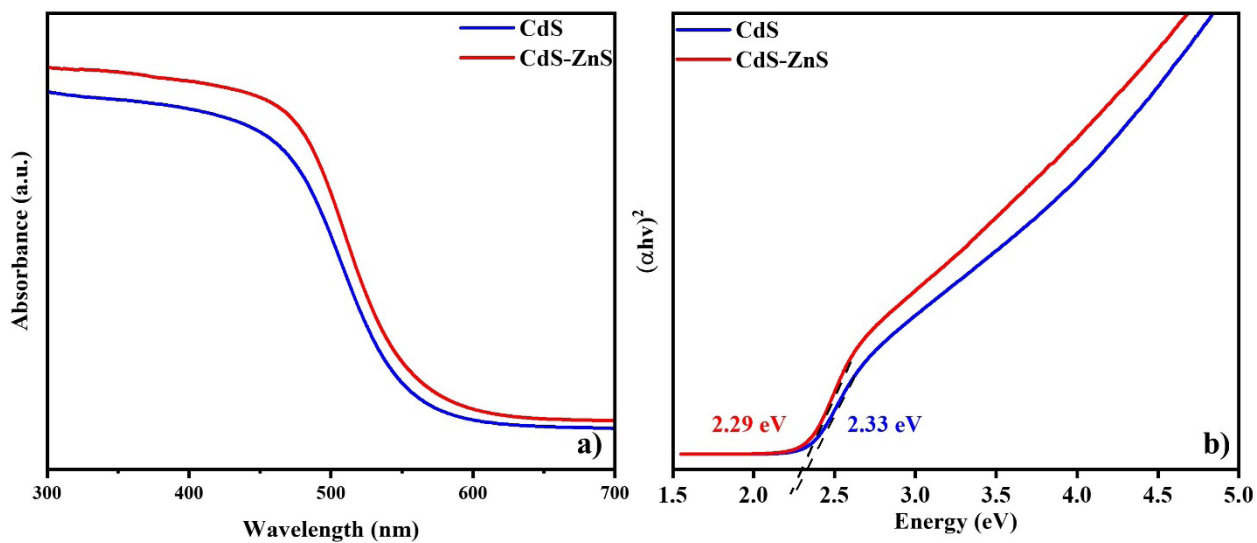
Figure 3 – (a) UV-vis absorption spectra;
(b) band gaps of CdS and CdS/ZnS estimated by $(\alpha h\upsilon)^2$ vs. photonenergy curve
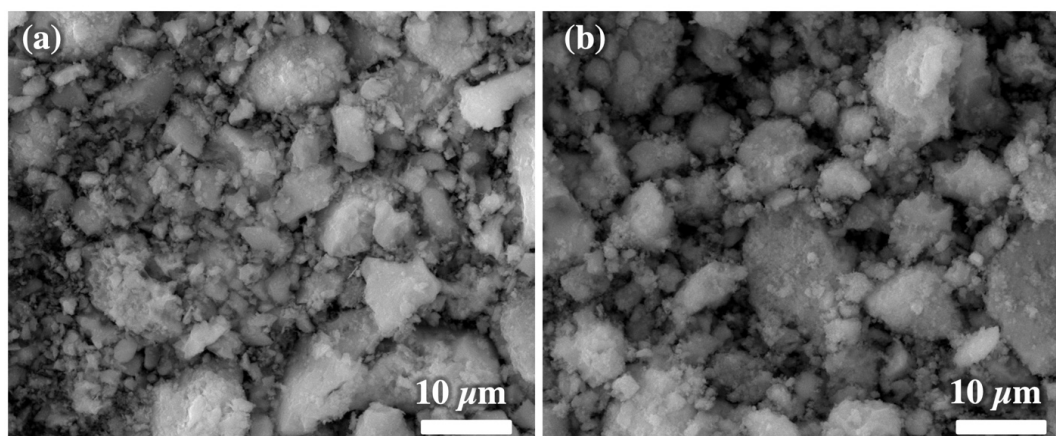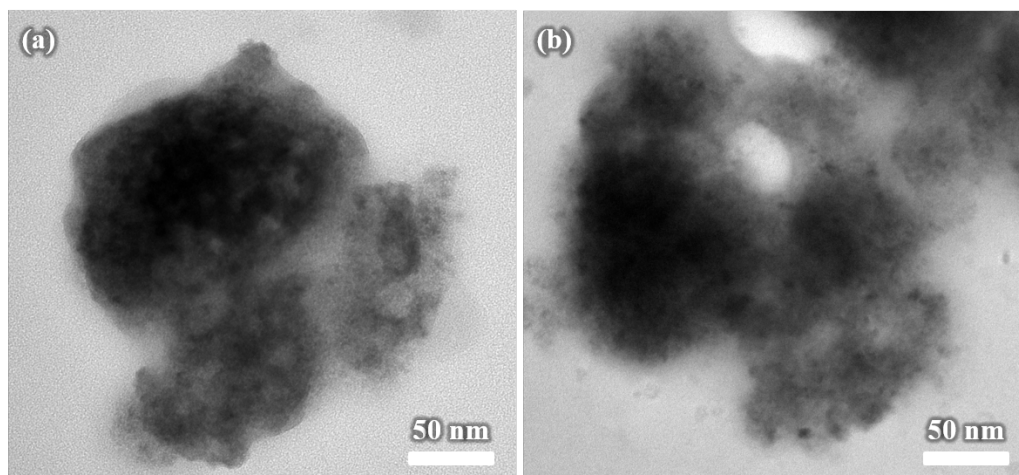

Figure 4 – SEM images of (a) CdS nanoparticles and (b) CdS/ZnS nanocomposites
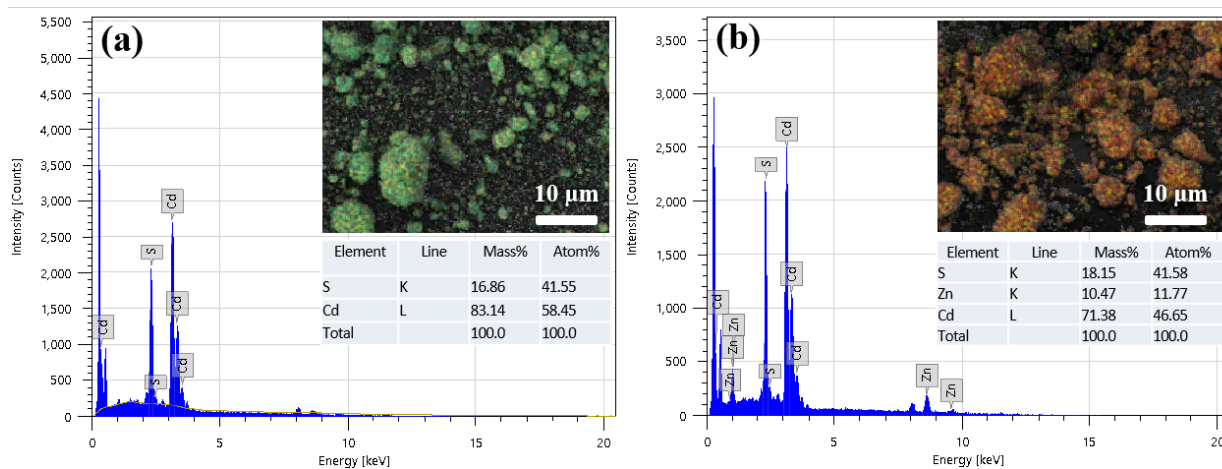
Figure 5 – SEM EDX spectrum images of (a) CdS nanoparticles and (b) CdS/ZnS nanocomposites

SEM EDX spectrum images of CdS nanoparticles and CdS/ZnS nanocomposites are presented in Figure 5. CdS nanoparticles were fabricated without contaminations. Doping with zinc sulfide occurred only on the surface of cadmium sulfide nanoparticles, and since the mass fraction of zinc in the nanocomposite according to the SEM EDX spectrum is around 10.5 %.

Figure 6 – TEM images of (a) CdS nanoparticles and (b) CdS/ZnS nanocomposites

TEM images are shown in Figure 6. Agglomerates of cadmium sulfide nanoparticles are actually composed of smaller particles of about 10 nm in size, as shown in Figure 6a. After doping cadmium sulfide nanoparticles with zinc ions, the morphology and size of the nanoparticles did not change, Figure 6b.

Photocatalytic activity. The results of the photocatalytic activity investigation of the composites prepared after different time are given in Figure 7a. According to the graph, after the starting of visible light irradiation, the samples immediately began to decompose the organic dye. The highest ability of Orange II degradation was demonstrated by CdS/ZnS (45 min) nanocomposite, indicating that 45 minutes of mechanochemical treatment is optimal for manifesting photocatalytic activity. It should be mentioned that the difference in the photocatalytic activity among the nanocomposites was not so big. The activity of the samples decreased from left to right as follows: CdS/ZnS (45 min), degraded about 99% molecules of Orange II → CdS/ZnS (30 min), (97%) → CdS/ZnS (15 min), (90%) → CdS/ZnS (60 min), (88%). The photocatalytic activity of the best photocatalyst, namely the CdS/ZnS (45 min) was compared with the bulk CdS (Figure 7b). As can be seen, CdS/ZnS (45 min) nanocomposite exhibits slightly worse activity.

The kinetics of the photocatalytic process was studied only for nanocomposites and depicted in Figure 7c. The order of the photocatalytic reactions was accepted as a pseudo-first-order reaction and the rate constants were found through the Langmuir–Hinshelwood kinetics model [42]:

$$ln\frac{C_0}{C} = kt \qquad (3)$$

where C_0 and C are initial concentrations of the model solution in the moment of time t and k (min^{-1}) is the rate constant of the process. The correlation coefficient R^2 served as proof of the kinetic order of decomposition of Orange II. The k and R^2 values are displayed in Table 1. Based on the data in Table 1 the k of the CdS/ZnS (45 min) is 1.34, 1.15 and 1.68 times higher than samples prepared during 15, 30 and 60 min, respectively, what indicates that CdS/ZnS (45 min) is a prospective candidate for the next study.

In addition, the cyclic tests for all nanocomposites were conducted, as the stability of the photocatalysts is one of the important properties [43]. Consequently, the results of the study (Figure 7d) demonstrate that during the first three cycles, the activity of the samples remains almost unchanged, after which there is a slight decrease in photocatalytic activity. Such results can be explained by the washing of powders from suspensions during each sampling. In general, the produced nanocomposites are relatively stable.
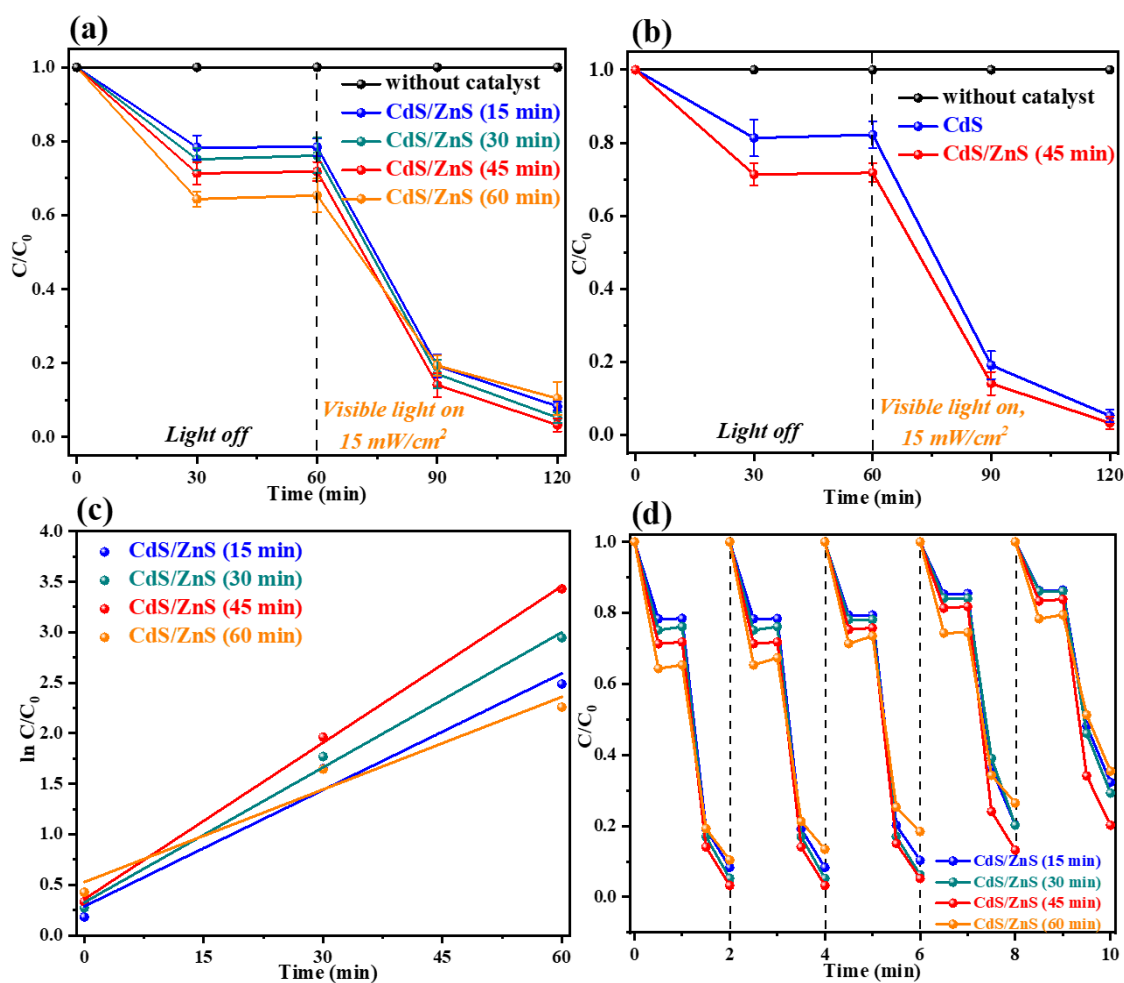
Figure 7 – a) Comparison of the photocatalytic activity of all nanocomposites;
b) comparison of the photocatalytic activity of CdS/ZnS (45 min) nanocomposite and CdS,
ZnS bulk materials; c) kinetic linear simulation curves for Orange II photocatalytic degradation by all nanocomposites;
d) Cycling degradation efficiency of all nanocomposites

Table 1 – The k and R^2 values of the CdS/ZnS nanocomposites

The sample	k, min^{-1}	R^2
CdS/ZnS (15 min)	0.0384	0.98
CdS/ZnS (30 min)	0.0446	0.99
CdS/ZnS (45 min)	0.0516	0.99
CdS/ZnS (60 min)	0.0306	0.96

The obtained results were similar to the study [44] and the behaviour of the bulk material, CdS and ZnS nanocomposites is almost the same. However, the slight difference in activity among the nanocomposites of this study should be clarified. It is known, that mechanochemical synthesis leads to the formation of defects in the lattice of the material [45], which can play the role of the active centres that can improve the photoconductivity of electrons of semiconductors. Moreover, this method of synthesis provides the increasing of the surface area of the crystals and such systems exhibit heterogeneity [46]. Thus, the 15 and

30 minutes duration of the mechanosynthesis, seems not enough for the formation of the needed amount of active centres on the surface of CdS and ZnS, while the duration of 60 minutes leads to the rapid recombination between electrons and holes, which retard the flow of photocatalytic reactions. This is why the 45-minute duration of mechanosynthesis produced the most photocatalyticaly active material.

Analysis of the literature sources revealed that photocatalyst based on CdS and ZnS were prepared by various methods. Table 2 provides a summary of methods and conditions for producing CdS and ZnS-based materials and their photocatalytic properties, including light source, type of organic dye, efficiency and rate constants. As can be seen from the data, the most time-consuming methods are solvothermal, precipitation, chemical precipitation, and hydrothermal. Most of the photocatalysts from the

Table 2 are used for photodegradation of Methylene blue (MB), Rhodamine B (RhB) and Methyl orange (MO). In general, all methods represented in Table 2 produced photocatalyst with high efiiciency. However, some of them require the use of toxic precursor, like Na$_2$S, which in addition easily catches the water, or methods represented by the complexity of execution where it is necessary to maintain certain conditions, such as temperature, concentration or pH. For example, the use of Thioacetamine (TAA) as a source of sulfide ions, as in [47], is complicated due to the fact the process requires constant monitoring of the pH of the medium, since the rate of formation of sulfide ions decreases with a decrease in pH [48]. The approach presented in this study is represented by simplicity and environmental friendliness, and the photocatalysts with high efficiency can pre prapred in this way.

Table 2 – The photocatalytic experiments of CdS@ZnS nanostructures prepared with different approaches on the degradation of organic dyes

Synthetic method	Experimental conditions		Precursors	Light source	Dye	Photocatalytic efficiency	Rate constant (min⁻¹)	[Ref]
	Time	T (°C)						
Solvothermal	10 h	180	Zn(Ac)$_2$, CS(NH$_2$)$_2$	-	Methylene blue (MB)	88.5%@12h	-	[49]
Ion adsoprtion	10 min	290	Cd(Ac)$_2$·2H$_2$O, Na$_2$S·9H$_2$O, Zn(Ac)$_2$·2H$_2$O	UV	Rhodamine B (RhB)	96.1%@35 min	0.0190	[50]
					MB	99.6%@35 min	0.0720	
Chemical precipitation	4 h	RT	Cd(NO$_3$)$_2$, H$_2$S, ZnCl$_2$	Vis	Acid blue (AB-29)	86.5%@90 min	0.0006	[51]
	9 h	80	CdCl$_2$×2H$_2$O, CS(NH$_2$)$_2$, ZnS	UV	Congo red	98%	-	[52]
Solvothermal & Precipitation	24 h	170	Cd(NO$_3$)$_2$×4H$_2$O, CS$_2$, Zn(Ac)$_2$×2H$_2$O	UV	MO (Methyl orange)	77%@75 min	-	[47]
					Pyronin B (PyB)	66%@75 min	-	
					RhB	84%@75 min	-	
					MB	85%@75 min	-	
Hydrothermal	12 h	140	CdCl$_2$×5H2O, CS(NH$_2$)$_2$, Zn(Ac)$_2$	Vis	MO	<95%@60 min	0.0625	[42]
Microwave-assisted	38 min	40	Pectin, NaOH, Cd(Ac)$_2$, TAA	Vis	RhB	98.7%@120 min	-	[17]
Two-step synthesis	3 h	180	Cd(Ac)$_2$, Na$_2$S, Zn(Ac)$_2$,	Vis	MO	<90%@90 min	0.0208	[44]
Sonochemical	40 min	RT	Zn(Ac)$_2$, TAA, CdS, NaOH,	UV	MB	42.6%@80 min	-	[53]
Mechanochemical	45 min	RT	Cd(NO$_3$)$_2$, (NH$_2$)$_2$CS, NaOH, Zn(CH$_3$COO)$_2$	Vis	Orange II	<99%@60 min	0.0516	this work

Hydrogen evolution by water splitting. Figure 8 displays the results of a photocatalytic experiment aimed to measure hydrogen evolution reaction (HER) using a photocatalyst. The experimental analysis involved monitoring the hydrogen release over a duration of 210 minutes. The obtained data reveals that the rate of hydrogen evolution when employing NiS-doped CdS/ZnS (45 min) photocatalyst exhibited an initial increase within the first 30 minutes, followed by a stabilization trend up to 180 minutes. The analysis indicates that the maximum rate of hydrogen evolution occurred at 19.3 μmolg^{-1}h^{-1} at the 120-minute mark. These findings suggest the existence of a synergistic effect and a direct correlation between the particle sizes of CdS and ZnS and their photocatalytic activity. These results imply that the high surface-to-volume ratio and the presence of defect sites at the photocatalyst interfaces play pivotal roles in enhancing the catalytic activity of nanostructured semiconductor composites. Additionally, the close interaction between CdS and ZnS particles emerges as a crucial factor contributing to enhanced photocatalytic activity [54]. Beyond the 180-minute mark, a decrease in hydrogen evolution is observed, attributed to the rapid recombination of electrons in the conduction band and holes in the valence band of CdS [55]. It is also noteworthy that ZnS exhibits limited absorption of visible light due to the excitation of certain defect states within the band gap [56]. These findings provide valuable insights for the design and optimization of photocatalytic systems for hydrogen production.
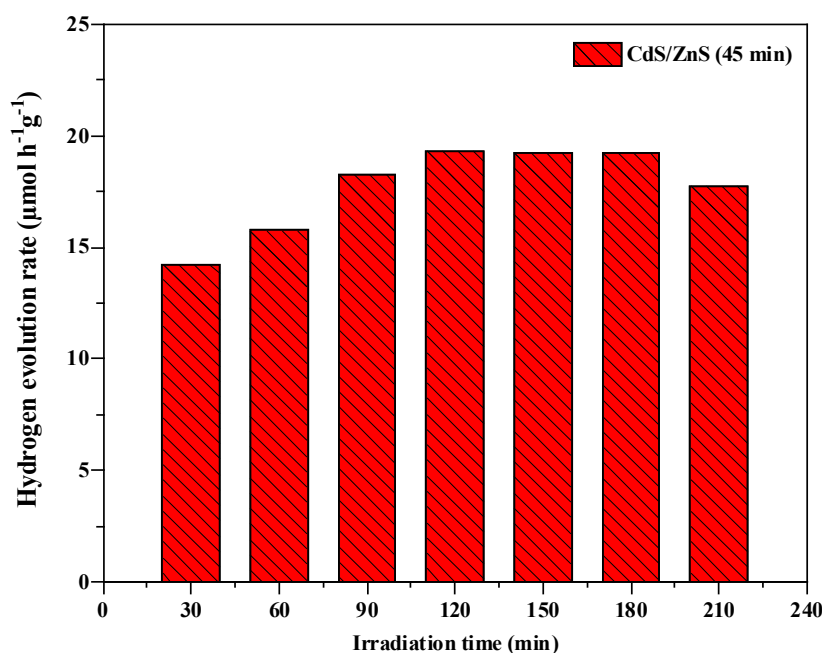
Figure 8 – Photocatalytic hydrogen generation performance
of CdS/ZnS sample synthesized in 45 min

Conclusion

In this paper, a new facile solvent-free technology for the production of CdS@ZnS nanocomposites was demonstrated. This composite was obtained by partial substitution of Cd^{2+} ions by Zn^{2+} ions on the nanoparticles surface during mechanochemical reaction. The new solid-state method has several advantages: the method is environmentally friendly, economically beneficial and easily scalable. The fabricated CdS@ZnS nanocomposites have increased photocatalytic activity and are suitable for use in water purification from organic pollutans under the visible light irradiation. The scientific results of the conducted research open up the possibility of creating and producing the new doped metal sulfides nanocomposites for various purposes.

Acknowledgements

References

1. Schwarzenbach R. P., Egli T., Hofstetter T. B., Von Gunten U., Wehrli B. Global water pollution and human health // Annual review of environment and resources. – 2010. – T. 35. – C. 109-136.

2. Madhav S., Ahamad A., Singh A. K., Kushawaha J., Chauhan J. S., Sharma S., Singh P. Water pollutants: sources and impact on the environment and human health // Sensors in water pollutants monitoring: Role of material. – 2020. – C. 43-62.

3. Mishra S., Sundaram B. A review of the photocatalysis process used for wastewater treatment // Materials Today: Proceedings. – 2023.

4. Nemiwal M., Zhang T. C., Kumar D. Recent progress in g-C3N4, TiO2 and ZnO based photocatalysts for dye degradation: Strategies to improve photocatalytic activity // Science of the total environment. – 2021. – T. 767. – C. 144896.

5. Zhang F., Wang X., Liu H., Liu C., Wan Y., Long Y., Cai Z. Recent advances and applications of semiconductor photocatalytic technology // Applied Sciences. – 2019. – T. 9, № 12. – C. 2489.

6. Koe W. S., Lee J. W., Chong W. C., Pang Y. L., Sim L. C. An overview of photocatalytic degradation: photocatalysts, mechanisms, and development of photocatalytic membrane // Environmental Science and Pollution Research. – 2020. – T. 27. – C. 2522-2565.

7. Munyai S., Hintsho-Mbita N. Green derived metal sulphides as photocatalysts for waste water treatment. A review // Current Research in Green and Sustainable Chemistry. – 2021. – T. 4. – C. 100163.

8. Hajiyeva F., Ramazanov M., Shirinova H., Maharramova G. Photosensitive hybrid polymer nanocomposites on the base PVDF+ CdS/ZnS for solar cells application // Composite Interfaces. – 2022. – T. 29, № 3. – C. 236-254.

9. Chen Y., Xing W., Liu Y., Zhang X., Xie Y., Shen C., Liu J. G., Geng C., Xu S. Efficient and stable CdSe/CdS/ZnS quantum rods-in-matrix assembly for white LED application // Nanomaterials. – 2020. – T. 10, № 2. – C. 317.

10. Sağlam Ö., Dilgin Y. Fabrication of Photoelectrochemical Glucose Biosensor in Flow Injection Analysis System Using ZnS/CdS-Carbon Nanotube Nanocomposite Electrode // Electroanalysis. – 2017. – T. 29, № 5. – C. 1368-1376.

11. Murugadoss G., Kumar M. R. Optical and structural characterization of CdS/ZnS and CdS:Cu2+/ZnS core–shell nanoparticles // Luminescence. – 2014. – T. 29, № 6. – C. 663-668.

12. Chen L., Liu Y., Lai C., Berry R., Tam K. Aqueous synthesis and biostabilization of CdS@ZnS quantum dots for bioimaging applications // Materials Research Express. – 2015. – T. 2, № 10. – C. 105401.

13. Fang D., Zhang Z., Wang Z., Ding Z. Study of photoluminescence of CdS/ZnS core/shell quantum dots // Physics Procedia. – 2012. – T. 32. – C. 920-925.

14. Hiemer J., Stöwe K. Continuous Flow Synthesis of Cd1-xZnxS and CdS/ZnS Core/Shell Semiconductor Nanoparticles by MicroJet Reactor Technology // ChemistryOpen. – 2022. – T. 11, № 12. – C. e202200232.

15. Bai L., Ge L., Gu J., Fang L., Li S. In situ synthesis of CdS/ZnS composite nanoparticles from ZIF-8 for visible light disposal of Cr (VI) // Journal of Sol-Gel Science and Technology. – 2021. – T. 99, № 1. – C. 211-219.

16. Huang M., Yu M., Si R., Zhao X., Chen S., Liu K., Pan X. Tailoring Morphology in Hydrothermally Synthesized CdS/ZnS Nanocomposites for Extraordinary Photocatalytic H2 Generation via Type-II Heterojunction // Catalysts. – 2023. – T. 13, № 7. – C. 1123.

17. Qin D., Yang G., Wang Y., Zhang J., Zhang L. Microwave-assisted synthesis of pectin-stabilised CdS/ZnS core/shell nanocrystals and enhanced photocatalytic performance // Micro & Nano Letters. – 2020. – T. 15, № 9. – C. 595-599.

18. Arab N., Fotouhi L., Salis A. Electrosynthesised CdS@ZnS quantum dots decorated multi walled carbon nanotubes for analysis of propranolol in biological fluids and pharmaceutical samples // Microchemical Journal. – 2021. – T. 168. – C. 106453.

19. Wang X., Li X.-y. Heterostructure CdS/ZnS nanoparticles as a visible light-driven photocatalyst for hydrogen generation from water // International Journal of Green Energy. – 2016. – T. 13, № 12. – C. 1201-1208.

20. Bujňáková Z., Baláž M., Dutková E., Baláž P., Kello M., Mojžišová G., Mojžiš J., Vilková M.,

Imrich J., Psotka M. Mechanochemical approach for the capping of mixed core CdS/ZnS nanocrystals: elimination of cadmium toxicity // Journal of Colloid and Interface Science. – 2017. – T. 486. – C. 97-111.

21. Baláž P., Baláž M., Dutková E., Zorkovská A., Kováč J., Hronec P., Kováč Jr J., Čaplovičová M., Mojžiš J., Mojžišová G. CdS/ZnS nanocomposites: from mechanochemical synthesis to cytotoxicity issues // Materials Science and Engineering: C. – 2016. – T. 58. – C. 1016-1023.

22. James S. L., Friščić T. Mechanochemistry // Chemical Society Reviews. – 2013. – T. 42, № 18. – C. 7494-7496.

23. Friščić T., Mottillo C., Titi H. M. Mechanochemistry for synthesis // Angewandte Chemie. – 2020. – T. 132, № 3. – C. 1030-1041.

24. Baláž P., Achimovičová M., Baláž M., Billik P., Cherkezova-Zheleva Z., Criado J. M., Delogu F., Dutková E., Gaffet E., Gotor F. J. Hallmarks of mechanochemistry: from nanoparticles to technology // Chemical Society Reviews. – 2013. – T. 42, № 18. – C. 7571-7637.

25. Li X., Yu J., Low J., Fang Y., Xiao J., Chen X. Engineering heterogeneous semiconductors for solar water splitting // Journal of Materials Chemistry A. – 2015. – T. 3, № 6. – C. 2485-2534.

26. Shalabayev Z., Baláž M., Khan N., Nurlan Y., Augustyniak A., Daneu N., Tatykayev B., Dutková E., Burashev G., Casas-Luna M. Sustainable synthesis of cadmium sulfide, with applicability in photocatalysis, hydrogen production, and as an antibacterial agent, using two mechanochemical protocols // Nanomaterials. – 2022. – T. 12, № 8. – C. 1250.

27. Khan N., Baláž M., Burkitbayev M., Tatykayev B., Shalabayev Z., Nemkayeva R., Jumagaziyeva A., Niyazbayeva A., Rakhimbek I., Beldeubayev A. DMSO-mediated solvothermal synthesis of S/AgX (X= Cl, Br) microstructures and study of their photocatalytic and biological activity // Applied Surface Science. – 2022. – T. 601. – C. 154122.

28. Oskenbay A., Salikhov D., Rofman O., Rakhimbek I., Shalabayev Z., Khan N., Soltabayev B., Mentbayeva A., Baláž M., Tatykayev B. Solid-state synthesis of ZnS/ZnO nanocomposites and their decoration with NiS cocatalyst for photocatalytic hydrogen production // Ceramics International. – 2023. – T. 49, № 19. – C. 32246-32260.

29. Kumar S., Sharma J. Stable phase CdS nanoparticles for optoelectronics: a study on surface morphology, structural and optical characterization // Materials Science-Poland. – 2016. – T. 34, № 2. – C. 368-373.

30. Maleki M., Sasani Ghamsari M., Mirdamadi S., Ghasemzadeh R. A facile route for preparation of CdS nanoparticles // Semiconductor Physics Quantum Electronics & Optoelectronics. – 2007.

31. Chen Q., Bao H., Shen X. Phase transition of CdS in the presence of ethylenediamine and formation of hollow CdS submicron particles with needle-like structure // Phase Transitions. – 2008. – T. 81, № 6. – C. 591-601.

32. Pathak C., Mishra D., Agarwala V., Mandal M. Blue light emission from barium doped zinc sulfide nanoparticles // Ceramics International. – 2012. – T. 38, № 7. – C. 5497-5500.

33. Zhang J., Wang L., Liu X., Li X. a., Huang W. High-performance CdS–ZnS core–shell nanorod array photoelectrode for photoelectrochemical hydrogen generation // Journal of Materials Chemistry A. – 2015. – T. 3, № 2. – C. 535-541.

34. Tang Y., Liu X., Ma C., Zhou M., Huo P., Yu L., Pan J., Shi W., Yan Y. Enhanced photocatalytic degradation of tetracycline antibiotics by reduced graphene oxide–CdS/ZnS heterostructure photocatalysts // New Journal of Chemistry. – 2015. – T. 39, № 7. – C. 5150-5160.

35. Rossetti R., Nakahara S., Brus L. E. Quantum size effects in the redox potentials, resonance Raman spectra, and electronic spectra of CdS crystallites in aqueous solution // The Journal of Chemical Physics. – 1983. – T. 79, № 2. – C. 1086-1088.

36. Brafman O., Mitra S. Raman effect in wurtzite-and zinc-blende-type ZnS single crystals // Physical Review. – 1968. – T. 171, № 3. – C. 931.

37. Zahn D., Maierhofer C., Winter A., Reckzügel M., Srama R., Thomas A., Horn K., Richter W. The growth of cubic CdS on InP (110) studied in situ by Raman spectroscopy // Journal of Vacuum Science & Technology B: Microelectronics and Nanometer Structures Processing, Measurement, and Phenomena. – 1991. – T. 9, № 4. – C. 2206-2211.

38. Sivasubramanian V., Arora A., Premila M., Sundar C., Sastry V. Optical properties of CdS nanoparticles upon annealing // Physica E: Low-dimensional Systems and Nanostructures. – 2006. – T. 31, № 1. – C. 93-98.

39. Yu J., Li C., Liu S. Effect of PSS on morphology and optical properties of ZnO // Journal of colloid and interface science. – 2008. – T. 326, № 2. – C. 433-438.

40. Liu L.-w., Hu S.-y., Pan Y., Zhang J.-q., Feng Y.-s., Zhang X.-h. Optimizing the synthesis of CdS/ZnS core/shell semiconductor nanocrystals for bioimaging applications // Beilstein Journal of Nanotechnology. – 2014. – T. 5, № 1. – C. 919-926.

41. Weller H. Colloidal semiconductor q-particles: chemistry in the transition region between solid state and molecules // Angewandte Chemie International Edition in English. – 1993. – Т. 32, № 1. – С. 41-53.

42. Xing R., Tong L., Liu X., Ren Y., Liu B., Ochiai T., Feng C., Chong R., Liu S. CdS/ZnS heterostructured porous composite with enhanced visible light photocatalysis // Journal of Nanoscience and Nanotechnology. – 2018. – Т. 18, № 10. – С. 6913-6918.

43. Wang H.-J., Cao Y., Wu L.-L., Wu S.-S., Raza A., Liu N., Wang J.-Y., Miyazawa T. ZnS-based dual nano-semiconductors (ZnS/PbS, ZnS/CdS or ZnS/Ag2S,): A green synthesis route and photocatalytic comparison for removing organic dyes // Journal of environmental chemical engineering. – 2018. – Т. 6, № 6. – С. 6771-6779.

44. Reddy C. V., Shim J., Cho M. Synthesis, structural, optical and photocatalytic properties of CdS/ZnS core/shell nanoparticles // Journal of Physics and Chemistry of Solids. – 2017. – Т. 103. – С. 209-217.

45. Mestl G., Verbruggen N., Knözinger H. Mechanically activated MoO3. 2. Characterization of defect structures // Langmuir. – 1995. – Т. 11, № 8. – С. 3035-3041.

46. Huang Z.-Q., Lu J.-P., Li X.-H., Tong Z.-F. Effect of mechanical activation on physico-chemical properties and structure of cassava starch // Carbohydrate polymers. – 2007. – Т. 68, № 1. – С. 128-135.

47. Liu S., Li H., Yan L. Synthesis and photocatalytic activity of three-dimensional ZnS/CdS composites // Materials Research Bulletin. – 2013. – Т. 48, № 9. – С. 3328-3334.

48. Monodispersed particles. / Sugimoto T.: Elsevier, 2019.

49. Wang L., Wei H., Fan Y., Liu X., Zhan J. Synthesis, optical properties, and photocatalytic activity of one-dimensional CdS@ ZnS core-shell nanocomposites // Nanoscale research letters. – 2009. – Т. 4. – С. 558-564.

50. Zhang K., Jin L., Yang Y., Guo K., Hu F. Novel method of constructing CdS/ZnS heterojunction for high performance and stable photocatalytic activity // Journal of Photochemistry and Photobiology A: Chemistry. – 2019. – Т. 380. – С. 111859.

51. Qutub N., Pirzada B. M., Umar K., Mehraj O., Muneer M., Sabir S. Synthesis, characterization and visible-light driven photocatalysis by differently structured CdS/ZnS sandwich and core–shell nanocomposites // Physica E: Low-Dimensional Systems and Nanostructures. – 2015. – Т. 74. – С. 74-86.

52. Fakhri F. H., Ahmed L. M. Incorporation CdS with ZnS as composite and using in photo-decolorization of congo red dye // Indonesian Journal of Chemistry. – 2019. – Т. 19, № 4. – С. 936-943.

53. Kaur G., Kaur A., Singh K. Study of Photo-catalytic Activity of Synthesized Intrinsic and Extrinsic CdS/ZnS Core-shell Nanostructures //.

54. He J., Ji W., Mi J., Zheng Y., Ying J. Y. Three-photon absorption in water-soluble ZnS nanocrystals // Applied physics letters. – 2006. – Т. 88, № 18.

55. Li Q., Guo B., Yu J., Ran J., Zhang B., Yan H., Gong J. R. Highly efficient visible-light-driven photocatalytic hydrogen production of CdS-cluster-decorated graphene nanosheets // Journal of the American Chemical Society. – 2011. – Т. 133, № 28. – С. 10878-10884.

56. Xie Y. P., Yu Z. B., Liu G., Ma X. L., Cheng H.-M. CdS–mesoporous ZnS core–shell particles for efficient and stable photocatalytic hydrogen evolution under visible light // Energy & Environmental Science. – 2014. – Т. 7, № 6. – С. 1895-1901.

G. Turlybay , E. Nurgaziyeva , D. Issayeva ,

A. Mentbayeva , Z. Bakenov , S. Kalybekkyzy*

[1]National Laboratory Astana, Astana, Kazakhstan
[2]School of Engineering and Digital Sciences, Nazarbayev University, Astana, Kazakhstan
[3]School of Sciences and Humanities,
Nazarbayev University, Astana, Kazakhstan
*e-mail: sandugash.kalybekkyzy@nu.edu.kz

Synthesis and characterization of LATP solid electrolyte by solution method

Abstract. Recently, considerable attention has been paid to the study of solid electrolytes in lithium-ion batteries. Ion conductive ceramic material NASICON-type $Li_{1+x}A_xTi_{2-x}(PO_4)_3$ (LATP) is a promising solid electrolyte for lithium-ion batteries due to its stability in air. In this work successfully produced pure solid electrolyte LATP powders with a rhombohedral NASICON-type structure. Here we report the results of LATP synthesis using the solution method. Pellets of dense electrolyte were made at 900 °C. It has been found that the ionic conductivity of LATP is largely influenced by the preparation method. Pure LATP was obtained with the grain size of 100-700 nm. These findings demonstrate the efficacy of the solution method in producing pure LATP. The resultant LATP has an activation energy of 0.465 eV and a total lithium-ion conductivity of 5.8×10^{-5} S cm-1 at ambient temperature. Its typical particle size is between 100 and 700 nm, and its relative density is 89.5 percent.

Key words: solid electrolytes, LATP, ionic conductivity, NASICON type, X-ray diffraction, SEM.

Introduction

In the last twenty years, the lithium-ion battery (LIBs) has gained popularity as a preferred option for rechargeable batteries because of its low redox potential, high energy density, minimal self-discharge, and lack of a memory effect. Currently, LIBs are extensively used in energy storage applications like 5G mobile networks, electric vehicles, and large-scale grid energy due to their lightweight and high energy density. LIBs incorporating organic liquid electrolytes face issues related to leakage and flammability, posing significant constraints, especially in the context of large-scale applications. These challenges not only compromise the safety of LIBs but also hinder their widespread implementation on a larger scale.However, the use of flammable organic liquid electrolytes in LIBs poses safety concerns, limiting their practical applications [1, 2, 4, 5]. The emergence of all-solid-state lithium-ion batteries (ASSLIBs), incorporating solid-state electrolytes (SSEs), is driven by the objective to improve safety without compromising the advantages of conventional LIBs. However, the practical application of ASSLIBs is hindered by the suboptimal ionic conductivity of these solid-state electrolytes. Consequently, there is a need for enhancements in both ionic conductivity and the mechanical and electrochemical stability of SSEs to unlock the full potential of ASSLIBs.

During battery operation, anions and cations move between electrodes, but anions, not participating in the oxidation-reduction reaction, cause concentration polarization on both sides of the electrolyte. This leads to rapid lithium dendrite growth, potentially penetrating the membrane and causing a short circuit, posing a safety risk [14].

Concerns over the frequent safety issues associated with traditional batteries have prompted a shift towards all-solid-state batteries. In addressing this, solid electrolytes are being employed to replace liquid electrolytes in the all-solid-state lithium-ion battery (ASSLIBs) system [11, 14]. This adaptation aims to eliminate electrolyte leakage, curb the growth of lithium dendrites, and elevate overall battery safety. The solid-state electrolyte holds a pivotal position in ASSLIBs, contributing significantly to advancements in carbon economy and energy technologies [12, 14].

Inorganic-based electrolytes typically exhibit high ion conductivity. Various solid inorganic materials show promise for application in lithium-ion batteries. Presently, advanced solid electrolytes, including lithium halide, lithium hydride perovskite, lithium nitride, garnet, argyrodite, and sulfide, demonstrate ionic conductivity within the range of 10^{-6}–10^{-2} S cm^{-1}. These materials hold potential for enhancing the performance of lithium-ion batteries through improved conductivity characteristics [3,4]. The sulfide type of electrolyte has the highest ionic conductivity among all other types of solid electrolytes, which is close to a liquid electrolyte (10^{-2} S cm^{-1}). However, it is unstable in air which prevents its mass production.

Among all types of solid electrolytes, NASICON structured electrolytes are the most stable in air and have sufficient ionic conductivity in the range of 10^{-6}-10^{-3} S cm^{-1} [1-13]. The NASICON-type electrolyte with the general formula of $NaM_2(PO_4)_3$ has a rhombohedral structure with the space group R3c. Na atoms can be replaced with Li atoms by converting them to $LiM_2(PO_4)_3$, where M is Ti, Zr or Ge [2]. The titanium-containing type is $LiTi_2(PO_4)_3$ (LTP), which demonstrates high chemical and thermal stability with an applicable ionic conductivity of 10^{-4} S cm^{-1} in grains and a total conductivity of about 10^{-8} and 10^{-6} S cm^{-1} due to high resistance at grain boundaries [10].

Various types of inorganic solid-state electrolytes, including garnet-type $Li_7La_3Zr_2O_{12}$ [3], perovskite-type $Li_{3x}La_{2/3-x}TiO_3$ [5,6], and NASICON-type systems [12,13], are currently under active investigation. Among these, the NASICON-type material lithium titanium phosphate, $LiTi_2(PO_4)_3$ (LTP), stands out as a particularly promising solid-state electrolyte due to its intrinsic safety features, cost-effectiveness, and high thermal and air stability at room temperature. LTP has demonstrated versatility, serving not only as an effective electrolyte in ASSLBs [4] but also in lithium-air and lithium-sulfide systems [2].

The $LiTi_2(PO_4)_3$ material, belonging to the NASICON type, adopts a rhombohedral structure characterized by octahedral TiO_6 units that share corners with tetrahedral PO_4 units. Within this structure, two types of Location vacancies are present: M1 vacancies, situated between tetrahedral PO_4 units, and M2 vacancies, formed between adjacent octahedral TiO_6 units. In the 3D NASICON network, the diffusion of Li$^+$ ions occurs along pathways that connect the M1–M2 vacancies. This intricate structure facilitates the movement of lithium ions within the material [15].

However, $LiTi_2(PO_4)_3$ suffers from a drawback of lower ionic conductivity at room temperature [14]. In the case of LTP, the grain boundary resistance significantly outweighs the contribution of the bulk to the total resistance. This indicates that the grain boundary resistance plays a pivotal role in governing the overall conductivity of $LiTi_2(PO_4)_3$. Therefore, the optimization of total conductivity crucially depends on controlling the density of an LTP electrolyte. To enhance density, researchers have explored the effects of incorporating fluxes or employing novel sintering techniques, some of which are briefly discussed below [15].

Studies show that Ti^{4+} can be replaced by various trivalent elements (such as Al^{3+}, Fe^{3+}, Y^{3+}, Cr^{3+}, Ga^{3+}, and Sc^{3+}) while preserving the rhombohedral NASICON-type structure [12-14]. Among these aliovalent substituents, Al^{3+} has proven effective in adjusting the NASICON cell volume to an optimal size for facilitating Li$^+$ transport, significantly improving conductivity in resulting $Li_{1+x}Al_xTi_{2-x}(PO_4)_3$ (LATP). Conversely, some research highlights that the aluminum additive primarily forms the Al-rich second phase $AlPO_4$, enhancing total ion conductivity by promoting densification and effectively creating a composite. However, the concentration of added Al is crucial, as at high levels, it hinders Li-ion conduction across the $LiTi_2(PO_4)_3$ grain boundaries. Therefore, maintaining overall control of the LTP microstructure is vital to maximize overall conductivity, striking a balance between achieving high density and ensuring that secondary phases do not impede ionic transport at the grain boundaries [15].

To address the microstructure challenge, an alternative approach involves utilizing low melting point fluxes to enhance the density of $LiTi_2(PO_4)_3$ (LTP) and related substituted solid electrolytes.

Currently, there are several known methods for the preparation of lithium aluminum titanium phosphate (LATP) samples. These include solid-phase reaction, sol-gel method, coprecipitation method, and melt quenching, as well as advanced techniques like spray drying, spark plasma sintering, and hydrothermal synthesis. These diverse methods offer researchers a range of options for tailoring LATP samples to specific requirements in terms of structure, composition, and performance [2,3,7,9].

Within these methods, the solid-phase reaction method encounters challenges related to the formation of secondary phases. Additionally, the melt quenching process demands elevated sintering temperatures. As a result, these factors need to be carefully considered and addressed to optimize the efficiency of the synthesis process [11]. The coprecipitation method

involve in the complexing agent or co precipitator, which results in higher production cost. Therefore, it is meaningful to explore a low-cost method for the preparation of LATP samples.

A sol-gel technique, specifically the solution method, stands out as a straightforward and cost-effective approach. This low-temperature process involves dissolving all precursors to form a homogeneous phase, facilitating the production of nanomaterials characterized by high crystallinity in a pure state. The simplicity and affordability of this method make it an attractive option for synthesizing materials with desired properties [1, 10].

The primary objective of this study is to acquire nanoparticles of lithium aluminum titanium phosphate (LATP) with a focus on solid electrolytes. In this research, we explore a straightforward solution method tailored for the large-scale production of nanoscale LATP (x=0.3). This method, utilizing purified water as a solvent, aims to circumvent the hydrolysis of titanium salt and achieve enhanced ionic conductivity. Furthermore, this work introduces a novel strategy for the synthesis of additional LATP solid electrolytes with varying x values, expanding the applicability of the proposed approach.

Materials and methods

Preparation of solid electrolyte. The preparation of $Li_{1.3}Al_{0.3}Ti_{1.7}(PO_4)_3$ solid electrolyte involved a solution-based method. Initially, $LiOH·H_2O$ was dissolved in purified water. Subsequently, Al_2O_3, TiO_2 and H_3PO were introduced into the solution under magnetic stirring. The resulting mixture underwent drying at 180 °C in an oven to eliminate excess water, leading to the formation of a viscous paste. This paste was subjected to calcination at 700 °C for 6 hours. The resultant precursor powders were then subjected to high-energy mechanical ball grinding, utilizing zirconium balls with a 12 mm diameter, at 650 rpm for 5 hours. The ground powders were subsequently pressed into pellets with a hydraulic press, featuring a diameter of 10 mm. These pellets underwent sintering at 900 °C for 12 hours in an air environment to yield the final LATP pellets.

This methodological approach ensures the systematic synthesis of $Li_{1.3}Al_{0.3}Ti_{1.7}(PO_4)_3$ solid electrolyte, employing a well-defined sequence of steps to achieve the desired material properties.

Characterization. The structure of LATP before and after sintering was studied using XRD (Rigaku smartLAB X-ray system) equipped with a Cu X-ray tube and a D-Text detector within 2θ = 10-70° with a step width of 0.06°.

The grain size and morphology of the LATP powder and pellet were studied using SEM (FESEM Auriga, Crossbeam 540). Gold with a thickness of 5 nm was applied to the surface of the powders using an automatic Q150T atomizer to improve electronic conductivity, since the electrolyte materials are electronic insulators. Ionic conductivity was measured by electrochemical impedance spectroscopy (potentiostat/galvanostat, Metrohm AutoLab 204, 1 Hz – 1 MHz).

Results and discussion

The solution method has proven effective in the successful synthesis of pure NASICON-structured lithium aluminum titanium phosphate (LATP). The X-ray diffraction (XRD) pattern, as depicted in Figure 1, reveals that the predominant phase is NASICON, characterized by the spatial group R3c. Notably, a common challenge in LATP material preparation lies in the significant formation of $AlPO_4$. In Figure 1, the arrow in the powder form points to the peak corresponding to $AlPO_4$. This undesirable phase typically arises during high-temperature sintering, leading to the loss of lithium through evaporation [13]. However, in the case of the obtained pellet powder, the intensity of the $AlPO_4$ peak decreases, indicating a reduction in the amount of $AlPO_4$. The lattice constants, calculated from the XRD data, are measured at 0.8471 nm and 2.0763 nm, aligning with the spatial group R3c.

These findings underscore the efficacy of the solution method in achieving the desired NASICON structure for LATP, while also addressing the challenge of minimizing the formation of $AlPO_4$ during the synthesis process. The reduced presence of $AlPO_4$ in the pellet powder indicates progress in optimizing the material composition and characteristics.

SEM images were acquired to analyze the morphology of the synthesized ATP. As per existing literature [2], the particles are expected to exhibit a cubic shape with dimensions ranging from 1 to 2 microns. Figure 2a reveals that LATP particles, obtained through the solution method, exhibit a reduced size in the range of 100-700 nm. This diminution in particle size is highly favorable, as it results in a smaller surface area, thereby minimizing the impact of grain boundaries on the overall conductivity of lithium ions [1-2].

Figure 2b provides a visualization of the surface morphology of the LATP pellets, offering valuable insights into the structural characteristics of the synthesized material.
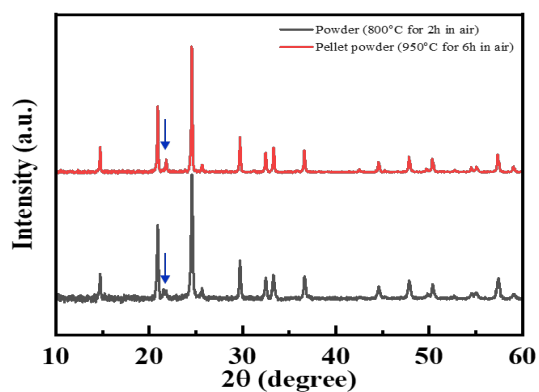
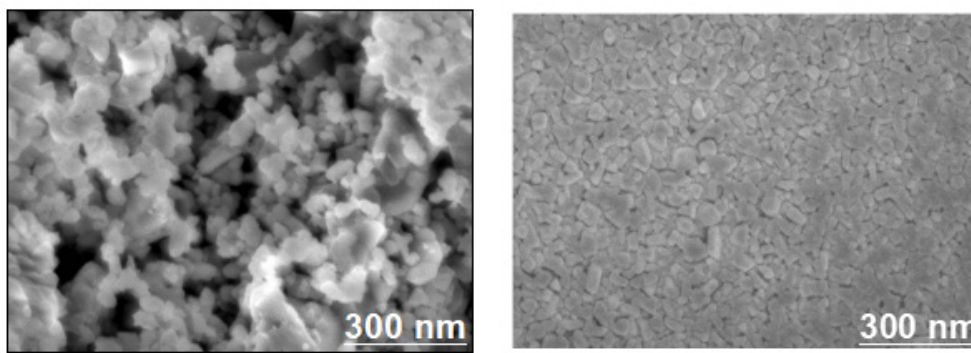**Figure 1** – XRD images of the prepared LATP in the form of powder and pellet

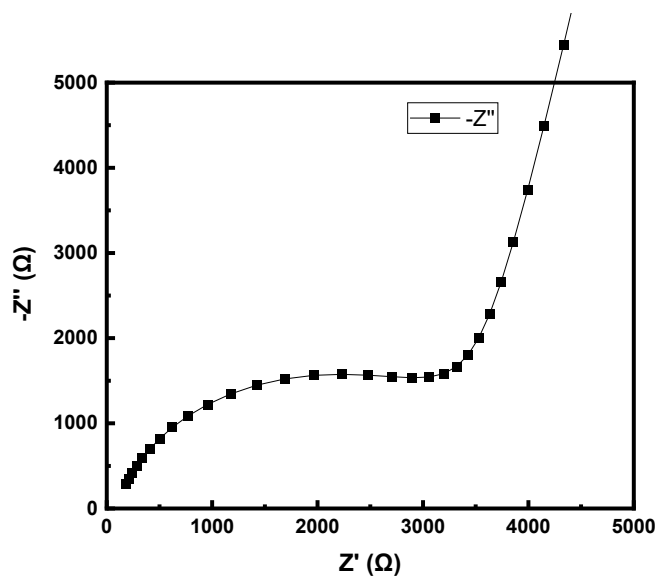**Figure 2** – SEM images of: a) LATP powder b) LATP pellet

Figure 3 – Impedance profile measured at room temperature for LATP pellet

According to the impedance spectrum (Figure 3), measured ionic conductivity of the above-obtained LATP pellet was 5.8×10^{-5} S cm^{-1}. The low ionic conductivity might be due to the density and activation energy of Li$^+$ transport. The ionic conductivity of LATP is directly proportional to its density in pellet form [5]. The calculated density of the obtained LATP pellet is 89.7 % (Table 1). This value is probably not enough to achieve ionic conductivity above 5.8×10^{-5} S cm^{-1}. Furthermore, calculated activation energy for Li$^+$ transport in LATP pellet is 0.465 eV.

Table 1 – Pellet parameters

Parametrs	Density, %	Ionic conductivity, S cm^{-1}	Activation energy, eV
Indicators	89.7	5.8×10^{-5}	0.465

Conclusion

In this work, pure solid electrolyte LATP powders with a rhombohedral NASICON-type structure were successfully obtained. Dense electrolyte pellets were prepared at 900 °C. These results show that the solution method is an effective approach for obtaining pure LATP. The resulting LATP with an average particle size of 100-700 nm and a relative density of 89.7 % demonstrates a total lithium-ion conductivity of 5.8×10^{-5} S cm^{-1} at room temperature and an activation energy of 0.465 eV. Based on the achieved parameters prepared LATP is a promising solid electrolyte for all solid-state lithium-ion batteries.

Acknowledgement

References

1. Kotobuki M., Koishi M. (2013) Preparation of Li1.5Al0.5Ti1.5(PO4)3 solid electrolyte via a sol–gel route using various Al sources. Ceramics International, vol. 39, no. 4, pp. 4645-4649, https://doi.org/10.1016/j.ceramint.2012.10.206.

2. Xiao W., Wang J., Fan L., Zhang J., Xifei Li. (2019) Recent advances in Li1+xAlxTi2−x(PO4)3 solid-state electrolyte for safe lithium batteries, Energy Storage Materials, vol. 19, pp. 379-400, https://doi.org/10.1016/j.ensm.2018.10.012.

3. Zhang, H., Wu, X., Yang, T., Liang, S., Yang, X. (2013). Cooperation behavior between heterogeneous cations in hybrid batteries, Chemical Communications, 49(85), 9977-9979. https://doi.org/10.1039/C3CC45895D

4. Zheng F., Kotobuki M., Song Sh., Lai M. O., Li Lu. (2018) Review on solid electrolytes for all-solid-state lithium-ion batteries, Journal of Power Sources, vol. 389, pp. 198-213, https://doi.org/10.1016/j.jpowsour.2018.04.022.

5. Bucharsky E.C., Schell K.G., Hintennach A., Hoffmann M.J. (2015) Preparation and characterization of sol–gel derived high lithium ion conductive NZP-type ceramics Li1+x AlxTi2−x(PO4)3, Solid State Ionics, vol. 274, pp.77-82, https://doi.org/10.1016/j.ssi.2015.03.009.

6. Sudreau F., Petit D., Boilot J.P.. (1989) Dimorphism, phase transitions, and transport properties in LiZr2(PO4)3, Journal of Solid State Chemistry, vol. 83, no.1, pp. 78-90, https://doi.org/10.1016/0022-4596(89)90056-X.

7. Jie Fu. (1997) Superionic conductivity of glass-ceramics in the system Li2O- Al2O3-TiO 2-P 2O5, Solid State Ionics, vol. 96, no. 3–4, pp. 195-200, https://doi.org/10.1016/S0167-2738(97)00018-0.

8. Hallopeau L., Bregiroux D., Rousse G., Portehault D., Stevens P., Toussaint G., Laberty-Robert Ch. (2018) Microwave-assisted reactive sintering and lithium ion conductivity of Li1.3Al0.3Ti1.7(PO4)3 solid electrolyte, Journal of Power Sources, vol. 378, pp. 48-52, https://doi.org/10.1016/j.jpowsour.2017.12.021.

9. Kwatek K., Nowiński J.L. (2017) Electrical properties of LiTi2(PO4)3 and Li1.3Al0.3Ti1.7(PO4)3 solid electrolytes containing ionic liquid, Solid State Ionics, vol. 302, pp. 54-60, https://doi.org/10.1016/j.ssi.2016.11.020.

10. Ma Q., Xu Q., Tsai Ch-L., Tietz F., Guillon O. (2016) A Novel Sol–Gel Method for Large-Scale Production of Nanopowders: Preparation of Li1.5Al0.5Ti1.5(PO4)3 as an Example, J. Am.

Ceram. Soc. vol. 99, no. 2, pp. 410-414, https://doi.org/10.1111/jace.13997

11. Huang L., Wen Z., Wu M., Wu X., Liu Y., Wang X. J. (2011). Electrochemical properties of Li1.4Al0.4Ti1.6(PO4)3 synthesized by a co-precipitation method, J. Power Sources, vol. 196, pp. 6943–6946, https://doi.org/10.1016/j.jpowsour.2020.11.140

12. Tolganbek N., Mentbayeva A., Uzakbaiuly B., Kanamura K., Bakenov Zh. (2020) Li1+xAlxTi2−x (PO4)3, NASICON-type solid electrolyte fabrication with different methods, Materials Today: Proceedings, vol. 25, pp. 97-100, https://doi.org/10.1016/j.matpr.2019.12.279

13. Tolganbek Nurbol, Serikkazyyeva Assel, Kalybekkyzy Sandugash, Sarsembina Madina, Kanamura Kiyoshi, Bakenov Zhumabay, Mentbayeva Almagul. (2022) Interface modification of NASICON-type Li-ion conducting ceramic electrolytes: a critical evaluation, Materials Advances, vol. 3, pp. 3055-3069, 10.1039/D1MA01239H

14. Tianyu Zhao, Qixin Gai, Xiaoyan Deng, Junwei Ma, Hongtao Gao. (2023) A new type of LATP doped PVDF-HFP based electrolyte membrane with flame retardancy and long cycle stability for solid state batteries, Journal of Energy Storage, vol 73, https://doi.org/10.1016/j.est.2023.108576

15. Yen P., Lee M., Gregory D., Liu W. (2020) Optimization of sintering process on Li1+Al Ti2-(PO4)3 solid electrolytes for all-solid-state lithium-ion batteries, Ceramics International, vol. 46, pp. 20529–20536, https://doi.org/10.1016/j.ceramint.2020.05.162

F. İslamoğlu* ID , N. Erdoğan ID , E. Hacıfazlıoğlu ID

Recep Tayyip Erdoğan University, Rize, Turkey
*e-mail: fatih.islamoglu@erdogan.edu.tr

Theoretical determination of electronic, geometric and spectroscopic properties of some 1,2,4-triazol derivatives

Abstract. In this study, molecular geometric optimization of five 4,5-dihydro-1H-1,2,4-triazol-5-one derivative compounds was obtained using Density Functional Theory, (DFT, B3LYP)/ Hartree Fock, (HF, B3LYP) methods on the basis set of 6-311G (d,p) in order to find the most stable geometric shape of the studied compounds. FT-IR and UV-vis spectral values were performed by using gauge independent atomic orbital (GIAO) methods with Gaussian G09W package program. IR frequency datas of investigated five compounds were calculated in gas phases and are multiplied with appropriate scala factors. The identification of the calculated IR data was performed in the veda4f program. In addition, bond angles, bond lengths, dipole moments, highest occupied molecular orbital (HOMO), lowest unoccupied molecular orbital (LUMO) energy and total energy, mulliken charges and molecular electrostatic potential (MEP) of five compounds were calculated using same methods and set.
Key words: Density functional theory, hartree fock, triazole derivatives.

Introduction

One of the most significant families of heterocyclic molecules includes triazoles and their derivatives. Due to their wide range of biological activities, 1,2,4-triazole derivatives have received a lot of attention in medicinal chemistry. Examples of these biological activities include antiviral [1], antibacterial [2], antifungal [3, 4] (examples of antifungal drugs are fluconazole [5, 6], itraconazole [7], ravuconazole [8], voriconazole [9-11] and posaconazole [12]), anti-tubercular [13-15], immunosuppressant [16], antihypertensive [17], anti-inflammatory [18,19], anticonvulsant [20, 21], analgesic [22], hypoglycemic [23], antidepressant [24, 25] and anticancer [26-28] activities. Derivatives of 1,2,4-triazoles are a significant class of antifungal medications that are frequently used to treat fungi [29]. Insecticides [30], antiasthmatics [31], antidepressants [32], insecticidal [33], and plant growth regulators [34] are all described uses for 1,2,4-triazole derivatives. Moreover, triazole-containing substances with anti-aromatase properties as vorozole, letrozole, and anastrozole have been demonstrated to be particularly helpful in preventing breast cancer [35-37]. According to reports, the 1,2,4-triazole moiety interacts well with heme iron, and the triazole's aromatic substituents are particularly successful in interacting with the active site of aromatase [38, 39].

Several properties in chemical systems have been predicted using computational chemical simulations. Because of this, the design of functional materials has been heavily utilized in these computations. Several organic compounds' spectroscopic, electrical, and thermodynamic properties have been clarified utilizing theoretical calculation techniques [40-44]. Due to their strong biological activity, Mannich bases have been able to capture the interest of numerous researchers. Due to this, publications on Mannich bases and their derivatives computational chemical computations were reported in the literature [45-48]. In order to determine the structural, spectroscopic, and electrical properties of the title chemical, we used a theoretical analysis approach. First off, the B3LYP(DFT)/6-311G(d,p) and B3LYP(HF)/ 6-311G(d,p) basis set have been used for all quantum chemical calculations of the molecules in issue. The optimized structure with B3LYP/6-311G(d,p) level was used to determine the 1H and 13C-NMR chemical shift values, vibrational frequencies, structural, and electronic parameters, HOMO-LUMO energies, and molecular electrostatic potential maps (MEP) of the title molecule. The spectral information generated using DFT/B3LYP and the 6-311G(d,p) basis set was connected to the vibrational frequencies of the

named molecular structure. The calculated and taken from the literature of experimental values of every spectroscopic parameter were compared.

If the predicted frequencies are scaled to account for the approximation handling of electron correlation, for basis set shortcomings, and for the anharmonicity, density functional theory calculations (DFT) are said to provide excellent vibrational frequencies of organic compounds [49, 50]. Several publications in the literature have discussed the calculation of the chemical shift of the Nuclear Magnetic Rezonans using quantum-chemistry techniques [51-55]. However, it was suggested that the single-point calculation of magnetic shielding by DFT methods was combined with a quick and accurate geometry-optimization procedure at the molecular mechanics level because as molecular size increases, computing-time limitations are introduced for obtaining optimized geometries at the DFT level [51].

One of the most popular methods for estimating nuclear magnetic shielding tensors is the gauge-including atomic orbital [56-57]. It has been demonstrated that, for the same basis set size, the results generated by the GIAO method are frequently more accurate than those estimated using other approaches [58]. When the electron correlation contributions were not insignificant, DFT approaches were favoured for the analysis of large organic compounds [59] and for GIAO 13C calculations [58].

Materials and methods

Studied molecules. In this article, five 1,2,4-triazol derivatives ((1) N-(3-methyl-5-oxo-1,5-dihydro-4H-1,2,4-triazol-4-yl)-2-phenylacet- amide, (2) N-(3-ethyl-5-oxo -1,5-dihydro-4H-1,2,4-triazol-4-yl)-2-phenylacetamide, (3) N-(3-benzyl-5-oxo-1,5-dihydro-4H-1,2,4-triazol -4-yl)-2-phenylacetamide, (4) N-{3-[(4-methylphenyl)methyl]-5-oxo-1,5-dihydro-4H-1,2,4-triazol-4-yl}-2-phenyl acetamide, (5) N-{3-[(4-chlorophenyl)methyl]-5-oxo-1,5-dihyd ro-4H-1,2,4-triazol-4-yl}-2-phenylacet amide) has been theoretically studied. Experimental studies on these molecules have been previously conducted and published as articles [60]. First of all, all molecules were optimized according to Density Functional Theory (DFT) and Hartree–Fock (HF) methods. Structure of the studied molecules is given on Figure 1.

	R
1	$-CH_3$
2	$-CH_2CH_3$
3	$-CH_2C_6H_5$
4	$-CH_2C_6H_4CH_3$ *(p-)*
5	$-CH_2C_6H_4Cl$ *(p-)*
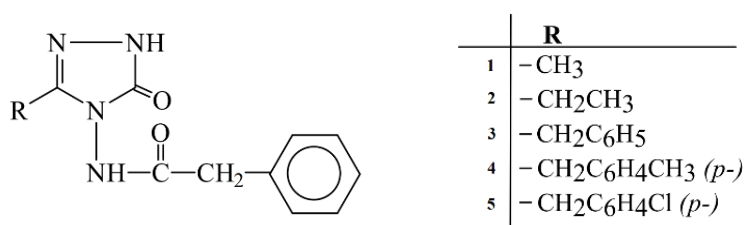
Figure 1 – Structure of the optimized molecules

Three dimensional drawing of molecules. The Gauss-view program is an interface included in the gaussian package programs that allows the three-dimensional design of a molecule to visually define the properties of the molecule, modify it, and start calculations by creating input data. Gaussview allows us to visualize molecules and move them in the direction we want, make changes in molecules and examine the results calculated for a molecule studied in the Gaussian 09W program. Guass-view graphical interface program is used to facilitate the Gaussian 09W program according to the bond numbers and positions of the atoms in the molecule. With the Gauss-view program, formula groups, symbols of atoms and their bonding shapes are available, and a three-dimensional Gauss-view image is obtained by using formulas and sambols and bonds that are suitable for the molecule to be drawn.

Bond angle and bond length. When determining and fine-tuning the structures of numerous molecules, correct knowledge of conventional bond lengths and bond angles is crucial. The experimental data from either X-ray crystallography or NMR studies are supplemented with ideal or target values for these geometrical parameters, which effectively increases the number of experimental observations in relation to the number of parameters being determined (the latter being the atomic co-ordinates and temperature factors). For the computational values of bond angle

and bond length, which are the geometrical structure parameters of all molecules, calculations were made using HF/DFT(B3LYP) methods and 6-311G(d,p) basic set in the Gaussian 09W package program.

Mulliken atomic charge. The electronic charge distribution in a molecule and the bonding, antibonding, or nonbonding nature of the molecular orbitals for specific atomic pairs can be described using Mulliken atomic charges. The concept of these Mulliken atomic charges was established; it was thought to be a real, normalized molecular orbital made up of two normalized atomic orbitals. The square of the wavefunction can be used to represent the charge distribution as a probability density. The result is obtained by integrating over all of the electronic coordinates and using the normalized molecular and atomic orbitals.

HOMO-LUMO. For the investigation of trends in -electronic configurations for conjugated systems simulated by different classes of chemical graphs, the HOMO-LUMO map has been proposed as a qualitative tool. The goal is to create a scatterplot of the Hückel HOMO vs LUMO eigenvalues and look at how the data clusters. The mappings proposed a conjecture for more general chemical graphs and a theorem for eigenvalue bounds for chemical trees. We used this simple device to re-examine some aspects of the qualitative theory of the electronic structure of 1,2,4-triazole derivatives and identify some plausible conjectures.

Dipole moment and total energy properties. When there is a separation of charge, dipole moments happen. Dipole moments, which result from variations in electronegativity, can happen between atoms in a covalent link or between two ions in an ionic bond. The dipole moment increases with the difference in electronegativity. The size of the dipole moment is also affected by the distance between the charge separations. The polarity of the molecule is determined by the dipole moment. By calculating the lowest feasible calculated energy, we may use the variation theorem to forecast the total energies of atoms. We can answer for the total energies of atoms with great precision using the outcomes of variation calculations, perturbation theory, Density Functional Theory, Hartree-Fock calculations, and/or configuration interaction.

IR spectral analysis. The study of how a molecule interacts with infrared light is known as infrared spectroscopy. Absorption, emission, and reflection measurements can be used to examine this in three different ways. This method is mostly employed in organic and inorganic chemistry. Chemists employ it to identify functional groups in compounds. By measuring atom vibrations using IR spectroscopy, the functional groups of molecules can be identified. Usually, heavier atoms and stronger bonds will vibrate with a higher stretching frequency (wavenumber).

UV Spectral analysis. UV-visible spectroscopy is a technique used to analyze the electronic transitions of molecules in the ultraviolet (UV) and visible (VIS) regions of the electromagnetic spectrum. It involves passing a beam of light of a specific wavelength through a sample and measuring the intensity of the light that is transmitted or absorbed. In UV-visible spectroscopy, the energy of the light is absorbed by the molecule and causes an electronic transition from the ground state to an excited state. The energy required to cause this transition is dependent on the chemical structure of the molecule, and thus each molecule has a unique absorption spectrum.

Molecular electrostatic potential (MEP). Molecular electrostatic potential (MEP) is a measure of the electrostatic potential energy at a given point in space around a molecule. It is a tool used in computational chemistry to study the distribution of electric charge in a molecule and its relationship to the molecule's properties. MEP is calculated by solving the Schrödinger equation for the molecule using quantum mechanical methods. This provides a description of the electron density around the molecule, which in turn allows the calculation of the electrostatic potential at each point in space. MEP for studied molecules using IQmol computer program for 6-311G(d) level.

Results and discussion

First, the bond lengths and bond angles of the molecules given in Table 1-2 were examined. When we evaluate the bonds between molecules, the longest bond length is 1.75963 Ao between C(38)-Cl(39) atoms in the 5th molecule according to the DFT model, and the shortest bond length is 0.99039 Ao between N(1)-H(7) atoms in the 2nd molecule according to the HF model was determined. When we consider in terms of angles, the widest bond angle is 131.59799 degrees between N(1)-C(2)=O(5) atoms in the 3rd molecule according to the DFT model and the narrowest bond angle is 100.75592 degrees between N(1)-C(2)-N(4) atoms in the 4th molecule according to the DFT model was determined.

Table 1 – The calculated bond angles (0) of all molecules as DFT (B3LYP) and HF (B3LYP) methods on the basis set of 6-311G (d,p).

Bond Angles (⁰)	Molecule 1 DFT / HF	Molecule 2 DFT / HF	Molecule 3 DFT / HF	Molecule 4 DFT / HF	Molecule 5 DFT / HF
H(7)-N(1)-C(2)	125.51734 / 125.76726	125.51958 / 125.78813	125.56632 / 125.83578	125.54830 / 125.82899	125.56176 / 125.84750
N(1)-C(2)=O(5)	131.54741 / 131.18307	131.50846 / 131.15371	131.59799 / 131.20935	131.56212 / 131.20538	131.57251 / 131.21932
N(1)-C(2)-N(4)	100.79764 / 101.64543	100.79403 / 101.65701	100.76333 / 101.62205	100.75592 / 101.62204	100.76218 / 101.62323
C(2)-N(4)-C(25)	109.00053 / 108.58199	109.04967 / 108.64197	108.97677 / 108.56856	108.98419 / 108.58452	108.91670 / 108.52508
N(4)-C(25)=N(3)	110.75049 / 110.72141	110.63013 / 110.56702	110.72754 / 110.63954	110.71453 / 110.61622	110.81169 / 110.71254
C(25)=N(3)-N(1)	105.05126 / 105.44952	105.14484 / 105.55789	105.06021 / 105.50403	105.05873 / 105.50629	105.04301 / 105.49273
N(3)-N(1)-H(7)	120.08212 / 120.62360	120.10128 / 120.62720	119.95986 / 120.49493	119.96302 / 120.49679	119.96822 / 120.50083
N(3)=C(25)-C(26)	125.36200 / 125.77546	125.91522 / 126.48111	126.58605 / 127.22220	126.64688 / 127.25754	126.43192 / 127.05017
H(28)-C(26)-H(27)	109.19119 / 109.55612	113.17004 / 113.14622	105.52697 / 105.82943	105.47604 / 108.02927	105.51012 / 105.83383
H(27)-C(26)-H(29)	107.50943 / 107.88766	-	110.26828 / 110.37114	-	110.27807 / 110.37329
H(28)-C(26)-H(29)	109.14532 / 109.51700	105.39778 / 105.89996	-	-	-
N(4)-C(25)-C(26)	123.88734 / 123.88734	123.45458 / 122.95187	122.68550 / 122.13827	122.63660 / 122.12624	122.75449 / 122.23729
C(25)-N(4)-N(6)	126.25664 / 125.93893	126.26731 / 125.89747	-	-	-
N(4)-N(6)-H(8)	115.48168 / 114.73649	115.63506 / 114.77904	115.46198 / 114.70483	115.54557 / 114.72428	115.41126 / 114.62772
N(4)-N(6)-C(9)	123.96491 / 121.76834	124.15527 / 121.81280	123.93710 / 121.71803	124.04090 / 121.73215	123.92439 / 121.66206
N(6)-C(9)=O(10)	118.34852 / 118.40623	118.36627 / 118.43522	118.35174 / 118.41488	118.36853 / 118.43318	118.26233 / 118.34988
N(6)-C(9)-C(11)	117.53223 / 116.57779	117.56948 / 116.58107	117.54833 / 116.59035	117.54943 / 116.58199	117.57960 / 116.61053
C(9)-C(11)-H(24)	111.18608 / 106.24476	111.19498 / 109.38708	111.19580 / 106.24680	111.16192 / 106.24229	111.14887 / 106.26400
C(9)-C(11)-H(23)	105.88265 / 109.37203	105.94016 / 106.22629	105.88335 / 109.38740	-	-
H(23)-C(11)-H(24)	106.92516 / 106.52050	106.97496 / 106.52562	106.96904 / 106.52356	107.00132 / 106.51549	107.00100 / 106.51418
C(9)-C(11)-C(12)	112.20308 / 113.59009	112.07661 / 113.58893	112.14749 / 113.55114	112.10077 / 113.55415	112.10718 / 113.54258
H(8)-N(6)-C(9)	113.09749 / 112.87271	113.25459 / 112.92184	113.02707 / 112.77322	113.12165 / 112.79664	112.92556 / 112.67060
O(10)=C(9)-C(11)	123.99698 / 125.00887	123.95400 / 124.97705	123.97874 / 124.98744	123.96900 / 124.97758	124.04234 / 125.03183
C(11)-C(12)-C(15)	120.11333 / 120.70956	120.12823 / 120.71591	120.14590 / 120.68941	120.11513 / 120.69286	120.09381 / 120.67225

Table continuation

Bond Angles (^{0})	Molecule 1 DFT / HF	Molecule 2 DFT / HF	Molecule 3 DFT / HF	Molecule 4 DFT / HF	Molecule 5 DFT / HF
C(11)-C(12)=C(17)	120.80145 / 120.46534	120.77136 / 120.46538	120.76011 / 120.48532	120.78723 / 120.48497	120.79365 / 120.49098
C(12)=C(17)-H(18)	119.58325 / 119.83456	119.57365 / 119.82820	119.57931 / 119.83749	119.57924 / 119.83444	119.60227 / 119.84954
H(24)-C(11)-C(12)	110.54616 / 110.49546	110.53736 / 110.49673	110.58156 / 110.50076	-	-
H(23)-C(11)-C(12)	109.85444 / 110.30918	109.88551 / 110.30744	109.82257 / 110.33337	109.85053 / 110.33409	109.84945 / 110.33356
C(12)=C(17)-C(16)	120.60550 / 120.76477	120.59195 / 120.76722	120.60424 / 120.76423	120.60457 / 120.76528	120.59117 / 120.75984
H(18)-C(17)-C(16)	119.81094 / 119.40046	119.83390 / 119.40439	119.81595 / 119.39815	119.81568 / 119.40015	119.80612 / 119.39049
C(17)-C(16)-H(19)	119.79467 / 119.78686	119.80222 / 119.78767	119.79459 / 119.79045	119.79564 / 119.78925	119.79472 / 119.79559
C(17)-C(16)=C(14)	120.05223 / 120.01650	120.05740 / 120.01731	120.05320 / 120.01637	120.05028 / 120.01759	120.05144 / 120.01212
C(16)=C(14)-H(22)	120.16083 / 120.23147	120.15890 / 120.23153	120.16367 / 120.22769	120.16269 / 120.22870	120.15672 / 120.22350
C(16)=C(14)-C(13)	119.66092 / 119.59057	119.66794 / 119.58860	119.65816 / 119.59138	119.65906 / 119.58987	119.66635 / 119.59777
C(14)-C(13)-H(21)	120.07682 / 120.04432	120.08252 / 120.04445	120.07632 / 120.04688	120.07179 / 120.04733	120.07575 / 120.04795
C(14)-C(13)=C(15)	120.28382 / 120.23409	120.27021 / 120.23505	120.28915 / 120.23103	120.29138 / 120.23142	120.28386 / 120.22914
C(13)=C(15)-H(20)	119.99873 / 119.74436	120.03393 / 119.74545	120.01165 / 119.74448	120.03926 / 119.74505	120.03707 / 119.74100
C(13)=C(15)-C(12)	120.31199 / 120.57274	120.31359 / 120.57503	120.30215 / 120.57479	120.29815 / 120.57678	120.29541 / 120.56723
H(21)-C(13)=C(15)	119.63924 / 119.72155	119.64710 / 119.72046	119.63440 / 119.72206	119.63673 / 119.72122	119.64029 / 119.72289
H(20)-C(15)-C(12)	119.68116 / 119.68153	119.64306 / 119.67814	119.67815 / 119.67945	119.65407 / 119.67689	119.65470 / 119.69054
H(7)-N(19)-C(2)	-	125.51958 / 125.78813	-	-	-
O(5)=C(2)-N(4)	-	127.68717 / 127.18339	127.62943 / 127.16283	126.67271 / 127.16680	127.65619 / 127.15181
C(2)-N(4)-N(6)	-	124.49850 / 124.96083	124.46635 / 124.96216	124.49208 / 124.93516	124.58774 / 125.03049
N(6)-N(4)-C(25)	-	126.25500 / 126.02905	126.33461 / 126.08436	126.29247 / 126.09151	126.25211 / 126.04678
C(25)-C(26)-H(28)	-	108.44966 / 108.19824	108.32520 / 107.90863	108.27469 / 107.85894	108.40364 / 108.02759
C(25)-C(26)-H(29)	-	108.45512 / 108.02851	113.79864 / 113.89156	-	-
C(26)-C(27)-H(31)	-	111.12290 / 111.15854	-	-	-
H(31)-C(27)-H(30)	-	108.49036 / 108.51343	-	-	-

Table continuation

Bond Angles (^{0})	Molecule 1	Molecule 2	Molecule 3	Molecule 4	Molecule 5
	DFT / HF	DFT / HF	DFT / HF	DFT / HF	DFT / HF
H(31)-C(27)-H(32)	-	107.57557 / 107.86320	-	-	-
H(29)-C(26)-C(27)	-	110.53421 / 110.64248	-	-	-
C(26)-C(27)-H(30)	-	109.94303 / 109.59954	-	-	-
C(26)-C(27)-H(32)	-	111.12634 / 111.11717	-	-	-
H(32)-C(27)-H(30)	-	108.48694 / 108.50503	-	-	-
C(13)-C(14)-H(22)	-	120.17290 / 120.17985	120.17795 / 120.18091	120.17804 / 120.18142	120.17671 / 120.17871
C(14)=C(16)-H(19)	-	120.14034 / 120.19491	120.15215 / 120.19309	120.15401 / 120.19307	120.15378 / 120.19219
C(17)=C(12)-C(15)	-	119.09577 / 118.81677	119.09033 / 118.82218	119.09401 / 118.81904	119.10927 / 118.83387
C(25)-C(26)-H(27)	-	-	108.27295 / 108.08503	-	-
H(28)-C(26)-C(29)	-	-	110.28981 / 110.39942	-	-
C(26)-C(29)-C(31)	-	-	120.57816 / 120.57232	120.86662 / 120.86084	120.74635 / 120.71445
C(26)-C(29)-C(30)	-	-	120.57162 / 120.53591	120.81562 / 120.85875	120.66345 / 120.66706
C(29)-C(31)-H(35)	-	-	119.61982 / 119.79019	119.66057 / 119.82719	119.82376 / 119.95904
C(29)-C(31)-C(34)	-	-	120.65440 / 120.64907	120.80140 / 120.85120	121.10752 / 121.06711
C(32)-C(30)-C(29)	-	-	120.66281 / 120.63927	120.81521 / 120.85249	121.12816 / 121.06035
H(33)-C(30)-C(29)	-	-	119.62982 / 119.77614	119.69431 / 119.84109	119.82199 / 119.94732
C(30)-C(29)-C(31)	-	-	118.85021 / 118.89041	118.31751 / 118.27806	118.58995 / 118.61800
C(31)-C(34)-H(38)	-	-	119.80029 / 119.78413	-	-
C(31)-C(34)-C(36)	-	-	120.09126 / 120.09425	-	-
H(38)-C(34)-C(36)	-	-	120.10834 / 120.12154	-	-
C(34)-C(36)-H(39)	-	-	120.16716 / 120.18540	-	-
C(34)-C(36)-C(32)	-	-	119.66277 / 119.62450	-	-
H(39)-C(36)-C(32)	-	-	120.16990 / 120.18997	-	-
C(36)-C(32)-H(37)	-	-	120.12235 / 120.12140	-	-

Table continuation

Bond Angles (^{0})	Molecule 1	Molecule 2	Molecule 3	Molecule 4	Molecule 5
	DFT / HF	DFT / HF	DFT / HF	DFT / HF	DFT / HF
C(36)-C(32)-C(30)	-	-	120.07852 / 120.10249	-	-
H(37)-C(32)-C(30)	-	-	119.79896 / 119.77602	-	-
C(32)-C(30)-H(33)	-	-	119.70736 / 119.58459	119.48996 / 119.30624	119.04984 / 118.99232
N(3)-N(1)-C(2)	-	-	-	114.47587 / 113.62284	114.45412 / 113.61732
H(27)-C(26)-C(29)	-	-	-	110.31199 / 110.40916	-
C(29)-C(26)-C(25)	-	-	-	113.92022 / 113.98235	113.62045 / 113.67489
H(35)-C(31)-C(34)	-	-	-	119.53796 / 119.32150	119.06866 / 118.97381
C(31)-C(34)-H(37)	-	-	-	119.40433 / 119.29469	120.78718 / 120.67751
H(37)-C(34)-C(38)	-	-	-	119.48461 / 119.63939	120.14655 / 120.16543
C(31)-C(34)-C(38)	-	-	-	121.11073 / 121.06563	119.06622 / 119.15702
C(34)-C(38)-C(32)	-	-	-	117.85812 / 117.88920	121.06720 / 120.93603
C(34)-C(38)-C(39)	-	-	-	120.95201 / 120.89916	119.45826 / 119.52603
C(39)-C(38)-C(32)	-	-	-	121.18188 / 121.20378	-
C(38)-C(39)-H(41)	-	-	-	111.43306 / 111.19182	-
H(40)-C(39)-C(38)	-	-	-	111.41971 / 111.22471	-
C(38)-C(32)-C(30)	-	-	-	121.09653 / 121.06302	119.04081 / 119.16149
C(38)-C(32)-H(36)	-	-	-	119.49359 / 119.68378	120.15811 / 120.17011
H(41)-C(39)-H(42)	-	-	-	107.30979 / 107.68553	-
H(42)-C(39)-H(40)	-	-	-	107.46650 / 107.75764	-
H(36)-C(32)-C(30)	-	-	-	119.40941 / 119.25285	120.80098 / 120.66833
CI(39)-C(38)-C(32)	-	-	-	-	119.47434 / 119.53777

Table 2 – The calculated bond lenghts (A0) of all molecules as DFT (B3LYP) and HF (B3LYP) methods on the basis set of 6-311G (d,p).

Bond Lenghts (A⁰)	Molecule 1	Molecule 2	Molecule 3	Molecule 4	Molecule 5
	DFT / HF	DFT / HF	DFT / HF	DFT / HF	DFT / HF
N(1)-H(7)	1.00581 / 0.99044	1.00576 / 0.99039	1.00586 / 0.99046	1.00582 / 0.99043	1.00597 / 0.99058
N(1)-N(3)	1.38360 / 1.37314	1.38340 / 1.37294	1.38302 / 1.37226	1.38325 / 1.37249	1.38247 / 1.37175
N(3)=C(25)	1.29459 / 1.26497	1.29446 / 1.26525	1.29349 / 1.26403	1.29345 / 1.26412	1.29343 / 1.26394
C(25)-C(26)	1.48540 / 1.48752	1.49287 / 1.49410	1.49834 / 1.49862	1.49850 / 1.49882	1.49847 / 1.49859
C(26)-H(28)	1.08908 / 1.08062	1.09593 / 1.08637	1.09509 / 1.08515	1.09504 / 1.08521	1.09479 / 1.08496
C(26)-H(27)	1.09304 / 1.08408	-	1.09558 / 1.08536	1.09587 / 1.08553	1.09561 / 1.08524
C(26)-C(27)	-	1.52977 / 1.52560	-	-	-
C(27)-H(30)	-	1.09173 / 1.08450	-	-	-
C(27)-H(31)	-	1.09124 / 1.08352	-	-	-
C(27)-H(32)	-	1.09124 / 1.08342	-	-	-
C(26)-H(29)	1.09315 / 1.08425	1.09594 / 1.08623	-	-	-
C(25)-N(4)	1.39016 / 1.38192	1.39131 / 1.38321	1.39185 / 1.38423	1.39219 / 1.38452	1.39088 / 1.38324
N(4)-C(2)	1.41673 / 1.38767	1.41643 / 1.38722	1.41641 / 1.38716	1.41647 / 1.38702	1.41728 / 1.38768
C(2)=O(5)	1.21146 / 1.19112	1.21156 / 1.19129	1.21164 / 1.19130	1.21179 / 1.19145	1.21112 / 1.19076
C(2)-N(1)	1.36895 / 1.34799	1.36904 / 1.34665	1.36885 / 1.34656	1.36869 / 1.34641	1.36927 / 1.34709
N(4)-N(6)	1.37300 / 1.36147	1.37277 / 1.36144	1.37316 / 1.36172	1.37305 / 1.36168	1.37354 / 1.36196
N(6)-H(8)	1.01460 / 0.99815	1.01446 / 0.99810	1.01469 / 0.99823	1.01460 / 0.99821	1.01478 / 0.99835
N(6)-C(9)	1.40482 / 1.39490	1.40384 / 1.39432	1.40516 / 1.39519	1.40460 / 1.39488	1.40635 / 1.39633
C(9)=O(10)	1.20647 / 1.18229	1.20675 / 1.18245	1.20642 / 1.18222	1.20656 / 1.18231	1.20608 / 1.18186
C(9)-C(11)	1.52568 / 1.51818	1.52565 / 1.51823	1.52566 / 1.51820	1.52568 / 1.51822	1.52546 / 1.51810
C(11)-H(24)	1.08979 / 1.08622	1.08962 / 1.08622	1.08985 / 1.08612	1.08983 / 1.08612	1.08989 / 1.08611
C(11)-H(23)	1.09538 / 1.08341	1.09536 / 1.08337	1.09537 / 1.08346	1.09532 / 1.08343	1.09537 / 1.08356
C(11)-C(12)	1.51419 / 1.51016	1.51420 / 1.51016	1.51440 / 1.51012	1.51430 / 1.51011	1.51434 / 1.51014
C(12)-C(15)	1.39873 / 1.38916	1.39860 / 1.38916	1.39876 / 1.38902	1.39876 / 1.38905	1.39870 / 1.38896
C(15)-H(20)	1.08505 / 1.07538	1.08503 / 1.07537	1.08508 / 1.07542	1.08509 / 1.07542	1.08509 / 1.07544
C(15)=C(13)	1.39226 / 1.38193	1.39237 / 1.38195	1.39226 / 1.38204	1.39221 / 1.38204	1.39218 / 1.38207
C(13)-H(21)	1.08435 / 1.07542	1.08435 / 1.07542	1.08436 / 1.07541	1.08436 / 1.07542	1.08432 / 1.07539

Table continuation

Bond Lenghts (A⁰)	Molecule 1 DFT / HF	Molecule 2 DFT / HF	Molecule 3 DFT / HF	Molecule 4 DFT / HF	Molecule 5 DFT / HF
C(13)-C(14)	1.39374 / 1.38637	1.39368 / 1.38636	1.39381 / 1.38627	1.39386 / 1.38627	1.39386 / 1.38623
C(14)-H(22)	1.08429 / 1.07538	1.08430 / 1.07539	1.08428 / 1.07538	1.08429 / 1.07538	1.08426 / 1.07535
C(14)=C(16)	1.39252 / 1.38211	1.39267 / 1.38213	1.39250 / 1.38222	1.39247 / 1.38221	1.39245 / 1.38225
C(16)-H(19)	1.08435 / 1.07552	1.08436 / 1.07553	1.08435 / 1.07552	1.08436 / 1.07552	1.08433 / 1.07549
C(16)-C(17)	1.39311 / 1.38634	1.39293 / 1.38633	1.39309 / 1.38622	1.39312 / 1.38624	1.39313 / 1.38617
C(17)-H(18)	1.08479 / 1.07668	1.08472 / 1.07668	-	1.08481 / 1.07670	1.08482 / 1.07673
C(17)=C(12)	1.39569 / 1.38578	1.39578 / 1.38581	-	1.39564 / 1.38585	1.39559 / 1.38584
C(26)-C(29)	-	-	1.51333 / 1.51237	1.51274 / 1.51178	1.51261 / 1.51185
C(29)-C(31)	-	-	1.39664 / 1.38704	1.39629 / 1.38686	1.39607 / 1.38635
C(31)-H(35)	-	-	1.08514 / 1.07633	1.08526 / 1.07656	1.08464 / 1.07579
C(31)-C(34)	-	-	1.39216 / 1.38398	1.39059 / 1.38231	1.39137 / 1.38305
C(34)-H(38)	-	-	1.08417 / 1.07537	-	-
C(34)-C(36)	-	-	1.39321 / 1.38434	-	-
C(36)-H(39)	-	-	1.08407 / 1.07527	-	-
C(36)-C(32)	-	-	1.39283 / 1.38417	-	-
C(32)-C(37)	-	-	1.08419 / 1.07536	-	-
C(32)-C(30)	-	-	1.39263 / 1.38418	1.39216 / 1.38447	1.39173 / 1.38334
C(30)-H(33)	-	-	1.08522 / 1.07626	1.08537 / 1.07648	1.08475 / 1.07574
C(30)-C(29)	-	-	1.39627 / 1.38687	1.39489 / 1.38482	1.39587 / 1.38612
C(32)-H(36)	-	-	-	1.08528 / 1.07624	1.08223 / 1.07324
C(32)-C(38)	-	-	-	1.39719 / 1.38735	1.38995 / 1.38028
C(38)-C(39)	-	-	-	1.50963 / 1.51034	-
C(39)-H(40)	-	-	-	1.09212 / 1.08418	-
C(39)-H(41)	-	-	-	1.09278 / 1.08473	-
C(39)-H(42)	-	-	-	1.09548 / 1.08702	-
C(38)-C(34)	-	-	-	1.39884 / 1.38946	1.39027 / 1.38054
C(34)-H(37)	-	-	-	1.08542 / 1.07644	1.08222 / 1.07324
C(38)-Cl(39)	-	-	-		1.75963 / 1.74441

Quantifying the distribution of electronic charge among the atoms in a molecule is the Mulliken atomic charge, which is a notion from quantum chemistry. This technique uses a quantum mechanical computation to take into account the overlap of atomic orbitals and their contributions to molecular orbitals in order to estimate the charge distribution on individual atoms within a molecule. The estimation of charge distributions inside molecules and comprehension of their chemical activity have traditionally been accomplished using mulliken atomic charges. Mulliken atomic charge values of the studied molecules in this article are given in Table 3. When the Mulliken atomic charge

values given in Table 3 were examined, it was determined that the highest value was calculated as 0.6880 in the C2 atom of the 2nd molecule according to the HF model, and the lowest value was calculated as -0.5025 in the O2 atom of the 4th molecule according to the HF model.

In quantum chemistry, the words HOMO and LUMO are used to characterize particular energy levels inside the electronic structure of molecules. They are essential for comprehending the electrical, bonding, and reactivity characteristics of molecules. The HOMO (Highest Occupied Molecular Orbital) is the highest energy molecular orbital that contains electrons.

Table 3 – Mulliken atomic charge values of the studied molecules according to DFT (B3LYP) and HF (B3LYP) methods on the basis set of 6-311G (d,p).

Molecule														
1			2			3			4			5		
Atom	DFT	HF	Atom	DFT	HF	Atom	DFT	HF	Atom	DFT	HF	Atom	DFT	HF
N1	-0.3023	-0.3683	N1	-0.3017	-0.3699	N1	-0.3026	-0.3695	N1	-0.3025	-0.3695	N1	-0.3022	-0.3694
C2	0.4984	0.6875	C2	0.4983	0.6880	C2	0.4990	0.6870	C2	0.4989	0.6868	C2	0.4999	0.6877
N3	-0.2158	-0.2762	N3	-0.2255	-0.2835	N3	-0.2046	-0.2597	N3	-0.2049	-0.2601	N3	-0.2052	-0.2599
N4	-0.3813	-0.4743	N4	-0.3909	-0.4859	N4	-0.3907	-0.4850	N4	-0.3906	-0.4850	N4	-0.3909	-0.4853
O5	-0.3674	-0.5011	O5	-0.3679	-0.2018	O5	-0.3682	-0.5018	O5	-0.3688	-0.5025	O5	-0.3658	-0.4993
N6	-0.2699	-0.3299	N6	-0.2689	-0.3286	N6	-0.2681	-0.3294	N6	-0.2682	-0.3291	N6	-0.2699	-0.3307
H7	0.2546	0.2639	H7	0.2541	0.2634	H7	0.2550	0.2645	H7	0.2545	0.2640	H7	0.2564	0.2659
H8	0.2478	0.2572	H8	0.2476	0.2568	H8	0.2475	0.2570	H8	0.2474	0.2568	H8	0.2481	0.2576
C9	0.3869	0.5478	C9	0.3885	0.5480	C9	0.3867	0.5477	C9	0.3867	0.5478	C9	0.3862	0.5472
O10	-0.3223	-0.4268	O10	-0.3236	-0.4276	O10	-0.3220	-0.4263	O10	-0.3226	-0.4269	O10	-0.3201	-0.4243
C11	-0.2739	-0.2544	C11	-0.2749	-0.2548	C11	-0.2747	-0.2547	C11	-0.2739	-0.2546	C11	-0.2738	-0.2546
C12	-0.0931	-0.0648	C12	-0.0937	-0.0651	C12	-0.0934	-0.0642	C12	-0.0938	-0.0643	C12	-0.0933	-0.0638
C13	-0.0994	-0.0806	C13	-0.0992	-0.0807	C13	-0.0995	-0.0803	C13	-0.0998	-0.0804	C13	-0.0995	-0.0800
C14	-0.0851	-0.1035	C14	-0.0854	-0.1036	C14	-0.0851	-0.1035	C14	-0.0851	-0.1036	C14	-0.0847	-0.1031
C15	-0.0486	-0.0692	C15	-0.0482	-0.0692	C15	-0.0484	-0.0701	C15	-0.0487	-0.0700	C15	-0.0492	-0.0705
C16	-0.0941	-0.0776	C16	-0.0941	-0.0777	C16	-0.0939	-0.0776	C16	-0.0939	-0.0776	C16	-0.0933	-0.0773
C17	-0.0555	-0.0909	C17	-0.0542	-0.0909	C17	-0.0558	-0.0906	C17	-0.0561	-0.0906	C17	-0.0564	-0.0905
H18	0.0799	0.0808	H18	0.0800	0.0809	H18	0.0800	0.0803	H18	0.0799	0.0805	H18	0.0801	0.0794
H19	0.0921	0.0966	H19	0.0921	0.0964	H19	0.0921	0.0967	H19	0.0919	0.0966	H19	0.0927	0.0972
H20	0.1155	0.0943	H20	0.1142	0.0943	H20	0.1162	0.0943	H20	0.1169	0.0943	H20	0.1169	0.0946
H21	0.1155	0.0999	H21	0.0936	0.0999	H21	0.0938	0.1000	H21	0.0937	0.0999	H21	0.0944	0.1006
H22	0.0926	0.0979	H22	0.0936	0.0977	H22	0.0926	0.0979	H22	0.0924	0.0978	H22	0.0932	0.0986
H23	0.1479	0.1333	H23	0.1333	0.1335	H23	0.1475	0.1321	H23	0.1472	0.1324	H23	0.1473	0.1309
H24	0.1435	0.1737	H24	0.1483	0.1736	H24	0.1433	0.1739	H24	0.1435	0.1738	H24	0.1431	0.1743
C25	0.3002	0.3919	C25	0.3566	0.4637	C25	0.3656	0.4743	C25	0.3656	0.4748	C25	0.3655	0.4742
C26	-0.2515	-0.1837	C26	-0.2156	-0.1929	C26	-0.1944	-0.1448	C26	-0.1949	-0.1475	C26	-0.1916	-0.1421

Molecule														
1			2			3			4			5		
Atom	DFT	HF	Atom	DFT	HF	Atom	DFT	HF	Atom	DFT	HF	Atom	DFT	HF
H27	0.1318	0.1228	C27	-0.2863	-0.2215	H27	0.1458	0.1399	H27	0.1453	0.1393	H27	0.1479	0.1424
H28	0.1318	0.1354	H28	0.1346	0.1204	H28	0.1418	0.1423	H28	0.1405	0.1412	H28	0.1438	0.1446
H29	0.1334	0.1183	H29	0.1324	0.1241	C29	-0.0936	-0.0913	C29	-0.0882	-0.1017	C29	-0.0936	-0.1003
			H30	0.1120	0.0980	C30	-0.0528	-0.0781	C30	-0.0549	-0.0581	C30	-0.0510	-0.0629
			H31	0.1213	0.1067	C31	-0.0479	-0.0776	C31	-0.0468	-0.0565	C31	-0.0449	-0.0617
			H32	0.1214	0.1081	C32	-0.0907	-0.0771	C32	-0.0706	-0.0833	C32	0.0259	0.0275
						H33	0.0839	0.0863	H33	0.0813	0.0843	H33	0.0925	0.0954
						C34	-0.0909	-0.0776	C34	-0.0743	-0.0879	C34	0.0254	0.0268
						H35	0.0836	0.0848	H35	0.0809	0.0829	H35	0.0921	0.0954
						C36	-0.0872	-0.1026	H36	0.0852	0.0889	H36	0.1203	0.1274
						H37	0.0964	0.1009	H37	0.0855	0.0889	H37	0.1204	0.1273
						H38	0.0966	0.1008	C38	-0.0967	-0.1208	C38	-0.2369	-0.2186
						H39	0.0970	0.1008	H40	0.1109	0.0972	CI39	-0.0691	-0.0994
									H41	0.1158	0.1078			
									H42	0.1289	0.1152			

In other words, it's the orbital where the last electron is placed when building up the electron configuration of a molecule. The HOMO is important because it determines how a molecule can interact with other molecules or undergo chemical reactions. Electrons in the HOMO are more readily available for participating in chemical reactions, such as bond formation or electron transfer.

The LUMO (Lowest Unoccupied Molecular Orbital) is the lowest energy molecular orbital that is devoid of electrons. It stands for the level of energy that is available after the HOMO. Because it shows the energy needed to remove an electron from a molecule or the energy obtained when an electron is supplied to the molecule, the LUMO is important. It is more likely for molecules with accessible, low-energy LUMOs to take electrons or engage in electron transfer reactions. When the HOMO and LUMO values given in Figure 2-6 were examined, it was determined that the highest HOMO value was calculated as EHOMO = 0.12572 in the 1st molecule according to the HF method, and the lowest value was calculated as EHOMO = -0.33409 in the 5th molecule according to the HF method. In LUMO values, it was determined that the highest value was calculated as ELUMO = 0.11845 in the 4th molecule according to the HF method, and the lowest value was calculated as ELUMO = -0.33166 in the 1st molecule according to the HF method. The HOMO-LUMO gap, or the energy difference between the HOMO and LUMO, is crucial in determining a molecule's optical and electrical properties.
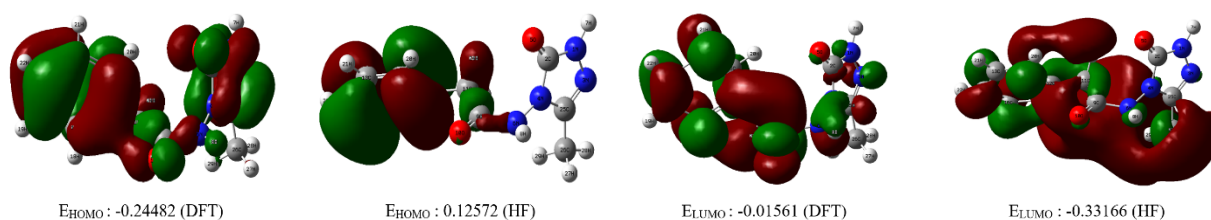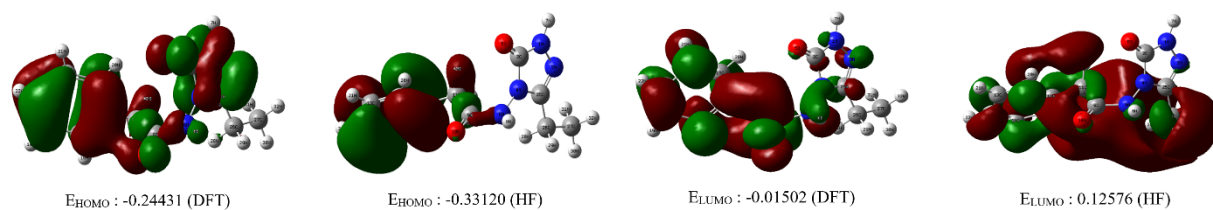

E$_{HOMO}$: -0.24482 (DFT)   E$_{HOMO}$: 0.12572 (HF)   E$_{LUMO}$: -0.01561 (DFT)   E$_{LUMO}$: -0.33166 (HF)

Figure 2 – The calculated HOMO-LUMO energies of molecule 1 according to DFT/B3LYP/6-311G (d,p) and HF/6-311G (d,p) levels

E_{HOMO} : -0.24431 (DFT) E_{HOMO} : -0.33120 (HF) E_{LUMO} : -0.01502 (DFT) E_{LUMO} : 0.12576 (HF)

Figure 3 – The calculated HOMO-LUMO energies of molecule 2 according to
FT/B3LYP/6-311G (d,p) and HF/6-311G (d,p) levels

E_{HOMO} : -0.24446 (DFT) E_{HOMO} : -0.33171 (HF) E_{LUMO} : -0.02153 (DFT) E_{LUMO} : 0.11643 (HF)
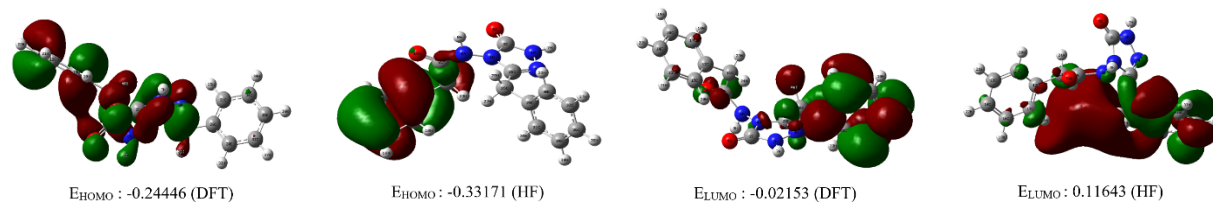
Figure 4 – The calculated HOMO-LUMO energies of molecule 3 according to
DFT/B3LYP/6-311G (d,p) and HF/6-311G (d,p) levels

E_{HOMO} : -0.24361 (DFT) E_{HOMO} : -0.32992 (HF) E_{LUMO} : -0.01919 (DFT) E_{LUMO} : 0.11845 (HF)
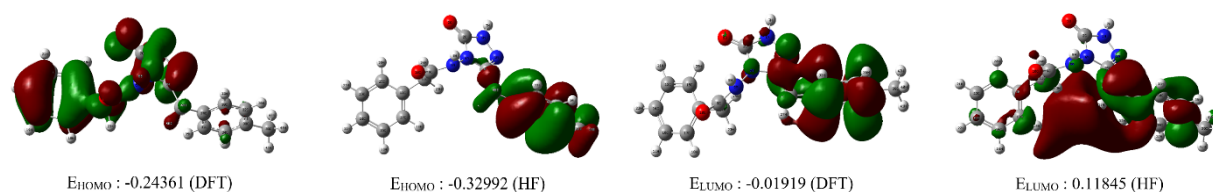
Figure 5 – The calculated HOMO-LUMO energies of molecule 4 according to
DFT/B3LYP/6-311G (d,p) and HF/6-311G (d,p) levels

E_{HOMO} : -0.24726 (DFT) E_{HOMO} : -0.33409 (HF) E_{LUMO} : -0.03456 (DFT) E_{LUMO} : 0.10618 (HF)
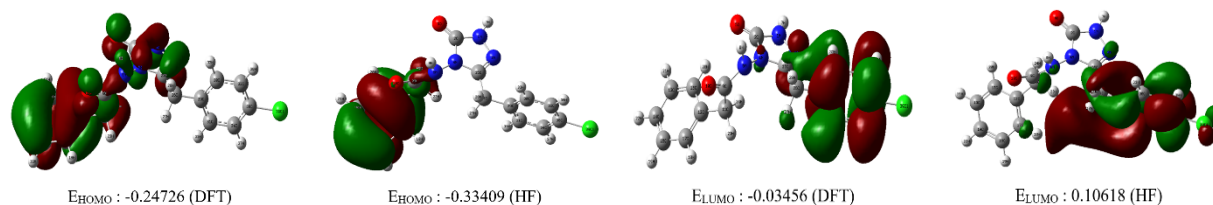
Figure 6 – The calculated HOMO-LUMO energies of molecule 5 according to
DFT/B3LYP/6-311G (d,p) and HF/6-311G (d,p) levels

Chemistry uses the phrases "dipole moment" and "total energy" to define crucial aspects of molecules, notably in relation to molecular structure, polarity, and stability. Due to variations in atom electronegativity, a dipole moment is a measurement of the separation of positive and negative charges within a molecule. In other words, it measures the level of polarity or charge imbalance within a molecule. An electron dipole molecule has a positive end (where there are fewer electrons) and a negative end (where there are more electrons). It is possible to visualize the dipole moment as a vector quantity with magnitude and direction. The highest dipole moment was calculated as μTotal = 4.6286 debye in the 4th molecule according to the HF technique, and the lowest dipole moment was calculated as μTotal = 1.9017 debye in the 5th molecule according to the HF method, according to the data presented in Table 4.

Table 4 – Dipole moment (debye) and total energy (a.u.) values

Molecule	Property		DFT	HF
1	Dipole Moment	μ_x	2.9971	-1.8265
		μ_y	-0.7008	3.2453
		μ_z	-2.1778	-1.0955
		μ_{Total}	3.7705	3.8818
	Total Energy		-796.04737247	-791.24048825
2	Dipole Moment	μ_x	3.3650	-2.3642
		μ_y	-0.7446	3.1523
		μ_z	-1.9495	-1.1001
		μ_{Total}	3.9596	4.0911
	Total Energy		-835.37126756	-830.28438620
3	Dipole Moment	μ_x	3.7860	3.5073
		μ_y	-0.7885	-2.1527
		μ_z	-1.2606	-0.8062
		μ_{Total}	4.0675	4.1935
	Total Energy		-1027.14715452	-1020.82813853
4	Dipole Moment	μ_x	4.2768	4.0775
		μ_y	-0.8039	-2.0416
		μ_z	-1.2495	-0.7937
		μ_{Total}	4.5275	4.6286
	Total Energy		-1066.47482216	-1059.87421405
5	Dipole Moment	μ_x	1.7914	1.5602
		μ_y	-0.5104	-1.0774
		μ_z	-0.4160	-0.1468
		μ_{Total}	1.9086	1.9017
	Total Energy		-1486.76855799	-1479.74965931

The sum of all the energy contributions made by a molecule's different parts, such as the electronic energy (energy of electrons), nuclear repulsion energy (caused by the positive charges of the atomic nuclei repelling one another), and other potential and kinetic energy terms, makes up the total energy of the molecule. A crucial characteristic that governs a molecule's stability and behavior is its total energy. The total energy of a molecule can be determined in quantum mechanics using techniques like the Hartree-Fock theory, density functional theory (DFT), or more sophisticated ab initio techniques. The stability of various molecular conformations, the strength of chemical bonds, and the energy changes brought on by chemical reactions are all factors that can be understood by energy calculations. When the total energy values are examined in the same Table 4, it is appears to be calculated the highest total energy is -791.24048825 a.u. in the 1st molecule according to the HF method and, the lowest total energy is -1486.76855799 a.u. in the 5th molecule according to the DFT method. All dipole moment and total energy values for studied compounds according to DFT/B3LYP/6-311G (d,p) and HF/6-311G (d,p) levels were given in Table 4. The graphical submission of these values is given on Figures 7-8.
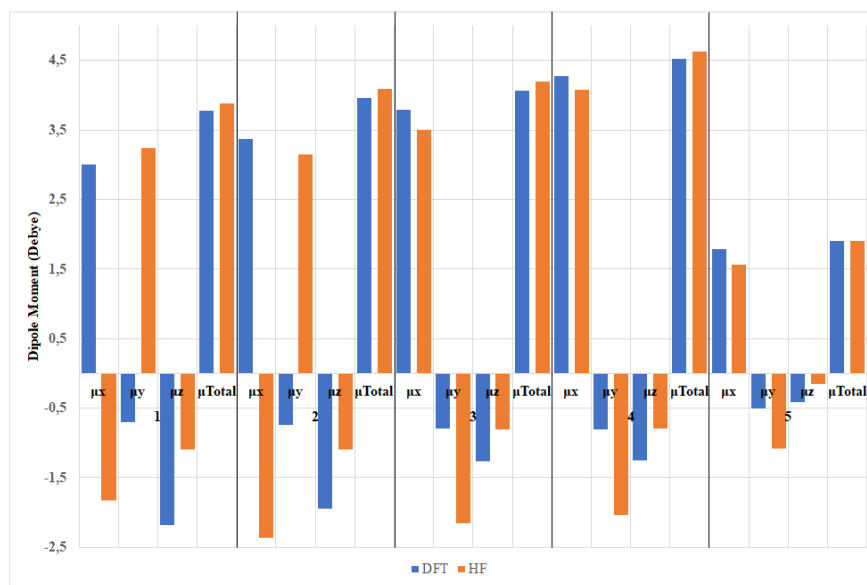
Figure 7 – Graphical submission of dipole moment values of studied molecules
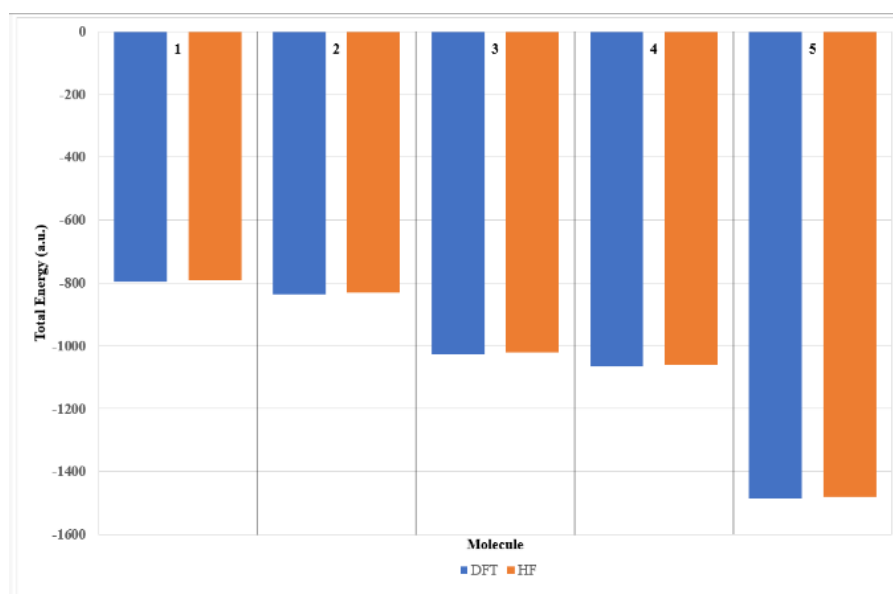

Figure 8 – Graphical submission of total energy values of studied molecules

IR spectrum analysis is the process of studying and analyzing the interaction between matter and infrared light using infrared (IR) spectroscopy. In order to recognize and describe the functional groups, chemical bonds, and molecular structures contained in a sample, IR spectroscopy is a technique that is frequently employed in chemistry, physics, and numerous other scientific disciplines. Longer wavelengths than visible light allow infrared light to interact with molecules' vibrational states. Every molecule contains unique vibrational frequencies, such as ν: stretching vibration, δ: bending vibration, γ: out-of plane bending vibration, τ: torsion vibration, connected to the motion of its atoms. It has been determined that the spectra obtained from these values and given in Figure 5-14 are compatible with each other with "vibration types and IR frequencies (cm^{-1})" values of molecules calculated according to DFT and HF methods and given in Table 5-9. The IR spectrum obtained from these values is also given on Figures 9-18.

Table 5 – Vibration types and IR frequencies (cm^{-1}) of molecule 1

Seq.	Vibration Types	DFT	HF
1	τ CCCC(46), τ CCNN(21), τ NCCC(12)	30	16
2	τ CCCC(33), τ CNNC(31)	34	32
3	τ NNCC(31), τ CCCC(15), τ NNC(13), τ NCCC(12)	42	54
4	τ NNCC(15), τ CNNC(30), δ NNC(10)	61	74
5	τ NCNN(62)	75	85
6	τ NNCC(12), ɣ CCCC(16), ɣ CNNC(19), δ CCC(19)	102	105
7	ɣ CCCC(12), ɣ CNNC(10), τ NNCC(12), τ HCCN(11)	133	140
8	τ HCCN(17), τ NCCC(23)	148	165
9	δ NCC(11), δ CCC(10), δ NNC(12)	243	249
10	δ NCC(15), δ CCC(23), τ CCCC(17)	249	274
11	δ CCN(45)	267	288
12	ɣ CCCC(19), ɣ CNNC(17), τ NNCN(14)	307	325
13	δ CNN(30)	312	354
14	δ OCN(14)	321	362
15	δ CCC(20), δ CCC(31)	343	452
16	τ HCCC(12), τ CCCC(42)	417	480
17	δ OCN(11), ν NC(12), ν NN(12)	441	492
18	δ OCN(10), τ HNNC(28)	467	503
19	τ HNNC(40)	471	537
20	τ CCCC(18)	496	579
21	ɣ ONNC(11), ɣ OCNC(15), τ HNNC(14)	534	643
22	τ HNNC(13), δ OCN(12), δ CCC(19)	583	667
23	δ CNN(18), δ CCN(12), δ OCN(14)	596	679
24	δ CCC(49)	637	707
25	ν CC(13), ν NN(12), δ CNN(11), δ OCN(11)	645	715
26	τ NNCN(42)	665	745
27	ɣ ONNC(13), ɣ OCNC(10), τ CCCC(12)	700	771
28	τ HCCC(10), τ CCCC(11), τ HCCC(28)	717	815
29	τ HCCC(46), ν CC(12)	750	868
30	ɣ ONNC(41), ɣ OCNC(39)	758	870
31	δ CNN(20), δ NNC(22)	804	893
32	ν CC(14)	830	921
33	τ HCCC(59)	860	946
34	δ NCN(11), ν NC(16)	900	993
35	τ HCCC(14), τ HCCN(10), τ HCCC(26), τ HCCN(10)	935	1021
36	τ HCCN(12), τ HCCC(16)	950	1046
37	τ HCCC(22), τ CCCC(18), τ HCCC(10)	983	1085
38	δ NNC(23), τ HCCN(16)	993	1087
39	τ HCCC(12), τ CCCC(18), τ HCCC(53)	1005	1095
40	δ CCC(56), ν CC(33)	1019	1115
41	δ HCC(18), δ CCC(10), ν CC(23)	1054	1121
42	δ CNN(10), ν NC(13), ν NN(35)	1057	1163

Table continuation

Seq.	Vibration Types	DFT	HF
42	τ HCCN(16), τ HCCN(25), δ HCH(10)	1067	1169
43	ν NN(27)	1100	1171
44	δ HCC(14), ν CC(25), ν CC(17), δ HCC(11)	1106	1191
45	δ HCC(33)	1174	1199
46	ν CC(12), δ HCC(65)	1183	1215
47	δ HCC(36), δ HCC(13), ν CC(10)	1209	1250
48	ν CC(13)	1218	1290
49	δ OCN(14), ν NC(18)	1233	1294
50	ν NN(17)	1238	1308
51	δ HCC(20), ν CC(13), ν NC(10)	1250	1334
52	δ NCN(19)	1328	1358
53	δ HCC(10), ν CC(27), ν CC(11), ν CC(16)	1339	1371
54	τ HCCN(25)	1359	1460
55	δ HCC(51), δ HCC(25)	1368	1471
56	δ HCH(11), δ HNN(65)	1397	1519
57	ν NN(12), δ HCH(51)	1422	1538
58	ν NC(19), ν NN(19), δ HNC(13)	1450	1559
59	δ HCH(29), δ HNC(42)	1467	1590
60	δ HNC(14), δ HCH(35)	1474	1591
61	τ HCCN(13), δ HCH(45)	1476	1593
62	δ HCC(21), ν CC(12)	1488	1604
63	δ HCH(29)	1491	1629
64	δ HCC(31), δ HCC(18), δ CCC(10)	1532	1639
65	δ CCC(12), ν CC(40)	1630	1656
66	δ HCC(12), ν CC(20)	1649	1772
67	ν NC(67)	1656	1798
68	ν OC(59)	1805	1873
69	ν NC(10), ν OC(54)	1834	1982
70	ν CH(14), ν CH(41)	3042	2001
71	ν CH(52), ν CH(25)	3043	3191
72	ν CH(49), ν CH(13)	3094	3198
73	ν CH(39)	3112	3244
74	ν CH(36)	3144	3250
75	ν CH(93)	3158	3293
76	ν CH(63), ν CH(27)	3164	3310
77	ν CH(44), ν CH(39)	3172	3320
78	ν CH(52), ν CH(22)	3180	3331
79	ν CH(85)	3189	3341
80	ν NH(50)	3538	3351
81	ν NH(50)	3682	3800
Note: *ν: stretching vibration, δ: bending vibration, γ: out-of plane bending vibration, τ: torsion vibration*			

Figure 9 – Theoretical IR spectrums according to DFT/B3LYP/6-311G (d,p) level for molecule 1
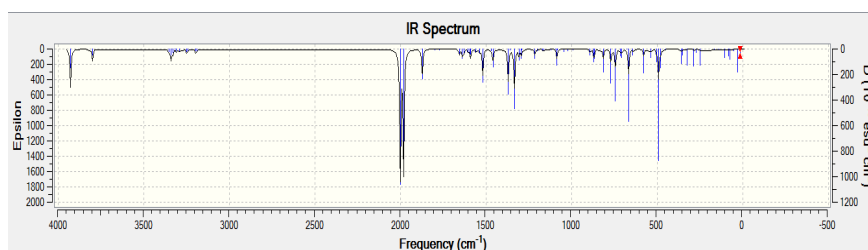
Figure 10 – Theoretical IR spectrums according to HF/B3LYP/6-311G (d,p) level for molecule 1.

Table 6 – Vibration types and IR frequencies (cm^{-1}) of molecule 2

Seq.	Vibration Types	DFT	HF
1	τ CCCC(70)	16	16
2	τ CCCC(18), τ CNNC(21), τ NCCC(29)	27	27
3	τ CNNC(55), τ CCCN(13)	32	48
4	τ NCNN(12), τ CNNC(15), τ CCCN(32), τ NNCC(38)	57	66
5	τ NCNN(54)	80	76
6	δ CCC(17), ɣ CCCC(14), ɣ CNNC(21), τ NNCC(12)	101	79
7	τ CNNC(13), τ NCCN(17), τ NNCN(11), ɣ CCCC(16), ɣ CNNC(12)	131	105
8	δ CCN(52), δ CCC(25)	176	134
9	τ HCCC(9)	214	192
10	δ CCC(11), τ CCCC(20)	248	232
11	τ CNNC(15), δ NCC(24), δ CCC(12)	255	257
12	δ CNN(17), δ CCC(12)	302	275
13	τ NNCN(13), ɣ CCCC(11)	310	325
14	δ CCC(19), δ CCC(11), δ OCN(10)	338	334
15	δ NCC(11), δ CCC(14), δ CCC(10), δ OCN(11)	345	358
16	τ CCCC(42), τ HCCC(13)	415	375
17	δ OCN(11), τ HNNC(27), δ OCN(14), ν NN(10)	467	452
18	τ NNCN(10), τ HNNC(42)	470	483
19	τ CCCC(17)	496	492
20	ɣ ONNC(14), ɣ OCNC(10), τ HNNC(16)	533	536
21	δ CCC(22), τ HNNC(10), τ HNCC(15)	582	578
22	δ CCC(24), δ CCC(49)	637	653
23	τ NNCN(42), τ CCCN(11)	657	679

Table continuation

Seq.	Vibration Types	DFT	HF
24	δ CCN(15), δ CCC(16), ν CC(10)	672	708
25	ɣ ONNC(10), ɣ OCNC(13)	698	718
26	τ CCCC(11;36), τ HCCC(29), τ HCCC(10)	716	741
27	ν CC(13), τ HCCC(45)	750	771
28	ɣ ONNC(40), ɣ OCNC(40)	757	815
29	δ CNN(11;31), δ NNC(13)	797	859
30	τ HCCN(17;16), τ HCCN(16;15;14)	803	863
31	ν CC(16;11)	832	876
32	τ HCCC(16)	855	896
33	τ HCCC(50), τ HCCC(22)	858	921
34	δ NCN(12), ɣ NC(16)	904	946
35	τ HCCC(28), τ HCCC(15)	935	996
36	τ HCCC(14), τ HCCC(10;11), δ NNC(19), ν CC(49)	949	1021
37	τ CCCC(18), τ HCCC(10;23), τ HCCC(23), τ HCCC(17)	981	1041
38	τ CCCC(17), τ HCCC(53), τ HCCC(12)	1004	1047
39	δ CCC(57), ν CC(33)	1019	1085
40	δ NNC(20), δ CCC(13)	1039	1095
41	δ CCC(10), δ HCC(13), ν CC(13;24)	1053	1115
42	ν NN(42), ν CC(17)	1073	1121
42	δ HCC(28), ν CC(25), ν CC(16)	1106	1135
43	τ HCCC(14), ν NN(18), ν CC(15), δ HCH(10)	1111	1169
44	τ HCCN(18), τ HCCC(21), δ HCH(12)	1115	1175
45	δ HCC(18;17)	1174	1199
46	δ HCC(15;12), δ HCC(44), ν CC(13)	1183	1211
47	δ HCC(40), δ HCC(15)	1208	1218
48	ν CC(35)	1219	1290
49	ν NC(19;20), ν NN(10), δ OCN(14)	1231	1294
50	ν NC(10), ν CC(12), δ HCC(10;14)	1251	1309
51	δ HCC(28;24)	1288	1335
52	δ CNN(11), δ NCN(13)	1292	1358
53	ν CC(11;27), ν CC(16)	1339	1368
54	τ HCCN(19;30)	1357	1395
55	δ HCC(15;16), δ HCC(24)	1367	1416
56	τ HCCN(28), δ HNC(17), ν NN(10)	1378	1471
57	δ HNC(55), ν NN(11)	1403	1513
58	δ HCH(95)	1422	1521
59	ν NC(18), ν NN(20), δ HNC(19)	1454	1545
60	δ HNC(33), δ HCH(39)	1470	1556
61	δ HCH(44;16), δ HNC(20)	1476	1591
62	δ HCH(31;24)	1480	1597
63	ν CC(13), δ HCC(41)	1488	1604
64	τ HCCC(12;11), δ HCH(75)	1496	1611
65	τ HCCC(10), δ HCH(63)	1509	1617

Seq.	Vibration Types	DFT	HF
66	δ CCC(10), δ HCC(38), δ HCC(18)	1532	1630
67	δ CCC(12), ν CC(39;11), δ HCC(11)	1629	1638
68	ν NC(48)	1648	1656
69	ν CC(12;14), ν NC(20)	1649	1772
70	ν OC(27)	1804	1798
71	ν OC(59)	1805	1865
72	ν OC(21;53)	1834	1981
73	ν CH(51;49	3025	2000
74	ν CH(38;15;40)	3043	3181
75	ν CH(44;52)	3046	3186
76	ν CH(96)	3048	3198
77	ν CH(11;39)	3114	3210
78	ν CH(45;50)	3115	3244
79	ν CH(51;46)	3119	3249
80	ν CH(11;39)	3144	3260
81	ν CH(93)	3158	3310
82	ν CH(63), ν CH(28)	3164	3320
83	ν CH(43;18), ν CH(38)	3172	3331
84	ν CH(52;15), ν CH(22)	3179	3341
85	ν CH(85)	3189	3351
86	ν NH(50)	3540	3800
87	ν NH(50)	3681	3929

Note: *ν: stretching vibration, δ: bending vibration, γ: out-of plane bending vibration, τ: torsion vibration*

Figure 11 – Theoretical IR spectrums according to DFT/B3LYP/6-311G (d,p) level for molecule 2
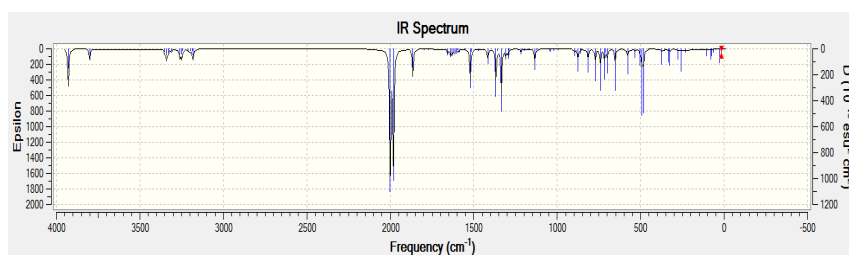
Figure 12 – Theoretical IR spectrums according to HF/B3LYP/6-311G (d,p) level for molecule 2

Table 7 – Vibration types and IR frequencies (cm^{-1}) of molecule 3

Seq.	Vibration Types	DFT	HF
1	τ CNNC(41), τ NCCN(38)	13	13
2	τ CNNC(15), τ CCCN(61)	23	23
3	τ CCCN(13), τ CCCC(59)	29	29
4	τ CCCC(84)	32	37
5	τ CCNN(33)	39	44
6	τ CNNC(45)	43	59
7	ɣ CCCC(29), δ CCC(19)	71	75
8	τ NNCC(64)	78	84
9	τ CCNN(15), τ CCCC(14;10), δ CCC(16;13)	101	112
10	ɣ NCNC(18), τ NNCC(43;12)	128	139
11	δ NCC(40)	185	196
12	τ CCCC(17;13), ν CC(12)	235	249
13	τ CCCC(34;13), δ CCC(12)	248	256
14	δ CCN(29), δ CCC(17)	251	287
15	ɣ NCNC(10), τ NNCC(21), τ CNNC(15;22)	294	305
16	δ NNC(25), δ OCN(15)	324	326
17	δ CCC(28)	333	339
18	δ CCC(51)	341	367
19	τ CCCC(77)	414	421
20	τ CCCC(48;15)	415	423
21	ν NC(11), ν NN(14)	428	446
22	τ HNNC(27), δ OCN(10)	466	486
23	ɣ NCNC(10), τ HNNC(46)	471	490
24	ɣ CCCC(18), τ CCCC(21)	484	496
25	τ CCCC(20;13)	497	521
26	ɣ ONNC(12;16), τ HNNC(14)	535	542
27	δ OCN(18), δ CCC(27)	566	573
28	τ HNNC(16;10), δ CCC(20)	586	605
29	δ NNC(12), δ OCN(19), δ CCC(17)	632	642
30	δ CCC(48;15)	636	648
31	δ CCC(53;23), δ CCC(15;11)	637	657
32	ɣ NCNC(39), τ HNNC(10)	660	669
33	τ CCCC(12)	698	708
34	τ CCCC(29)	704	716
35	τ CCCC(10), τ HCCC(17), τ HCCC(52)	715	734
36	τ CCCC(21;12), τ HCCC(10), τ HCCC(29)	717	745
37	τ CCCC(12), τ HCCC(43)	750	763
38	ɣ ONNC(40;41)	758	776
39	τ CCCC(11), τ HCCC(13), δ CNN(16)	780	798
40	δ NNC(12), δ CNN(10)	805	824
41	ν CC(26)	830	442
42	τ HCCC(26)	835	849

Table continuation

Seq.	Vibration Types	DFT	HF
42	ν CC(18)	843	857
43	τ HCCC(54)	853	861
44	τ HCCC(16)	855	865
45	τ HCCC(22), τ HCCC(50)	859	879
46	ν NC(14), δ OCN(10)	906	925
47	τ HCCN(10;11), δ HCC(13)	930	938
48	τ HCCN(15), τ HCCC(18), τ HCCC(17)	933	946
49	τ HCCN(16), τ HCCC(14), τ HCCC(25)	935	954
50	τ HCCN(14;10), τ HCCC(13)	951	969
51	τ CCCC(11), τ HCCC(17), τ HCCC(57)	976	981
52	τ CCCC(13), τ HCCC(25), τ HCCC(18;11;24)	982	1002
53	τ CCCC(18;27), τ HCCC(10), τ HCCC(55), τ HCCC(49)	1004	1010
54	ν CC(19;17), ν CC(15;13), δ CCC(29;26), δ CCC(26;21)	1019	1020
55	δ NNC(34), δ CCC(10)	1027	1045
56	ν CC(18;13), δ HCC(16), δ CCC(10)	1052	1064
57	ν CC(37), δ HCC(13), δ CCC(10)	1053	1085
58	ν NN(61)	1084	1092
59	ν CC(43), δ HCC(10)	1105	1115
60	ν CC(28), δ HCC(13,12)	1106	1121
61	δ HCC(20,19)	1174	1199
62	ν CC(14), δ HCC(66), δ HCC(67)	1183	1208
63	ν CC(19), δ HCC(39), δ HCH(18)	1205	1251
64	ν CC(24), δ HCC(36;13)	1208	1269
65	τ HCCN(13), δ HCC(20,22)	1210	1290
66	τ HCCN(10)	1219	1294
67	ν CC(11), ν CC(10)	1222	1298
68	ν NC(21;17), δ OCN(13), δ CNN(10)	1231	1302
69	τ HCCN(12)	1250	1308
70	τ HCCN(10;11), δ OCN(13)	1285	1323
71	ν CC(52), ν CC(23)	1339	1335
72	ν CC(69), δ HCC(12)	1340	1349
73	τ HCCN(24), δ HCC(14)	1355	1359
74	δ HCC(54), δ HCH(24)	1361	1367
75	δ HCC(51;25)	1367	1413
76	τ HCCN(22), ν NN(12)	1371	1457
77	δ HNN(66)	1401	1471
78	ν NC(21), ν NN(23), δ HNC(15)	1450	1476
79	δ HNC(35), δ HNC(27)	1470	1513
80	δ HNC(19), δ HCH(58)	1474	1521
81	δ HCC(81)	1476	1538
82	ν CC(24), δ HCC(12), δ HCC(27,11)	1487	1553
83	ν CC(14), δ HCC(21), δ HCC(12;10)	1488	1557
84	ν CC(11), δ HCC(28;16), δ HCC(31,13), δ CCC(11)	1532	1591

Table continuation

Seq.	Vibration Types	DFT	HF
85	ν CC(12), ν CC(27), ν CC(20), δ CCC(12)	1629	1633
86	ν CC(28;15,14), δ CCC(13)	1631	1656
87	ν NC(52), ν CC(12)	1645	1681
88	ν CC(48), δ HCC(12)	1649	1761
89	ν NC(13), ν CC(38)	1652	1772
90	ν OC(59;26)	1805	1980
91	ν OC(55;21)	1833	2002
92	ν CH(51;47)	3030	3158
93	ν CH(41;37;11;10)	3042	3165
94	ν CH(50;48)	3058	3195
95	ν CH(39;11)	3111	3199
96	ν CH(93), ν CH(69), ν CH(29)	3158	3220
97	ν CH(38;11), ν CH(11), ν CH(39)	3160	3225
98	ν CH(62;10;28)	3163	3242
99	ν CH(31;30;17), ν CH(19)	3170	3244
100	ν CH(43;16;38)	3171	3310
101	ν CH(54;16;23)	3179	3312
102	ν CH(64;24)	3180	3320
103	ν CH(86)	3189	3329
104	ν CH(85)	3191	3340
105	ν NH(50)	3537	3799
106	ν NH(50)	3681	3928

Note: *ν: stretching vibration, δ: bending vibration, γ: out-of plane bending vibration, τ: torsion vibration*
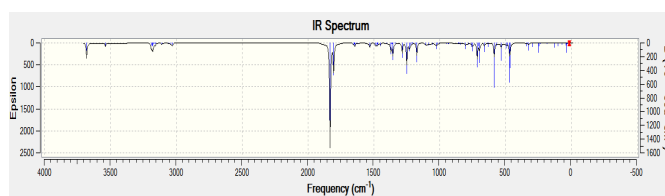
Figure 13 – Theoretical IR spectrums according to DFT/B3LYP/6-311G (d,p) level for molecule 3
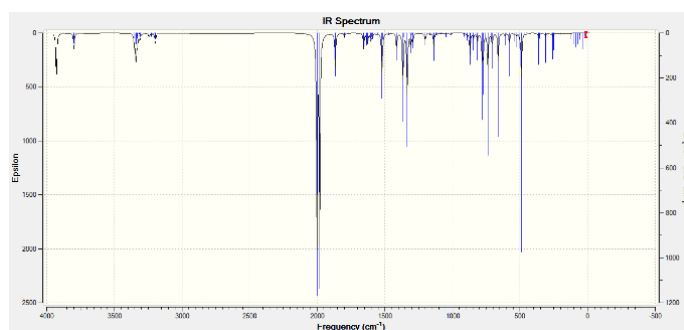
Figure 14 – Theoretical IR spectrums according to HF/B3LYP/6-311G (d,p) level for molecule 3

Table 8 – Vibration types and IR frequencies (cm⁻¹) of molecule 4

Seq.	Vibration Types	DFT	HF
1	τ CNNC(13), τ CCCN(36;34)	11	8
2	τ CCCC(21), τ CCCC(21;18)	20	11
3	τ CNNC(24;15), τ CCCN(18;12)	27	16
4	τ CNNC(18), τ NNCC(10), τ CCCN(30)	33	21
5	τ HCCC(60), τ CCCN(11)	37	36
6	δ CCN(10), τ CNNC(20), τ NNCC(22)	39	49
7	τ CNNC(11;12), τ CCCN(23)	40	57
8	δ CCC(11), τ CCCC(19), τ NNCC(15)	59	70
9	δ NNC(11), τ CCNN(56)	78	80
10	τ NNCC(16), ɣ CCCC(15), ɣ CCCC(16)	101	104
11	τ CNNC(11), τ NNCC(42), ɣ NCNC(17)	126	128
12	δ CCN(22), τ CCCC(13)	148	161
13	δ CCN(23)	192	209
14	τ CCCC(17), τ CCCC(10)	248	253
15	δ CCN(33), δ CCC(11)	249	275
16	δ CCC(13), τ CNNC(11)	279	296
17	τ CNNC(13), τ NNCC(22)	298	319
18	δ CNN(10), τ CCCC(11)	312	341
19	δ CNN(21)	331	365
20	δ CCC(16;13)	342	368
21	δ CCC(12;10), δ CCC(13;12)	379	407
22	τ HCCC(13), τ HCCC(19), τ CCCC(61;28), τ CCCC(57;12)	416	425
23	ν NC(12), ν NN(15), δ OCN(10)	425	455
24	τ HNNC(30)	466	462
25	τ HNNC(43)	470	490
26	τ CCCC(13), ɣ CCCC(19)	489	530
27	ɣ CCCC(21;15)	502	543
28	δ CCC(11), ɣ CCCC(10)	523	564
29	τ HNNC(14), ɣ ONNC(15;11)	534	579
30	δ CCC(22), τ HNNC(15)	583	653
31	δ OCN(27)	619	679
32	δ CCC(49), δ CCC(23;15)	636	699
33	δ CCC(18;17), ɣ NCNC(18)	654	713
34	δ CCC(13), ɣ NCNC(26)	664	736
35	τ HCCC(28), τ HCCC(10), τ CCCC(36;11)	717	758
36	ν CC(15)	739	772
37	ν CC(11), τ HCCC(43)	751	792
38	ɣ ONNC(40)	757	815
39	ν CC(10), τ HCCC(32)	767	830
40	δ CNN(21), δ NNC(17)	800	865
41	ν CC(17), τ HCCC(17)	829	869
42	ν CC(18), τ HCCC(16)	840	901

Table continuation

Seq.	Vibration Types	DFT	HF
42	τ HCCC(98)	846	921
43	ν CC(10)	854	929
44	τ HCCC(60), τ HCCC(16)	860	941
45	ν CC(13), τ HCCC(13)	863	946
46	ν NC(14)	909	1001
47	ν CC(10), δ HCC(15), δ HCC(12), τ HCCN(21;11)	929	1009
48	τ HCCC(27;14), τ HCCN(13)	935	1022
49	τ HCCC(15), τ HCCN(12;10)	951	1046
50	τ HCCC(70)	963	1069
51	τ HCCC(82)	970	1085
52	τ HCCC(21;19;10), τ HCCC(22), τ CCCC(18)	983	1092
53	τ HCCC(50), τ HCCC(14), τ CCCC(17)	1005	1115
54	ν CC(11), δ HCH(18), τ HCCC(44)	1010	1121
55	ν CC(32), δ CCC(10)	1019	1137
56	δ CNN(11;10), δ NNC(33)	1027	1161
57	δ HCH(13), δ CCC(30;29)	1040	1169
58	ν CC(23;13), δ HCC(18), δ CCC(10)	1053	1178
59	δ HCH(15), τ HCCC(52;12)	1063	1199
60	ν NN(61)	1084	1208
61	ν CC(25), ν CC(17), δ HCC(14;11)	1106	1251
62	ν CC(12), ν CC(22), δ HCH(53)	1140	1269
63	δ HCC(15), δ HCC(16)	1175	1290
64	ν CC(12), δ HCC(65)	1183	1294
65	ν CC(11), δ HCC(13), δ HCC(20), τ HCCN(13;11)	1208	1298
66	ν CC(17), δ HCC(30), δ HCH(70)	1209	1302
67	ν CC(37), ν CC(37), ν CC(17;13)	1222	1308
68	ν NC(14;20), δ OCN(11)	1231	1323
69	ν CC(16;10), δ CCC(13), δ HCH(19)	1234	1335
70	δ HCC(12), δ HCC(11)	1251	1349
71	δ NCN(12), δ CNN(11), τ HCCN(11)	1286	1359
72	ν CC(37), ν CC(25), δ HCH(13)	1332	1367
73	ν CC(27;11), ν CC(16), δ HCC(10)	1339	1413
74	ν CC(12), δ HCH(70)	1349	1457
75	τ HCCN(15;38)	1356	1471
76	δ HCC(48), δ HCC(23)	1368	1476
77	ν NN(10), τ HCCN(32)	1371	1513
78	δ HNN(66)	1400	1521
79	δ HCH(89)	1416	1538
80	ν CC(18), δ HCH(39)	1444	1553
81	ν NC(20), ν NN(23), δ HNC(13)	1449	1557
82	δ HNC(41), δ HCH(24)	1470	1591
83	δ HNC(11), δ HCH(62)	1473	1597
84	δ HNC(10), δ HCC(77)	1476	1604

Table continuation

Seq.	Vibration Types	DFT	HF
85	ν CC(12), δ HCC(22), δ HCC(12;10)	1488	1608
86	δ HCH(70), τ HCCC(16)	1491	1612
87	δ HCH(65), τ HCCC(14)	1497	1625
88	δ HCC(31), δ HCC(18), δ CCC(10)	1532	1633
89	δ HCH(59)	1551	1656
90	ν CC(12), ν CC(22;21), δ CCC(11)	1619	1681
91	ν CC(12), ν CC(40), δ CCC(12)	1629	1761
92	ν NC(64)	1647	1772
93	ν CC(20;16;12), δ HCC(11)	1649	1798
94	ν CC(55), δ HCH(18)	1661	1812
95	ν OC(59;26)	1805	1980
96	ν OC(55;21)	1832	2001
97	ν CH(97)	3023	3158
98	ν CH(50;47)	3028	3165
99	ν CH(38;11;10), ν CH(41)	3043	3195
100	ν CH(48;49)	3056	3199
101	ν CH(90)	3076	3220
102	ν CH(89)	3103	3225
103	ν CH(10)	3110	3242
104	ν CH(39;11)	3111	3244
105	ν CH(77;23)	3153	3310
106	ν CH(93)	3158	3312
107	ν CH(62), ν CH(29)	3164	3320
108	ν CH(99)	3169	3329
109	ν CH(41;18), ν CH(39)	3171	3330
110	ν CH(99)	3172	3333
111	ν CH(54;17), ν CH(20)	3179	3340
112	ν CH(86)	3189	3351
113	ν NH(50)	3539	3799
114	ν NH(50)	3681	3928

Note: *ν: stretching vibration, δ: bending vibration, γ: out-of plane bending vibration, τ: torsion vibration*

Figure 15 – Theoretical IR spectrums according to DFT/B3LYP/6-311G (d,p) level for molecule 4.

Figure 16 – Theoretical IR spectrums according to HF/B3LYP/6-311G (d,p) level for molecule 4.

Table 9 – Vibration types and IR frequencies (cm^{-1}) of molecule 5

1	τ NCCC(47), γ NCCN(17), τ CCCN(20)	10	10
2	τ NCCC(18), τ CCCN(34), τ CCCC(30)	18	15
3	τ CCCN(11;30), τ CCCC(33)	24	19
4	τ NCCC(16), τ CCCN(40), τ CCCC(19)	30	34
5	δ CCC(14), δ NCC(12), δ CCC(10), τ CCCC(16), γ CCCC(31)	38	43
6	δ CNN(14), γ NCCN(34)	39	56
7	τ CNNC(37;15)	54	69
8	δ NNC(11), τ CCNN(52)	78	78
9	δ CCC(12), τ CCCC(11), γ NCCN(13)	100	104
10	γ NCNC(17), τ NNCC(32), τ CNNC(32)	125	127
11	δ NCC(17), δ CCC(12), τ CCCC(32), γ ClCCC(18)	135	148
12	δ NCC(22)	182	199
13	δ ClCN(31), γ NCCN(14)	243	251
14	δ CCC(12), δ ClCC(43)	248	268
15	δ CCC(10), τ CCCC(35;13)	254	276
16	τ NNCC(33), τ CNNC(10)	297	315
17	γ CCCC(16), γ ClCCC(29), τ CCCC(16)	307	336
18	δ CCC(49)	328	355
19	δ CCC(19), δ OCN(10), δ NNC(24)	341	365
20	δ CCC(22;20), δ ClCC(30)	366	396
21	ν ClC(22), δ CCC(12)	401	435
22	τ HCCC(16), τ CCCC(16;15)	415	452
23	τ HCCC(17), τ CCCC(79)	418	456
24	τ HNNC(12)	446	483
25	τ HNNC(31;14)	466	493
26	δ OCN(16)	472	503
27	τ CCCC(29;18;10)	495	536
28	τ CCCC(21;22), γ CCCC(15), γ ClCCC(22)	508	557
29	δ CCC(13), τ HNNC(11), γ ONNC(13;11)	534	579
30	δ OCN(36)	582	647
31	δ CCC(51;18;15)	608	679
32	δ CCC(28;18;14)	636	694
33	γ NCNC(26)	647	712
34	ν ClC(13)	674	724

Table continuation

35	τ HNNC(12)	694	743
36	τ HCCC(10), τ CCCC(36)	701	756
37	τ HCCC(13), τ HCCC(12), τ CCCC(23;15)	717	772
38	τ HCCC(17)	748	813
39	τ HCCC(10), τ CCCC(11)	757	826
40	δ CNN(13;15)	759	863
41	ɣ ONNC(41;39), τ CNNC(10)	796	869
42	ν CC(16)	828	891
42	ν CC(14)	831	899
43	δ CCC(11)	834	921
44	τ HCCC(99)	859	934
45	τ HCCC(58), τ HCCC(27)	864	946
46	τ HCCC(47), ɣ CCCC(12)	909	953
47	ν NC(13), δ CCN(12)	933	1002
48	δ HCC(15), δ HCC(16), τ HCCC(16), τ HCCN(12)	935	1016
49	τ HCCC(16;10), τ HCCN(21)	951	1022
50	τ HCCC(46;11), τ HCCC(18)	964	1045
51	τ HCCC(71), τ CCCC(10)	972	1076
52	ν CC(42), δ CCC(53)	983	1085
53	τ HCCC(42;11), τ HCCC(84), τ CCCC(16;14)	1006	1095
54	δ CCC(12), δ CCC(59), δ HCC(10)	1019	1106
55	τ HCCC(34;16), τ CCCC(21)	1026	1115
56	ν CC(32), δ CCC(13;11), δ HCC(15)	1033	1121
57	δ CNN(11), δ NNC(40)	1053	1137
58	ν CC(28), δ HCC(19)	1086	1169
59	ν CC(29), δ HCC(21)	1102	1172
60	ν CC(11), ν CC(35), ν ClC(22), δ HCC(13)	1106	1195
61	ν CC(19), ν CC(27;10), δ HCC(14)	1132	1204
62	δ HNN(12)	1173	1247
63	ν CC(26), δ HCC(28)	1183	1290
64	ν CC(25), δ HCC(34), δ HCC(13)	1204	1292
65	ν CC(10), δ HCC(67)	1208	1294
66	ν CC(12), ν NN(61), δ HCC(13), δ HCC(22;16)	1209	1308
67	δ HCC(12;11), τ HCCN(12)	1222	1310
68	ν CC(12), ν CC(11), δ HCC(15)	1230	1333
69	ν NC(20), ν CC(10)	1250	1343
70	δ HCC(20), δ HCC(10;26), τ HCCC(10)	1287	1358
71	ν CC(12), δ HCC(16), δ HCC(10)	1321	1362
72	ν NC(28)	1339	1365
73	ν NC(11)	1341	1414
74	ν NC(13), δ CNN(17), δ NNC(10), τ HCCN(14)	1355	1445
75	δ HCC(85)	1367	1471
76	δ HCC(16), δ HCC(20;17;24)	1401	1513
77	ν NC(11), ν CC(12), τ HCCN(29)	1439	1521

Table continuation

78	ν CC(15), τ HCCN(33)	1450	1552
79	ν CC(11), ν CC(14), δ HCC(39)	1470	1554
80	δ HNN(60)	1474	1590
81	δ HCC(42;32), τ HCCN(11)	1476	1598
82	δ HCC(50;42)	1488	1604
83	ν CC(14), δ HCC(42)	1526	1627
84	ν NC(13), δ HNC(48)	1532	1632
85	ν NC(32;18), δ HNC(20)	1619	1656
86	δ CCC(11), δ HCC(33), δ HCC(13)	1629	1660
87	ν CC(16), δ CCC(10), δ HCC(55)	1641	1762
88	ν CC(51), δ CCC(14;10)	1648	1795
89	ν CC(37;27), ν CC(12;22), δ CCC(11), δ HCC(10)	1649	1798
90	ν CC(12), ν CC(29), δ HCC(20)	1807	1866
91	ν CC(48), δ HCC(12)	1834	1983
92	ν NC(69)	3031	2003
93	ν OC(59;15)	3042	3197
94	ν OC(65;19)	3058	3198
95	ν CH(68), ν CH(31)	3059	3229
96	ν CH(29), ν CH(66)	3111	3243
97	ν CH(53), ν CH(46)	3158	3309
98	ν CH(44), ν CH(51)	3164	3320
99	ν CH(20), ν CH(69)	3169	3328
100	ν CH(74), ν CH(13)	3170	3329
101	ν CH(24;49), ν CH(19)	3171	3331
102	ν CH(52;23), ν CH(16)	3179	3341
103	ν CH(85), ν CH(11)	3189	3351
104	ν CH(89)	3203	3365
105	ν CH(93)	3204	3366
106	ν CH(28), ν CH(72)	3371	3430
107	ν CH(24), ν CH(75)	3372	3433
108	ν NH(50)	3536	3797
109	ν NH(50)	3679	3926

Note: ν: stretching vibration, δ: bending vibration, ɣ: out-of plane bending vibration, τ: torsion vibration

Figure 17 – Theoretical IR spectrums according to DFT/B3LYP/6-311G (d,p) level for molecule 5
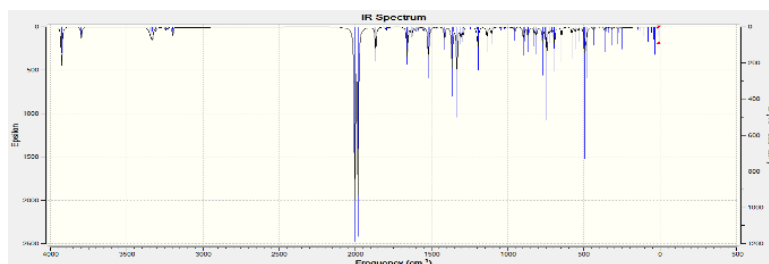
Figure 18 – Theoretical IR spectrums according to HF/B3LYP/6-311G (d,p) level for molecule 5

To examine how molecules interact with ultraviolet light, scientists employ a technique called UV (ultraviolet) spectral analysis in analytical chemistry and other disciplines. Since ultraviolet light has shorter wavelengths and more energy than visible light, it can excite molecular electrons to states with higher energies. This interaction between UV light and molecules can reveal important details about the composition, characteristics, and chemical structure of the substances being examined. UV spectral analysis includes shining UV light through a sample and observing how much of it is absorbed or transmitted at various wavelengths. The UV absorption spectra that results can shed light on the electronic transitions occurring inside the molecules in the sample. Compounds may be identified, their concentrations can be measured, and numerous chemical processes and interactions can be researched using this data. When the theoretical UV-visible spectrum of the molecules drawn according to the DFT and HF methods and given in Figure 19-23 are examined, it has been observed that the spectra drawn according to both methods are generally compatible with each other.

DFT (B3LYP, 6-311G(d))   HF (B3LYP, 6-311G(d))
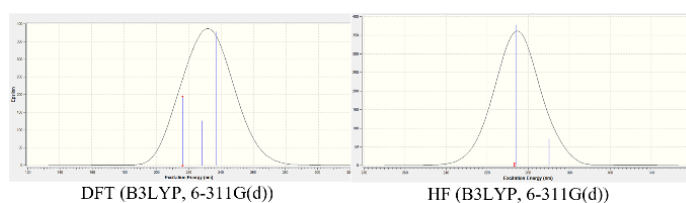
Figure 19 – Theoretical UV-visible spectrum for studied molecule 1

DFT (B3LYP, 6-311G(d))   HF (B3LYP, 6-311G(d))
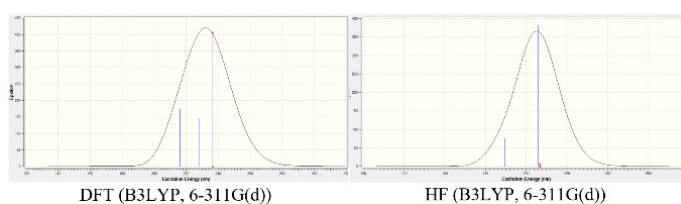
Figure 20 – Theoretical UV-visible spectrum for studied molecule 2

DFT (B3LYP, 6-311G(d))   HF (B3LYP, 6-311G(d))
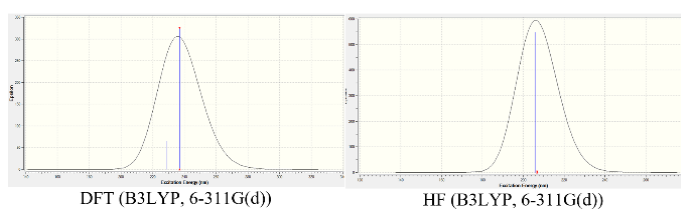
Figure 21 – Theoretical UV-visible spectrum for studied molecule 3

DFT (B3LYP, 6-311G(d))   HF (B3LYP, 6-311G(d))
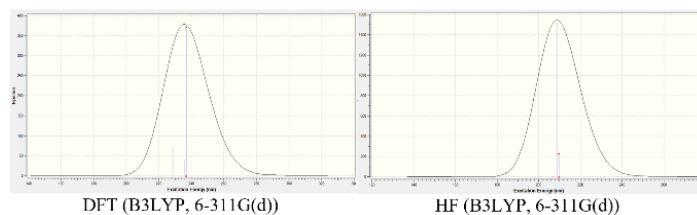
Figure 22 – Theoretical UV-visible spectrum for studied molecule 4

DFT (B3LYP, 6-311G(d))   HF (B3LYP, 6-311G(d))
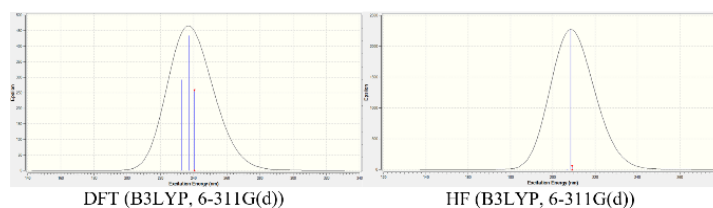
Figure 23 – Theoretical UV-visible spectrum for studied molecule 5

In computational chemistry, the idea of molecular electrostatic potential (MEP) is used to examine and depict molecules' electrostatic characteristics. It offers information about how electric charges are distributed within molecules, which in turn affects a number of molecular interactions, characteristics, and forces, including bonding and reactivity. The partial atomic charges that are given to the atoms in a molecule are the source of MEP and are frequently computed using quantum mechanical techniques like density functional theory (DFT) or Hartree-Fock computations. The distribution of electron density surrounding each atom is represented by these partial charges, which also contribute to the molecule's overall electrostatic potential. Typically, color maps or contour plots are used to show the MEP graphically. In these figures, the blue patches with positive MEP often denote electron-poor regions, which are places with an electron-deficient environment. In contrast, areas with negative MEP are frequently depicted in red to denote electron-rich zones. Neutral areas are usually shown in white. When the Molecular Electrostatic Potential (MEP) shapes we obtained in this framework and given in Figure 24-28 are examined, it is seen that electron-poor regions, electron-rich regions and neutral regions of each molecule are clearly distinct.
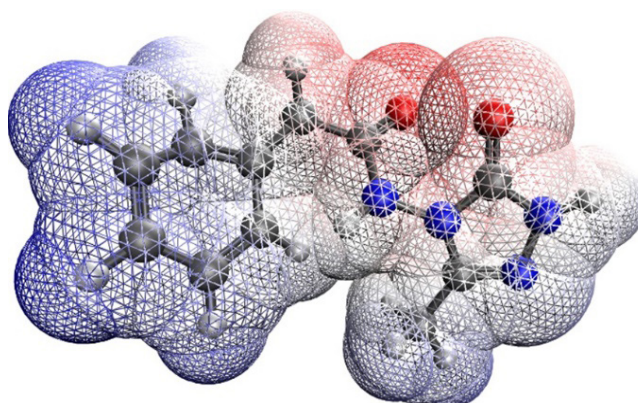
Figure 24 – Molecular electrostatic potential (MEP) for molecule 1
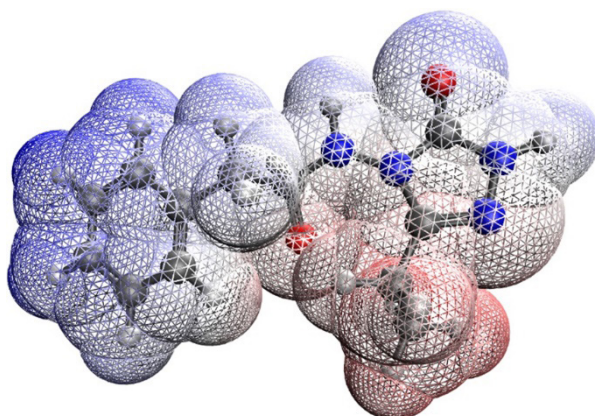
Figure 25 ж Molecular electrostatic potential (MEP) for molecule 2
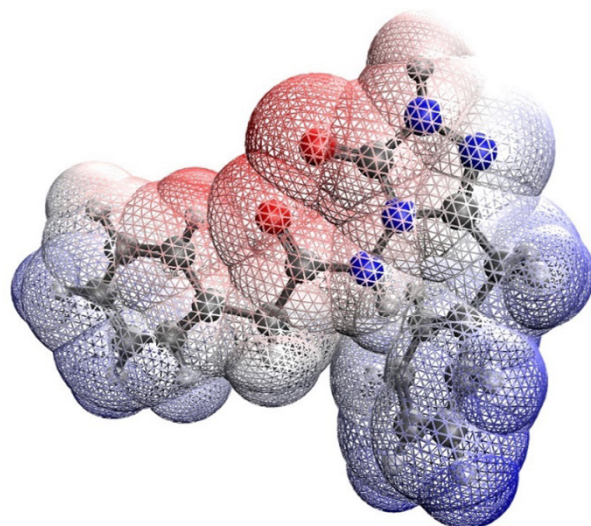
Figure 26 – Molecular electrostatic potential (MEP) for molecule 3
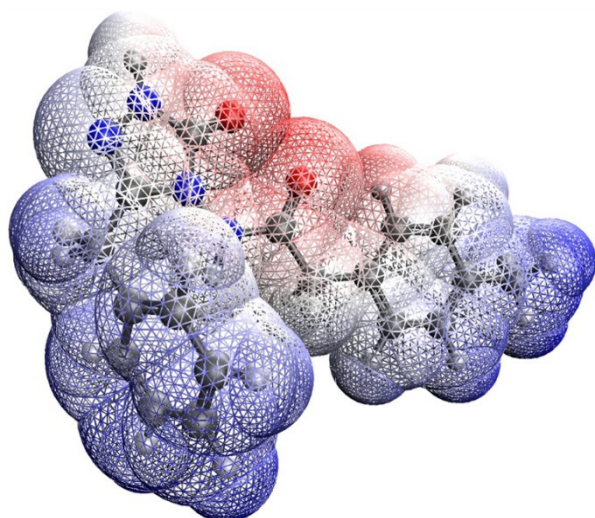
Figure 27 – Molecular electrostatic potential (MEP) for molecule 4
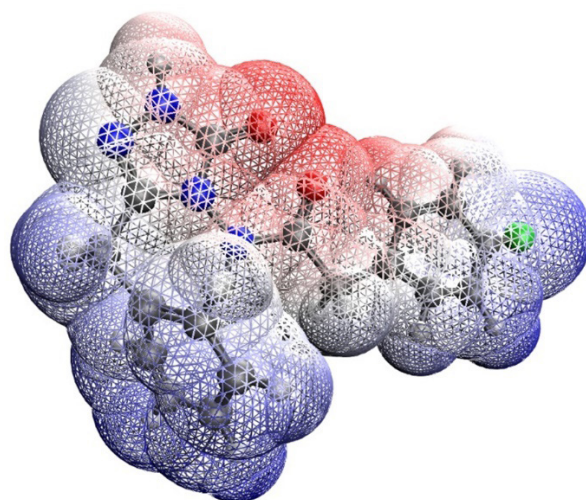
Figure 28 – Molecular electrostatic potential (MEP) for molecule 5

Conclusion

By conducting theoretical studies of these five molecules, which we had previously synthesized, we showed that they could be evaluated especially in drug development. It is especially important that the Density Functional Theory, (DFT, B3LYP) / Hartree Fock, (HF, B3LYP) methods we used in this theoretical study are widely used in the literature. Properties such as FT-IR and UV-vis spectral values, bond angles, bond lengths, dipole moments, highest occupied molecular orbital (HOMO), lowest unoccupied molecular orbital (LUMO) energy and total energy, mulliken charges and molecular electrostatic potential (MEP). Determination is important so that these molecules can be used for purposes other than being used as drug active ingredients.

References

1. Cao, X.; Wang, W.; Wang, Sh. and Bao, L. Asymmetric synthesis of novel triazole derivatives and their in vitro antiviral activity and mechanism of action. Eur. J. Med. Chem. 2017, 139, 718-725.

2. Gao, F.; Wang, T.; Xiao, J. and Huang, G. Antibacterial activity study of 1, 2, 4-triazole derivatives. Eur. J. Med. Chem. 2019, 173, 274-281.

3. Sadeghpour, H.; Khabnadideh, S.; Zomorodian, K.; Pakshir, K.; Hoseinpour, K.; Javid, N.; Faghih-Mirzaei, E. and Rezaei, Z. Design, synthesis, and biological activity of new triazole and nitro-triazole derivatives as antifungal agents. Molecules 2017, 22, 1150-1161.

4. Cheng, Y.N.; Jiang, Zh.H.; Sun, L.Sh.; Su, Z.Y.; Zhang, M.M. and Li, H.L. Synthesis of 1,2,4-triazole benzoyl arylamine derivatives and their high antifungal activities. Eur. J. Med. Chem. 2020, 200, 112463-112474.

5. Tsukuda, T.; Shiratori, Y.; Watanabe, M.; Ontsuka, H.; Hattori, K.; Shirai, M. and Shimma, N. Modeling, synthesis and biological activity of novel antifungal agents-I. Bioorg. Med. Chem. Lett. 1998, 8, 1819-1829.

6. Arndt, C.A.S.; Walsh, T.J.; Pizzo, F.M. and Poplack, D.G. Cerebrospinal fluid penetration of fluconazole: implications for antifungal therapy in patients with acquired immunodeficiency syndrome. J. Infect. Dis. 1988, 157(1), 178-180.

7. Mbailey, E.; Krakovsky, D.J. and Rybak, M.J. The triazole antifungal agents: A review of itraconazole and fluconazole. Pharmacotherapy 1990, 10,146-153.

8. Roberts, J.; Schock, K.; Marino, S. and Andriole, V.T. Efficacies of two new antifungal agents, the triazole ravuconazole and the echinocandin LY-303366, in an experimental model of invasive aspergillosis. Antimicrob. Agents Chemother. 2000, 44(12), 3381-3388.

9. Espinel-Ingroff, A. In vitro activity of the new triazole voriconazole (UK-109, 496) against opportunistic filamentous and dimorphic fungi and common and emerging yeast pathogens. J. Clin. Microbiol. 1998, 36, 198-202.

10. Sabo, J.A. and Abdel-Rahman, S.M. Voriconazole: a new triazole antifungal. Ann. Pharmacother. 2000, 34(9), 1032-1043.

11. Johnson, L.B. and Kauffman, C.A. Voriconazole: a new triazole antifungal agent. Clin. Infect. Dis. 2003, 36(5), 630-637.

12. Pfaller, M.A.; Messer, S. and Jones, R.N. Activity of a new triazole, Sch 56592, compared with those of four other antifungal agents tested against clinical isolates of candida spp. and saccharomyces cerevisiae. Antimicrob. Agents. Chemother. 1997, 41(2), 233-235.

13. Neenu, G.; Arun K, S.; Manisha, S.; Venkaraddi Mangannavar, C. and Gurubasavaraj Veeranna, P. Antitubercular potential of novel isoxazole encompassed 1, 2, 4-triazoles: design, synthesis, molecular docking study and evaluation of antitubercular activity. Anti-Infect. Agents 2021, 19(2), 147-161.

14. Mohan Krishna, K.; Inturi, B.; Pujar, G.V.; Purohit, M.N. and Vijaykumar, G.S. Design, synthesis and 3D-QSAR studies of new diphenylamine containing 1, 2, 4-triazoles as potential antitubercular agents. Eur. J. Med. Chem. 2014, 84, 516-529.

15. Keri, R.S.; Patil, S.A.; Budagumpi, S. and Nagaraja, B.M. Triazole: a promising antitubercular agent. Chem. Biol. Drug. Des. 2015, 86(4), 410-423.

16. Chinthakindi, P.K.; Sangwan, P.L.; Farooq, S.; Aleti, R.R.; Kaul, A.; Saxena, A.K.; Murthy, Y.L.N.; Vishwakarma, R.A. and Koul, S. Diminutive effect on T and B-cell proliferation of non-cytotoxic α-santonin derived 1, 2, 3-triazoles: A report. Eur. J. Med. Chem. 2013, 60, 365-375.

17. Liu, J.; Liu, Q.; Yang, X.; Xu, Sh.; Zhang, H.; Bai, R.; Yao, H.; Jiang, J.; Shen, M.; Wu, X. and Xu, J. Design, synthesis, and biological evaluation of 1, 2, 4-triazole bearing 5-substituted biphenyl-2-sulfonamide derivatives as potential antihypertensive candidates. Bioorg. Med. Chem. 2013, 21(24), 7742-7751.

18. Abuo-Rahma, G.E.-D.A.; Abdel-Aziz, M.; Farag, N.A. and Kaoud, T.S. Novel 1-[4-(Aminosulfonyl) phenyl]-1H-1, 2, 4-triazole derivatives with remarkable selective COX-2 inhibition: Design, synthesis, molecular docking, anti-inflammatory and ulcerogenicity studies. Eur. J. Med. Chem. 2014, 83, 398-408.

19. Abdel-Aziz, M.; Beshr, E.A.; Abdel-Rahman, I.M.; Ozadali, K.; Tan, O.U. and Aly, O.M. 1-(4-Methoxyphenyl)-5-(3, 4, 5-trimethoxy phenyl)-1H-1,2,4-triazole-3-carboxamides: Synthesis, molecular modeling, evaluation of their anti-inflammatory activity and ulcerogenicity. Eur. J. Med. Chem. 2014, 77, 155-165.

20. Huang, L.; Ding, J.; Li, M.; Hou, Z.; Geng, Y.; Li, X. and Yu, H. Discovery of [1, 2, 4]-triazolo [1, 5-a] pyrimidine-7 (4H)-one derivatives as positive modulators of GABAA1 receptor with potent anticonvulsant activity and low toxicity. Eur. J. Med. Chem. 2020, 185, 111824-111833.

21. Plech, T.; Luszczki, J.J.; Wujec, M.; Flieger, J. and Pizon, M. Synthesis, characterization and preliminary anticonvulsant evaluation of some 4-alkyl-1, 2, 4-triazoles. Eur. J. Med. Chem. 2013, 60, 208-215.

22. Vijesh, A.M.; Isloor, A.M.; Shetty, P.; Sundershan, S. and Fun, H.K. New pyrazole derivatives containing 1, 2, 4-triazoles and benzoxazoles as potent antimicrobial and analgesic agents. Eur. J. Med. Chem. 2013, 62, 410-415.

23. Kholodnyak, S.V.; Schabelnyk, K.P.; Zhernova, G.O.; Sergeieva, T.Yu.; Ivchuk, V.V.; Voskoboynik, O.Yu.; Kovalenko, S.I.; Trzhetsinskii, S.D.; Okovytyy, S.I. and Shishkina, S.V. Hydrolytic cleavage of the pyrimidine ring in 2-aryl-[1, 2, 4] triazole [1, 5-c] quinazolines: physico-chemical properties and the hypoglycemic activity of the compounds synthesized. News of Pharmacy 2015, 83(3), 9-17.

24. Chelamalla, R.; Akena, V. and Manda, S. Synthesis of N-arylidene-2-(5-aryl-1H-1, 2,4-triazol-3-ylthio) acetohydrazides as antidepressants. Med. Chem. Res. 2017, 26, 1359-1366.

25. Radhika, C.; Venkatesham, A. and Sarangapani, M. Synthesis and antidepressant activity of di substituted-5-aryl-1,2,4-triazoles. Med. Chem. Res. 2012, 21, 3509-3513.

26. El-Sherief, H.A.; Youssif, B.G.M.; Bukhari, S.N.A.; Abdelazeem, A.H.; Abdel-Aziz, M. and Abdel-Rahman, H.M. Synthesis, anticancer activity and molecular modeling studies of 1, 2, 4-triazole derivatives as EGFR inhibitors. Eur. J. Med. Chem. 2018, 156, 774-789.

27. El-Sherief, H.A.M.; Youssif, B.G.M.; Bukhari, S.N.A.; Abdel-Aziz, M. and Abdel-Rahman, H.M. Novel 1, 2, 4-triazole derivatives as potential anticancer agents: Design, synthesis, molecular docking and mechanistic studies. Bioorg. Chem. 2018, 76, 314-325.

28. Turky, A.; Bayoumi, A.H.; Sherbiny, F.F.; El-Adl, K. and Abulkhair, H.S. Unravelling the anticancer potency of 1, 2, 4-triazole-N-arylamide hybrids through inhibition of STAT3: synthesis and in silico mechanistic studies. Mol. Divers. 2021, 25(1), 403-420.

29. Xu, K.; Huang, L.; Xu, Zh.; Wang, Y.; Bai, G.; Wu, Q.; Wang, X.; Yu, Sh. and Jiang, Y. Design, synthesis, and antifungal activities of novel triazole derivatives containing the benzyl group. Drug Des. Devel. Ther. 2015, 9, 1459-1467.

30. Chaia, B.; Qian, X.; Cao, S.; Liu, H. and Song, G. Synthesis and insecticidal activity of 1,2,4-triazole derivatives. Arkivoc 2003, ii, 141-145.

31. Naito, Y.; Akahoshi, F.; Takeda, S.; Okada, T.; Kajii, M.; Nishimura, H.; Sugiura, M.; Fukaya, C. and Kagitani, Y. Synthesis and pharmacological activity of triazole derivatives inhibiting eosinophilia. J. Med. Chem. 1996, 39(15), 3019-3029.

32. Oruc, E.E.; Rollas, S.; Kabasakal, L. and Uysal, M.K. The in vivo metabolism of 5-(4-nitrophenyl)-4-phenyl-2,4-dihydro-3H-1,2,4-triazole-3-thione in rats. Drug. Metabol. Drug. Interact. 1999, 15(2-3), 127-140.

33. Maddila, S.; Pagadala, R. and Jonnalagadda, S.B. Synthesis and insecticidal activity of tetrazole linked triazole derivatives. J. Het. Chem. 2014, 52(2), 487-491.

34. Oh, K.; Yamada, K.; Asami, T. and Yoshizawa, Y. Synthesis of novel brassinosteroid biosynthesis inhibitors based on the ketoconazole scaffold. Bioorg. Med. Chem. Lett. 2012, 22(4), 1625-1628.

35. Santen, J.R. Inhibition of aromatase: insights from recent studies. Steroids 2003, 68(7-8), 559-567.

36. Clemons, M.; Coleman, R.E. and Verma, S. Aromatase inhibitors in the adjuvant setting: bringing the gold to a standard? Cancer Treat. Rev. 2004, 30, 325-332.

37. Delea, E.; El-Ouagari, K.; Karnon, J. and Sofrygin, O. Cost-effectiveness of letrozole versus tamoxifen as initial adjuvant therapy in postmenopausal women with hormone-receptor positive early breast cancer from a Canadian perspective. Breast Cancer Res. Treat. 2008, 108(3), 375-387.

38. Christova, K.; Shilkaitis, A.; Green, A.; Mehta, R.G.; Grubbs, C.; Kelloff, G. and Lubet, R. Cellular responses of mammary carcinomas to aromatase inhibitors: Effects of vorozole. Breast Cancer Res. Treat. 2000, 60, 117-128.

39. Roman, G.; Rahman, M.N.; Vukomanovic, D.; Jia, Z.; Nakatsu, K. and Szarek, W.A. Heme oxygenase inhibition by 2-oxy-substituted 1-azolyl-4-phenyl butanes: effect of variation of the azole moiety. Xray crystal structure of human heme oxygenase-1 in complex with 4-phenyl-1- (1H-1,2,4-triazol-1-yl) -2-butanone. Chem. Biol. Drug. Des. 2010, 75(1), 68-90.

40. Pagacz-Kostrzewa, M.; Bronisz, R. and Wierzejewska, M. Theoretical and matrix isolation FTIR studies of 3-amino-1,2,4-triazole and its isomers. Chem. Phys. Lett. 2009, 473(4-6), 238-246.

41. Al-Tamimi, A.S. Electronic structure, hydrogen bonding and spectroscopic profile of a new 1,2,4-triazole-5(4H)-thione derivative: A combined experimental and theoretical (DFT) analysis. J. Mol. Str. 2016, 1120, 215-227.

42. Ayeni, A.O.; Watkins G.M. and Hosten, E.C. Polymorphism of a new Mannich base-[-4-methyl-2-((4-(4-nitrophenyl)piperazin-1-yl)methyl) phenol]. J. Mol. Str. 2018, 1160, 38-45.

43. Raj, A.D.; Jeeva, M.; Shankar, M.; Prabhu, G.V.; Vimalan, M.; Potheher, I.V. Synthesis, growth, physicochemical properties and DFT calculations of 2-naphthol substituted Mannich base 1-(morpholino (phenyl) methyl) naphthalen-2-ol: A non linear optical single crystal. J. Mol. Str. 2017, 1147, 763-775.

44. Boobalan, M.S.; Amaladasan, M.; Ramalingam, S.; Tamilvendan, D.; Prabhu, G.V. and Bououdina, M. First principles and DFT supported investigations on vibrational spectra and electronic structure of 2-((phenyl amino)methyl)isoindoline-1,3-dione–An antioxidant active Mannich base. Spectrochim. Acta A Mol. Biomol. Spectrosc. 2015, 137, 962-978.

45. Fu, A.; Li, H.; Si, H.; Yuan, S. and Duan, Y. Theoretical studies of stereoselectivities in the direct syn- and anti-Mannich reactions catalyzed by different amino acids. Tetrahedron: Asymmetry 2008, 19(19), 2285-2292.

46. Pająk, J.; Rospenk, M.; Maes, G. and Sobczyk, L. Matrix-isolation FT-IR and DFT theoretical studies of the intramolecular hydrogen bonding in Mannich bases. Chem. Phys. 2006, 320(2), 229-238.

47. Al-Wabli, R.I.; Govindarajan, M.; Almutairi, M.S. and Attia, M.I. Spectral characterization, computed frequencies analysis and electronic structure calculations on (1E)-N-hydroxy-3-(1H-imidazol- 1-yl)-1-phenylpropan-1-imine: An oxime-bearing precursor to potential antifungal agents. J. Mol. Str. 2018, 1168, 264-279.

48. Diez-Martinez, A.; Tejero, T. and Merino, P. Experimental and theoretical studies on Mannich-type reactions of chiral non-racemic N-(benzyloxyethyl) nitrones. Tetrahedron: Asymmetry 2010, 21(24), 2934-2943.

49. Abramov, Yu. A.; Volkov, A.V. and Coppens, P. On the evaluation of molecular dipole moments from multipole refinement of X-ray diffraction data. Chem. Phys. Lett. 1999, 311(1-2), 81-86.

50. Handy, N.C.; Maslen, P.E.; Amons, R.D.; Audrows, J.S.; Murroy, C.W. and Lawing, G. The harmonic frequencies of benzene. Chem. Phys. Lett. 1992, 197(4-5), 506-515.

51. Forsyth, D.A. and Sebag. A.B. Computed 13C NMR Chemical Shifts via Empirically Scaled GIAO Shieldings and Molecular Mechanics Geometries. Conformation and Configuration from 13C Shifts. J. Am. Chem. Soc. 1997, 119(40), 9483-9494.

52. Sebag, A.B.; Forsyth, D.A. and Plante, M.A. Conformation and configuration of tertiary amines via GIAO-derived (13)C NMR chemical shifts and a multiple independent variable regression analysis. J. Org. Chem. 2001, 66 (24), 7967-7973.

53. Turhan Irak, Z. and Gümüş, S. Heterotricyclic compounds via click reaction: A computational study. Noble Int. J. Sci. Res. 2017, 1(7), 80-89.

54. Beytur, M.; Turhan Irak, Z.; Manap, S. and Yüksek, H. Synthesis, characterization and theoretical determination of corrosion inhibitor activities of some new 4,5-dihydro-1H-1,2,4-triazol-5-one derivatives. Heliyon 2019, 5(6), 1-8.

55. Turhan Irak, Z. and Beytur, M. Theoretical study on the investigation of antioxidant properties of some 4-benzylidenamino-4,5-dihydro-1H-1,2,4-triazol-5-one derivatives. Iğdır Univ. J. Inst. Sci. Tech. 2019, 9(1), 512-521.

56. Ditchfield, R. Self-consistent perturbation theory of diamagnetism. Mol. Phys. 1974, 27(4), 789-807.

57. Wolinski, K.; Hinton, J.F. and Pulay, P. Efficient implementation of the gauge-independent atomic orbital method for NMR chemical shift calculations. J. Am. Chem. Soc. 1990, 112, 8251-8260.

58. Cheeseman, J.R.; Trucks, G.W.; Keith, T.A. and Frisch. M.J. A comparison of models for calculating nuclear magnetic resonance shielding tensors. J. Chem. Phys. 1996, 104(14), 5497-5509.

59. Friesner, R.A.; Murphy, R.B.; Beachy, M.D.; Ringnalda, M.N.; Pollard, W.T.; Dunietz, B.D. and Cao, Y. Correlated ab initio electronic structure calculations for large molecules. J. Phys. Chem. A 1999, 103(13), 1913-1928.

60. Alkan, M.; Yüksek, H.; İslamoğlu, F.; Bahçeci, Ş.; Calapoğlu, M.; Elmastaş, M.; Akşit, H. and Özdemir, M. A study on 4-acylamino-4,5-dihydro-1H-1,2,4-triazol-5-ones. Molecules 2007, 12, 1805-1816.

D. Narin[1]* , Y. Cosgun[2] , G. Korukluoglu[2] , M. Kavutcu[1]

[1]Gazi University, Ankara, Turkey
[2]National Virology Reference Laboratory, Ankara, Turkey
*e-mail: deniz_narin@hotmail.com

Investigation of serum neopterin levels and adenosine deaminase enzymatic activity in measles infection

Abstract. The aim of this study was to investigate the serum neopterin level and ADA activity in acute measles infection and determine whether there is a correlation between the measles optical density values, and the neopterin and ADA levels. The neopterin level and ADA activities were investigated in the samples of 136 measles IgM-positive patients along with those of 40 measles IgM-negative patients as the control group. The most important findings of the study were the determination of significantly higher neopterin levels and ADA activity in the measles IgM-positive group when compared to the measles IgM-negative group. The high neopterin level and ADA activity in measles before IgM becomes positive in some of the patients in the first 3 days suggested that they can be used as a preliminary and supportive marker for the preliminary diagnosis of measles. These findings have shown that the neopterin level and ADA activity can assist in the diagnosis of measles in the acute period as biomarkers.
Key words: Measles, neopterin, adenosine deaminase, biomarkers, ELISA.

Introduction

Neopterin is used as a trendy biological marker in recent years in severe conditions such as in transplantation, inflammatory diseases, and autoimmune and malignant diseases, where the cellular immune system is activated [1]. Cytokines are an indicator of proinflammatory immune state delivered by human monocytes and macrophages upon stimulation by interferon-gamma [2-6]. Neopterin may be a prognostic determinant in the early stages of the disease [7, 8]. Neopterin also increases in conditions that accompany the increase of endogenous interferons, such as viral infections (especially HIV), infection of intracellular pathogens (tuberculosis, malaria, etc.), autoimmune diseases, inflammatory diseases, allograft rejection, malignant diseases, and hereditary pteridine metabolism. In studies conducted, has IFN-leds to neopterin production and release in human monocytes and macrophages *in vitro* [1, 8, 9].

Numerous clinical and experimental studies have demonstrated the relationship between neopterin production and cellular immune activation, and a strong link between neopterin levels and the severity and progression of infectious and inflammatory diseases has been demonstrated [10, 11]. Adenosine deaminase (ADA) is an enzyme required for purine metabolism that plays an important role in the differentiation of lymphoid cells. ADA deficiency causes autosomal recessive diffuse combined immunodeficiency disease with impaired cellular immunity, B- and T-lymphocyte dysfunction, and decreased immunoglobulin production [12]. ADA deficiency progresses with lymphopenia, severely impaired cellular and humoral immunity, growth retardation, and serious fatal infections [12, 13]. Measles (Rubeola, Measles, Morbili) is an acute viral disease of childhood with rash [14]. Humoral and cellular immunity occurs in those who suffer from the disease. Immunity after natural infection is thought to be lifelong [15]. In immunocompromised patients, measles may have a longer, more severe, and fatal course, and the severity of the disease depends on the severity of the cellular immunity disorder. Antibody formation is considered in the diagnosis of the disease, but immunity is mainly dependent on T-lymphocyte functions and memory [15]. The purpose of the current study was to 1) investigate the serum neopterin level and ADA activity in acute measles infection; 2) determine whether there is a correlation between measles optical density (OD) values, and neopterin and ADA levels; 3) to examine the values between the acute phase of the disease and

the recovery period; and 4) to compare the results with the control group and examine the relationship of the obtained data with the demographic findings.

Materials and methods

Serum samples of a total of 176 patients, comprising 102 women and 74 men, were included in the study. During the measles epidemic in Turkey in 2014–2015, serum samples that fit the case definition of measles and were confirmed by the laboratory were used in the current study. A pool of 176 samples, from 136 IgM-positive measles patients and 40 measles IgM-negative patients (control group), were created from the samples separated at the National Virology Reference Laboratory of the General Directorate of Public Health and stored at –80 (±10) °C. The neopterin level and ADA activity were investigated in all of the samples. The micro ELISA method (Neopterin ELISA, IBL, Germany), and ELISA washer and reader devices were used for the neopterin test. ADA analysis was performed spectrophotometrically using a Shimadzu UVmini 1240 spectrophotometer (Kyoto, Japan) following the method described by Giusti. The Enzygnost Anti-Measles Virus/IgM (Siemens, Marburg, Germany) kit was used for the determination of the measles IgM antibodies. The method was based on the indirect ELISA principle, and the test study was conducted in accordance with the instructions in the package insert of the commercial kit used.

Statistical analysis. SPSS Statistics for Windows 15.0 (SPSS Inc., Chicago, IL, USA) was used to evaluate the data obtained from the study and create tables. The mean, standard deviation, median, minimum, and maximum values were used for the presentation of the continuous variables (quantitative variables) obtained by the measurements, and the frequency and percentage values were used for presentation of the categorical variables (qualitative variables). The Fisher Exact test was used to evaluate the categorical variables. In the comparison of the quantitative variables, whether the parametric test conditions (investigation of conformity to normal distribution) were achieved was investigated using the Kolmogorov-Smirnov or Shapiro-Wilk test. The Mann-Whitney U test was used to compare 2 independent groups, as the parametric test conditions were not met. The Spearman correlation coefficient was used to examine the relationships between the variables and the relationships were also shown as a scatter plot. In all of the statistical analyses, statistical significance was accepted as $P < 0.05$.

Results and discussion

A significant difference was found between the OD, neopterin and ADA levels in the IgM-positive and IgM-negative measles groups, and the results are summarized. Of the samples that exhibited positive results, 86.8% consisted of blood samples taken within the first 0 to 5 days from the date of rash onset, and 13.2% were taken between days 6 and 15. All of the samples that exhibited negative results consisted of blood samples taken in between days 0 and 5. In the measles IgM-positive group, there were no statistically significant differences between days 0 and 5, and days 6 and 15 in terms of the measles IgM OD values with regards to the date of rash onset ($P = 0.579$). In the measles IgM-positive group, the median neopterin level between days 0 and 5 with regards to the date of rash onset was 37.58, and the median value between days 6 and 15 was 18.83. There was a statistically significant difference between days 0 and 5, and days 6 and 15 ($P = 0.002$). In the measles IgM positive group, according to the date of the rash, ADA values were found to be higher in the 0-5-day period, but there was no statistically significant difference between the 6-15-days period ($P = 0.082$) (Figure 1).

When the OD values between days 0 and 5 in the measles IgM-positive and IgM-negative groups were compared, it was determined that the measles IgM OD values were higher between days 0 and 5, and a statistically significant difference was found between them. The neopterin levels and ADA values were found to be higher between days 0 and 5 in the measles IgM-positive group, and a statistically significant difference was found when compared to the measles IgM-negative group ($P < 0.001$ for all) (Figure 2).

In the measles IgM-positive group, the median neopterin level value was found to be higher in the males, and a statistically significant difference was found between the males and the females, ($P = 0.032$). No statistically significant difference was found between the males and the females in terms of the ADA activity ($P = 0.807$). There were no statistically significant differences between the males and females in the measles IgM-negative group in terms of the neopterin level and ADA activity ($P = 0.871$ and $P = 0.705$). In the measles IgM-positive group, there was no statistically significant correlation between the measles IgM OD and neopterin levels with regards to age. The P-values were calculated as 0.068 and 0.640, respectively. There was a significant negative correlation between ADA and age ($P = 0.008$). In the

measles IgM-negative group, there was no statistically significant correlation between the measles IgM OD and ADA values with regards to age. The P-values were calculated as 0.833 and 0.542, respectively. There was a significant negative correlation between the neopterin level and age (P = 0.019) (Figure 3).
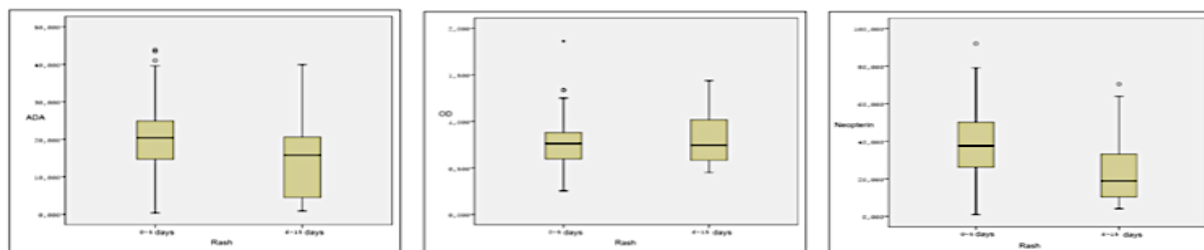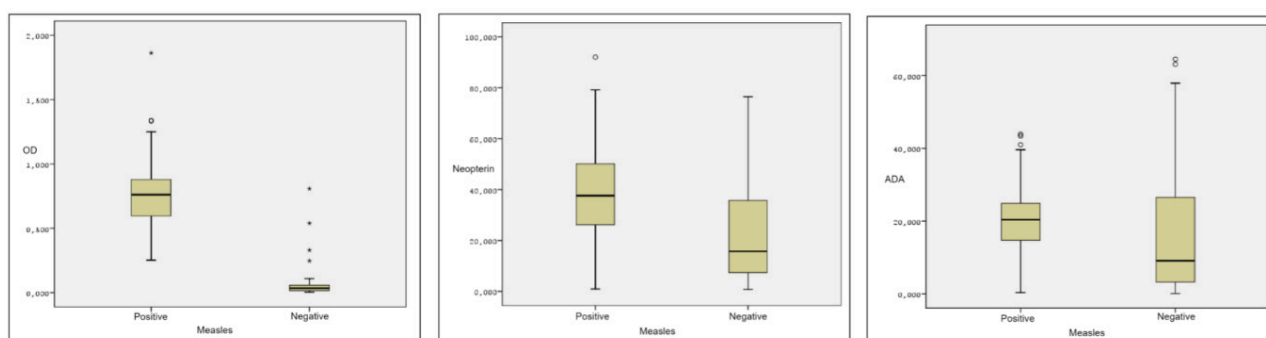

ADA: adenosine deaminase

OD: Optical density

Figure 1. Box-plot graph of the OD value, neopterin levels, and ADA activity in the IgM-positive measles groups with regards to the date of rash onset.

Figure 1 – Box-plot graph of the OD value, neopterin levels, and ADA activity in the IgM-positive measles groups with regards to the date of rash onset, where: ADA – adenosine deaminase; OD – Optical density

Figure 2 – Box-plot graph of the OD values, neopterin levels, and ADA activity between days 0 and 5 in the IgM-positive and IgM-negative measles groups, where: ADA – adenosine deaminase; OD – Optical density
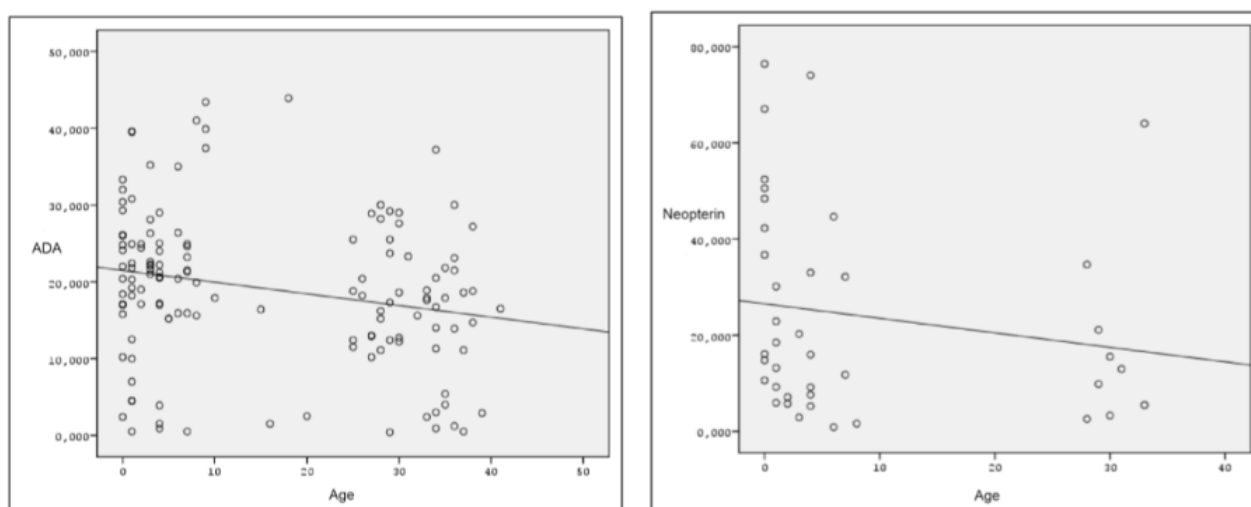
Figure 3 – Plot of the negative correlation between the ADA activity and age in the IgM-positive measles group

Neopterin is considered to be a biochemical marker of stimulated cellular immune response [1]. It is known that increased neopterin levels occur in viral infection. The literature comprises very old studies of measles in patients with subacute sclerosing panencephalitis (SSPE); however, there have been no follow-up studies thus far, regarding neopterin levels and ADA activity in patients suffering from acute measles infection [16, 17]. Neopterin may actually be a visible early diagnosis marker. Recommendations have been made that neopterin should be useful as a prognostic marker in a retrospective study for HIV positivity [18]. In studies conducted on patients with tuberculosis, serum neopterin levels were reported to be higher than the control group [19]. In another study, it was stated that increased neopterin levels were associated with mortality [20]. In the current study, the measles IgM OD values were expressed as minimum, median, and maximum values in the IgM-positive measles group, respectively, as 0.25, 0.76, and 1.86 (Table 1).

Table 1 – OD value, and neopterin and ADA levels in the IgM-positive and IgM-negative measles groups

		OD					Z	P
		Mean	Standard deviation	Median	Minimum	Maximum		
Measles	Positive	0.77	0.25	0.76	0.25	1.86	-9.21	<0.001
	Negative	0.08	0.15	0.03	0.01	0.10		
		Neopterin					Z	P
		Mean	Standard deviation	Median	Minimum	Maximum		
Measles	Positive	36.48	18.77	35.11	0.94	92.02	-3.77	<0.001
	Negative	23.92	21.48	15.73	0.86	76.45		
		ADA					Z	P
		Mean	Standard deviation	Median	Minimum	Maximum		
Measles	Positive	19.13	9.86	19.10	0.40	43.90	-2.54	0.011
	Negative	16.94	18.77	9.10	0.10	64.50		

Since an OD value above 0.20 is considered positive, this indicated that the study group included a large patient sample with low-positive, positive, and high-positive values. Significantly higher neopterin levels were observed in the measles IgM-positive group when compared to the measles IgM-negative group, which was one of the main objectives of this study, and emerged as one of the most important findings of the study (P < 0.001). Although there are no studies in the literature regarding neopterin levels in acute measles infection, similar results were obtained in studies investigating neopterin levels in other infectious diseases. [21]. Reported that serum neopterin levels in patients with chronic kidney disease were significantly correlated when inflammatory markers such as hsCRP, IL-6, and IFN-were increased [21]. In our study, the neopterin level measured in the measles IgM positive group was found to be significantly higher than in the negative group (p <0.001). This supported the idea that neopterin can be used as a biomarker in the early diagnosis of measles. When analyzed according to the date of rash onset, it was observed that the neopterin levels were found to be significantly higher in the blood samples taken in the first 5 days when compared to those taken between days 6 and 15 (P = 0.002). In measles patients, specific IgM antibodies cannot be detected in 20% of the patients in the first 3 days, and the presence of a virus can only be detected by molecular tests. For this reason, high levels of neopterin and ADA in the first 5 days can be helpful in the diagnosis of measles in the acute period. In a study conducted on acute respiratory diseases, neopterin levels in the early period and the recovery period were compared, and the mean neopterin levels were determined as 34.2 nmol/L in the acute serum of the patients and 5.1 nmol/L in the healing sera [22]. This showed that neopterin levels can be helpful in diagnosis, especially in the first days of the disease and in the acute phase. In the measles IgM-positive group herein, no statistically significant correlation was found between the neopterin levels and age (P = 0.64). In the IgM-negative measles group, a significant negative correlation was found

between the neopterin levels and age (P = 0.019). In other words, it was observed that the younger the age, the higher the neopterin level. In another study conducted, it was shown that serum neopterin levels changed with age, without any association with any disease [22]. Neopterin levels were found to be high in the serum of patients under the age of 18 and above the age of 75, while the age-related neopterin levels did not change in patients between 18 and 75 years of age [23, 24]. In a study conducted by Daito et al. on 14 patients with chronic hepatitis B, where 8 patients were over 30 years of age and 6 were under 30 years of age, no significant relationship was found between the serum neopterin levels and age [24]. In the study of Lucas et al., it was shown that serum neopterin levels increased significantly as the age of the patients increased, in 302 healthy adults, without infectious disease, under stress [25]. The reason for such a correlation in the negative patient group was thought to be due to the fact that this group of patients had a fever with a non-measles rash or that the median age value of the negative patient group was lower than that of the positive group. Considering that the group of patients with measles IgM-negative was actually the group of patients with a fever, rash complaints, and whose samples were sent with a pre-diagnosis of measles, the lower neopterin levels in this group suggested that neopterin can also be used in the differential diagnosis of other rash and fever agents in the acute phase of measles.

ADA is recognized as a nonspecific marker of T-lymphocyte activation and cellular immunity [26]. It is known that ADA activity increases in infectious diseases, such as tuberculosis, in which T-lymphocytes play an important role [27-29]. In the present study, higher median values were obtained in the measles IgM-positive group when compared to the measles IgM-negative group in terms of ADA activity, and the difference was found to be statistically significant (P = 0.011). There are no studies in the literature regarding ADA activity in acute measles infection. There are studies reporting increased pleural fluid ADA activity in patients with TB pleurisy [30, 31]. In a study by Solomon et al., the pleural fluid levels and serum ADA activity were investigated, and it was found that serum ADA activity was higher in patients with TB than in those with malignancy, pneumonia, and rheumatoid arthritis [32]. Herein, a negative correlation was found between age and ADA activity in the measles IgM-positive group, and it was found to be statistically significant (P = 0.008). No significant correlation was found in the measles IgM-negative group. In a study of Kaya et

al., 73 hepatitis B and 71 hepatitis C patients were examined, and serum the ADA and transaminase activity was found to be significantly higher than in the control group [33]. One of the limitations of this study was that the patients could not be followed-up in terms of the prognosis of the disease, mortality and morbidity, development of complications, such as SSPE, etc. Another limitation of this study was that vaccination information could not be obtained for all of the patients; hence, no comparison could be made between IgM positivity due to vaccine and IgM positivity due to wild virus in terms of the neopterin levels and ADA activity. The median neopterin value was found to be higher in the men in the measles IgM-positive group, and a statistically significant difference was found between females and the males (P = 0.032). Although a clear explanation could not be made regarding the reason for this, different results were obtained in different studies depending on the population in which the study was conducted [2, 29, 30, 34].

Conclusion

Significantly higher neopterin levels and ADA activity in the measles IgM-positive group when compared to the measles IgM-negative group emerged as one of the most important findings of this study. When analyzed according to the date of rash onset, it was observed that the neopterin levels and ADA activity were found to be significantly higher in blood samples taken during the first 5 days when compared to those taken between days 6 and 15. With these findings, both parameters were found to be higher in the acute period when compared to the recovery period, suggesting that they behaved like an acute phase reactant. The high neopterin level and ADA activity in measles before IgM becomes positive in some of the patients in the first 3 days suggested that they can be used as a preliminary and supportive marker for the preliminary diagnosis of measles. In conclusion, the findings herein showed that the neopterin level and ADA activity, as biomarkers, can help diagnose measles in the acute phase.

References

1. Fuchs D, Weiss G, Wachter H. Neopterin, biochemistry and clinical use as a marker for cellular immune reactions. Int Arch Allergy Immunol. 1993;101(1):1-6. doi:10.1159/000236491.

2. Wachter, P. Europium chalcogenides: EuO, EuS, EuSe and EuTe. Handbook on the Physics and

Chemistry of Rare Earths, (2), Chapter 19, 1979; P:507-574.

3. Rokos H, Rokos K, Frisius H, et al. Altered urinary excretion of pteridines in neoplastic disease. Determination of biopterin, neopterin, xanthopterin, and pterin. *Clin Chim Acta*. 1980;105(2):275-286. doi:10.1016/0009-8981(80)90470-2

4. Stea B, Halpern RM, Halpern BC, et al. Urinary excretion levels of unconjugated pterins in cancer patients and normal individuals. *Clin Chim Acta*. 1981;113(3):231-242. doi:10.1016/0009-8981(81)90277-1

5. Dhondt AA, Schillemans J, De Laet J. Blue tit territories in populations at different density levels. *Ardea-Wageningen.* 1982; 70, 185-188.

6. Chan CP, Choi JW, Cao KY, et al. Detection of serum neopterin for early assessment of dengue virus infection. *J Infect*. 2006;53(3):152-158. doi:10.1016/j.jinf.2005.11.008

7. Kaleli I, Demir M, Cevahir N, et al. Serum neopterin levels in patients with replicative and nonreplicative HBV carriers. *BMC Infect Dis*. 2006; 6:157. Published 2006 Oct 31. doi:10.1186/1471-2334-6-157

8. Wachter H, Fuchs D, Hausen A, et al. Neopterin as marker for activation of cellular immunity: immunologic basis and clinical application. *Adv Clin Chem*. 1989; 27:81-141. doi:10.1016/s0065-2423(08)60182-1

9. Müller MM, Curtius HC, Herold M, et al. lNeopterin in clinical practice. *Clin Chim Acta*. 1991;201(1-2):1-16. doi:10.1016/0009-8981(91)90019-9

10. Baize S, Leroy EM, Georges AJ, et al. Inflammatory responses in Ebola virus-infected patients. *Clin Exp Immunol*. 2002;128(1):163-168. doi:10.1046/j.1365-2249.2002.01800.x

11. Rieder J, Lirk P, Hoffmann G. Neopterin as a potential modulator of tumor cell growth and proliferation. *Med Hypotheses*. 2003;60(4):531-534. doi:10.1016/s0306-9877(03)00002-1

12. Balis ME. Adenosine deaminase and malignant cells. *Ann N Y Acad Sci*. 1985; 451:142-149. doi:10.1111/j.1749-6632.1985.tb27105.x

13. Rosi F, Tabucchi A, Carlucci F, et al. 5'-nucleotidase activity in lymphocytes from patients affected by B-cell chronic lymphocytic leukemia. *Clin Biochem*. 1998;31(4):269-272. doi:10.1016/s0009-9120(98)00017-4

14. Kliegman, R. M., Behrman, R. E., Jenson, H.B., et al. B. M. Nelson textbook of pediatrics e-book. Edinburgh: Elsevier Health Sciences,2007;88-89.

15. Redd SC, Markowitz LE, and Katz SL. Measles vaccine. (Edt. Plotkin, S. A. and Orenstein, W. A.) In: Vaccines, 3rd Edition. Philadelphia: WB Saunders Company,1999; 222-266.

16. Murata R, Hattori H, Matsuoka O, et al. Ferritin, creatine kinase, and neopterin in subacute sclerosing panencephalitis. *Brain Dev*. 1992;14(6):391-395. doi:10.1016/s0387-7604(12)80346-9

17. Tousoulis D, Kampoli AM, Stefanadi E, et al. New biochemical markers in acute coronary syndromes. *Curr Med Chem*. 2008;15(13):1288-1296. doi:10.2174/092986708784534965

18. Baier-Bitterlich G, Fuchs D, Wachter H. Chronic immune stimulation, oxidative stress, and apoptosis in HIV infection. *Biochem Pharmacol*. 1997;53(6):755-763. doi:10.1016/s0006-2952(96)00651-x

19. Koşar F, Yurt S, Arpınar Yiğitbaş B, et al. The comparative value of pleural fluid adenosine deaminase and neopterin levels in diagnostic utility of pleural tuberculosis. *Tuberk Toraks*. 2015;63(4):243-249. doi:10.5578/tt.9973

20. Adamik B, Kübler-Kielb J, Golebiowska B, et al. Effect of sepsis and cardiac surgery with cardiopulmonary bypass on plasma level of nitric oxide metabolites, neopterin, and procalcitonin: correlation with mortality and postoperative complications.*Intensive Care Med*. 2000;26(9):1259-1267. doi:10.1007/s001340000610

21. Yadav AK, Sharma V, Jha V. Association between serum neopterin and inflammatory activation in chronic kidney disease. *Mediators Inflamm*. 2012; 2012:476979. doi:10.1155/2012/476979

22. Berdowska A, Zwirska-Korczala K. Neopterin measurement in clinical diagnosis. *J Clin Pharm Ther*. 2001;26(5):319-329. doi:10.1046/j.1365-2710.2001.00358.x

23. Hamerlinck FF. Neopterin: a review. Exp Dermatol. 1999;8(3):167-176. doi:10.1111/j.1600-0625.1999.tb00367.x

24. Daito K, Suou T, Kawasaki H. Serum and urinary neopterin levels in patients with chronic active hepatitis B treated with interferon. *Res Commun Chem Pathol Pharmacol*. 1994;83(3):303-316.

25. Lucas RM, Ponsonby AL, Dear K. Mid-life stress is associated with both up- and down-regulation of markers of humoral and cellular immunity. *Stress*. 2007;10(4):351-361. doi:10.1080/10253890701379023

26. Ateş Y, Ergün H, Tüzün A, et al. Serum adenosine deaminase levels and lymphocyte subgroups

in familial mediterranean fever. [In Turkish: Ailesel Akdeniz Ateşi olan hastalarda lenfosit alt grupları ve serum adenozin deaminaz düzeyleri.] *Akad Gastroenteroloji Dergi.* 2005; 4 (2): 112-116

27. Collazos J, España P, Mayo J, et al. Sequential evaluation of serum adenosine deaminase in patients treated for tuberculosis. *Chest.* 1998;114(2):432-435. doi:10.1378/chest.114.2.432

28. Bittencourt PL, Farias AQ, Porta G, et al. Frequency of concurrent autoimmune disorders in patients with autoimmune hepatitis: effect of age, gender, and genetic background. *J Clin Gastroenterol.* 2008;42(3):300-305. doi:10.1097/MCG.0b013e31802dbdfc

29. Teufel A, Weinmann A, Kahaly GJ, et al. Concurrent autoimmune diseases in patients with autoimmune hepatitis. *J Clin Gastroenterol.* 2010;44(3):208-213. doi:10.1097/MCG.0b013e3181c74e0d

30. Burgess LJ, Maritz FJ, Le Roux I, et al. Use of adenosine deaminase as a diagnostic tool for tuberculous pleurisy. *Thorax.* 1995;50(6):672-674. doi:10.1136/thx.50.6.672

31. Bañales JL, Pineda PR, Fitzgerald JM, et al. Adenosine deaminase in the diagnosis of tuberculous pleural effusions. A report of 218 patients and review of the literature. *Chest.* 1991;99(2):355-357. doi:10.1378/chest.99.2.355.

32. Al-Shammary FJ. Adenosine deaminase activity in serum and pleural effusions of tuberculous and non-tuberculous patients. *Biochem Mol Biol Int.* 1997;43(4):763-779. doi:10.1080/15216549700204581

33. Kaya S, Cetin ES, Aridogan BC, et al. Adenosine deaminase activity in serum of patients with hepatitis -- a useful tool in monitoring clinical status. *J Microbiol Immunol Infect.* 2007;40(4):288-292.

34. Fukushima T, Nixon JC. Analysis of reduced forms of biopterin in biological tissues and fluids. *Anal Biochem.* 1980;102(1):176-188. doi:10.1016/0003-2697(80)90336-x

Content